

AFRL-AFOSR-UK-TR-2011-0029



**Study for Air Vehicles at High Speeds
Identifying the Potential Benefits to Transport Aircraft
of a Continuously Variable Geometry Trailing-Edge
Structure that can be Utilized for Aircraft Control,
Trim, Load-Alleviation and High Lift**

Raj K Nangia

**Nangia Aero Research Associates
West Point, 78 Queens Road, Clifton
Bristol, United Kingdom BS8 1QU**

EOARD GRANT 10-3090

August 2011

Final Report for 27 September 2010 to 27 March 2011

Distribution Statement A: Approved for public release distribution is unlimited.

**Air Force Research Laboratory
Air Force Office of Scientific Research
European Office of Aerospace Research and Development
Unit 4515 Box 14, APO AE 09421**

REPORT DOCUMENTATION PAGE				Form Approved OMB No. 0704-0188	
Public reporting burden for this collection of information is estimated to average 1 hour per response, including the time for reviewing instructions, searching existing data sources, gathering and maintaining the data needed, and completing and reviewing the collection of information. Send comments regarding this burden estimate or any other aspect of this collection of information, including suggestions for reducing the burden, to Department of Defense, Washington Headquarters Services, Directorate for Information Operations and Reports (0704-0188), 1215 Jefferson Davis Highway, Suite 1204, Arlington, VA 22202-4302. Respondents should be aware that notwithstanding any other provision of law, no person shall be subject to any penalty for failing to comply with a collection of information if it does not display a currently valid OMB control number. PLEASE DO NOT RETURN YOUR FORM TO THE ABOVE ADDRESS.					
1. REPORT DATE (DD-MM-YYYY) 22-08-2011		2. REPORT TYPE Final Report		3. DATES COVERED (From – To) 27 September 2010 – 27 March 2011	
4. TITLE AND SUBTITLE Study for Air Vehicles at High Speeds, Identifying the Potential Benefits to Transport Aircraft of a Continuously Variable Geometry Trailing-Edge Structure that can be Utilized for Aircraft Control, Trim, Load-Alleviation, and High Lift				5a. CONTRACT NUMBER FA8655-10-1-3090	
				5b. GRANT NUMBER Grant 10-3090	
				5c. PROGRAM ELEMENT NUMBER	
6. AUTHOR(S) Dr. Raj K Nangia				5d. PROJECT NUMBER	
				5d. TASK NUMBER	
				5e. WORK UNIT NUMBER	
7. PERFORMING ORGANIZATION NAME(S) AND ADDRESS(ES) Nangia Aero Research Associates West Point, 78 Queens Road, Clifton Bristol, United Kingdom BS8 1QU				8. PERFORMING ORGANIZATION REPORT NUMBER N/A	
9. SPONSORING/MONITORING AGENCY NAME(S) AND ADDRESS(ES) EOARD Unit 4515 BOX 14 APO AE 09421				10. SPONSOR/MONITOR'S ACRONYM(S) AFRL/AFOSR/RSW (EOARD)	
				11. SPONSOR/MONITOR'S REPORT NUMBER(S) AFRL-AFOSR-UK-TR-2011-0029	
12. DISTRIBUTION/AVAILABILITY STATEMENT Approved for public release; distribution is unlimited. (approval given by local Public Affairs Office)					
13. SUPPLEMENTARY NOTES					
14. ABSTRACT One of the technologies emerging in recent years concerns variable aerofoil shaping (or morphing), using "clever" internal mechanisms. Previous studies have noted potential aerodynamic efficiency gains, gust loads alleviation, stagnation point control for laminar flow onset or Shock position / strength control. Previous work along some of these lines has also been in TACT & MAW programs. Although such mechanisms may provide a lower sectional C _{lmax} , compared with a point design high-lift system, the main advantage is that these mechanisms could be utilized across the entire flight envelope for different functions. It is also known that to obtain optimum L/D performance at high-lift, TE deflections may need to be accompanied by LE deflections or devices. Many, varied aspects of VTE technology have been assessed. At high and low speed, a VTE capable wing provides higher L/D. This advantage can be assimilated in a variety of ways, increased range efficiency gives typically 5% to 15% increase in range, Take-Off field lengths are reduced by 10% to 15% depending upon C _{lmax} capability. A wing with VTE capability can control "off-design" gust loads thereby reducing structural strength requirements leading to a lighter wing. Using simplified but modest assumptions, the wing weight saving can be immediately absorbed as increased payload within given MTOW. On current, reasonably fuel efficient, long-range civil transports this leads to 45% increased efficiency. On small, comparatively inefficient long-range executive transports the wing weight reduction virtually doubles the design payload leading to 70% to 80% increase in efficiency.					
15. SUBJECT TERMS EOARD, Aerodynamics, Control System					
16. SECURITY CLASSIFICATION OF:			17. LIMITATION OF ABSTRACT SAR	18. NUMBER OF PAGES 133	19a. NAME OF RESPONSIBLE PERSON Gregg Abate
a. REPORT UNCLAS	b. ABSTRACT UNCLAS	c. THIS PAGE UNCLAS			19b. TELEPHONE NUMBER (Include area code) +44 (0)1895 616021

Study for Air Vehicles at High Speeds
Identifying the Potential Benefits to Transport Aircraft of
a Continuously Variable Geometry Trailing-Edge
Structure that can be Utilized for Aircraft Control, Trim,
Load-Alleviation, and High-Lift.

Dr R K Nangia

SUMMARY

One of the technologies emerging in recent years concerns variable aerofoil shaping (or morphing), using “clever” internal mechanisms. Previous studies have noted potential aerodynamic efficiency gains, gust loads alleviation, stagnation point control for laminar flow onset or Shock position / strength control. Previous work along some of these lines has also been in TACT & MAW programmes. Although such mechanisms may provide a lower sectional C_{Lmax} , compared with a point design high-lift system, the main advantage is that these mechanisms could be utilized across the entire flight envelope for different functions. It is also known that to obtain optimum L/D performance at high-lift, TE deflections may need to be accompanied by LE deflections or devices.

Many, varied aspects of VTE technology have been assessed. At high and low speed, a VTE capable wing provides higher L/D. This advantage can be assimilated in a variety of ways, increased range efficiency gives typically 5% to 15% increase in range, Take-Off field lengths are reduced by 10% to 15% depending upon C_{Lmax} capability. A wing with VTE capability can control “off-design” gust loads thereby reducing structural strength requirements leading to a lighter wing. Using simplified but modest assumptions, the wing weight saving can be immediately absorbed as increased payload within given MTOW. On current, reasonably fuel efficient, long-range civil transports this leads to 45% increased efficiency. On small, comparatively inefficient long-range executive transports the wing weight reduction virtually doubles the design payload leading to 70% to 80% increase in efficiency.

The work performed in this report was requested by the Air Force Research Laboratory, Air Vehicles Directorate, Low Speed Aerodynamics Configuration Branch with the technical monitors identified as Mr. Gary Dale & Mr. Peter Flick

EOARD Grant No.10-3090

Consulting Engineers
Nangia Aero Research Associates
WestPoint, 78 Queens Road, Clifton
Bristol BS8 1QU, UK

The work performed in this report was requested by the Air Force Research Laboratory, Air Vehicles Directorate, Low Speed Aerodynamics Configuration Branch with the technical monitor identified as Mr. Gary Dale. It was facilitated via the USAF - EOARD, 86 Blenheim Crescent, Ruislip, London HA4 7HB, UK and was carried out under the terms of Grant No 10 – 3090

INITIAL DISTRIBUTION LIST

1	Dr. Gregg Abate	USAF-EOARD, 86 Blenheim Crescent, Ruislip London HA4 7HB, UK
1	Mr Gary Dale	AFRL/RBAL, Bldg 45, 2130 8 th Street, WPAFB, OH 45433 -7542
1.	Mr. Peter Flick	AFRL/RBSD, Bldg 45 , 2130 Eighth St, WPAFB, OH 45433 -7542
1	Mr. Dieter Multhopp	AFRL/RBAA Bldg 45, 2130 8 th Street, WPAFB, Ohio, USA 5433-7542
1	Dr. Carl P. Tilmann	AFRL/RBAA Bldg 45, 2130 8 th Street, WPAFB, Ohio, USA 5433-7542
1	Mr. William Blake	AFRL/RBCA Bldg 146, 2130 8 th Street, WPAFB, Ohio, USA 45433-7542
1	Mr. Cale Zeune	AFRL/RBAA Bldg 45 8 th St, Bldg 45, Rm 262, WPAFB, Ohio, USA 45433- 7542
1	Mr. Ryan Plumley	AFRL/RBAA Bldg 45 8 th St, Bldg 45, Rm 262, WPAFB, Ohio, USA 45433- 7542
2	Dr. R.K. Nangia	Nangia Aero Research Associates, WestPoint, 78-Queens Road, Clifton, BRISTOL BS8 1QU, UK.

CONTRACTUAL DECLARATIONS

“The Contractor, Dr. R. K. Nangia,, hereby delcares that, to the best of its knowledge and belief, the technical data delivered herewith under Grant No10-3090 is complete, accurate, and complies with all requirements of the grant.”

DATE: July 2011 Name and Title of Authorized Official: Dr R K Nangia

“I certify that there were no subject inventions to declare as defined in FAR 52.227-13, during the performance of this contract.”

DATE: July 2011 Name and Title of Authorized Official: Dr R K Nangia

CONTENTS

SUMMARY

DISTRIBUTION LIST AND CONTRACTUAL DECLARATIONS

1. INTRODUCTION AND OVERVIEW

- 1.1. Technology Advances in Aerofoil Design (Adaptation Across Flight Envelope)
- 1.2. Content and Layout of this Report

2. TECHNICAL DETAILS AND METHODOLOGIES

- 2.1. Fuel Efficiency Perspective
- 2.2. Present Context
- 2.3. Methodologies

3. SETTING UP SCOPE AND PHASING OF THE PROGRAMME

- 3.1. Scope and Phasing
- 3.2. Work Programme Envisaged (Statement of Work)

4. PREVIOUS EXPERIENCE ON RELATED HIGH-LIFT

- 4.1. High Lift Devices
- 4.2. Fokker 100 (F-100)
- 4.3. Gulfstream III (G-III)
- 4.4. Assessing and Matching Performance Data

5. ASPECT RATIO 6 WING CONFIGURATION

- 5.1. Geometry and Modelling
- 5.2. High Speed (M 0.75) Performance, TE Deflection and Variable TE
- 5.3. Low Speed (M 0.20) Performance
- 5.4. Stability and Control, Laterals

6. ASPECT RATIO 10 WING CONFIGURATION

- 6.1. Nominal AR 10 wing Configuration, Performance, Geometry and Modelling
- 6.2. High Speed (M 0.75) Performance, Clean Wing, Plain Flaps and Variable TE
- 6.3. Low Speed (M 0.20) Performance
- 6.4. Stability and Control, Laterals

7. INTEGRATING VARIABLE CAMBER

- 7.1. VTE Capability into High Speed Wing Design and Low Speed Application
- 7.2. VTE integration into Cruise Wing Design, Effect on Payload – Range Efficiency
- 7.3. Low Speed, Take-Off and Landing, Performance
- 7.4. Transport Aircraft Design Comparison, Conventional Flaps v Variable Camber

8. CONCLUDING REMARKS

9. FURTHER WORK

ACKNOWLEDGEMENTS

REFERENCES

LIST OF SYMBOLS AND ABBREVIATIONS

FIGURES 1.1.1-31, 2.1.1-12, 2.3.1, 4.1.1-9, 4.2.1-15, 4.3.1-4, 4.4.1, 5.1.1-5, 5.2.1-17, 5.3.1-27, 5.4.1, 6.1.1-4, 6.2.1-11, 6.3.1-24, 7.2.1-4, 7.3.1-2 (173 Total)

1. INTRODUCTION AND OVERVIEW

Presently there is great emphasis on achieving efficient and optimised flight. The current and future budgets recognise this and stress the need for the work to be done. We have been working in this field for several years (e.g. Refs.1-3). The need for overall energy savings is being felt in all spheres of defence and commercial aviation. The military scene includes many different types of aircraft designed for fulfilling many diverse roles.

In our previous studies under USAF- EOARD grant 08-3023, we have looked at current Transports (Jets and Turbo-Props), Surveillance, Reconnaissance and Tankers. We have developed Fuel Efficiency related metrics (Refs.4-8).

The studies have brought out the significance of achieving balance (compromises) between aerodynamic, propulsive and structural efficiencies through a series of metrics involving payload, range and block fuel for different missions and flight envelopes.

Newer technologies and improvements can be evaluated through these metrics.

1.1. Technology Advances in Aerofoil Design (Adaptation Across Flight Envelope)

One of the technologies emerging in recent years concerns variable aerofoil shaping (or morphing), using “clever” internal mechanisms. Studies have noted potential aerodynamic efficiency gains, gust loads alleviation, stagnation point control for laminar flow onset or Shock position / strength control, Refs.9-10.

In its simplest form, continuously varying trailing edge geometry is used for gust alleviation on A380 and will be further developed for the A350.

It is noted in Ref.11 that commercial considerations demand that there is “fleet commonality” in civil transport aircraft. Airframe manufacturers therefore design and size wings of “launch” concepts to accommodate future fuselage stretches for higher capacity variants. The wing discussed in Ref.11 for four-engined, long-range capability is also used in a twin-engined high capacity configuration. Optimum performance is achieved at high wing loadings that will occur later in a concept development programme. Variable camber implies that the wing can be “re-designed” to tune performance throughout the flight envelope (Take-Off, Cruise, Landing) and for a range of operational requirements (Short Range High Capacity or Longer Ranges). Variable camber therefore allows for smaller wing areas to be considered from the outset of a new design.

Several interesting and beneficial concepts related to variable camber are discussed in detail in Ref.12 and are reviewed briefly here. Primary design requirements and typical wing area trade-offs that arise from a basic wing design (cruise C_L capability 0.3 to 0.7) are shown in **Fig.1.1.1**. Incorporated into a four-engined, long range aircraft, the wing provides cruise C_L 0.4 to 0.6. Higher capacity, stretched, long-range variants will take advantage of the higher cruise C_L capability (up to 0.7). In a twin-engined, short-range concept, the lower C_L capabilities will be used. A stretched version will be afforded C_L capability up to 0.6 of the common wing. The principles of variable camber and anticipated L/D improvements are shown in **Fig.1.1.3**. **Fig.1.1.2** is an Aerodynamic Development Concept Flow chart for a wing incorporating variable camber. The effect of variable camber downwash on the tail design is noted. Both high speed cruise design and low speed take-off and landing capabilities are considered.

It was noted in **Fig.1.1.3(b)**, Airbus A320 studies, that a variable camber design would give a 3% L/D increment at C_L 0.5 and 10% increment at C_L 0.6. The primary advantage arises from the lower design C_L requirements (end of cruise case) for the VTE capable wing. The higher C_L required at start of cruise is achieved by deflections of the VTE geometry. Pressure

distributions on a conventional, highly loaded, aerofoil and on one suitably designed for variable camber operation are compared in **Fig.1.1.4**. Note the reduced supersonic flow region, low dC_p/dx near C_p^* (establishes stable shock) and reduced rear loading (reduces adverse pitching moment). **Fig.1.1.5** shows theoretical effects of Reynolds number on pressure distribution and drag for a 3.5° camber deflection. As flight Re is approached, the distribution is almost shock free with increased skin friction near the TE (separation is delayed). Aerodynamic efficiency ($M.L/D$) contours are compared on a $C_L - M$ grid in **Fig.1.1.6** for the fixed and variable camber cases. At any $M.L/D$ value the variable camber case covers a wider $C_L - M$ envelope. A 20% increase in C_L optimum is noted for the variable camber case.

Further comments on **Figs.1.1.7 to 20** will help to introduce the concepts.

Previous work along some of these lines has also been in the TACT and MAW programmes, **Figs.1.1.21-22** (Ref.9). Although such mechanisms may provide a lower sectional C_{Lmax} , compared with a point design high-lift system, the main advantage is that these mechanisms could be utilized across the entire flight envelope for different functions. It is also known that to obtain optimum L/D performance at high-lift, TE deflections may need to be accompanied by LE deflections or devices.

It is worth mentioning that adaptive TE technologies can be used efficiently with Close Formation Flying (CFF) (no controls hinge-line penalties). We have developed an “inverse” design method that allows the TE shape / camber and twist variation along the span to be determined. See Refs.13-14. Substantial Lift- Induced drag (C_{Di}) benefits are available, depending on the relative sizes of the aircraft in formation and their numbers in formation. This subject is in revival currently. Early proving work has been conducted by NASA on FA-18 formations.

In the time-scale to 2012, Ref.15 mentions flight research (NASA & AFRL) into Adaptive Compliant Trailing Edge (ACTE) on a Gulfstream-III, **Fig.1.1.23**. The conventional TE flaps (19 ft span x 3 ft chord) of the aircraft are to be replaced by morphing composite wing structures. The studies hope to demonstrate fuel savings and noise reduction.

For the proposed work, it will be required to know quantitatively, the significance of this technology, in more practical terms, applied to different types of aircraft (e.g. mobility aircraft, transports, tankers, Reconnaissance, Sensor-craft etc.). In the first instance, transport and mobility aircraft are of interest (**Figs.1.1.24-25** for Jets and Turbo-props respectively). The transports have a wider flight envelope compared with Civil types. **Fig.1.1.26** shows the Payload, Range and Weight characteristics of C-17 Globemaster transport aircraft operating under different g conditions and with different reserve fuel limits. Further details are in Refs. 4-6. Other beneficial applications of variable camber technology will include Sensorcraft, long endurance platforms, **Fig.1.1.27**, Tanking and Mobility, **Fig.1.1.28** and future transport concepts, **Fig.1.1.29**.

It is noted in Ref.11, that the spanwise load distributions are dependent upon configuration and flight conditions. Various examples were generated using Fourier analysis and estimates of Lift-induced drag efficiencies ($e = 1/k$) were derived, **Fig.1.1.30**. For the clean wing with elliptic loading, $e = 1.000$, (a). For a trapezoidal wing with constant aerofoil sections $e = 0.976$. Fuselage interference on case (a) reduced e to 0.948, (c). Wing mounted engine pod, pylon and pod plus pylon and fuselage interference effects progressively reduced e to 0.884, (e to g). For the wing-fuselage case in the high lift configuration e is 0.549, (h). Several asymmetric cases were also considered, **Fig.1.1.31**. For the basic wing (elliptic loading design) in sideslip e reduces to 0.975. Using differential aileron for Roll control gives $e = 0.741$. The wing distribution is less affected using differential tail for Roll control, $e = 0.792$.

Using wing spoiler for Roll control has less impact on ϵ (0.922). These observations will have a considerable bearing on the application of variable camber in preference to conventional devices for high lift and control aspects.

The **Objective** of this study is to identify the potential benefits to transport aircraft of a continuously variable geometry trailing edge structure that can be utilized for aircraft control, trim, load alleviation, and high lift. Efficiency and Endurance are part of this.

The **Approach** would be to evaluate the technology for several different missions and assess the impact on the vehicle design and performance. It is anticipated the new trailing edge technology would be applied to the entire trailing edge of a new vehicle (designs over next 10-20 years).

As in our previous programmes (both subsonic and supersonic) with AFRL over last two decades, the product of the studies will be reports, briefings and Conference papers (as required).

1.2. Content and Layout of this Report

The remainder of this report is contained in **Sections 2 to 9**.

Section 2 relates to Technical Details

Section 3 establishes the scope and phasing of the programme, depending on funds and resources availability.

Section 4 discusses Previous Experience on related High lift aspects.

Section 5 assess Aspect Ratio 6 configuration, conventional flaps and variable camber.

Section 6 refers to Aspect Ratio 10 configuration.

Section 7 looks at integrating Variable Camber technology into future Transport designs.

Section 8 Concluding Remarks.

Section 9 outlines Further Work.

2. TECHNICAL DETAILS AND METHODOLOGIES

2.1. Fuel Efficiency Perspective

In Ref.2, Nangia presented results from an appreciable data exercise on modern commercial (jet) aircraft, taking into account the distinction between Maximum Payload performance, occurring at Pt A on the Payload-Range diagram, **Fig.2.1.1** and the Design Payload performance, Pt D. Several figures from Ref.2 are reproduced and discussed as a reminder of the basic efficiency principles. **Fig.2.1.1** compares the Payload-Range performance of the Boeing 757-200 and the much larger Boeing 747-400. The significance of mandatory fuel reserves has also been considered. Pt B on the Payload-Range diagram is also of interest. At Pt B the aircraft is at maximum fuel capacity with a reduced payload and at the MTOW limit. In payload terms, passenger payload is inefficient! Pt F corresponds to maximum fuel capacity with zero payload essentially for Ferrying Range.

Civil aircraft are designed, initially, for a particular passenger payload over a given Range (Pt B). Variants of the initial design may carry additional passengers (more densely seated) or additional cargo over shorter Ranges, closer to Pt A. Civil freighters are, in general, derivatives of passenger aircraft and they will not be aligned to a specific design point. Similarly, military transport aircraft will be required to operate over the entire scope of the Payload-Range envelope.

For the Civil aircraft, trends of aircraft component weight ratios (with respect to MTOW), OEW/MTOW, WP/MTOW, (OEW+WP)/MTOW, WFB/MTOW and WFR/MTOW are

derived in **Fig.2.1.2.** (Pt A) and **Fig.2.1.3** (Pt D) against Range. We note the slight shift in the trends for the more modern High By-Pass Ratio (HBPR) engines.

Payload Range Efficiency (PRE) is an important and useful efficiency parameter. It is the product of Payload (WP) and Range (R) divided by Fuel burnt to complete the mission (WFB). $PRE = WP * R / WFB$.

These results have been correlated into reliable “first-order” non-dimensional trends in terms of PRE/X and Z, using the Breguet Range equation.

$$X = V L/D / SFC, \quad Z = R / X$$

$Z = R/X = \log_e [W1 / (W2)]$ where W1 and W2 signify the weights at start and end of cruise.

$W2 = W1 - WFBC$ where WFBC is weight of the Fuel burnt during cruise.

$W1 = MTOW - WFBS$ where WFBS refers to the Fuel used for take-off, manoeuvring additional to the cruise. This is of the order of 2.2% of MTOW (Ref.6).

Total Block fuel is then $WFB = WFBC + WFBS$.

Figs. 2.1.4-5 summarise the WFB/WP and PRE/X trends, distinguishing between A and D point operation. Radial lines of constant WFB/WP are shown. In fuel efficiency terms, aircraft perform best at Pt. A and the optimum design Range is about 2500 - 3500nm, depending on the aircraft Range parameter X. Note that from practical size and Range considerations, Pt A curves extend to Z near 0.4.

The work on efficiency of civil aircraft has been extended to civil freighters, Refs.2-3.

The variations of freighter aircraft component weight ratios (with respect to MTOW), OEW, WP, OEW+WP, WFB and WFR at Pt A with Range are presented in **Fig.2.1.6** together with trends for the civil passenger aircraft. The OEW ratio trends for the freighter aircraft are near 10%TOW less than those of the passenger aircraft. This allows a corresponding increase in WP ratio for the freighters.

Fig.2.1.7 shows civil freighter PRE variation with Range at varying payload fractions (100%, 80%, 60% and 40% of WP_{max}). The band-widths for each payload fraction indicate scatter in the plotted data. This is partly due to variations in efficiency for freighters of varying age and design technology but may also be indicative of the accuracy of the performance data available. Also shown are “radial” lines of constant WFB/WP. This indicates that at Pt A, the freighters are achieving a WFB/WP ratio of about 0.8. When non-dimensionalised by Z, the trends of **Fig.2.1.7** take on a different emphasis, **Fig.2.1.8**. Here, PRE/X for a given payload fraction remains almost constant as Z varies. Also included in **Fig.2.1.8** is the Pt A PRE/X – Z trend for the civil passenger aircraft indicating the greater efficiency of the freighter aircraft at all payload fractions.

We also need to consider other issues e.g.

- Acknowledge that some military transports were adapted from the civil scene (except the heavy lifters)
- Traditionally, military aircraft are designed to specific roles – fighter, bomber, reconnaissance, land-based / carrier-based. Currently, with significant awareness of costs, multi-role designs for different operating scenarios becoming the norm.
- Modern materials and controls will allow morphing structures to expand the flight envelopes in future (adaptive intakes, morphing wings optimised for T/O, cruise, Landing)

- Consideration of fuel Efficiency Parameters should allow greater flexibility in the design of future transports.

The ratio of maximum static, Sea Level, thrust available over MTOW (T/W) is plotted against Range in **Fig.2.1.9**. The trends derived for the civil passenger aircraft at Pt A are in **Fig.2.1.9** (a) and for Pt B in **Fig.2.1.9** (b). Corresponding data for the civil freighter aircraft fall within these trends. Data for the military transports are shown at various g ratings. Turbo-prop transport aircraft data are added to the trends for Pt A in **Fig.2.1.9** (c) and for Pt B in **Fig.2.1.9** (d). There is a considerably wider variation in T/W at a given range for the turbo-prop aircraft than for the civil and military jets. This indicates a wider range of design requirements, e.g. short field performance (Saab 2000 & A400M) or older, quieter performance trends.

The variation of component weight ratios at Pt A against Range for the military jet transports are compared with those for civil freighters in **Fig.2.1.10**. These are essentially similar. These aircraft span several technology levels (years) and each has its own set of design parameters. The component weight ratios for the C-17 at Pt A lie close to the civil passenger aircraft trends. The An-124 weight ratios lie within the civil freighter trends.

The variation of PRE with Range as WP varies from 100% WP_{max} (circle symbol) to 40% WP_{max} for the military transport aircraft is shown in **Fig.2.1.11**. PRE – Range regions encompassing points of equal decrements (20%) of WP_{max} are shown the figure. Also shown are bands for similar payload fractions for the civil freighter aircraft. At a given range, the C-141 operates at about 2/3rds PRE of the civil freighters. The C-5 compares with the best of the civil freighters. Results for the An-124 are slightly better than those for the C-5. The validity of the matched data for the An-124 is yet to be confirmed.

Also shown in **Fig.2.1.11**, are radial lines for constant WFB/WP (lb of block fuel per lb of payload). The trends for the civil freighters operating at Pt A (100% WP_{max}) achieve about 0.8 WFB/WP. At 60% WP_{max} the civil freighters achieve 2.0 WFB/WP. At Pt A operation, the C-5 achieves WFB/WP = 0.7 whereas the An-124 achieves a slightly better value near 0.6.

When non-dimensionalised by the appropriate X value for each aircraft, the data presented in **Fig.2.1.12** tend to collapse into distinct trends. We note immediately that the fractional payload trends for the civil freighters are at near constant PRE/ X values as Z varies. The familiar Pt A PRE/ X – Z variation for the civil passenger aircraft is shown as a dashed line. The C-5 and C-141 lie close to the civil passenger aircraft Pt A trend. The An-124 data lies at the mid-point of the civil freighter trends for all payload fractions shown. Note PRE/ X – Z regions encompassing points of equal decrements (20%) of WP_{max} .

The inclusion of Variable Trailing Edge (VTE) Geometry to replace conventional Trailing Edge Part-Span Flaps (TEF) in an aircraft configuration (either as retro-fit or new design) must show clear performance advantages without weight penalties.

Two aspects will emerge

- VTE capability allows for lower design C_L and higher cruise L/D immediately increasing range parameter X and
- VTE capability allows control over structural loading experienced by the wing (e.g. RBM), relieving safety load factors, resulting in a lighter wing structure.

The assessment of VTE integration then becomes a multi-aspect, iterative process having impact on a wide range of performance parameters.

2.2. Present Context

We need to identify the potential benefits to transport aircraft of a continuously variable geometry trailing edge structure (VTE) that can be utilized for aircraft control, trim, load alleviation, and high lift, throughout the flight envelope.

The approach is to evaluate the technology for several different missions and assess the impact on the vehicle design and performance. It is anticipated the new TE technology would be applied to the entire TE of a new vehicle.

As mentioned earlier, the variable-camber TE would not provide the same sectional C_{Lmax} as existing high lift systems, however it could be utilized across the entire flight envelope for various functions.

The TE flap would be capable of variable camber along the span for optimal L/D at all times during the mission, it would enable wing root bending moment (RBM) reduction during symmetric manoeuvres and gusts, it would reduce losses associated with the flow around edges of wing trailing edge surfaces, etc. However, there could be differences in trim that need to be accounted.

For transport applications with a full-span TEF the possible deflections ranges are $+40^\circ$ -10° for trim at high lift and $\pm 10^\circ$ for control and load alleviation (at typical aileron and frequency response rates). Typically, Transport aircraft operate with 2.25g to 3g limits (c.f. Commercial Aircraft 2.5g). This expands the missions and design space scope.

2.3. Methodologies

For expedience in the early studies, we assume no weight or power penalties compared with conventional control surfaces. However, the structure penalties or advantages can be introduced in a parametric way as required. Typical wing weight is of the order of 20-30% of the OEW, depending upon design range. Flaps weights will be a proportionally smaller percentage (say 15% of wing weight).

A thorough and in-depth assessment is made to establish knowledge and techniques available from previous related studies on variable camber. We assess the levels of influence of various parameters to establish their beneficial effects on future designs.

In the first instance, it is anticipated that conceptual design level methodologies could be utilized to quantify the potential benefits to an existing planform, as well as to conduct trades of conceptual design variables such as wing area to understand the impact of such a technology on the design space for a variety of transport missions.

It is also anticipated that minimization of fuel required for a particular mission would be the metric for the study. To allow broad-based comparisons between conventional high-lift configurations, TEF, and those equipped with VTE geometry we establish two simplified methods for estimating wing weight and Take-Off Field Length.

Wing Weight

In general, wings are sized for extreme loads experienced at take-off, high weight landing or high-g manoeuvres and then further factored for the ultimate load case, e.g. 2.5g loading. Effectively the wing strength (weight) is proportional to the extreme RBM that may be experienced. In the overall aircraft weight breakdown, Wing weight is a function of MTOW, wing size and shape and ultimate load factor. In Ref.16, an estimate of wing weight is given by

$$0.036 (MTOW \cdot \eta_{UL} \cdot S \cdot AR^{1.5} (1.1 + 0.5\lambda) f_E \cdot f_q^{1.5}) / f_T \cdot (\cos \Lambda_{25})^{1.5})^{0.649}$$

where η_{UL} is Ultimate Load Factor, λ Taper Ratio and f_E , f_q and f_T are Engine, Dynamic Pressure and Thickness Factors.

Whilst it is entirely feasible that VTE could reduce wing RBM by 20% further work and analysis is required to establish accurate “trade-off” rates between RBM capability and wing weight. At present we have taken a simplistic and possibly optimistic “one-for-one” rate, i.e 1% reduction in RBM equates to 1% reduction in wing weight.

Take-Off Field Length

Take-Off Field Length is defined as the total distance from brake release to the point at which the aircraft clears a height of 35 ft. The clearance height is increased to 50 ft for military and small civil aircraft. Here we consider only the “all engines operating” Field Length (AEFL) evaluation and 35 ft height clearance. The AEFL comprises two parts, the ground roll from brake release to lift-off (GR) plus the distance from lift-off to 35 ft height clearance. Various methods of estimating GR and AEFL are given in Refs.16 to 19. Considering each of the methods given we adopt a semi-empirical approach to estimate GR and factor this distance to give AEFL. The GR multiplying factors are 1.15 for straight wing aircraft, 1.36 for swept wing and 1.58 for deltas, Ref.16.

The GR is a function of C_{Lmax} , wing loading (W/S), rolling friction (μ), Thrust (T) and Lift Induced Drag factor (k). V_{STALL} is based on C_{Lmax} and V_{TO} is taken as 110% of V_{STALL} . In its simplest form $GR = (2gK_A)^{-1} \ln(1.0 + (K_A/K_T)V_{TO}^2)$,

where $K_T = T/W - \mu$ and $K_A = (\rho/2.0 * (W/S)) * (\mu C_L - C_{Do} - k C_L^2)$

Values of C_{Lmax} used are nominal, achieved with best TEF configuration near rotation point C_L and C_{Di} ($k C_L^2 / \pi AR$) are affected by the presence of the ground during the GR phase due to constraint of tip vortices, trailing vortices and upwash. The $k C_L^2$ term in K_A is factored as follows $C_{DiGE}/C_{DiOGE} = (16.(h/b)^2) / (1.0 + 16.(h/b)^2)$

A final factor is applied to GR to accommodate all the variations and inaccuracies in the estimation of k, μ , C_{Lmax} , etc. to correct predicted AEFL to known values. The method has been validated against published AEFL data for B707-320, B767-300 and B747-400, **Fig.2.3.1** (Sea Level, ISA). The $\delta AEFL / \delta MTOW$ gradients are predicted well. However, at nominal TOW AEFL is over-predicted by 16% for the B707, 6% for the B767 and under-predicted by 6% for the B747. The method is adequate for estimating reductions in AEFL afforded by VTE integration.

3. SETTING UP SCOPE AND PHASING OF THE PROGRAMME

Scientists Consulted: Mr. Gary Dale, Mr Peter Flick, Mr. William Blake, Mr Cale Zeune, Dr. Surya Surampudi, Dr. Gregg Abate and others.

3.1. Scope and Phasing

From the viewpoint of setting up the scope of the Programme, the first step is towards using some of the existing knowledge on Transport Aircraft.

The subsequent stages are to exploit the knowledge within the context of the present programme in a more integrated sense. This then initiates the main body of work.

Final stages will lead to firming up on the inferences and recommendations for future work. Including comments on methodology and improvements.

This subject is considered very timely in view of the proposed time-frames for incorporating fuel-efficient technologies. However, the scope of the work remains broad.

3.2. Work programme envisaged (Statement of Work)

The scope of the work is broad. The work programme is being phased in line with availability of funds. Following recent discussions with AFRL Technical Monitors (Mr. Peter Flick and Mr Gary Dale), the proposals are to work through selections from the following aspects (based on Section 2). Phase 1 is addressed in more detail at this stage. Phase 1 should make a continuing case for further work in subsequent phases.

PHASE 1

Task 1.1: Use 1-3 existing configurations to derive guide-lines including Flight Envelope Payload – range diagrams, Mach – L/D capability, CG variation and Trim, Control sizing, etc. Useful data on flow benefits and penalties is available from studies on Airbus Aircraft and possibly also on Boeing Aircraft.

Task 1.2: Select / derive an initial simplified generic configuration (jet transport). Assume Flight envelope (Mach, altitude), payload – range capability. Focus is on how the technologies can affect the transport missions. We are limited by financial constraints. Work through selected aspects e.g.

- Design without and with Conventional and New TE controls. Look at Performance, trim and S & C aspects, Longitudinal and lateral sense.
- Assess requirement for LE devices in both cases
- Assess at important points on flight envelope (Low and High Speeds, g-variation)
- Stagnation Point Control – Laminar flow or Shock strength reduction control
- Span loadings, Load Alleviation, Root Bending Moment control (g-variation)
- Assess Impact on L/D, Range weight, Block Fuel, Thrust / weight ratio penalties / benefits, field lengths
- Wing area increase, span as well as chord or both.

Identify where the greater benefits are.

4. PREVIOUS EXPERIENCE ON RELATED HIGH LIFT

High-Lift devices are used to increase $C_{L_{max}}$ at low speed for Take-Off and Landing. Using Trailing Edge (TE) devices only may demand very high α to achieve adequate lift. High α may result in Leading Edge (LE) flow separation, hence the use of Leading Edge (LE) devices to control LE flow. We look briefly at TEF and LEF development and the control of flow separation and the performance capabilities of the Fokker 100 and Grumman Gulfstream III aircraft, especially at high-lift.

4.1. High Lift Devices

Various high lift devices are illustrated in **Fig.4.1.1**, Ref.20. They are arranged in ascending order of maximum sectional Lift coefficient (C_{LL}). The basic clean wing establishes a datum C_{LL} of 1.4. Suitable LE devices or a simple Plain flap can increase C_{LL} to 2.4. Split flap takes the C_{LL} to 2.6. In general, Fowler flaps translate rearwards as the deflection angle increases. They may be Split (single slotted) or Plain with additional segments deployed (multi-slotted). Combinations of LE and TE devices, together with upper surface suction, take C_{LL} to 4.0 in these examples.

Fig.4.1.2 shows typical combinations of LE and TE segments related to flight phase. In the cruise configuration all segments are at 0° deflection, **Fig.4.1.2(a)**. For Take-Off, LE Slat and TE flap are deflected (TE Fowler about 25°), both without gaps. In the Landing configuration, **Fig.4.1.2(c)**, the LE Slat is deployed (maximum) with gap. The TE Fowler flap is also deployed to its maximum. In this case with three intermediate segments, four gaps are generated.

A significant amount of research on High-Lift devices, theory and experiment, was carried out by Boeing during design of the B-727, **Fig.4.1.3**, Ref.20. Typical Inboard and Outboard TEF deflections are shown in **Fig.4.1.3(a)** for Take –Off ($\delta_{TE} 20^\circ$) and Landing ($\delta_{TE} 40^\circ$). Outboard flap gaps are closed in the Take-Off configuration. Wind tunnel $C_L - \alpha$ results are in **Fig.4.1.3(b)** for single and double slotted TEF (D & C) and triple slotted TEF (A & B). Flap A has superior $C_{L_{max}}$ by virtue of its increased rearward translation (cf B). A similar classification for LE device performance, $C_L - \alpha$ experiment, are in **Fig.4.1.3(c)**. Four types of LE device were considered, LE slot, drooped LE, Kruger LEF and LE Slat. Although the Kruger LEF achieved the highest $C_{L_{max}}$, its stall characteristics are particularly unfavourable. The optimized LEF and TEF layout is shown in **Fig.4.1.3(d)**, LE Slats (outboard) and LE Flaps (inboard) occupy the entire wing LE. The inboard and outboard TEF are separated by the inboard, high-speed, aileron. The low speed aileron is outboard. **Fig.4.1.3(e)** shows $C_L - \alpha$ experimental results for clean wing and triple slotted TEF (Landing) without and with LE devices. The LE devices increase $C_{L_{max}}$ from 1.9 to 2.7. Streamlines over the wing, LE and TE devices for Cruise, Take-Off and Landing configuration are in **Fig.4.1.3(f)**.

Various flow separation regimes and the effects on chordwise pressure distributions are shown in **Fig.4.1.4** for a wing with TEF, without and with LE Slat. **Figs.4.1.4(a to c)** are for the wing with TEF but without LE device. In **Fig.4.1.4(a)** flow separates from the TE of the TEF. In **Fig.4.1.4(b)** the separation is on TE of wing and in **Fig.4.1.4(c)** separation occurs at the wing LE. With the LE Slat deployed, separation may occur on the slat itself, **Fig.4.1.4(d)** resulting in loss of LE suction. Increasing the Slat angle further reduces the slat suctions and flow separates from the TE of the main wing, **Fig.4.1.4(e)**. At higher slat angles, separation may occur at the LE of the wing, **Fig.4.1.4(f)**.

Ref.21 describes 2-D results for F-28 aerofoil section with slotted TEF at 42° . The geometry is shown in **Fig.4.1.5(a)**. Inviscid and viscous theory results, $C_L - \alpha$, are compared with wind tunnel data in **Fig.4.1.5(b)**. The tunnel model experienced separation over the TE of the Flap

resulting in lower C_{L0} . Inviscid theory gives higher C_{L0} . Lift curves slopes agree well in the attached flow range. Note the expanded C_{LL} scale. Both viscous theory and tunnel data show C_{LL} break at about $\alpha 10^\circ$. **Fig.4.1.5(c)** shows development of “wake displacement bodies” as α increases. At $\alpha 10^\circ$ the wing wake impinges upon the Flap and Slat wakes resulting in the loss of lift evident in **Fig.4.1.5(b)**. This implies the need for increased flap segments at these higher deflections.

A statistical analysis of C_{Lmax} achieved by a wide range of transport aircraft is shown in **Fig.4.1.6**. The data are plotted against $\Lambda_{25\%}$ chord sweep angle. Increasing the LE and TE device complexities and reducing sweep increase the levels of C_{Lmax} possible. **Fig.4.1.6** also shows the advantages of forward sweep achieving similar C_{Lmax} levels at higher sweeps than conventional backward swept wings. C_{Lmax} for the B-727 at nominal $\Lambda_{25\%} 35^\circ$ compares well with the trends for triple slotted TEF with LE devices. Both the Fokker 100 and Gulfstream III, discussed in the following sections, have fixed LE geometry. Typical C_{Lmax} variation with $\Lambda_{25\%}$ for a Plain TEF ($\delta_{TE} 40^\circ \sim 60^\circ$) shows the expected scope for current analysis.

A current adaptive wing research programme, Dryden Flight Research Centre, uses the Gulfstream G-III as a flight test platform. The General Assembly and Performance data are in **Fig.4.1.7**. The wing has straight LE and TE with AR 6. There are conventional, part-span TE Flaps (TEF) inboard and ailerons outboard. There are no LE devices. **Fig.4.1.8** illustrates full-span TE adaptive wing technology on a typical combat configuration, Ref.22. Deflection angle definitions for Conventional TEF and the Adaptive Wing are shown. The variation of C_L with C_D and $C_{L\eta}$ (Flap Efficiency) with α in **Fig.4.1.9** compares a conventional TEF with “Form Variable Trailing Edge Section” flap. The benefits of lower drag at given C_L and improved flap efficiency (+25%) for the variable geometry case are evident.

4.2. FOKKER 100 (F-100)

The Fokker 100 is a short-haul airliner (2000 nm), seating up to 100 passengers, **Fig.4.2.1**. It is a twin engined (rear fuselage mounted turbofans) Tee-tailed configuration. The wing has fixed Leading Edge (LE) geometry, inboard and mid span Trailing Edge Flaps (TEF) of approximately 30% local chord and ailerons ($0.6 < \eta < 0.93$) of approximately 20% chord. Wing span is 92.1 ft, area 1070 ft², AR 8 and $\Lambda_{25\%}$ is about 18° . MTOW is 98,000 lb for the Intermediate and 101,000 lb for the High Gross Weight variants.

A considerable amount of theoretical and experimental data is generally available for the Fokker 100, in particular Ref.21. In the 1980s, Fokker developed a non-planar, thin, lifting surface programme, NPLS, based on a panel method developed at NLR. We review, briefly, some salient points relating to drag breakdown for TEF cases, from Ref.21.

Boundary layer growth and flow separation effects on the TEF upper surface cause the effective flap angle (δ_{TE-EFF}) to be less than the geometric flap angle (δ_{TE}). For the Fokker 100, δ_{TE-EFF} is 85% to 90% δ_{TE} . **Fig.4.2.2** shows wind tunnel and theoretical $C_L - \alpha$ curves with $\delta_{TE} 0^\circ, 20^\circ$ and 42° ($\delta_{TE-EFF} 0^\circ, 17.6^\circ$ and 35.5°). Airworthiness requirements determine that climb out speed (V_2) is greater than stall speed (V_S), in general, $V_2 > 1.2V_S$. This establishes the approximate operating limits circled in **Fig.4.2.2**.

Spanwise lift distributions are shown in **Fig.4.2.5** for $\delta_{TE} 0^\circ, 20^\circ$ and 42° , at $\alpha 0^\circ, 3^\circ$ and 6° . The average C_{LL} for the inner and outer panels is noted. To estimate Form Drag for varying δ_{TE-EFF} , C_{LL} is converted to local α (**Fig.4.2.3**) and then related to the 2-D characteristics to give drag due to δ_{TE} for single slotted, double slotted and compound TEF in **Fig.4.2.6**. Average sectional lift dependent drag relationship ($C_{LL} - C_{DIL}$) is in **Fig.4.2.4** and this is used to give drag increase on the outer panel due to TEF. It is also used in conjunction with

Fig.4.2.6 to give average drag due to TEF on the inner panel, **Fig.4.2.7**. Theoretical C_{Di} variation with C_L^2 for varying δ_{TE} is in **Fig.4.2.8**. We note immediately the non-linearity with respect to δ_{TE} .

Trim drag variation with C_L^2 for δ_{TE} 0° , 20° and 42° , is in **Fig.4.2.12** derived from **Figs.4.2.9** to **11**. These assess Tail-Off $C_m - C_L$ relationships and hence average downwash at the tail.

Drag increments due to lift induced, profile and flap track fairings are shown in **Fig.4.2.13**. To these are added trim drag increments (**Fig.4.2.12**) and the basic clean wing drag polar to give drag polars for varying flap angles, **Fig.4.2.14**. From the derived theoretical, wind tunnel and flight test data, L/D variation with C_L is established for varying δ_{TE} in **Fig.4.2.15**. We note the operational limits imposed by typical safety margins of $1.2V_S$, $1.3V_S$ and $1.4V_S$. These limits have allowed us to establish applicability ranges for $C_L - \alpha$ and $L/D - C_L$ results for configurations with AR 6 and AR 10 wings.

4.3. GULFSTREAM III (G-III)

The Gulfstream III is a twin engined (rear fuselage mounted turbofan) long-range executive transport, typically capable of carrying 11 to 19 passengers up to 4100 nm, **Fig.4.3.1**. The wing has fixed Leading Edge (LE) geometry, TEF ($0.12 < \eta < 0.64$) and ailerons ($0.66 < \eta < 0.88$). Wing span is 77.8 ft, area 950 ft², AR 6 and $\Lambda_{25\%}$ is about 27° . MTOW is 70,000 lb. The type has been extensively used by the military (search and rescue, fisheries protection, VIP transport, etc). A test vehicle is operated by Dryden Flight Research Centre.

The G-III was developed from the G-II with the aim of achieving a design capable of M 0.78 whilst retaining the original wing box. LE and Tip extensions were applied to the wing planform, increasing area by 15%, Λ_{LE} by 3° and maintaining AR 6, **Fig.4.3.3(a)**. The chord extension decreased t/c from 12% to 10%. The original aerofoil sections were accordingly modified and further adapted to reduce shock losses, **Fig.4.3.3(c)**. The Drag rise characteristics of the G-II wing were improved, **Fig.4.3.3(b)**, the improvement being greater than that attributable to the t/c reduction alone.

Further analysis was carried out to assess the effects of engine nacelle and spillage on the wing root pressure distributions. This is an aspect that will need to be considered in future designs using variable camber wings.

4.4. Assessing and Matching Performance Data

The Gulfstream III is a long-range executive transport. As a fraction of MTOW, the payload is extremely small and OEW relatively high. In simple terms a large fraction of aircraft (OEW) uses a high proportion of fuel (WFB) to fly small payloads (WP) over long Ranges (R). A nominal Payload – Range diagram is in **Fig.4.4.1**. The efficiency parameter PRE was discussed and defined in Section 2.1. The PRE values noted at Pt A and Pt B in **Fig.4.4.1** are very low, less than 1000 nm. Long-range, high capacity, civil transports generate PRE of the order of 2500 to 3500 nm.

It will become evident that although the G-III is a suitable vehicle on which to assess and evaluate the mechanics of VTE geometry, it is not suitable for assessing the overall efficiency advantages.

5. ASPECT RATIO 6 WING CONFIGURATION

The configuration is based upon a simplified version of the Gulfstream III. The trapezoidal wing has AR 6.0, λ 0.34 and Λ_{LE} 30.95°. For a span of 77.8 ft, standard mean chord (smc) is 25.9 ft and aerodynamic mean chord (amc) is 28.9 ft.

5.1. Geometry and Modelling

The configuration planform is shown in **Fig.5.1.1**. Typical Plain Flap (TEF), Fowler Flap (FTEF) and Variable TE-geometry (VTE) locations are also shown. Conventional TEF and FTEF lie at $0.12 < \eta < 0.64$. Aerofoil section spanwise distribution for a M 0.75, C_L 0.5 design case is in **Fig.5.1.2** (t/c varying 12% to 9% across semi-span). TEF, FTEF and VTE geometries, for nominal TE deflections (δ_{TE}), are shown in **Fig.5.1.3**.

TEF are simply deflections of TE about a hinge line. For the AR 6 wing they extend from 15% to 60% semi-span.

FTEF occupy the same spanwise region but slide out from the stowed (0°) position as δ_{TE} increases. To simplify the modelling, FTEF has been represented by a second lifting surface positioned at the wing TE. Flap angles of 25° and 40° are shown.

The variable camber of the VTE type is applied as a quadratic function in z over the flap chord (x). VTE angle is defined as the mean chord line slope at TE. Note the VTE δ_{TE} 40° TE z displacement is only 50% that of the equivalent TEF.

The c.g. is located such that the configuration is 6.3% stable (amc) at M 0.75. A tailplane deflection of -1.45° (LE down) is required to trim (C_L 0.5, C_m 0.0) at M 0.75. Low speed trim is achieved by deflecting the Elevator. Typical panelled geometry is in **Fig.5.1.4**.

Fuselage Interference Effects

Currently, the configuration is modelled as lifting wing and tailplane. Fuselage pitching moment effects are assumed to be small. When determining L/D ratios, Fuselage drag (Form and Skin Friction) is included in the C_{D0} term.

Initially, a simple symmetric body has been generated to represent a mid-wing configuration. The resulting panelling is in **Fig.5.1.5**.

To be completed.

5.2. High Speed (M 0.75) Performance, TE Deflection and Variable Camber

Conventional TEF are not operated at high speed. Variations in C_L and trim during cruise are accommodated by climbing to alternative altitudes and the use of elevator to achieve efficient flight. As a brief insight into the possibilities of vari-camber, we look, initially, at small deflections of full-span plain TEF. We then consider the effects of distributed vari-camber at high speed to control load distribution, Root Bending Moment (RBM).

Clean Wing (δ_{TE} 0°) and Full-Span Trailing Edge Flaps (Plain)

The effects of full-span TEF deflection (δ_{TE} 0°, 1° & 2°) on $C_L - \alpha$ and $C_m - C_L$ are shown in **Figs.5.2.1 & 2**. Each δ_{TE} case is trimmed over a range of C_L (0.4 to 0.9). The variation of θ_{ELEV} and α required to trim is shown in **Fig.5.2.2(a)** and $C_m - C_L$ trends, varying δ_{TE} , trimmed at C_L 0.5, 0.6 and 0.7 are in **Fig.5.2.2(b)**. The variation of α required with θ_{ELEV} to trim at constant C_L values is in **Fig.5.2.2(c)**.

Loadings for the datum case ($\delta_{TE} 0^\circ$) are shown in **Fig.5.2.3**. At M 0.75, cruise C_L is 0.50, α 4.68° . To trim, θ_{TP} is -1.45° and θ_{ELEV} is 0° . At these conditions, L/D is 15.82 and the wing centre of pressure lies at 40.3% semi-span.

Full-span TE deflection effectively alters the overall camber. Accordingly, as δ_{TE} increases, the shape of the spanwise distributions remains unaltered, with local values increasing in proportion to δ_{TE} and the trimmed C_L . Loadings for $\delta_{TE} 1^\circ$ and trimmed C_L 0.5 and 0.7 are in **Figs.5.2.4 & 5** respectively. Loadings for $\delta_{TE} 2^\circ$ and trimmed C_L 0.5, 0.7 and 0.9 are in **Figs.5.2.6 to 8** respectively. At the higher trimmed C_L values, C_{LL} increases in the region η 0.6. This may lead to onset of flow breakdown.

The variation $C_D - C_L$ at M 0.75, for the trimmed cases is in **Fig.5.2.9**. C_{Di} for wing plus tailplane has been determined from a first order panel method and therefore includes components of form drag. The value of C_{Do} added to derive L/D allows for this whilst including the usual C_{Do} components (skin friction, boundary layer, form drag, etc) for all items in the configuration (fuselage, wing, tailplane and fin). The variation of L/D with C_L at M 0.75, is in **Fig.5.2.10**. We note the 3% increase in L/D at C_L 0.5 resulting from an additional 2° TEF. This may not be achievable due to flow separation arising on the flap. However this gives an indication of the benefits that may arise using full-span VTE.

Constant α 4.68° trimmed C_L cases, δ_{TE} and θ_{ELEV} vary

In general it is desirable to keep M.L/D constant during the cruise. Higher altitudes give better L/D and lower fuel consumption (sfc). As fuel is consumed during cruise the aircraft weight and therefore C_L decrease and hence the aircraft must climb to maintain M.L/D. Full-span VTE allows a wide range of trimmed C_L to be achieved during cruise at constant α .

For full-span TEF, from **Fig.5.2.2(c)**, for α 4.68° , M 0.75, δ_{TE} 2.85° , 1.45° , 0.0° and -1.35° are required for C_L 0.7, 0.6, 0.5 and 0.4 respectively. The resulting L/D – C_L variation is in **Fig.5.2.11** (dashed line). It was noted in **Fig.1.1.3(b)**, Airbus A320 studies, that a variable camber design would give a 3% L/D increment at C_L 0.5 and 10% increment at C_L 0.6. The primary advantage arises from the lower design C_L requirements (end of cruise case) for the VTE capable wing. This effectively reduces C_{Do} on the wing. The higher C_L required at start of cruise is achieved via VTE. Assuming a 3% increase in L/D at C_L 0.5 for the AR 6 wing configuration, C_{Do} reduces by about 10 drag counts, effectively a reduced camber design wing. At C_L 0.6 (start of cruise), full-span TEF, α 4.68° trimmed, would give 6% L/D increase over the basic clean wing case, **Fig.5.2.11** (solid line). Further C_{Do} reductions can be included as the configuration is trimmed to constant α throughout cruise, reducing fuselage drag contributions. Using distributed VTE, the wing C_{Di} contribution may be reduced via more favourable spanwise load distributions yielding further L/D increments.

Distributed, Full-Span Variable Camber, Root Bending Moment

We vary δ_{TE} linearly from root to tip. Nominal VTE δ_{TE} distributions are in **Fig.5.2.12(a)**. In addition to those shown, $\delta_{TE} +2.5^\circ / \Delta -5^\circ$ was also assessed to look at non-linearity. For an initial assessment, the variations are such that the mean δ_{TE} in each case is 0° . All cases were trimmed at C_L 0.5. The effect of distributed VTE on total loads are shown in **Figs.5.2.12(b-c)**. With respect to the datum case ($\delta_{TE} 0^\circ / \Delta 0^\circ$), deflecting the root TE up ($\delta_{TE} -5^\circ$) and tip TE down ($\Delta +10^\circ$) reduces C_L at given α . Reversing the δ_{TE} spanwise variation ($\Delta -10^\circ$) reverses this trend. The loadings are shown in **Fig.5.2.13**. The effect of reducing root camber and increasing tip camber can be clearly seen. Reversing the sense of the spanwise distributed variable camber has a more favourable effect on the tip pressure distributions. However, the

spanwise loading becomes very triangular, implying reduced RBM, increased Drag and hence reduced L/D.

For each of the distributed VTE cases, α varies to achieve trimmed C_L 0.5. We need to interpolate the δ_{TE} / Δ variations for cases that will achieve trimmed C_L 0.5 at α 4.68° (datum case) for valid comparisons.

Constant α , constant C_L Distributed, Full-Span Variable Camber

From the above analysis, VTE spanwise distributions were interpolated that would trim to C_L 0.5, M 0.75 at constant α 4.68°. This ensures a balanced comparison with the basic cruise wing. Nominal distributions are $\delta_{TE} +1.8^\circ / \Delta -5^\circ$, $-1.85^\circ / \Delta +5^\circ$ and $-3.7^\circ / \Delta +10^\circ$. The loadings are shown in **Fig.5.2.14** with typical chordwise pressure distributions for $\delta_{TE} +1.8^\circ / \Delta -5^\circ$ case. Assuming constant C_{D0} values for these small deflections, L/D variations with C_L are in **Fig.5.2.15**. We note the 1.3% increase in L/D for the $\delta_{TE} -1.85^\circ / \Delta +5^\circ$ case. However, the loading has increased outboard giving rise to increased RBM and possible unacceptable wing weight increments.

Wing root bending moment was evaluated for the trimmed cases as the product of wing Lift and distance from centre of pressure to fuselage side (10% semi-span). The variation of % Increments in RBM and L/D, as distributed VTE angle varies, with respect to the datum case, is shown in **Fig.5.2.16**. Simple, constant δ_{TE} deflections across the span of 1° and 2° increased L/D by 2% to 3% but also increased RBM by similar amounts. More significant was the reduction in α (4.68° to 3.41°) as δ_{TE} increased (0° to 2°). Distributing VTE δ_{TE} across the span such that Δ_{TE} increased from -5° to $+10^\circ$ resulted in RBM increments ranging from -15% to $+15\%$ with α increasing from 4.11° to 5.26°. A maximum L/D increment of 0.5% was achieved at the expense of a 5% increase in RBM.

The M 0.75, constant α (4.68°), constant C_L 0.5 trimmed cases achieved a maximum L/D gain of 1.3% but with an increase in RBM of 8%. A 5% reduction in RBM would result in a 3% reduction in L/D. In general, a reduction in RBM could lead to a lighter wing structure, reducing OEW and cruise C_L requirements. The lower cruise C_L may or may not compensate for the initial reduction in L/D. This type of trade-off requires further analysis from the structures aspect.

We again assume a reduction of 10 C_{D0} drag counts for a VTE capable wing, designed for a lower Cruise C_L . The higher C_L required at start of cruise is achieved via VTE. Applying a reduced C_{D0} term applicable to a lower design C_L wing we obtain the % Increments in RBM and L/D variation, as distributed VTE angle varies with respect to the datum case, shown in **Fig.5.2.17**. A 10% reduction in RBM could be achieved without L/D penalty. A wing load distribution that would leave RBM unchanged would result in a 3.2% increase in L/D and a 10% increase in RBM capability would lead to a 4.8% increase in L/D. These “trade-offs” are discussed in Section 7.

5.3. Low Speed (M 0.20) Performance

We look at Plain Flaps (TEF), Fowler Flaps (FTEF) and Variable TE-geometry (VTE).

Plain Flaps (Conventional), Clean Wing (δ_{TE} 0°) and δ_{TE} 25° and 40°

The effects of TEF δ_{TE} on $C_L - \alpha$ and $C_m - C_L$ are shown in **Figs.5.3.1 & 2**. There is small, wing C_{L0} , contribution at each trimmed δ_{TE} case. The negative tailplane contribution, providing positive C_m , can be seen at each δ_{TE} setting. Elevator and α requirements to trim at various C_L and δ_{TE} conditions are shown in **Fig.5.3.2(a)**. Typical operating limits (attached flow) are shown. The $C_m - C_L$ relationships show stable trends.

We look at wing loadings (spanwise and chordwise pressure distributions) for various trimmed C_L , δ_{TE} cases. Loadings for C_L 1.2, clean wing (δ_{TE} 0°) are in **Fig.5.3.3**. To achieve C_L 1.2 without TEF requires α 14.4° . This implies an unacceptable fuselage incidence. The high suctions at LE indicate requirement for LE devices. At higher C_L (1.4), **Fig.5.3.4**, α 17.0° is required and even higher LE suctions occur. Deflecting the part-span TEF 25° allows C_L 1.2 to be achieved at α 5.5° . Loadings are in **Fig.5.3.5**. The LE suctions are greatly reduced. However, high suctions occur at the TEF hinge-line, implying possible, local flow separation for the plain flap configuration. These could be reduced using slotted flaps and multi-segment flaps. C_L 1.4 requires α 8.2° . This is less than half α required for the datum wing and LE suctions are greatly reduced, **Fig.5.3.6**.

For part-span TEF δ_{TE} 0° , 25° and 40° , trimmed at C_L 0.8, 1.2 and 1.6 respectively, **Fig.5.3.7** shows drag component contributions as C_L varies. We note that C_{D0} contribution varies with δ_{TE} . The resulting $L/D - C_L$ variation is in **Fig.5.3.8**. For fully attached flow predictions, trimming at any C_L (elevator deflection to trim C_m with α correction to required C_L) does not affect the overall L/D value. TEF deflection is required to extend the attached flow C_L range. Typical operating limits (attached flow) are shown together with constant α 8° line.

Full-Span Plain Flaps, δ_{TE} 10° and 15°

Deflecting full-span TEF (constant angle across the span) is effectively an increase in overall wing camber. We look briefly at total forces and wing loadings for δ_{TE} 10° and 15° , for trimmed C_L 1.2 and 1.4 in each case.

The effects of full-span δ_{TE} on $C_L - \alpha$ and $C_m - C_L$ are shown in **Figs.5.3.9 & 10**. Typical operating limits (attached flow) are shown. The $C_m - C_L$ relationships show stable trends, although slightly reduced for the deflected TE cases.

Loadings for the clean wing, C_L 1.2, α 14.4° case are in **Fig.5.3.3**. With full-span δ_{TE} 10° , C_L 1.2 is achieved at α 7.9° . Loadings are in **Fig.5.3.11**. The LE suctions are greatly reduced compared to the clean wing case and are of the same order as those achieved with part-span δ_{TE} 25° . C_L 1.4 requires α 10.4° and suctions near the tip are again approaching high levels, **Fig.5.3.12**. With full-span δ_{TE} 15° , C_L 1.2 is achieved at α 4.7° . Loadings are in **Fig.5.3.13**. The LE suctions are very significantly reduced compared to the clean wing case. C_L 1.4 requires α 7.2° and LE suctions are well behaved, **Fig.5.3.14**.

For full-span TEF δ_{TE} 0° , 10° and 15° , trimmed at C_L 0.8, 1.2 and 1.6 respectively, **Fig.5.3.15** shows drag component contributions as C_L varies. We note that C_{D0} levels are proportional to those for part-span TEF. The resulting $L/D - C_L$ variation is in **Fig.5.3.16**. Also included are results for the part-span TEF (δ_{TE} 25° and 40°). The full-span cases approach the clean wing predictions at higher C_L which cannot be achieved without TEF deflection. At C_L 1.2, full-span δ_{TE} 10° gives 43% L/D improvement over part-span δ_{TE} 25° . At C_L 1.6, full-span δ_{TE} 15° gives 66% L/D improvement over part-span δ_{TE} 40° .

Fowler Flaps, Clean Wing (δ_{TE} 0°) and δ_{TE} 25° and 40°

To be completed. Modelling of Fowler Flaps to be improved.

Variable Camber (Full-Span implicit)

The effects of varying the camber at the TE (VTE, δ_{TE} 0° , 10° & 20°) on $C_L - \alpha$ and $C_m - C_L$ are shown in **Figs.5.3.17 & 18**. Loadings for clean wing (δ_{TE} 0°), C_L 1.2, α 14.4° are in **Fig.5.3.3**. We note the high LE suctions near the tip, implying onset of flow separation. Applying VTE increases wing rear loading providing higher Lift. Loadings for δ_{TE} 10° , C_L 1.2

and 1.4 are in **Figs.5.3.19 & 20** and for δ_{TE} 20°, C_L 1.2 and 1.4 in **Figs.5.3.21 & 22**. The LE suction for C_L 1.4, δ_{TE} 20° are of the same order as those for C_L 1.2, δ_{TE} 10°.

The variation of C_D (includes wing and tailplane Form drag component) with C_L at M 0.20, for the trimmed cases, is shown in **Fig.5.3.23**. The value of C_{D0} added to derive L/D allows for wing and tailplane skin friction fuselage and interference drags. It is estimated that this will not vary significantly with VTE angle. Since C_{D0} is constant and total C_D for all three δ_{TE} cases lies on the same curve, increase in wing C_{Di} is matched by reducing trim C_{Di} as δ_{TE} increases. The variation of L/D with C_L at M 0.20, for the trimmed cases, is shown in **Fig.5.3.24**. The wing has effectively been redesigned at each higher trim C_L . We now compare the part-span TEF and VTE cases at α 8°, C_L 1.4 (trimmed).

Constant α and trimmed C_L Comparison

Effective flow onset incidence (relative to horizontal datum plus sink rate angle) is typically 5° to 10° during the Landing phase. It will depend upon several factors, e.g size and type of aircraft (large civil transport or small combat aircraft), high lift devices available, landing zone (runway, neighbouring structures, climate and altitude). We consider α 8°, C_L 1.4 (trimmed) at M 0.20 for a comparison between conventional part-span flaps (TEF) and full-span variable camber (VTE).

For C_L 1.4 at α 8°, the part-span TEF is deflected δ_{TE} 25.6° and θ_{ELEV} +5.08° is required to trim. At these conditions, L/D is 9.0. For C_L 1.4 at α 8°, VTE δ_{TE} 20.8° and θ_{ELEV} +2.25° are required to trim, giving L/D 12.1, a 34% improvement over the TEF. C_{D0} applied is equal to that of the basic, “clean” wing. However, it is possible that VTE δ_{TE} of 20.8° may give rise to some additional boundary layer growth and flow separations. A more conservative estimate of L/D still yields a 25% improvement.

Distributed, Full-Span Variable Camber, Root Bending Moment

By varying δ_{TE} across the span, the shape of the spanwise load distributions and hence center of pressure location and RBM can be controlled. The loadings (spanwise and chordwise pressure distributions) obtained for linear spanwise δ_{TE} distributions of 0° to 40°, 20° to 20° and 40° to 0°, trimmed at C_L 1.4, are shown in **Fig.5.3.25(b to e)** together with the corresponding δ_{TE} distributions **Fig.5.3.25(a)**. The pressure distributions for the 0° to 40° case show very high suction towards the tip. Conversely, tip pressures for the 40° to 0° case are very much ameliorated. A target δ_{TE} distribution (38° / 11° / 11°) to give C_L 1.4 at α 8° when trimmed with θ_{ELEV} +4.96° is also shown. The loadings for the target case are shown in **Fig.5.3.26**. The spanwise distributions are very triangular and the centre of pressure has moved inboard to 39.3% semi-span. This implies a reduction in RBM close to 3% with an increase in L/D of 27.1% over the part-span TEF configuration (δ_{TE} 25.6°).

The variation of % Increments in RBM and L/D, M 0.20, C_L 1.4, as VTE angle varies is shown in **Fig.5.3.27**. The increments are based on the part-span TEF δ_{TE} 25.6° which achieved C_L 1.4 at α 8°, giving L/D 9.0. Increasing root camber (VTE) δ_{TE} +40° and linearly decreasing to 0° at the tip, reduces RBM by about 6% with a 25% increase in L/D. A uniform δ_{TE} +20°, increases RBM by 9% and L/D by 35%. Totally reversing the initial additional camber to 0° root to 40° tip loads up the tip giving an increase in RBM of 24% and in L/D of 27%. The “tuned” distribution (36.3° / 11.3° / 11.3°), giving C_L 1.4 at α 8°, gave 3% reduction in RBM and 27% increase in L/D.

Changes in RBM need to be quantified in terms of wing weight changes. For a given TOW aircraft (undercarriage strength, engine performance, Take-Off and Landing capabilities, etc.

pre-defined) a reduction in wing weight might allow an increase in payload or fuel (hence range). These changes need to be balanced against the corresponding changes in L/D and their effect on Take-Off and Landing performance and range.

5.4. Stability and Control, Laterals

Lateral stability and control aspects, at high speed and low speed, at design and off-design, need to be assessed during the design process. Aircraft performance at anticipated off-design situations will size and position control surfaces and need to be considered when defining thrust requirements. Each of these aspects will contribute towards the overall sizing of the aircraft and hence its performance. In assessing the benefits of variable camber (VTE) over conventional part-span flaps (TEF), we look, briefly at low speed performance.

At present, the geometries comprise wing and tailplane only. The fuselage will have a significant effect in sideslip and this will need to be modelled for further analysis. Typical panelled geometry (part-span, plain $\delta_{TE} 25.6^\circ$) is in **Fig.5.4.1**. Sign convention for typical parameters has been annotated. We look at the M 0.20, $\alpha 8^\circ$, $C_L 1.4$ (trimmed) cases.

Sideslip, $\beta 5^\circ$, has reduced the trimmed C_L to 1.39 for all three cases considered. Loadings for the conventional part-span TEF ($\delta_{TE} 25.6^\circ$) are in **Fig.5.4.2**. The pressure distributions are somewhat complex but higher LE suctions on the lead, left wing can be identified. Similarly the increased loading over the left wing TEF area is evident. Loadings for the full-span VTE $\delta_{TE} 20.8^\circ$ are in **Fig.5.4.3**. These show much smoother distributions although high loadings near the tips and over the TE area are evident. Distributed VTE has further ameliorated the tip loading, **Fig.5.4.4**.

At zero sideslip, the constant VTE $\delta_{TE} 20.8^\circ$ case gave 34% increase in L/D and a 9% increase in RBM compared with the TEF $\delta_{TE} 25.6^\circ$. The distributed VTE $\delta_{TE} 36.3^\circ / 11.3^\circ / 11.3^\circ$ case gave 27% increase in L/D and a 3% reduction in RBM. In positive sideslip (nose to right), there is an increase in RBM on the left, lead wing with a similar but not necessarily equal reduction in RBM on the trail wing. From a structural safety limitation view we consider the RBM increments on the lead wing. **Fig.5.4.5** shows the % RBM variation with β for the three TEF cases considered. The conventional plain TEF at zero sideslip is taken as datum. At 5° sideslip, RBM increases by 7% on the part-span TEF. RBM increases at a very slightly lower rate on both the constant VTE and the distributed VTE cases. However, the distributed VTE case starts from reduced RBM at zero sideslip.

At M 0.20, $\alpha 8^\circ$, in $C_L 1.4$ (trimmed) condition, the constant VTE case exhibits 4.3% less $C_{l\beta}$ and the distributed VTE 8.7% less $C_{l\beta}$ than the TEF case. This implies less control surface deflection to trim for the VTE cases. In turn, smaller control surface deflections imply less induced yawing moment requiring smaller vertical surfaces to trim and reduced thrust requirement.

All these advantages are interactive and cumulative and further analysis from a structures viewpoint is required.

6. ASPECT RATIO 10 WING CONFIGURATION

The higher AR wing configuration is based on the Bombardier, C-Series. The wing has AR 10.0, $\lambda 0.20$ and $\Lambda_{LE} 29.2^\circ$. For a span of 115.1 ft, standard mean chord (smc) is 11.5 ft and aerodynamic mean chord (amc) is 12.9 ft.

6.1. Nominal AR 10 wing Configuration, Performance, Geometry and Modelling

The C-Series, **Fig.6.1.1**, is in development and published performance data is sparse. Nominal layout and sizing are shown in **Fig.6.1.1(a)**. From data available we have generated a typical payload range diagram for a modern, medium capacity, medium range civil transport **Fig.6.1.1 (b)**. It was noted in Section 4.4 that the Gulfstream III is a long-range executive transport with a very small payload fraction. In terms of PRE, less than 1000 nm, it is an inefficient transport aircraft and predicted performance advantages arising from VTE will not be representative. The nominal AR 10 wing configuration has PRE values of the order of 2500 nm and will therefore be more suitable for VTE integration in terms of predicted performance. The simplified configuration planform is shown in **Fig.6.1.1(c)**. Typical Plain Flap (TEF), Fowler Flap (FTEF) and Variable TE-geometry (VTE) locations are also shown. Conventional TEF and FTEF lie at $0.12 < \eta < 0.64$.

Aerofoil section spanwise distribution for a M 0.75, C_L 0.5 design case is in **Fig.6.1.2** (t/c varying 14%, 11% to 9% across semi-span). TEF, FTEF and VTE geometries, for nominal TE deflections (δ_{TE}), are shown in **Fig.6.1.3**. Flap type definitions are discussed in Section 5.1. Again we note the VTE δ_{TE} 40° TE z displacement is only 50% that of the equivalent TEF. The c.g. is located such that the configuration is 11.6% stable (amc) at M 0.75. A tailplane deflection of -2.00° (LE down) is required to trim C_L 0.55 at M 0.75. Trim is achieved by rotating the “all-moving” Tailplane. Typical panelled geometry is in **Fig.6.1.4**.

Fuselage Interference Effects

Currently, the configuration is modelled as lifting wing and tailplane. Fuselage pitching moment effects are assumed to be small. When determining L/D ratios, Fuselage drag (Form and Skin Friction) is included in the C_{D0} term. Fuselage interference effects may need to be assessed in future.

6.2. High Speed (M 0.75) Performance, Clean Wing, Plain Flaps and Variable Camber

Conventional TEF are not operated at high speed. Variations in C_L and trim during cruise are accommodated by climbing to alternative altitudes and the use of elevator to achieve efficient flight. Based on the initial work on the AR 6 wing, Section 5, we consider small δ_{TE} full-span TEF, both constant and varying δ_{TE} , and the effects of distributed VTE at high speed to control load distribution, Root Bending Moment (RBM). The δ_{TE} distributions assessed are in **Fig.6.2.1**.

Wing root bending moment was evaluated for the trimmed cases as the product of wing Lift and distance from centre of pressure to fuselage side (10% semi-span).

The effects of full-span TEF deflection (δ_{TE} varying root to tip: $0.0^\circ / 0.0^\circ$, $2.5^\circ / 1.0^\circ$ & $5.0^\circ / 2.0^\circ$) on total loads are in **Fig.6.2.2**, (a) $C_L - \alpha$ and (b) $C_m - C_L$. Loadings for the datum case (δ_{TE} 0°) are shown in **Fig.6.2.3**. At M 0.75, cruise C_L is 0.55. To trim, θ_{TP} is -2.00° . At these conditions, L/D is 17.98. Constant, positive δ_{TE} across the span effectively implies an increase in camber, resulting in progressively increased C_{L0} , **Fig.6.2.2(a)**. Each δ_{TE} case is trimmed at C_L 0.55, **Fig.6.2.2(b)**. Loadings for δ_{TE} $2.5^\circ / 1.0^\circ$ are in **Fig.6.2.4** and for δ_{TE} $5.0^\circ / 2.0^\circ$ in **Fig.6.2.5**. In this series δ_{TE} rises more rapidly at the root, increasing inboard loading at constant C_L and reducing RBM. The variation $C_D - C_L$ at M 0.75, for the trimmed cases is in **Fig.6.2.6**. C_{Di} for wing plus tailplane has been determined from a first order panel method and therefore includes components of form drag. The value of C_{D0} added to derive L/D allows for this whilst including the usual C_{D0} components (skin friction, boundary layer, form drag, etc) for all items in the configuration (fuselage, wing, tailplane and fin). The variation of L/D with C_L at M 0.75, is in **Fig.6.2.7**. The increased camber affords higher L/D, 4% and 8%

increments for the $\delta_{TE} 2.5^\circ / 1.0^\circ$ and $\delta_{TE} 5.0^\circ / 2.0^\circ$ respectively. Corresponding reductions in RBM are 2.6% and 5.0%.

Constant, full-span, $\delta_{TE} 1.0^\circ$ and 2.0° cases were also assessed. These gave 2% to 5% L/D increments together with about 1% RBM increase. Distributed VTE cases gave more favourable results. Nominal $\delta_{TE} +5.0^\circ / -5.0^\circ$ gave 16% reduction in RBM at the expense of only 2% reduction in L/D. There was zero L/D penalty for $\delta_{TE} +2.5^\circ / -2.5^\circ$ but an 8% reduction in RBM. As expected, $\delta_{TE} -2.5^\circ / +2.5^\circ$ gave an increase in RBM, 8%, and nearly 2% loss in L/D. These results are summarised in **Fig.6.2.10**.

Constant α , constant C_L Distributed, Full-Span Variable Camber

From the above analysis, VTE spanwise distributions were interpolated that would trim to $C_L 0.55$, $M 0.75$ at constant $\alpha 4.37^\circ$. This ensures a balanced comparison with the basic cruise wing. Nominal distributions are $\delta_{TE} +5.23^\circ / \Delta -15^\circ$, $+3.40^\circ / \Delta -10^\circ$ and $+1.70^\circ / \Delta -5^\circ$. The loadings are shown in **Fig.6.2.8** with typical chordwise pressure distributions for $\delta_{TE} +5.23^\circ / \Delta -15^\circ$ case. Assuming constant C_{D0} values for these small deflections, L/D variations with C_L are in **Fig.6.2.9**. We note the 1.3% increase in L/D for the $\delta_{TE} -1.85^\circ / \Delta +5^\circ$ case. However, the loading has increased outboard giving rise to increased RBM and possible unacceptable wing weight increments.

Wing root bending moment was evaluated for the trimmed cases as the product of wing Lift and distance from centre of pressure to fuselage side (10% semi-span). The variation of % Increments in RBM and L/D as distributed VTE angle varies, with respect to the datum case, is shown in **Fig.6.2.10**.

Simple, constant δ_{TE} deflections across the span of 1° and 2° increased L/D by 2% to 5% but also increased RBM by 1% to 2%. More significant was the reduction in α (3.84° to 3.32°) as δ_{TE} increased (0° to 2°). Distributing VTE δ_{TE} across the span such that Δ increased from -10° to $+5^\circ$ resulted in RBM increments ranging from -16% to +9%. A maximum L/D increment of 0.25% was achieved with a 5% reduction in RBM.

The $M 0.75$, constant α (4.37°), constant $C_L 0.55$ cases explored so far, achieved significant reductions in RBM, up to 25% but with corresponding reduction in L/D of 8%. A reduction in RBM could lead to a lighter wing structure, reducing OEW and cruise C_L requirements. The lower cruise C_L may or may not compensate for the initial reduction in L/D. This type of trade-off requires further analysis and assessment from a structures point of view.

We note from work on the AR 6 (Section 5.2) and Airbus studies a possible C_{D0} reduction of 10 counts for a VTE capable wing, designed for a lower Cruise C_L . The higher C_L required at start of cruise is achieved via VTE. Applying a reduced C_{D0} term applicable to a lower design C_L wing we obtain the % Increments in RBM and L/D variation, as distributed VTE angle varies with respect to the datum case, shown in **Fig.6.2.11**. A 20% reduction in RBM would result in a 2.7% loss in L/D. A 10% reduction in RBM would result in a 1.5% gain in L/D and a wing load distribution leaving RBM unchanged would result in a 3.4% increase in L/D. These “trade-offs” are discussed in Section 7.

6.3. Low Speed (M 0.20) Performance

We look at Plain Flaps (TEF), Fowler Flaps (FTEF) and Variable TE-geometry (VTE).

Plain Flaps (Conventional), Clean Wing ($\delta_{TE} 0^\circ$) and $\delta_{TE} 25^\circ$ and 40°

The effects of TEF deflection on $C_L - \alpha$ and $C_m - C_L$ are shown in **Figs.6.3.1& 2**. Tailplane rotation and α requirements to trim at various C_L and δ_{TE} conditions are shown in **Fig.6.3.2(a)**. Typical operating limits (attached flow) are shown.

Loadings for trimmed C_L 1.2, clean wing (δ_{TE} 0°) are in **Fig.6.3.3**. To achieve C_L 1.2 without TEF requires α 12.7° . This implies an unacceptable fuselage incidence. The high suctions at indicate the requirement for LE devices. Deflecting the part-span TEF 25° allows C_L 1.2 to be achieved at α 1.2° . Loadings are in **Fig.6.3.4**. The LE suctions are greatly reduced. However, high suctions occur at the hinge-line, implying possible, local flow separation for the TEF configuration. These could be reduced using slotted flaps and multi-segment flaps. C_L 2.0 requires α 10.4° , **Fig.6.3.5**. This is less than half α required that would be predicted for the datum wing. Using part-span δ_{TE} 40° , C_L 2.0 is achieved at α 4.1° . Loadings are in **Fig.6.3.6**. High suctions occur at LE and hinge-line, although LE suctions are significantly reduced from δ_{TE} 25° , C_L 2.0 case.

For part-span TEF δ_{TE} 0° , 25° and 40° , trimmed at C_L 1.2 and 2.0, **Fig.6.3.7** shows drag component contributions as C_L varies. We note that C_{D0} contribution varies with δ_{TE} . The resulting $L/D - C_L$ variation is in **Fig.6.3.8**. For fully attached flow predictions, trimming at any C_L (elevator deflection to trim C_m with α correction to required C_L) does not affect the overall L/D value. TEF deflection is required to extend the attached flow C_L range. Typical operating limits (attached flow) are shown.

Fowler Flaps, Clean Wing (δ_{TE} 0°) and δ_{TE} 25° and 40°

The effects of TEF deflection or the addition of a deflected FTEF on $C_L - \alpha$ and $C_m - C_L$ are shown in **Figs.6.3.9**. Also shown is typical panel geometry for the wing, flap and tail geometry. At α 0° , deflecting TEF, δ_{TE} 40° increases the wing contribution by $1.5 C_L$. Adding a FTEF component to the undeflected wing adds additional $0.25 C_L$ and increases the wing contribution by $1.2 C_L$. The long chain lines indicate Wing $C_L - \alpha$ variation, the short chain lines include the FTEF contribution and the solid lines are $C_L - \alpha$ for each configuration.

Loadings and pressure distributions for FTEF δ_{TE} 25° , α 11.01° , trimmed C_L 2.0, are in **Fig.6.3.10**. C_{DL} and C_{mL} distributions show the component contributions for wing, tail and FTEF. We note the significant contribution to drag arising from the FTEF. The pressure distributions show high LE suctions on both the wing and FTEF. The FTEF modelling may require improvement to more accurately represent air flow around this type of high lift device. With FTEF δ_{TE} 40° , trimmed C_L 2.0 is achieved at α 6.00° , **Fig.6.3.11**. The loadings show the increased contributions to C_L and C_D borne by the FTEF.

Nominal L/D variation with C_L is in **Fig.6.3.12**. Results for the current modelling indicate slightly reduced L/D for the FTEF compared with TEF. However, in practice, FTEF should provide greater C_L attached flow range.

Should further evaluation of Fowler Flap be required, the model panelling will require refinement, relaxed wake and viscous effects will need to be included. Higher order methods will be used to confirm results.

Full-Span Plain Flaps

As an intermediate step towards full-span TE variable camber the TE was deflected 10° across the span. This is a simple representation of change in camber, although appropriate C_{D0} term for 10° Plain flap is added. The resulting $L/D - C_L$ relationship is shown in **Fig.6.3.13**. Naturally, the full-span flap is very much superior to the part-span flap. The constant α 8° line is very informative. This implies, assuming attached flow, TEF 25° gives C_L 1.7 with L/D

about 10. A full-span TEF of 10° would require higher α to achieve C_L 1.7 but L/D would rise to 12.

Variable Camber (Full-Span implicit)

The effects of full-span VTE on $C_L - \alpha$, $C_m - C_L$ and $C_D - C_L$ were assessed at M 0.20. Typical VTE geometry deflections (δ_{TE}), are shown in **Fig.6.1.3**. Tailplane rotation and α requirements to trim at various C_L and δ_{TE} conditions are shown in **Fig.6.3.14**. This may be compared with **Fig.6.3.2(a)** for the conventional part-span TEF. We note for trimmed C_L 2.0 at α 8° , TEF requires 31° deflection with 2.7° tailplane rotation. The VTE requires 32° deflection and 3.9° tailplane to trim.

Loadings and pressure distributions for VTE δ_{TE} 10° , trimmed C_L 1.2, are in **Fig.6.3.15**. An incidence of 8.14° is required. To achieve trimmed C_L 2.0 with VTE δ_{TE} 10° , a 17.1° is required. The loadings are in **Fig.6.3.16**. With VTE δ_{TE} 40° , trimmed C_L 2.0 is achieved at α 5.35° , **Fig.6.3.17**. Comparing this with **Fig.6.3.6** (TEF 40° , C_L 2.0) the pressure distributions for the VTE case are much smoother, indicating reduced separation tendencies. The resulting L/D - C_L variations for a range of VTE δ_{TE} deflections are in **Fig.6.3.18**. These lie close to the fully attached flow, clean wing values over the higher C_L ranges. These high C_L could not be achieved by the clean wing. Also shown are L/D - C_L trends for the full-span TEF 10° and the part-span TEF 25° .

The various high lift devices need to be compared at the same trimmed C_L at constant α .

Constant α and trimmed C_L Comparison

As noted for the AR 6 case, Section 5.3, effective flow onset incidence during Landing is typically 5° to 10° . We consider α 8° , C_L 2.0 (trimmed) at M 0.20 for a comparison between conventional part-span flaps and full-span variable camber.

Loadings for part-span δ_{TE} 30.5° are in **Fig.6.3.19**. To trim, $\theta_{T/P}$ is $+2.65^\circ$. At these conditions, L/D is 9.0. Loadings for variable camber δ_{TE} 32.4° are shown in **Fig.6.3.20**. To trim, $\theta_{T/P}$ is $+3.95^\circ$. At these conditions, L/D is 13.5, a 50% improvement over the conventional flap. The C_{D0} applied is equal to that of the basic, “clean” wing. However, it is possible that variable camber δ_{TE} of 32.4° may give rise to some additional boundary layer growth and flow separations. A more conservative estimate of L/D still yields a 40% improvement.

Constant α and trimmed C_L Relaxed Wakes Comparison

Initial estimates of trimmed L/D at low speed were conducted with both rigid and relaxed trailing wakes. It was noted that relaxing the wakes affected C_m slightly but did not affect C_L . After “re-trimming” the relaxed wake cases to the required C_L , the associated change in trim drag returned L/D to the original rigid wake value.

Relaxed wake analysis was also carried for the constant α 8° cases. Wing relaxed wake geometry is in **Fig.6.3.21** for the part-span δ_{TE} 30.5° , trimmed to C_L 2.0. The required $\theta_{T/P}$ is $+1.74^\circ$, a small reduction to correct ΔC_m -0.069 . The resulting L/D value of 8.90 is less than 1% lower than the rigid wake estimate and therefore within expected theoretical limits. Wing relaxed wake geometry is in **Fig.6.3.22** for variable camber δ_{TE} 32.4° . To trim, $\theta_{T/P}$ is reduced to $+3.46^\circ$ to correct ΔC_m -0.035 . Trimmed L/D is less than 0.3% lower than the rigid wake estimates.

These two first order panel method cases confirm that our simplified model has been more than adequate to indicate “gross effect” advantages of full-span variable camber flaps. Further accuracy and definition may be achieved with increased panelling and higher order methods

(second order panel, Euler or Navier Stokes methods). However, the general trends and magnitude of increments will remain unaltered.

Spanwise Distribution Control via Tuned Variable TE Camber, Constant α 8°

By varying δ_{TE} across the span, the shape of the spanwise load distributions and hence center of pressure and RBM can be controlled. The loadings obtained for linear spanwise δ_{TE} distributions of 40° to 0°, 20° to 20° and 0° to 40° are shown in **Fig.6.3.23** together with the corresponding δ_{TE} distributions. A target δ_{TE} distribution is also shown that would give C_L 2.0 at α 8° when trimmed with $\theta_{T/P} + 7.09^\circ$. The resulting loadings are in **Fig.6.3.24**. The spanwise distributions are very triangular and the wing centre of pressure has moved inboard to 45.4% semi-span. This implies a reduction in RBM of near 3% with an increase in L/D of 37.8% over the part-span flap configuration (δ_{TE} 30.5°).

6.4. Stability and Control, Laterals

Stability and Control effects in sideslip have been briefly assessed for the AR 6 configuration. These aspects need to be addressed for the AR 10 configuration.

7. INTEGRATING VARIABLE CAMBER

The advantages offered by Variable TE geometry (VTE) over conventional wing geometry with Training Edge Flaps (TEF) may be assimilated in a variety of ways. At low speed (Take-Off or Landing), for a given M, α , trimmed C_L condition, VTE offers higher L/D. At high speed (Cruise), VTE allows the wing geometry to be “tuned” for best efficiency, higher L/D, as flight conditions vary (Wing loading reduction as fuel is burnt, buffet response, etc.). VTE capability allows a wing to be designed at the outset for lower cruise C_L .

We assess the advantages of VTE on various size aircraft with differing AR wings in terms of specific Performance Factors, namely:

Payload Range Efficiency (PRE) = Payload (WP) x Range (R) / Fuel Consumed (WFB)

Field Length (Take-Off and Landing)

Aircraft size (Span and Wing Area, Take-Off weight (TOW) and Thrust) required to transport a given Payload over a given Range.

7.1. VTE Capability into High Speed Wing Design and Low Speed Application

VTE capability: lower design C_L , High Speed Cruise

It was noted in Section 1.1 and Ref.12 that VTE capability allows the cruise wing design C_L to be biased to end of cruise conditions. This lower design C_L reduces C_{D0} by approximately 10 counts for aircraft types considered here, Gulfstream G-III (AR 6) and Bombardier C-Series (AR 10).

VTE capability: RBM control at high g, High Speed and Low Speed

For a conventional wing design, safety factors are built in to accommodate normal load variation, Take-Off to Landing. These factors are increased to account for off-design dynamic loading experienced during manoeuvres, gusts and wind shear (nominally 2.5g loading). All these considerations significantly increase the weight of the wing structure.

VTE geometry can control wing load distribution and hence control wing RBM. It can therefore reduce the ultimate load factor requirements currently applied, effectively reducing wing structural weight.

VTE capability: Low Speed, Take-Off and Landing, Performance

At low speed, VTE gives higher L/D at given C_L compared to conventional wings with part-span TEF. For a given TOW this implies shorter take-off run capability, or for a given thrust level and take-off run, variable camber allows a higher TOW.

7.2. VTE integration into Cruise Wing Design, Effect on Payload – Range Efficiency

We consider three aircraft types. The Gulfstream G-III is a long-range executive transport, AR 6 wing. The Bombardier C-Series, still in development, are intended to be medium-range civil transports, AR 10. The A340-500 is a typical, current large, long-range civil transport, AR 8.5. The A340-500 was selected for large aircraft assessment as extensive performance data was most readily available. Also, the work in Ref.12 was for typical new generation long to medium range aircraft, e.g A340 and A330.

The aircraft component weight breakdowns (WFB, Reserves, WP, OEW and Wing contribution), with respect to MTOW at the Design point, are shown in **Fig.7.2.1**. We note the similar WFB fraction for the G-III and A340, both effectively long-range. Also of note is that WP fraction on the G-III is less than the reserves fuel fraction.

The WP – R diagrams are compared in **Fig.7.2.2**. This exemplifies the dissimilarity between the three types – A340: large payloads over very long ranges, C-Series: medium payloads over medium ranges and the G-III: small payloads over long ranges. Also noted in the figure are PRE values at the Design points. The inverse of PRE gives Fuel burnt (lb) per nm per lb of WP. The A340 type uses 0.586 lb of fuel per lb of payload per 1000 nm. Initial, possibly optimistic, estimates for the C-Series predict 0.433 lb of fuel per lb of payload per 1000 nm. The G-III consumes 4.386 lb of fuel per lb of payload per 1000 nm. This appears very fuel inefficient but to do the same task the A340 type would consume over 17 lb of fuel per lb of payload per 1000 nm.

It will be interesting to compare the effects of VTE integration into the three classifications.

VTE capability into Cruise Wing Design – Improved L/D

For AR 6 and 10 wings, designing for lower cruise C_L with VTE capability results in lower C_{D0} and higher L/D, approximately 3.3% gain. This benefit results in a proportional increase in Range Parameter (X) and hence Range whilst WP and MTOW remain unchanged.

VTE RBM control on Cruise Wing Design – Lower Wing Weight

VTE capability gives a 3.3% gain in Range for the cruise design wing. Furthermore, the VTE capability allows control over the magnitude of RBM experienced during high g manoeuvres or gust loads. This results in a relaxation of ultimate load factors applied to the wing design with a subsequent reduction in wing weight. It was shown in Sections 5.2 and 6.2 that, for both AR 6 and AR 10 wings, a 20% reduction in RBM could be achieved with modest deflections of distributed (spanwise) VTE. We assume that this equates to 20% reduction in wing weight. The weights are redistributed whilst maintaining MTOW and Fuel content (WFT). The absolute wing weight reduction is applied as an increase in WP at Points A, B and Design point. The resulting aircraft component weight breakdowns with respect to MTOW at the Design point, are shown in **Fig.7.2.3**.

We note a 25% increase in WP_{Des} for the A340 and an almost doubling of WP_{Des} for the G-III. We need to refer to these payload increments in absolute terms to ensure that the respective fuselages have available capacity.

The basic A340 design point is 313 pax in three class configuration at 210 lb each (65,730 lb). Maximum seating, one class, is 440 (92,400 lb), an additional 127 pax, **Fig.7.2.4**. Estimated wing weight reduction was of the order of 26,600 lb equating exactly to 127 pax should it be

necessary to redistribute this weight saving as seated pax. This leads to a 46% increase in PRE. The increase in maximum payload (WPA) to 139,480 lb may be beyond the A340 fuselage structural capability. Overall, WPA is limited by structural integrity and volume.

The G-III seats up to 19 pax, easily accommodating the increment from 8 to 14 pax at design point. The C-Series are intended to carry 100 to 125 and 120 to 149 pax depending upon variant. Again the wing weight saving is readily accommodated within increased seating density.

The resulting WP – R diagrams are compared, for the three aircraft types, in **Fig.7.2.4**. Also shown are WP – R diagrams for the conventional aircraft together with original and improved PRE values and corresponding % changes. Although in PRE terms the G-III is inefficient, the application of VTE would provide a very significant 78% increase in PRE at the design point. Applied to typical civil transport aircraft, medium to very long-range, VTE offers 15 % to 45% PRE increases.

7.3. Low Speed, Take-Off and Landing, Performance

Take-Off Performance

At low speed, VTE gives higher L/D at given C_L compared to conventional wings with part-span TEF. For a given TOW this implies shorter take-off run capability, or for a given thrust level and take-off run, variable camber allows a higher TOW. At present we consider Sea Level, ISA conditions.

For AR 6 configuration we consider trimmed C_L 1.4, α 8°, M 0.2 data for conventional TEF and VTE geometry cases. Predicted variations of Field Length, all engines, (AEFL) with TOW are in **Fig.7.3.1**. Results for conventional TEF 25.6° assuming C_{Lmax} 1.9 are compared with those for VTE 20.8°, C_{Lmax} ranging from 1.7 to 2.1. The AR 6 configuration is based on the Gulfstream G-III and G350 class of aircraft and the theoretical predictions compare well with G350 data (Field Length of 5050 ft at MTOW 70,900 lb) assuming C_{Lmax} of 1.9. Based on conventional TEF at TOW 70,000 lb, if VTE is limited to C_{Lmax} 1.7, AEFL increases by 6%. However, if VTE can match C_{Lmax} AEFL is reduced by 6% and if C_{Lmax} can be improved to 2.1 AEFL reduces by 15%.

For AR 10 configuration we consider trimmed C_L 2.0, α 8°, M 0.2 data for conventional TEF and VTE geometry cases. Predicted variations of AEFL with TOW are in **Fig.7.3.2**. Results for conventional TEF 30.5° assuming C_{Lmax} 2.0 and 2.2 are compared with those for VTE 32.4°, C_{Lmax} ranging from 1.8 to 2.2. Published AEFL, Sea Level, ISA data are also shown for typical Boeing and Bombardier C-Series aircraft in this TOW range. Claimed C_{Lmax} for the B737-200ADV is 2.1 to 2.3 and its AEFL lies close to the predicted C_{Lmax} 2.2 line. Claimed C_{Lmax} for the B737-300 is 2.2 to 2.5. Its AEFL lies in the region for predicted C_{Lmax} extrapolated to 2.5. The C-Series data lie on typical increasing TOW trends close to predicted C_{Lmax} 2.4. Based on conventional TEF at TOW 120,000 lb with C_{Lmax} 2.2, VTE with C_{Lmax} 2.0 gives almost identical AEFL relationship. If VTE is limited to C_{Lmax} 1.8 AEFL increases by 12%. However, if VTE can achieve C_{Lmax} 2.2 AEFL reduces by 12%.

In the above comparisons, the VTE applied in the AR 6 case resulted in a 10% increase in RBM. This, of course, may be relieved by selecting suitable VTE distributions. The VTE applied in the AR 10 case did not result in RBM changes.

The next phase of assessment will consider a current generation aircraft, with known capabilities and performance, and compare that with one of equal capability (powerplant, fuselage capacity, payload, range, field length, etc.) but incorporating VTE into a smaller, lighter, more aerodynamically efficient wing.

Landing Performance

The increased L/D at given C_L afforded by VTE implies less thrust requirement during Approach. This would be advantageous in the civil aircraft scene. In general, with higher L/D it may be possible to increase “glide slope” and reduce Landing speed.

To transport a given payload over a given range, the application of VTE technology allows a much smaller aircraft to be designed. This would naturally have a shorter Landing Field.

Further work is required to fully evaluate these advantages.

7.4. Transport Aircraft Design Comparison, Conventional Flaps v Variable Camber

A further assessment will include a redesign of the entire configuration (fuselage, wing, tail, powerplant) such that all advantages afforded by VTE throughout the flight envelope can be incorporated. Continuous buffet alleviation leads to reductions in stress safety factors resulting in a smaller, lighter wing structure. A smaller wing may have reduced fuel capacity but the improved fuel efficiency may result in Range being unaffected. Improved L/D assures greater range for given fuel capacity or reduced fuel requirements for given range. Reduced fuel weight would allow for a larger payload within a given MTOW limit.

A first order “re-design” for an aircraft with A340-500 Design Point capability (313 pax over 8550 nm) incorporating VTE technology shows over 50% PRE improvement, **Fig.7.4.1**. The new design has a 30% reduction in MTOW and 35% reduction in OEW. The effectively scaled down wing (AR maintained) has a 35% reduction in fuel capacity. Retaining the original engines the AEFL is halved. However, if the engine thrust is scaled according to MTOW, AEFL returns to the original value. Further work is required to assess the engine thrust trade-off for cruise efficiency and take-off performance.

8. CONCLUDING REMARKS

The benefits of Variable Trailing Edge geometry (VTE) over conventional part-span Trailing Edge Flaps (TEF) have been assessed on AR 6 and AR 10 wings at high and low speed, effectively covering the whole range of transport aircraft. In all cases, VTE provides L/D increments over conventional wing design.

A wing that is to have VTE capability may be designed for lower cruise C_L . This immediately implies improved cruise performance of the order of 3% to 5% L/D leading directly to similar increase in range. In addition, VTE capability allows a degree of load alleviation at high g, off design situations. Wing load design factors may therefore be relaxed, resulting in a lighter wing structure. For a given MTOW design, the wing weight saving may be redistributed as increased payload.

It was shown that with distributed VTE of quite modest deflection angles, 20% reductions in RBM could be achieved on both AR 6 and AR10 wings.

At low speed, VTE capability provides increased L/D , resulting in shorter Take-Off Field Length of the order of 10% to 15% depending upon C_{Lmax} capability.

Fuel Efficiency, Payload – Range performance, without and with VTE capability, was assessed on Gulfstream G-III, Bombardier C-Series and the Airbus A340-500. The design points for these three aircraft vary widely. The G-III, AR 6, is a long-range executive transport. The C-Series, AR 10, still in development, are intended to be medium-range civil transports. The A340-500, AR 8.5, is a typical, current large, long-range civil transport.

The theoretical assessment of VTE capability on AR 6 and 10 wings was biased towards typical performance data for corresponding aircraft. For example, low speed trimmed C_L for the AR 6 case was 1.2 and 2.0 for AR 10. Nevertheless, there do not appear to be significant differences in advantages for VTE on AR 6 or AR 10 wings.

In terms of Payload – Range fuel Efficiency (PRE), the most significant benefits appear on the G-III, AR 6 configuration. The G-III is a comparatively inefficient long-range executive transport. In this case, a 20% reduction in wing weight results in a doubling of design payload, leading to a 78% increase in PRE. For current, long-range civil transports, VTE capability will result in 40% to 50% increase in PRE at the Design point. It should be noted that performance criteria developed for long-range civil transports may not be entirely applicable to cases such as the G-III. However, comparative assessments are valid.

Summarising:-

- VTE capability 3% to 5% increase in L/D and Range
- 20% reductions in RBM give 20% reductions in wing weight, 20% increase in payload
- 10% to 15% reduction in Take-Off Field Length
- 78% increase in PRE for relatively inefficient long-range executive transports
- 40% to 50% increase in PRE at the Design point for long-range civil transports

It should be mentioned that these advantages are in general at least partially cumulative but not always totally additive. However, the gains are favourable and encouraging.

The benefits of VTE now need to be assessed on larger, high wing military transports and other, more diverse configurations e.g. sensorcraft (joined-wing), reconnaissance types, manned and un-manned concepts (UAV, UCAV, etc.).

9. FURTHER WORK

The very favourable benefits of variable training edge (VTE) technology determined so far lead to several avenues of further work. The work has focussed on assessment of trends rather than the determination of exact values. Various analysis and comparative methods need to be developed and calibrated, e.g. Take-Off Field length and load alleviation / wing weight trade-off.

The next phase should concentrate on evaluating the concept on larger, high wing military transport configurations.

Application of the concept can be further explored on a wider range of applications (joined-wing, long-endurance reconnaissance, smaller manned and un-manned combat aircraft, supersonic aircraft). A VTE capable wing is a better match at all conditions throughout the flight envelope.

The beneficial “knock-on” effects appear to be endless and, at first sight, not necessarily related. For example, integration of VTE into a future design results in a much smaller combat aircraft for a give weapons load. A more efficient combat aircraft could operate from smaller carriers and out of smaller airfields.

Within the context of VTE evaluation on Heavy Lift, High-wing, military transports, several areas require further development:-

Modelling

- Fuselage Interference effects have been taken into account but need further validation
- Nacelle and Spillage Effects on basic and vari-camber designs need to be considered
- Relaxed wake effects have been shown to be negligible for cases considered

Improve modelling of segmented TEF without and with gaps, e.g. Fowler Flap.

Stability and Control
 Sideslip without and with Fuselage Effects

High Speed L/D advantages can be exploited as
 improved high speed performance - Increased Range (better efficiency)
 Smaller wing at design stage - Lower OEW, lower drag

Future designs with VTE considered at the design stage:
 Wing sizing (reduced area and span)
 Engine sizing (reduced thrust requirement)
 Nacelle location and possible spillage effects (Sect 4.3)

High speed cruise, RBM controlled, L/D against wing weight trade-offs to be validated

Efficiency improvements in Loiter applicable to Surveillance, Tankers, etc.

Low Speed L/D advantages can be exploited as
 Improved performance
 Reduced Take-Off Field Length or
 Increased TOW
 Increased Payload or
 Increased Range (more fuel aboard at Take-Off)

Further comparison of achievable C_{Lmax} (TEF and VTE)

Use of LE devices for very high lift ($CL = 3.0$) cases requires assessment

New Heavy Lift Design incorporating VTE
 (comparison with conventional design at specific Payload – Range)
 Determine appropriate sweep, t/c, area, AR
 Redesign wing for end of cruise CL requirements (as per Airbus work)
 Develop fully integrated “morphing” wing design
 Resize engines for smaller MTOW
 Field performance, re-evaluate to include altitude and temperature effects

Complementary / Additional theoretical methods:-
 Develop more accurate assessment of wing weight model using higher order models
 More accurate trade-off rates for RBM, wing structure, wing weight
 Weight penalties for VTE actuation systems
 (current research suggests no weight penalties)

Other ideas are to be discussed with the technical monitors.

ACKNOWLEDGEMENTS

The author has pleasure in acknowledging helpful technical comments and discussions with Dr Surya Surampudi and recently Dr Gregg Abate (both from USAF-EOARD), Mr. Gary Dale, Mr Peter Flick and Mr. Cale Zeune (US-AFRL). The technical help of Dr. M. E. Palmer is appreciated.

This material is based upon work supported by the European Office of Aerospace Research and Development, Air Force Office of Scientific Research, Air Force Research Laboratory, under Grant No. 10-3090.

Any opinions, findings and conclusions or recommendations expressed in this material are those of the author(s) and do not necessarily reflect the views of the European Office of Aerospace Research and Development, Air Force Office of Scientific Research, Air Force Research Laboratory.

REFERENCES

1. NANGIA, R.K., "Energy Efficiency of Military Aircraft & Operations (Jet Transports)", RKN/AERO/REPORT/2008-30, January 2008.
2. NANGIA, R.K., "Energy Efficiency of Military Aircraft & Operations (Turbo-prop Aircraft)", RKN/AERO/REPORT/2008-40, July 2008.
3. NANGIA, R.K., "Energy Efficiency of Military Aircraft and Operations, Surveillance, 3-Reconnaissance and Tankers", RKN/AERO/REPORT/2009-50, August 2009.
4. NANGIA, R.K., "Efficiency Parameters for Modern Commercial Aircraft", RAeS Aeronautical Journal, Volume 110, no 1110, pp 495-510, August 2006
5. NANGIA, R.K., "Operations and Aircraft Design Towards "Greener" Civil aviation Using Air-to-Air Refuelling", RAeS Aeronautical Journal, Volume 110, No. 1113, pp. 705-721, November 2006.
6. NANGIA, R.K., "Greener" Civil Aviation Using Air-to-Air Refuelling - Relating Aircraft Design Efficiency & Tanker Offload Efficiency", RAeS Aeronautical Journal, Vol. 111, No. 1123, pp. 589-592, September 2007.
7. NANGIA, R.K., ZEUNE, C & BLAKE, W., "Operating Efficiency of Military Jet Transports", AIAA Paper 2009-0044, January 2009.
8. NANGIA, R.K., ZEUNE, C. & BLAKE, W., "Operating Efficiency of Military Transports (Jets & Turbo-Props) & Comparisons with Civil Aircraft", AIAA- 2010-0848, January 2010.
9. CARTER, D.L., OSBORN, R.F., HETRICK, J.A. & KOTA, S., "The Quest for Efficient Transonic Cruise", AIAA-2007-7812, September 2007.
10. KOTA, S., OSBORN, R.F., ERVIN, G., MARIC, D., FLICK, P.M. & PAUL, D., "Mission Adaptive Compliant Wing – Design, Fabrication and Flight Test", RTO-MP-AVT-168, Paper 18, 2009.
11. BOPPE, C., AGARD Lecture Series R 783
12. GREFF, E., "Aerodynamic Design and Integration of a Variable Camber Wing for a New Generation Long/Medium Range Aircraft", ICAS-88-2.2.3, 1988.
13. NANGIA, R.K. & PALMER, M.E., "Formation Flying of Commercial Aircraft – Assessment using a New Approach - Wing Span Load & Camber Control", AIAA 45th Aerospace Sciences Meeting, Reno, AIAA-2007-0250, January 2007.
14. NANGIA, R.K., PALMER, M.E., "Formation Flying of Commercial Aircraft – Variations in Relative Size / Spacing – Induced Effects & Control", AIAA Paper 2007-4163, June 2007.
15. NORRIS, G., "Adaptive Wing", Aviation Week & Space Technology, March 08, 2010, pp51-52.
16. FIELDING, J.P., "Introduction to Aircraft Design", Cambridge University Press, 1999.
17. RAYMER, D.P., "Aircraft Design: A Conceptual Approach", AIAA Education Series, 1992.
18. McCORMICK, B.W., "Aerodynamics, Aeronautics & Flight Mechanics", John Wiley & Sons, 1979.
19. JENKINSON, L.R., SIMPKIN, P. & RHODES, D., "Civil Jet Aircraft Design", Arnold, 1999.
20. ANDERSON, J.D.Jr., "Aircraft Performance and Design", McGrawHill, 1999.

21. OBERT, E., “Aerodynamic Design of Transport Aircraft”, Delft University Press, 2009.
22. BREITSAMTER, C., “Aerodynamic Efficiency of Maneuverable Aircraft Applying Adaptive Wing Trailing Edge Section”, ICAS, 2004.

LIST OF SYMBOLS AND ABBREVIATIONS

Only the general symbols are defined here. Other symbols are of local significance within the Section they arise in.

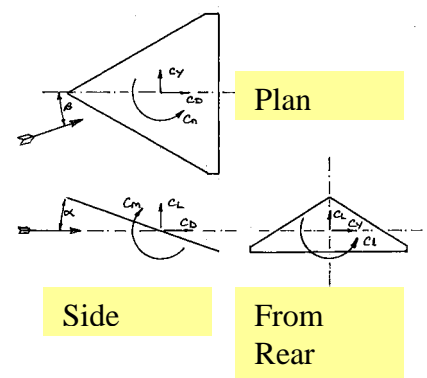
Performance Related

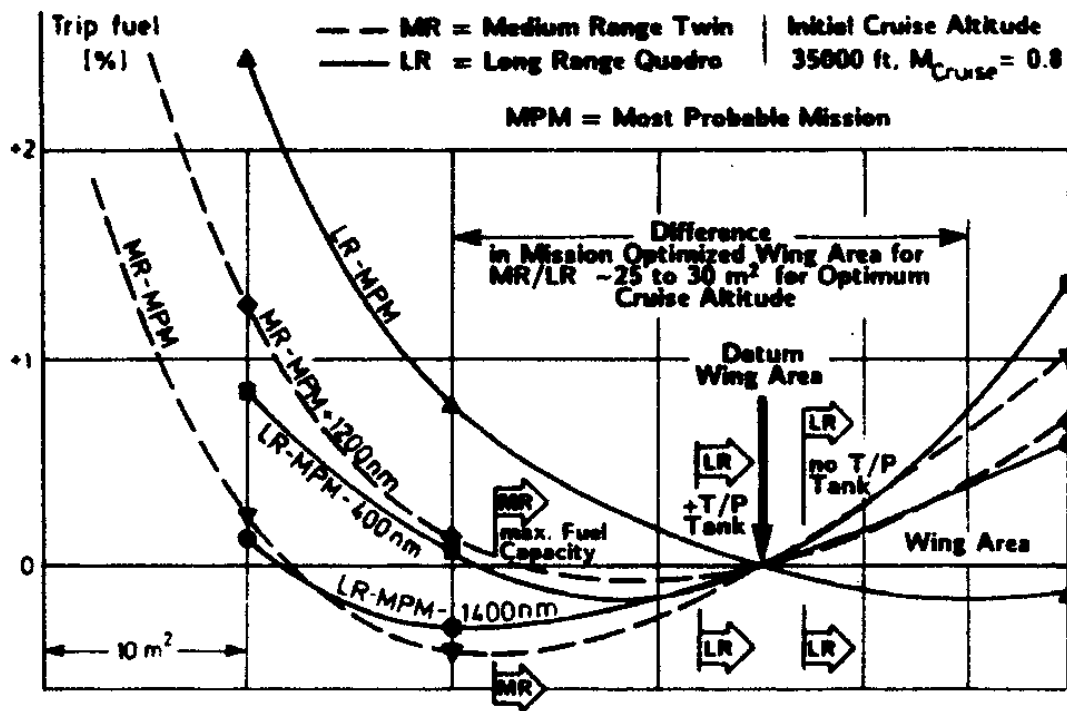
AEFL	Field Length (All Engines)
EXP	Exponential
HBPR	High By-Pass Ratio Engines
OEW	Operating Empty Weight
PRE	= $WP * R / WFB$, Payload Range Efficiency
Pt	Point
R	Range (nm or km)
Radius	Radius of Operation (Tankers, Surveillance and Bombers)
SFC	Specific Fuel Consumption
T	Thrust
WFB	Block Fuel Load
WFB / WP	Fuel Payload Fraction (FPF)
WFR _{es}	or WFR, Reserve Fuel Load
WFT	Total Fuel Load
WP	Payload
WP/WFB	Payload Efficiency
X	= $V * (L/D) / SFC$
Z	= R/X
ZFW	Zero Fuel Weight (MZFW, Maximum)

General

AoA	Angle of Attack (α), usually referred to the body axis
AR	Aspect Ratio
A	Axial Force along wing-plane x-axis (for definition of C_A)
b	= $2 s$, Wing span
BL	Boundary Layer
c	Local Wing Chord
c_{aero}	= c , Mean Aerodynamic Wing Chord
c_{ave}	= $c = c_{ref}$, Average Wing Chord
C_A	= $A/(q S)$, Axial Force Coefficient, measured in Wing plane
C_{AL}	= Local Axial Force Coefficient
C_D	= Drag Force $/(q S)$, Drag Coefficient
C_{D0}	Drag Coefficient at zero lift (see text)
$C_{D0}^{\#}$	Drag Correction added to Panel Method Drag to give Total Drag (see text)
C_{Di}	Lift Induced Drag
cg	Centre of Gravity
C_l	= $l/(q S b)$, Rolling Moment Coefficient (Body Axis), positive right tip up
C_L	= $CL = L/(q S)$, Lift Coefficient
C_{LL}	= Local Lift Coefficient
C_{Lmax}	Maximum Lift Coefficient
C_m	= $m/(q S c)$, Pitching Moment Coefficient (Body Axis), positive nose up
C_{mo}	C_m at zero Lift
C_n	= $n/(q S b)$, Yawing Moment Coefficient (Body Axis), positive nose to left
C_N	= $N/(q S)$, Normal Force Coefficient
CoP	Centre of Pressure

C_p	Coefficient of Pressure
c_r, c_t	Wing Root chord, Wing Tip chord
C_Y	$= Y/(q S)$, Side Force Coefficient, positive to right
D	Drag Force
DOF	Degrees Of Freedom
k	$= \pi A C_{Di}/C_L^2$, Lift Induced Drag Factor
l	Rolling moment (Body Axis), positive right tip up
l	Length
L	Lift Force
LE	Leading Edge
m	Pitching moment (Body Axis), positive nose up
L/D	Aircraft Lift / Drag Ratio
M	Mach Number
MRC	Moment Reference Centre
n	Yawing moment (Body Axis)
N	Normal Force
q	$= 0.5 \rho V^2$, Dynamic Pressure
r	Aerofoil radius
r_n	Aerofoil radius normal to c
R	Reynolds Number, based on c_{ave} (unless otherwise stated)
s	Wing semi-span
S	Wing Area
t	Aerofoil thickness
TE	Trailing Edge
V	Airstream Velocity
VTE	Variable Trailing Edge
x, y, z	Orthogonal Wing Co-ordinates, x along body axis
x_{ac}	Location of Aerodynamic Centre along x -axis
x_{cp}	Location of Centre of pressure along x -axis
Y	Side Force, positive to right
α	Angle of Attack (AoA), usually referred to the body axis
β	Sideslip angle, positive nose to right
λ	Wing Taper Ratio
Λ	LE Sweep Angle
ρ	Air Density
η	$= y/s$, Non-dimensional spanwise Distance
$\theta_{T/P}$	Tailplane Setting Angle (relative to Wing Datum)
θ_{ELEV}	Elevator Setting Angle (relative to Tail Plane Datum)
δ_{TE}	Flap Setting Angle (relative to Wing Datum)



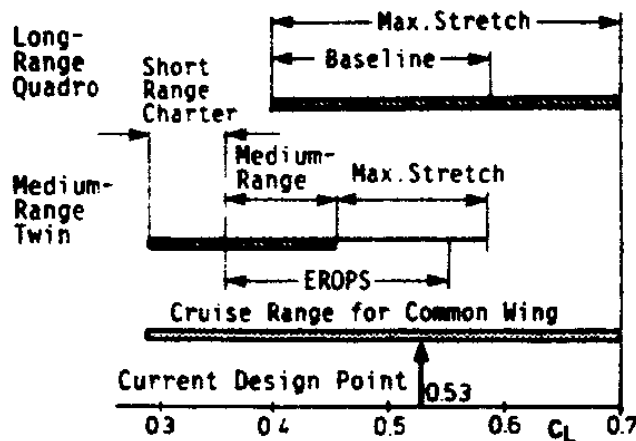


(a) WING AREA TRADE-OFFS FOR MEDIUM / LONG RANGE

• AIRBUS A300	ca. 25%
• AIRBUS A310	ca. 16% *
• BOEING 747	ca. 17%
• BOEING 767	ca. 15% *
• MC DONNELL DOUGLAS DC 10	ca. 37% **
• LOCKHEED 1011 TRISTAR	ca. 19%

TOW Increase
of Wide Body A/C

- * Further Increase Possible
- ** Span Increase + Structure Reinforcement



Mach-No.	TOBFL (ft)	Approach-Speed (kts)
0.82	10000-13000	135 - 145
Initial Cruise Altitude ~ 35000 ft		
0.78 - 0.82	8000-10000	135 - 145

C_L - Range

(b) WING DESIGN REQUIREMENTS

FIG. 1.1.1. WING DESIGN REQUIREMENTS WING AREA TRADE-OFF POSSIBILITIES (Ref.Greff)

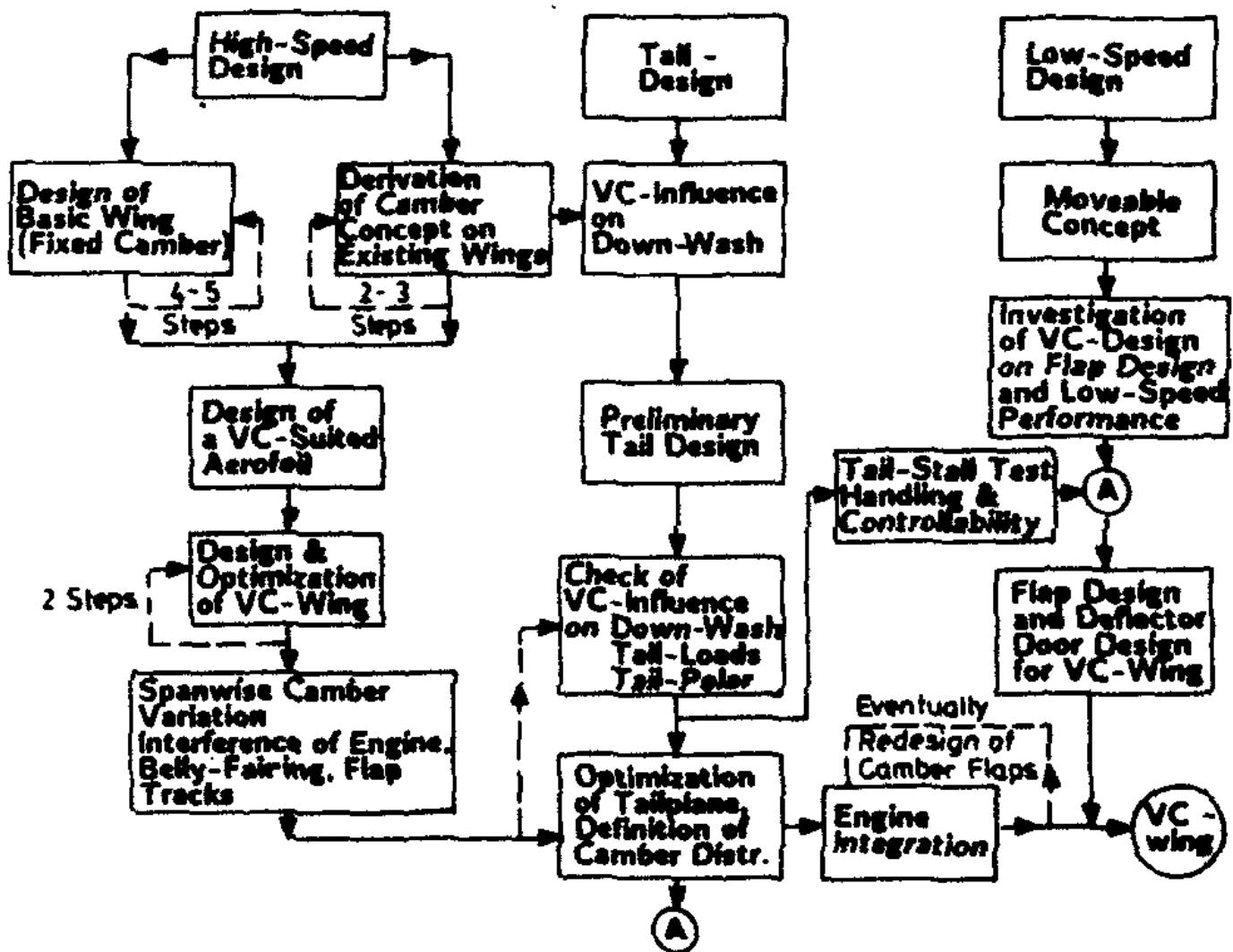
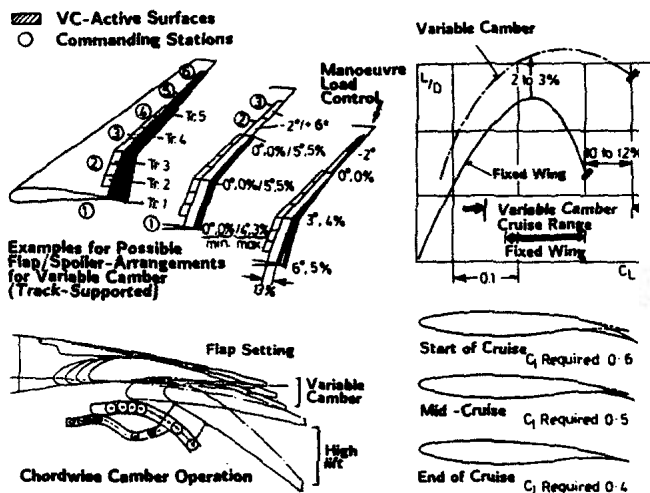
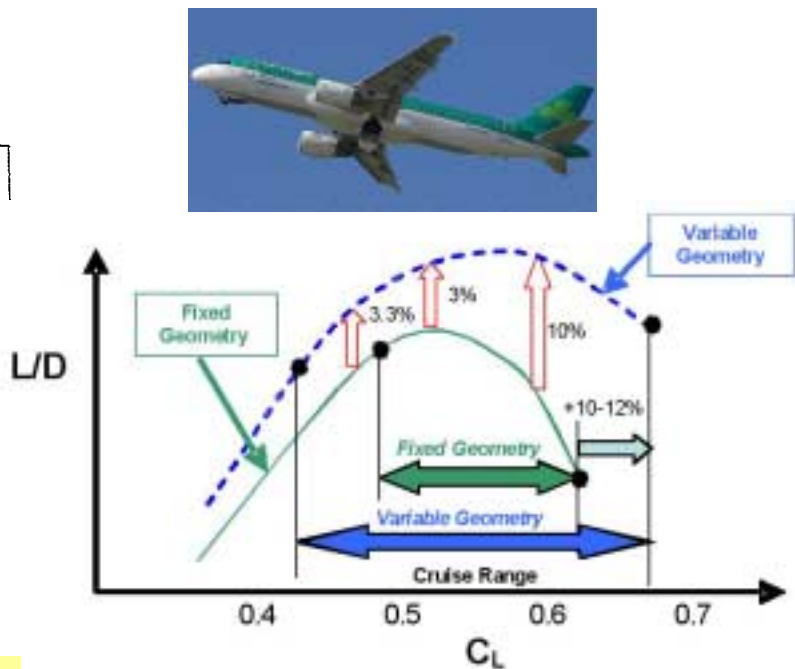


FIG. 1.1.2. AERODYNAMIC DEVELOPMENT CONCEPT FOR VARIABLE-CAMBER WING (Ref.Greff)



(a) Trailing Edge Deflection Mechanism



(b) L/D Improvements on A320 (Airbus Programme)

FIG. 1.1.3. VARIABLE-CAMBER PRINCIPLES AND ANTICIPATED L/D IMPROVEMENTS (Ref.Greff)

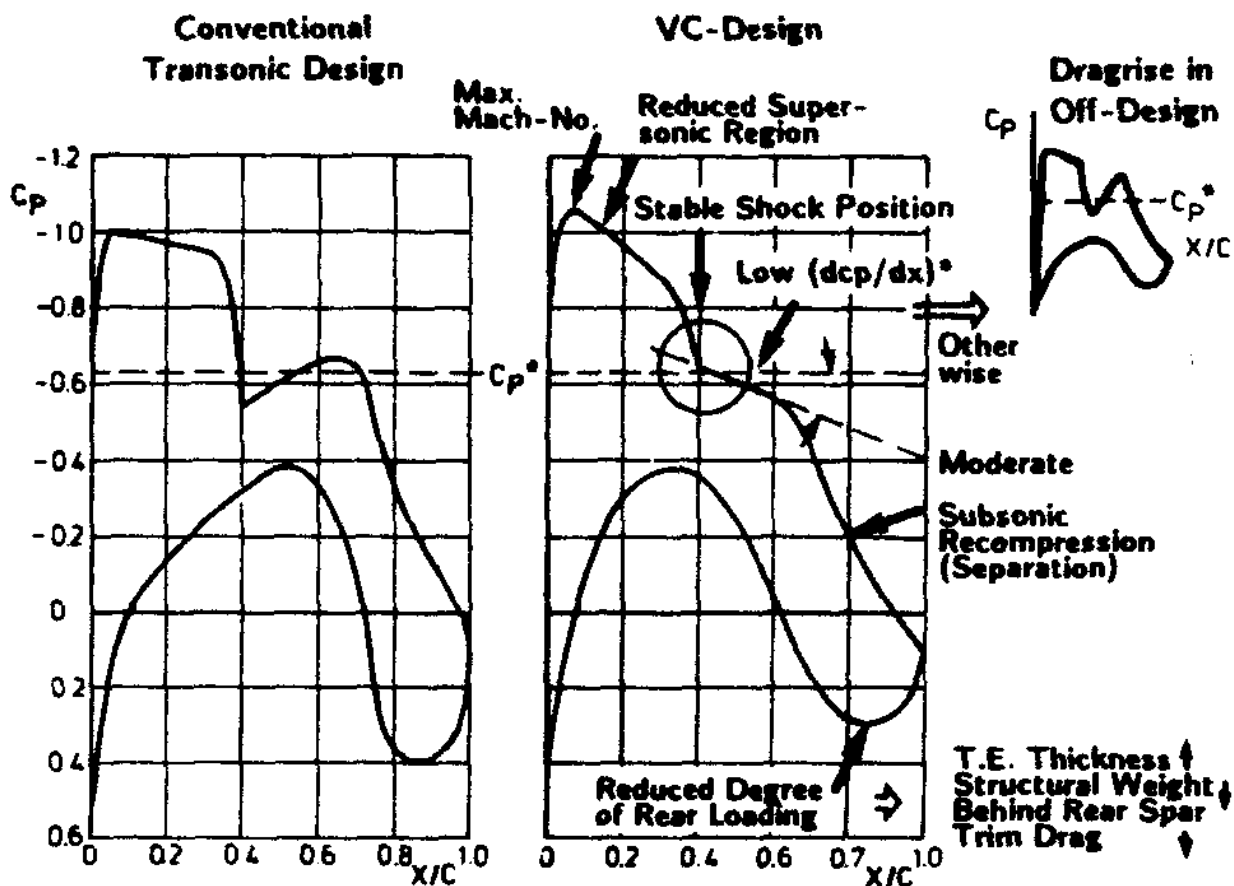


FIG. 1.1.4. CORRECTLY PRESCRIBED PRESSURE DISTRIBUTION FOR VARIABLE CAMBER (Ref.Greff)

$$M_{20} = 0.74, \hat{M}_{Cruise} = 0.81, C_L = 0.67$$

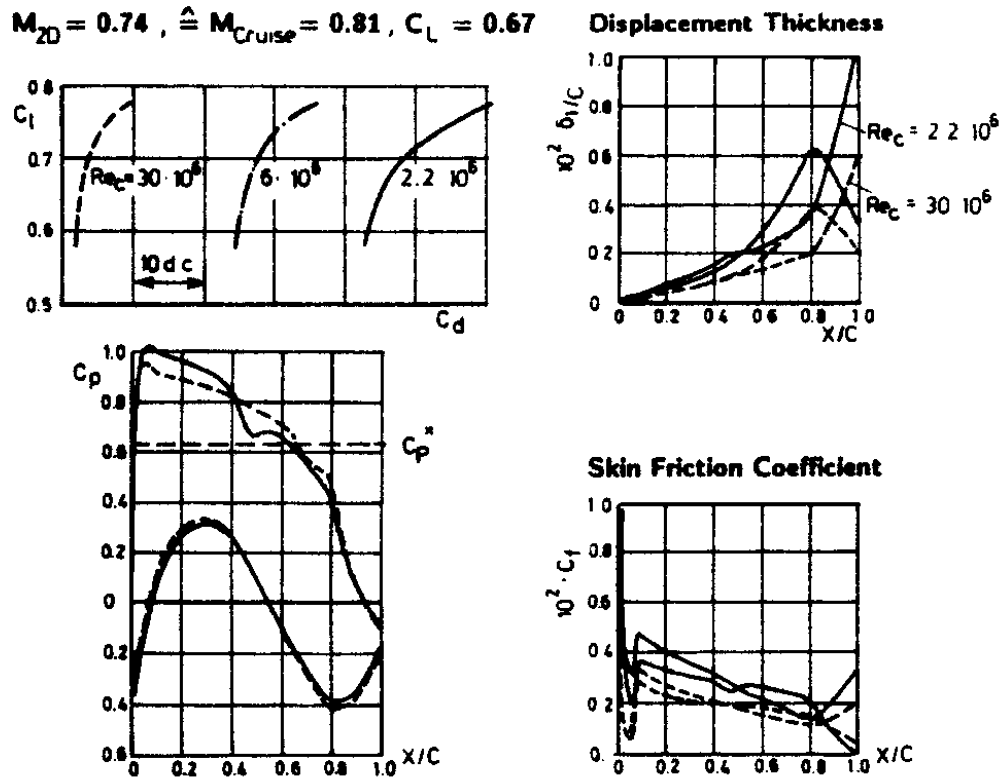


FIG. 1.1.5. REYNOLDS NUMBER EFFECTS ON C_p DISTRIBUTIONS (Ref.Greff)

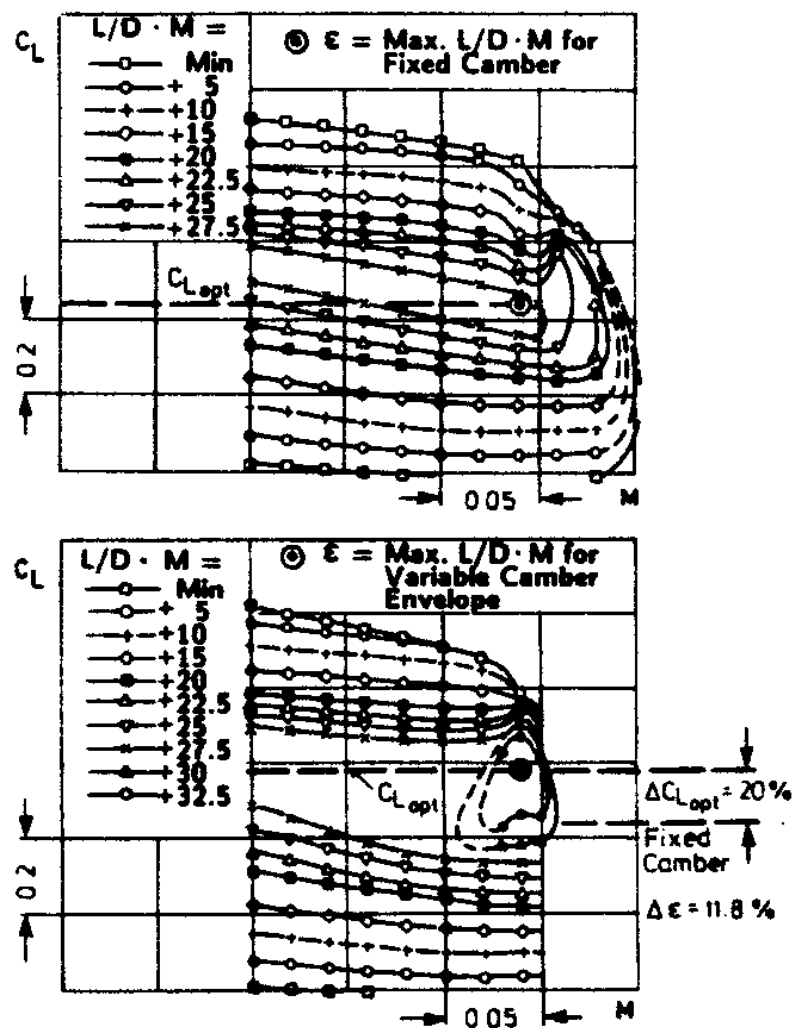


FIG. 1.1.6. C_L - M , $M.L/D$ CONTOURS, FIXED AND VARIABLE CAMBER (Ref.Greff)

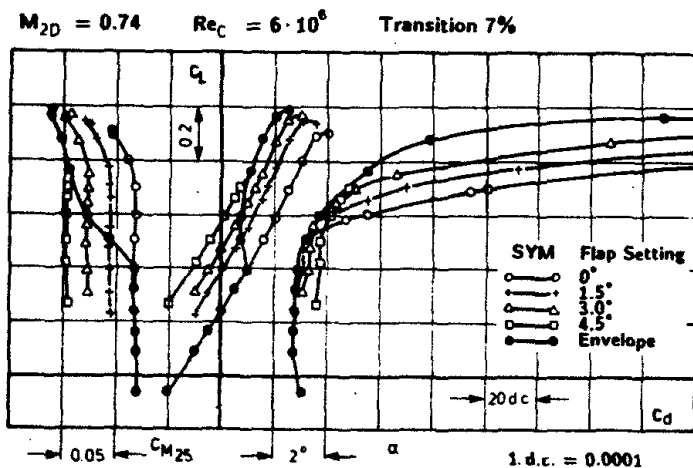


FIG. 1.1.7. $C_m - C_L$, $C_L - \alpha$, $C_L - C_D$ VARIATION, VARIABLE CAMBER FLAP SETTING (Ref.Greff)

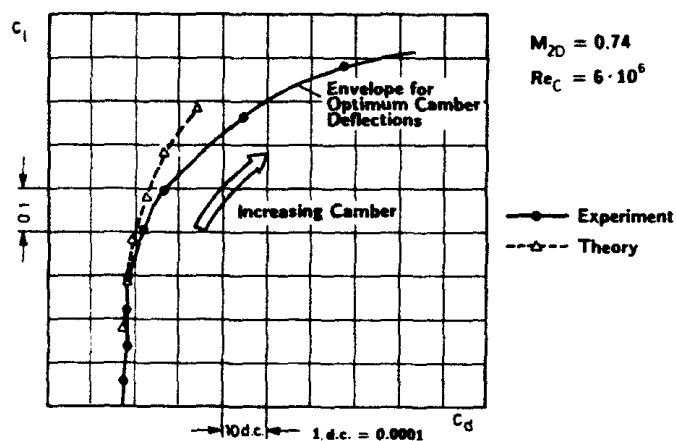


FIG. 1.1.8. $C_D - C_L$ ENVELOPE, CAMBER VARIES THEORY and EXPERIMENT (Ref.Greff)

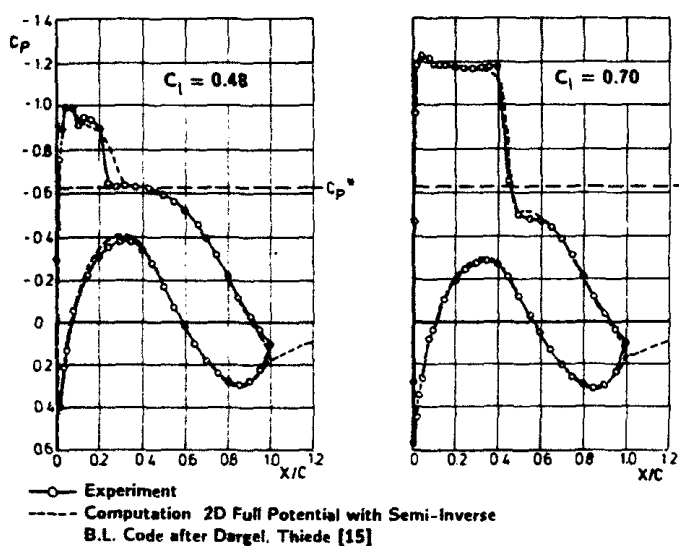


FIG. 1.1.9. $C_p - x/c$, C_{LL} 0.48 & 0.70 THEORY and EXPERIMENT (Ref.Greff)

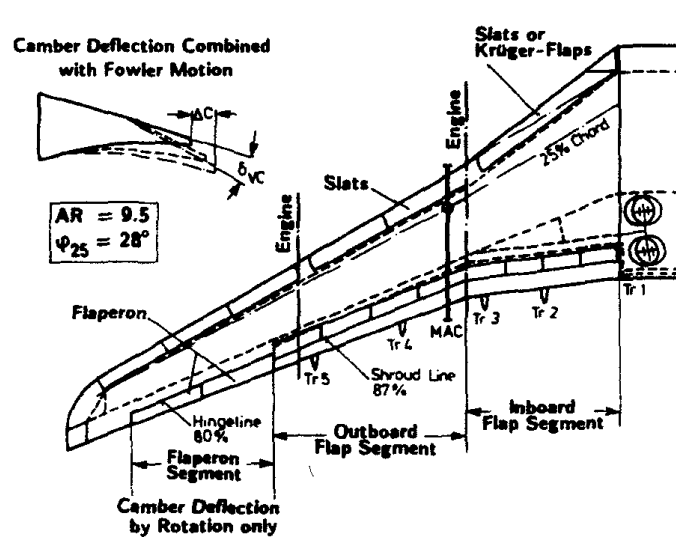
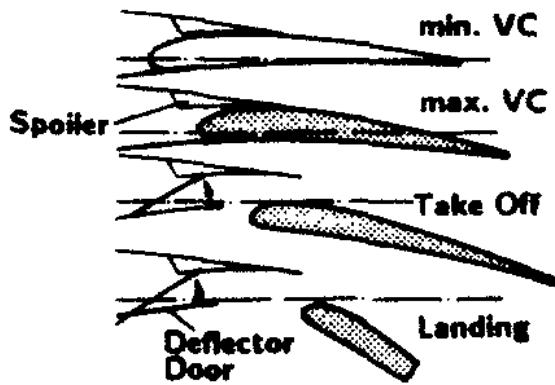
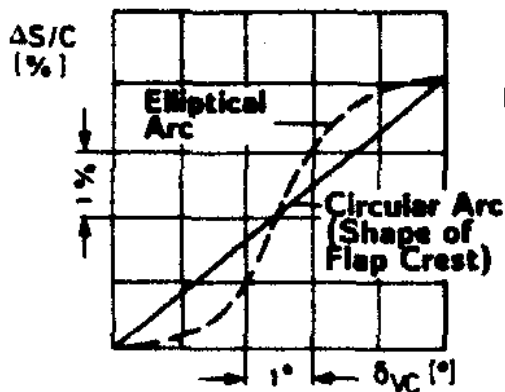
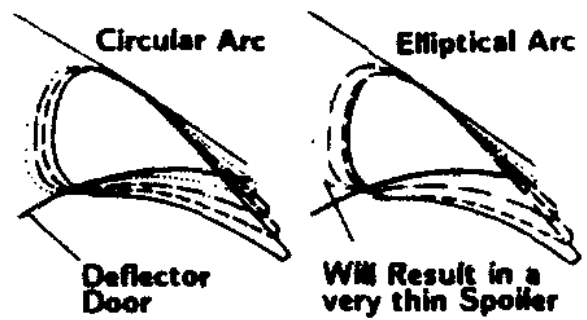


FIG. 1.1.10. VARIABLE CAMBER RESEARCH WIND TUNNEL MODEL (Ref.Greff)

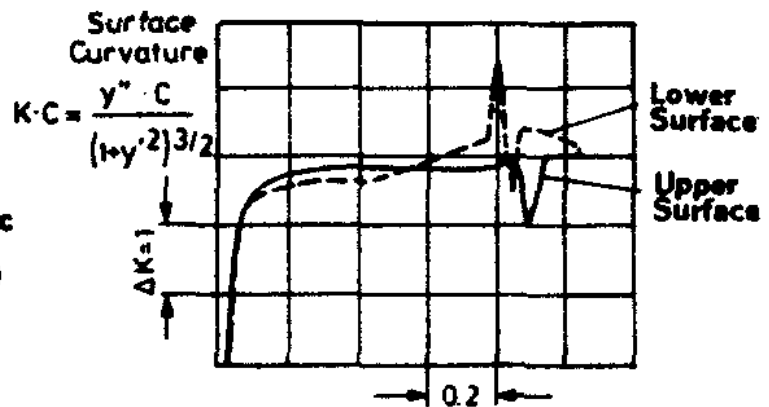
Flap Position / Configuration



Influence of Transfer Function of Flap Body Contour



Transfer Function of Fowler / Camber Motion



Influence of Circular Flap Crest (Linear VC-Transfer Function) on Curvature

FIG. 1.1.11. CONSTRAINTS ON VARIABLE CAMBER / FOWLER FLAP MODELLING (Ref.Greff)

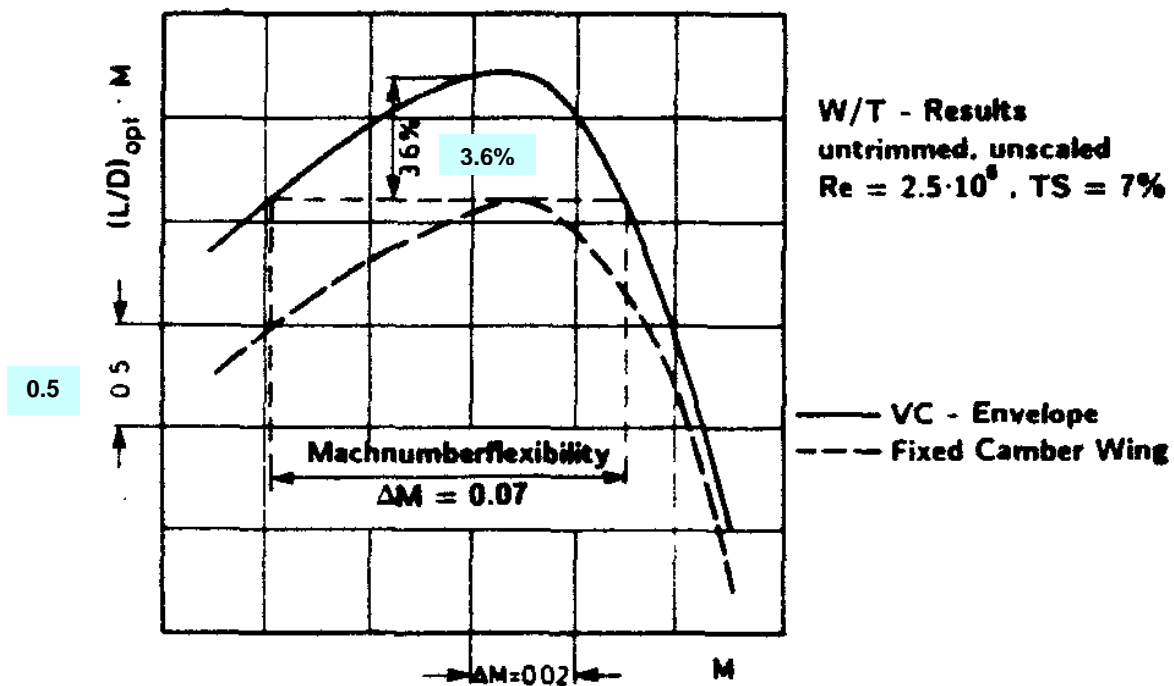
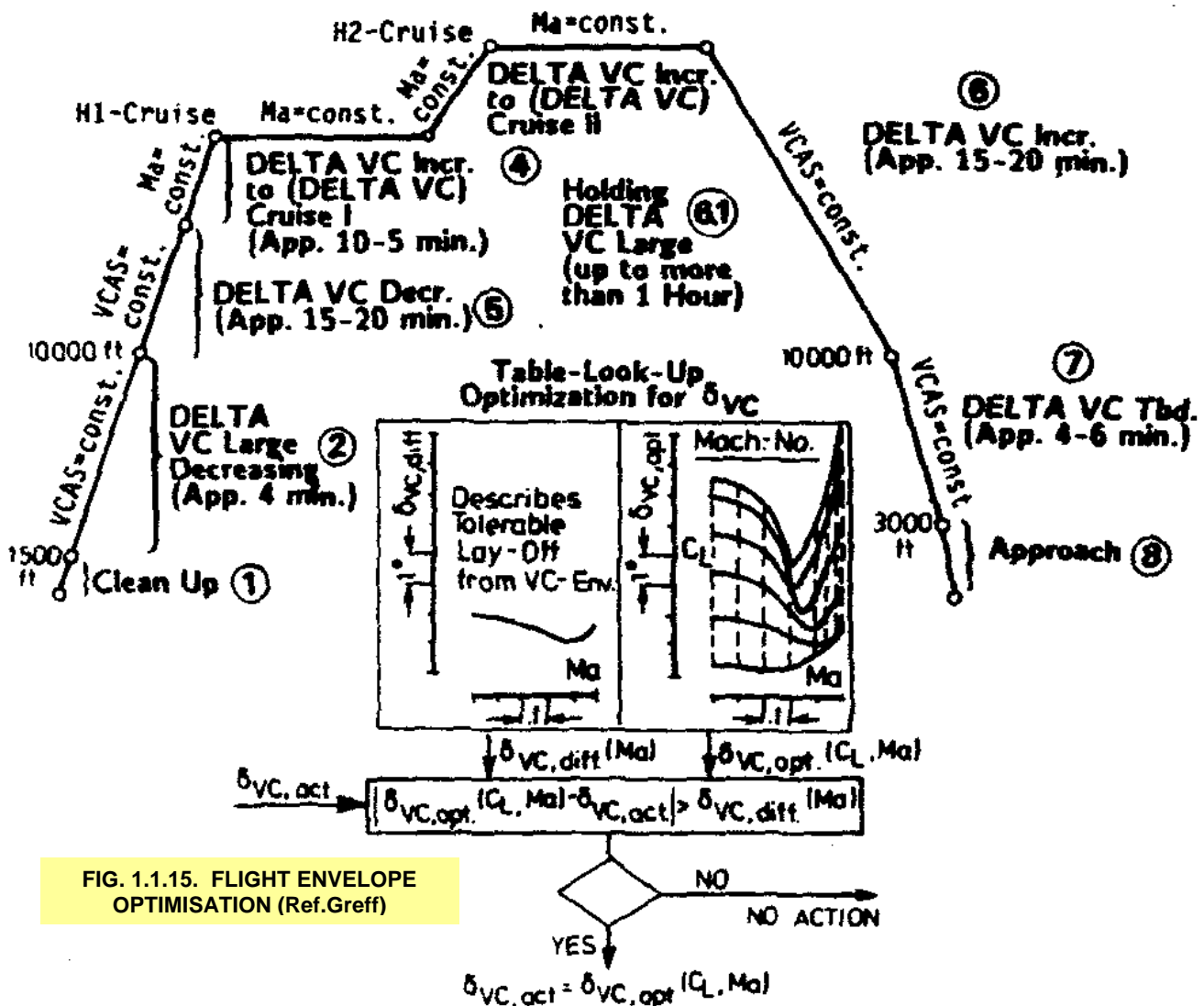
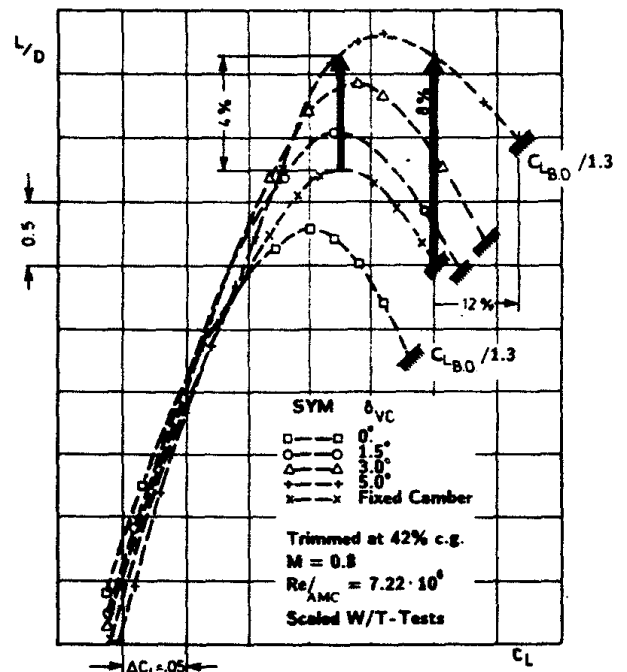
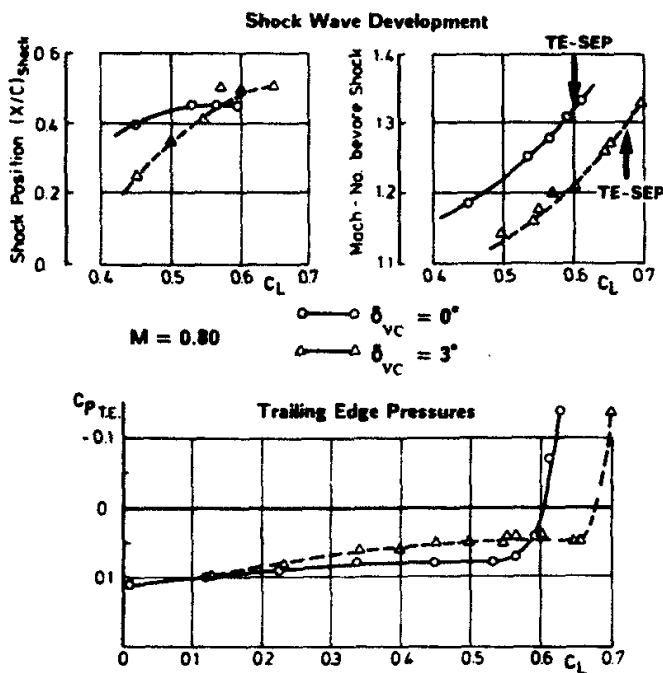
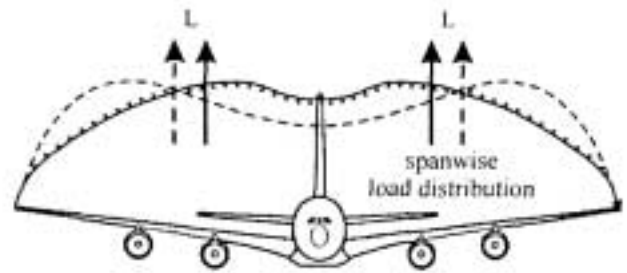
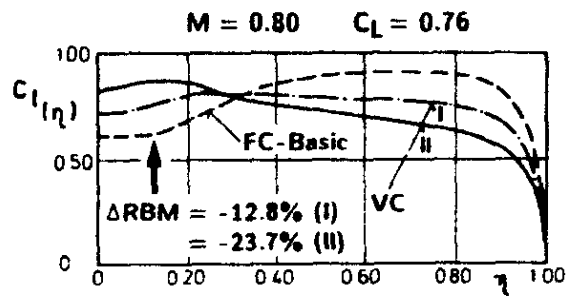
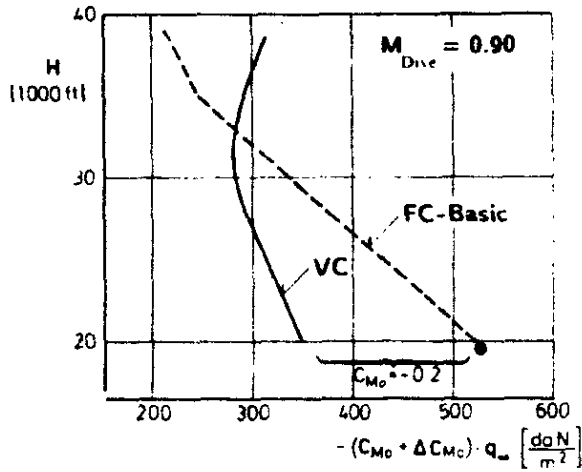


FIG. 1.1.12. $M/L/D - M$, EXPERIMENT (Not Trimmed) FIXED AND VARIABLE CAMBER (Ref.Greff)

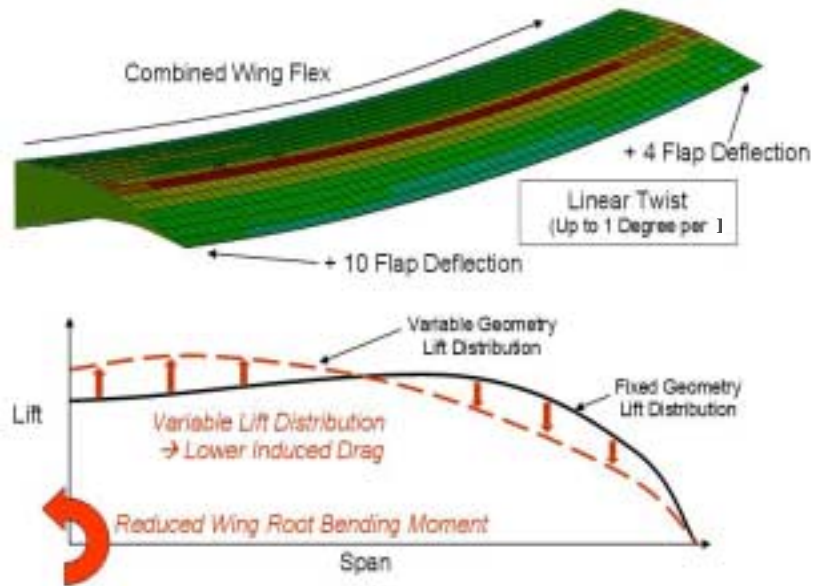




(b) Spanwise Loading and yCP control



(a) Spanwise Distributions and effect on RBM variation with Altitude



(c) Wing Flexing Considerations

FIG. 1.1.16. LOAD CONTROL VIA VARIABLE CAMBER (Ref.Greff)

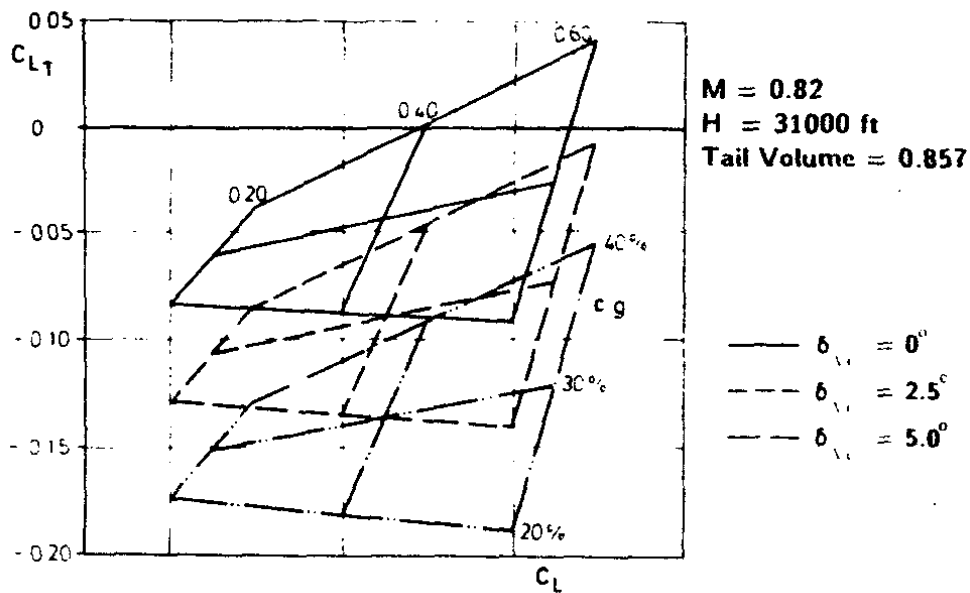


FIG. 1.1.17. $C_{Ltail} - C_L$
 EFFECT OF VARIABLE CAMBER and c.g. LOCATION & Tail Demand (Ref.Greff)

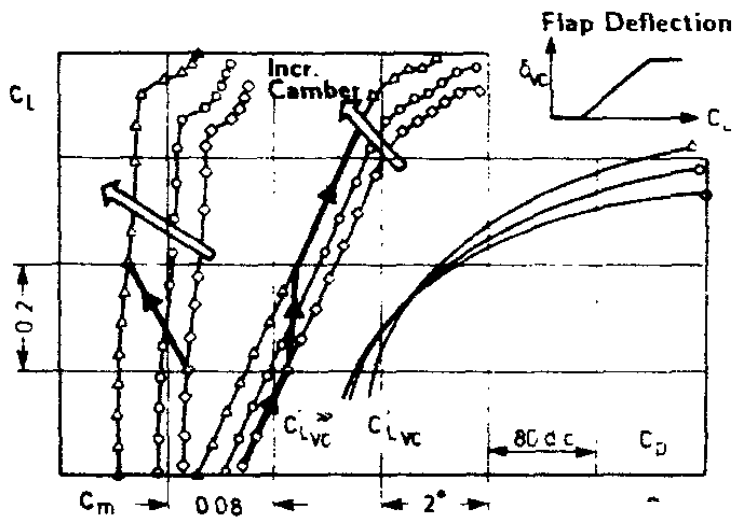


FIG. 1.1.18. FUSELAGE INCIDENCE and WING ROOT SETTING ANGLE EFFECT OF VARIABLE CAMBER (Ref.Greff)

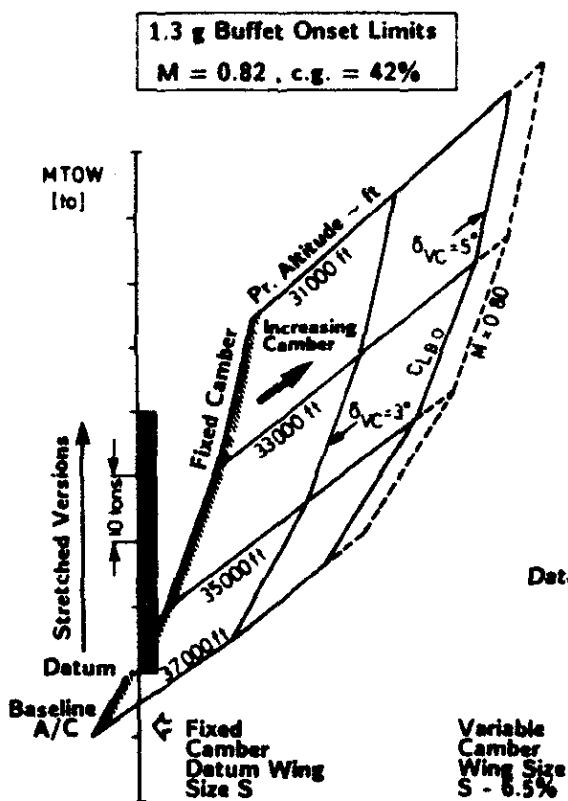
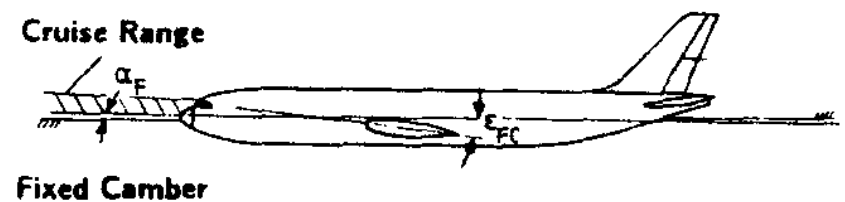
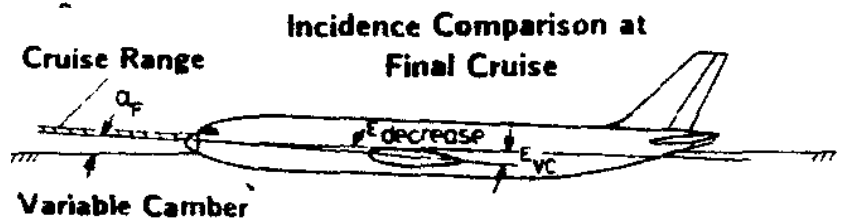


FIG. 1.1.19. MTOW, CRUISE ALTITUDE, Operational Buffet Limits, VARIABLE CAMBER EFFECTS (Ref.Greff)

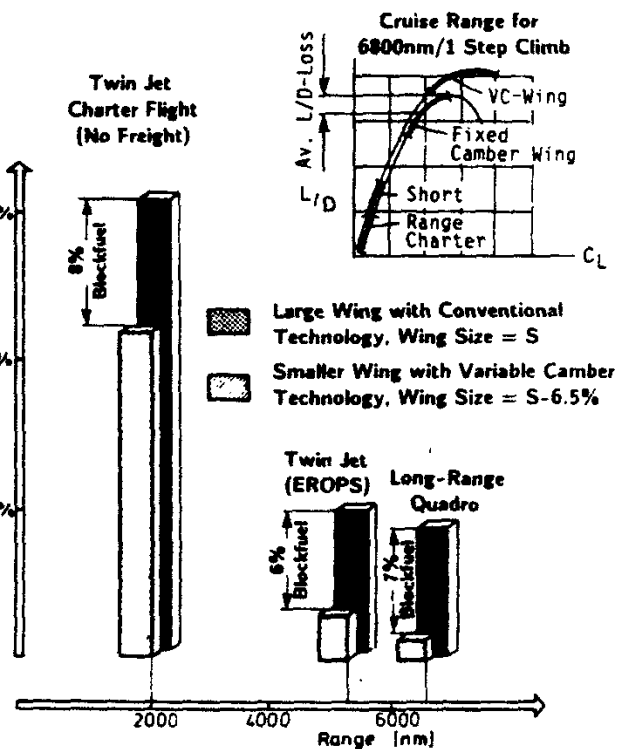
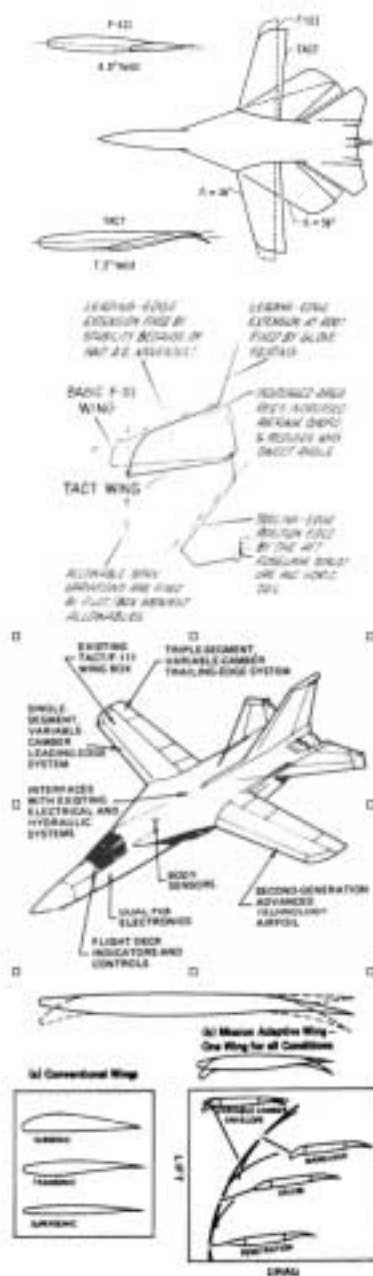


FIG. 1.1.20. POSSIBLE BLOCK FUEL REDUCTIONS EFFECT OF VARIABLE CAMBER (Ref.Greff)



- Joint USAF / NASA
- 1969 – 1975
- Investigate Applicability of Supercritical Airfoil on Tactical Aircraft
- Improve Transonic Cruise
- Improve Maneuverability
- No Degradation of High or Low Speed Performance



FIG. 1.1.21 Transonic Aircraft Technology (TACT) Programme

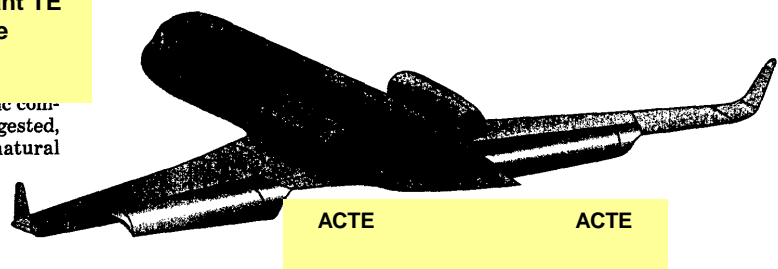
- Joint USAF / NASA
- 1979 – 1988
- Investigate Functional Utility of Supercritical Airfoils
 - Improved Range
 - Buffet-free Lift
 - Sustained Load Factor
 - Reduced Wing Root Bending During Maneuvers
 - Reduced Response to Turbulence



FIG. 1.1.22 Mission Adaptive Wing (MAW) Programme

FIG. 1.1.23 Adaptive Compliant TE Flaps (ACTE) Programme

are congested, natural

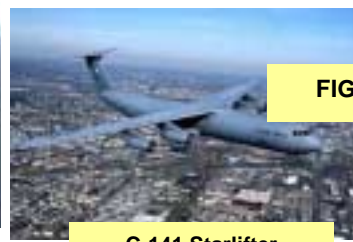




C-5 Galaxy



C-17 Globemaster



C-141 Starlifter

FIG. 1.1.24 JET TRANSPORTS



Lockheed C130 Hercules

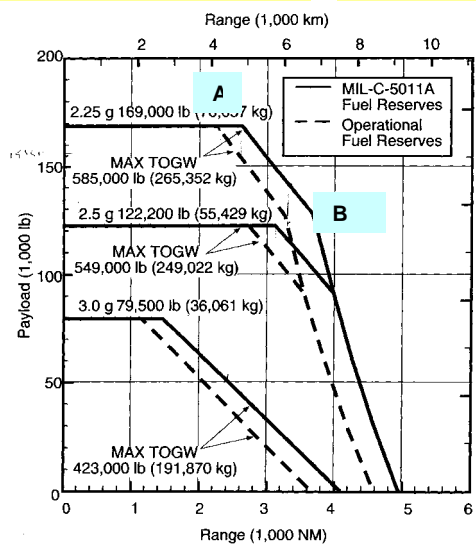


Alenia - Lockheed C27J Spartan



Airbus A400M

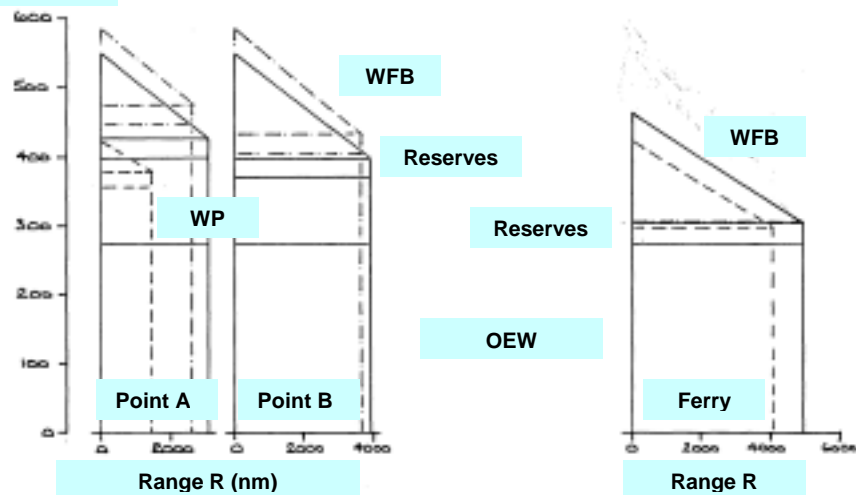
FIG. 1.1.25 TURBO-PROP TRANSPORTS



(a) WP - Range, 2.00g, 2.25g & 3.00g

- Operating Empty Weight (OEW) of 277,000 lb (125,645 kg)
- JP-8 or Jet A-1 at 6.74 lb/gal (0.81 kg/liter)

W (1000 lb)



(b) Weights Breakdown, g Limitation Effects

Fig. 1.1.26 C-17 GLOBEMASTER III, MIL-C-5011A & AMC Reserves



Lockheed C130J Hercules



KC-135



A310/A330MRTT



AIRBUS A400M



KC-10A



Fig. 1.1.27 SENSORCRAFT (Generic Picture)

Endurance 40 hrs

Fig. 1.1.28 TANKERS & MOBILITY TURBO-JET and TURBO-PROP POWERED



NASA

Military

Civil



ESTOL CONCEPTS

Fig. 1.1.29 NOTIONAL NEXT GENERATION MOBILITY & TRANSPORTS & CIVIL AIRCRAFT

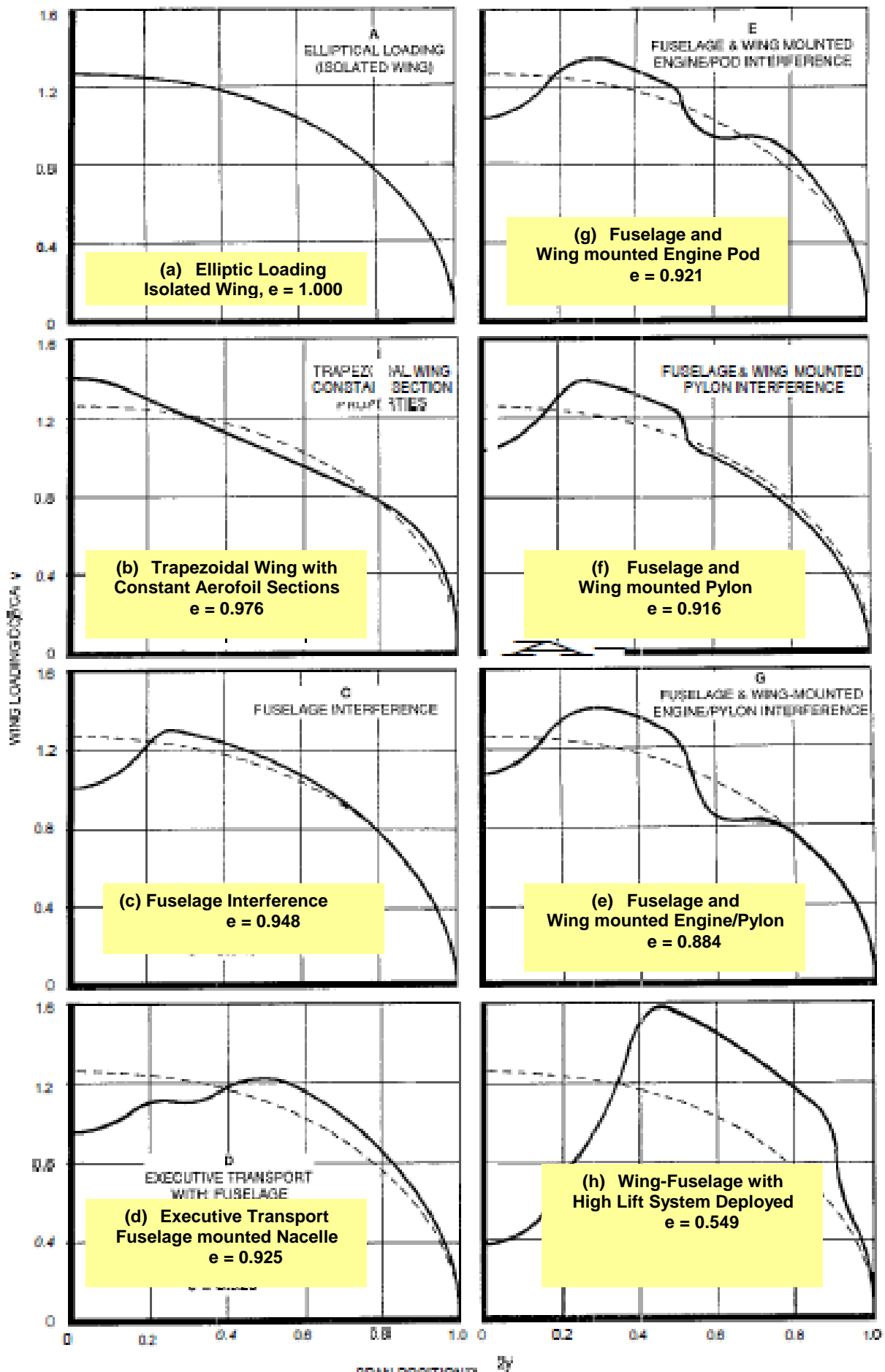


Fig. 1.1.30 EXAMPLES OF SPANWISE LOADINGS & $e = 1/k$ VALUES (Ref: Boppe)

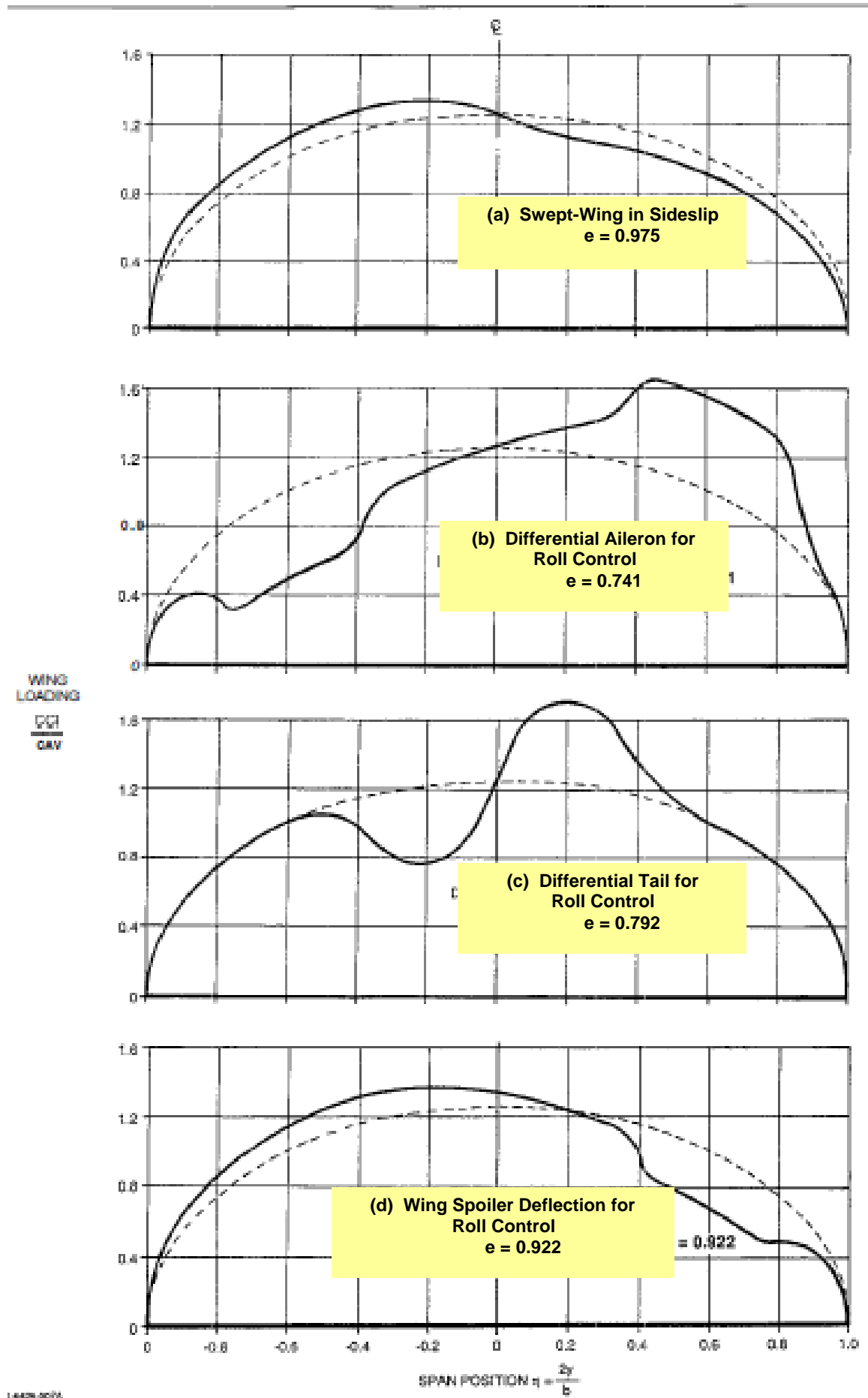


Fig. 1.1.31 EXAMPLES OF ASYMMETRIC SPANWISE LOADINGS & $e = 1/k$ VALUES (Ref: Boppe)

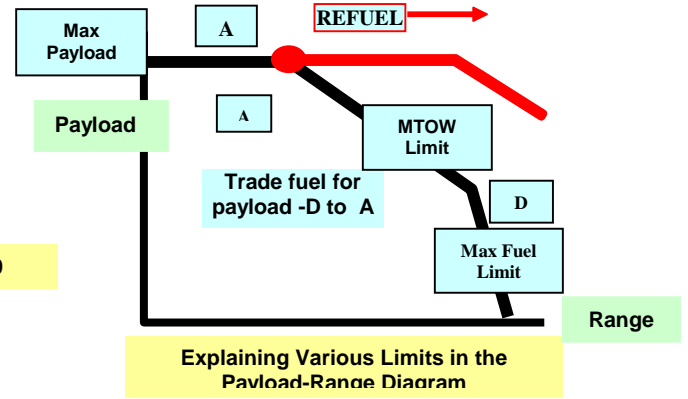
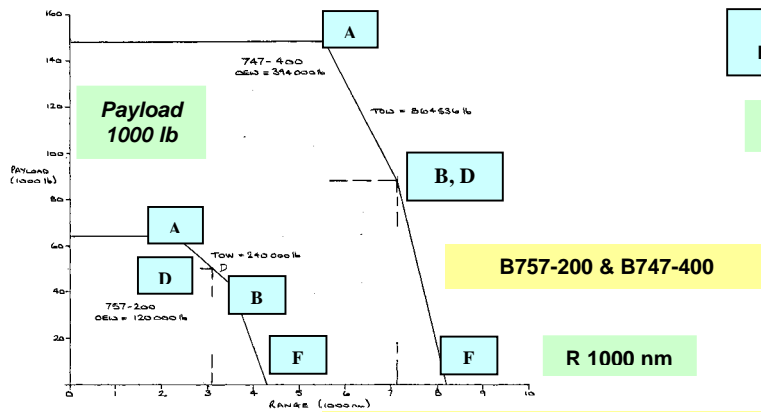


Fig. 2.1.1 TYPICAL PAYLOAD RANGE DIAGRAMS, LIMITS

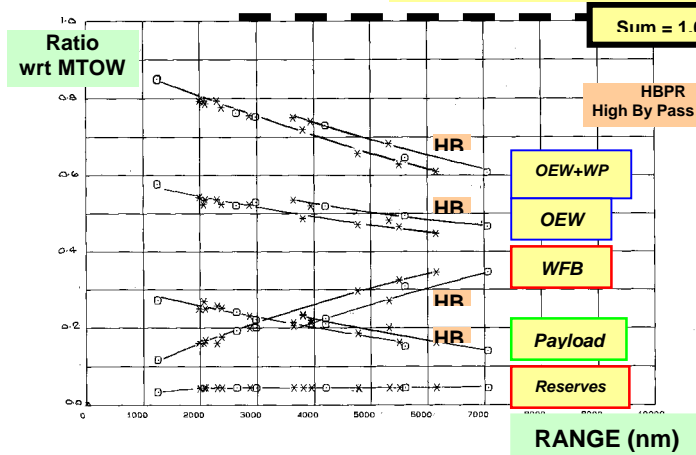


Fig. 2.1.2. Pt A, COMMERCIAL AIRCRAFT, DERIVED OEW, FUEL & PAYLOAD RATIO TRENDS

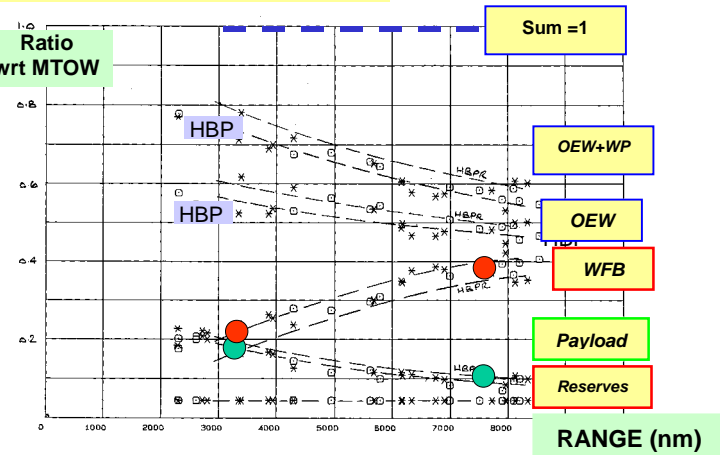


Fig. 2.1.3 Pt D, COMMERCIAL AIRCRAFT, DERIVED OEW, FUEL & PAYLOAD RATIO TRENDS

A:

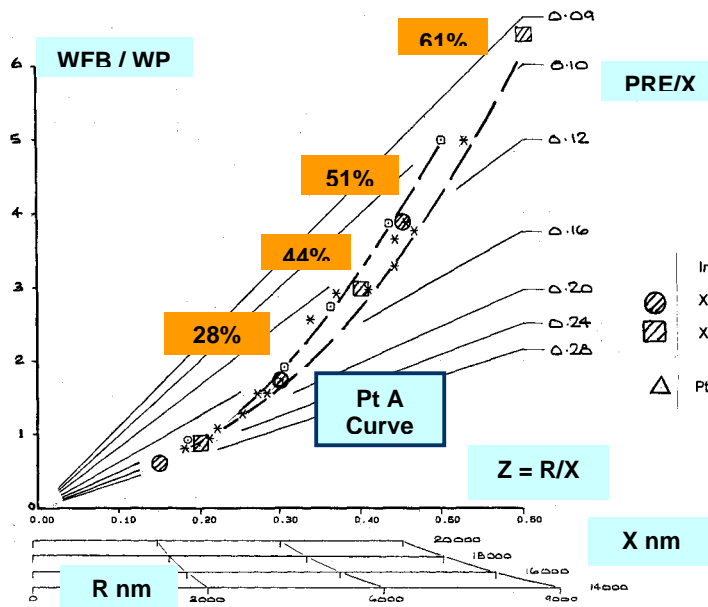


Fig. 2.1.4 WFB / WP vs $Z = R/X$, Pt A & Pt D
Note: Parallel Scales of R Implied for Different X Values

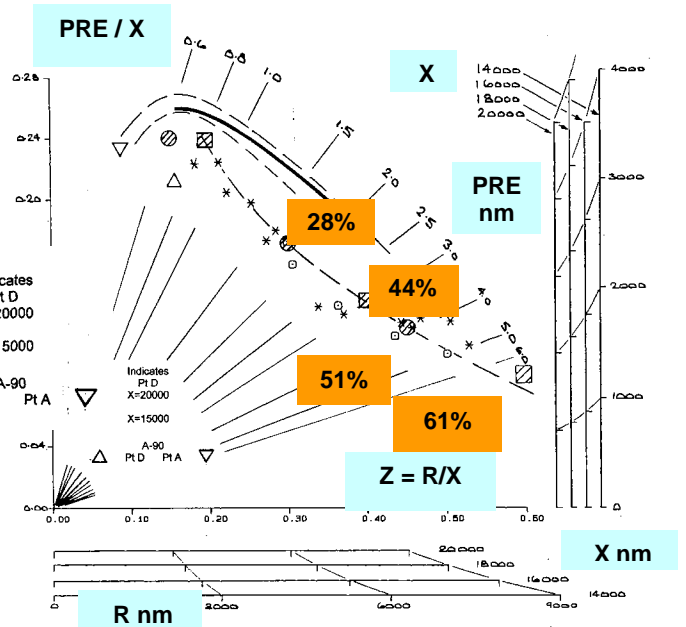


Fig. 2.1.5 PRE/X vs $Z = R/X$, Pt A & Pt D
Note: Parallel Scales of PRE Implied for Different X

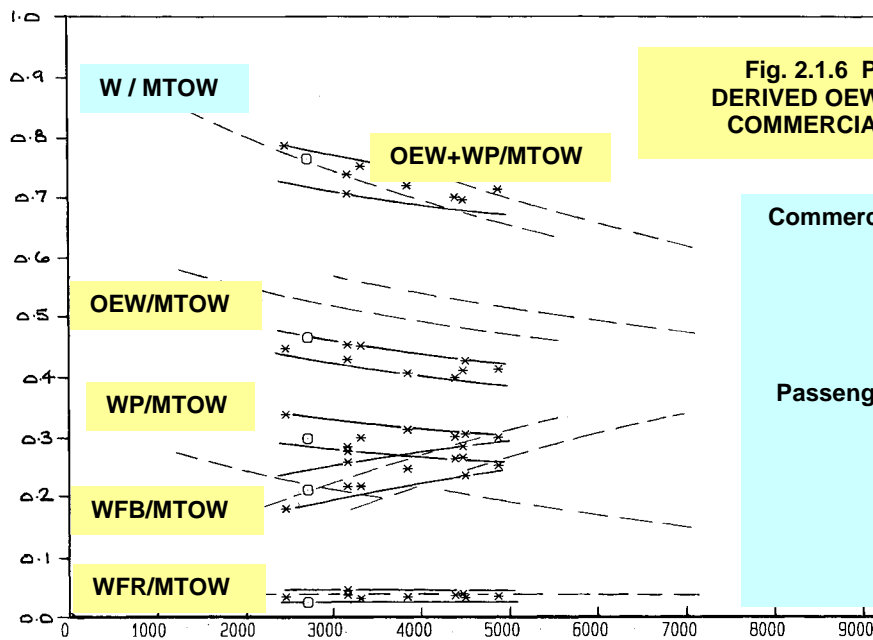


Fig. 2.1.6 Pt A, CIVIL FREIGHTER AIRCRAFT, DERIVED OEW, FUEL & PAYLOAD RATIO TRENDS, COMMERCIAL PASSENGER AIRCRAFT TRENDS

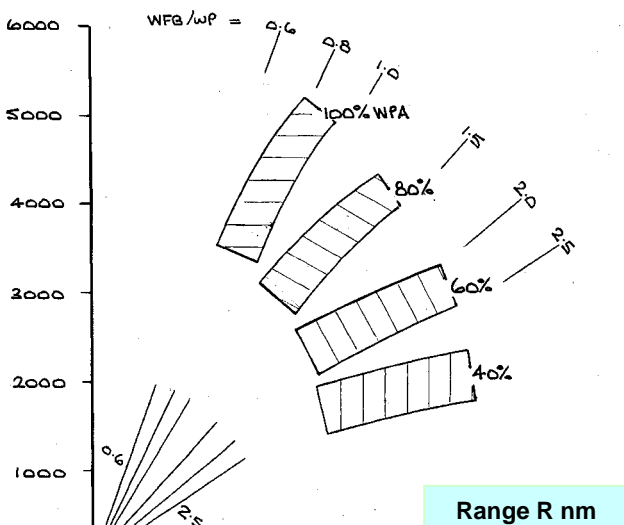


Fig. 2.1.7 PRE vs RANGE, BANDS FOR VARYING PAYLOAD FRACTION, FREIGHTERS, Constant WFB/WP (Radial lines)

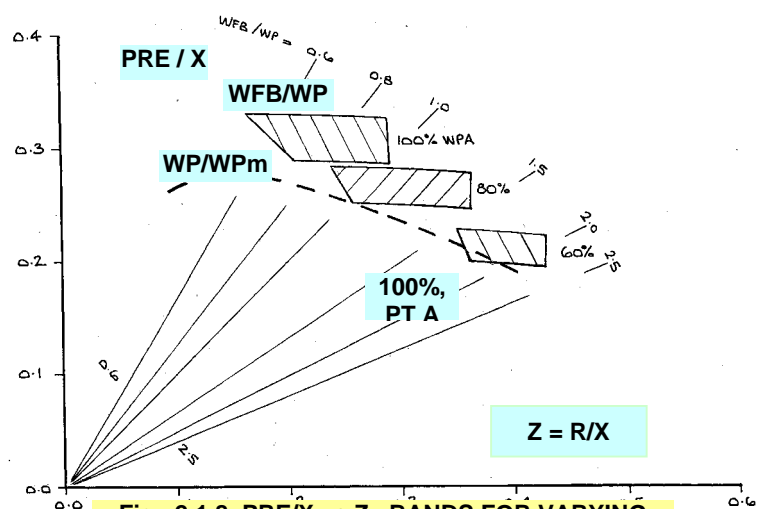


Fig. 2.1.8 PRE/X vs Z , BANDS FOR VARYING PAYLOAD FRACTION, FREIGHTERS, Civil Aircraft Pt A Trends, Constant WFB/WP (Radial lines)

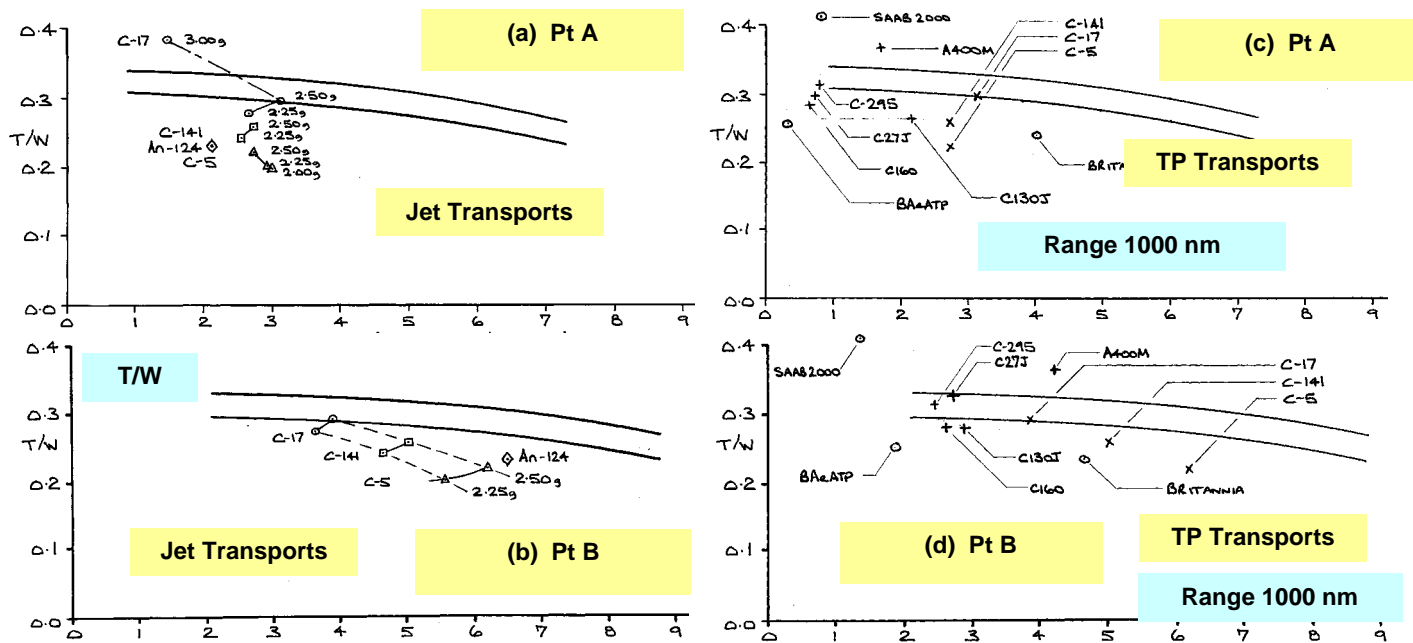


Fig. 2.1.9 T/W - RANGE, CIVIL PASSENGER AND FREIGHTER AIRCRAFT TRENDS AND MILITARY TRANSPORT AIRCRAFT

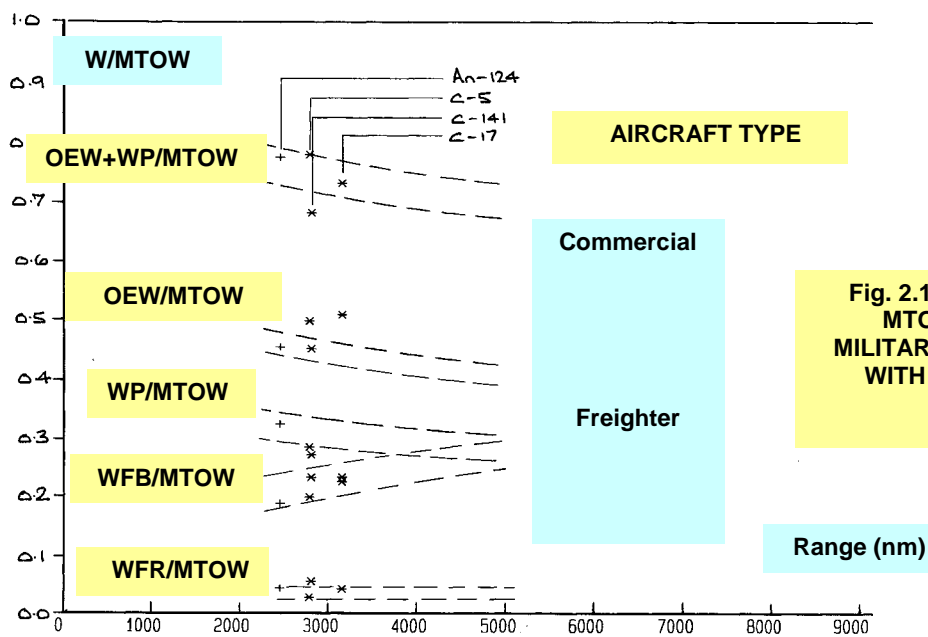


Fig. 2.1.10 WEIGHT RATIOS wrt MTOW v POINT A RANGE, MILITARY TRANSPORT AIRCRAFT WITH FREIGHTER AIRCRAFT TRENDS

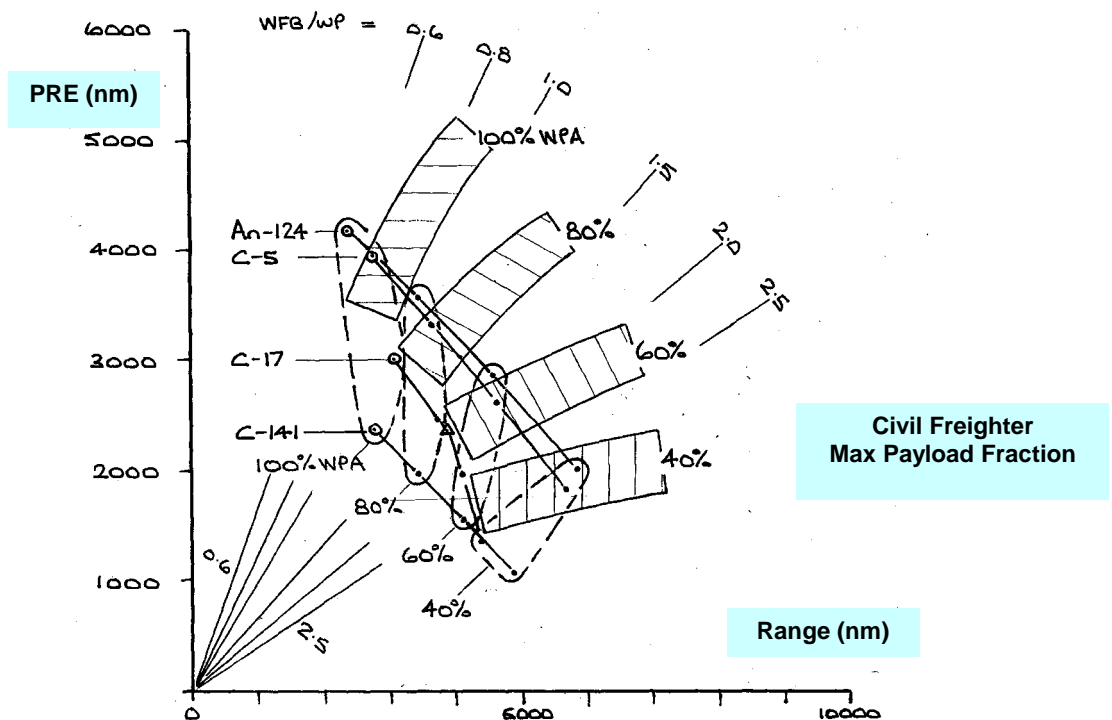


Fig. 2.1.11 PRE - RANGE, MILITARY TRANSPORTS, CIVIL FREIGHTER AIRCRAFT MAX PAYLOAD FRACTION TRENDS, CONSTANT WFB/WP (RADIAL LINES)

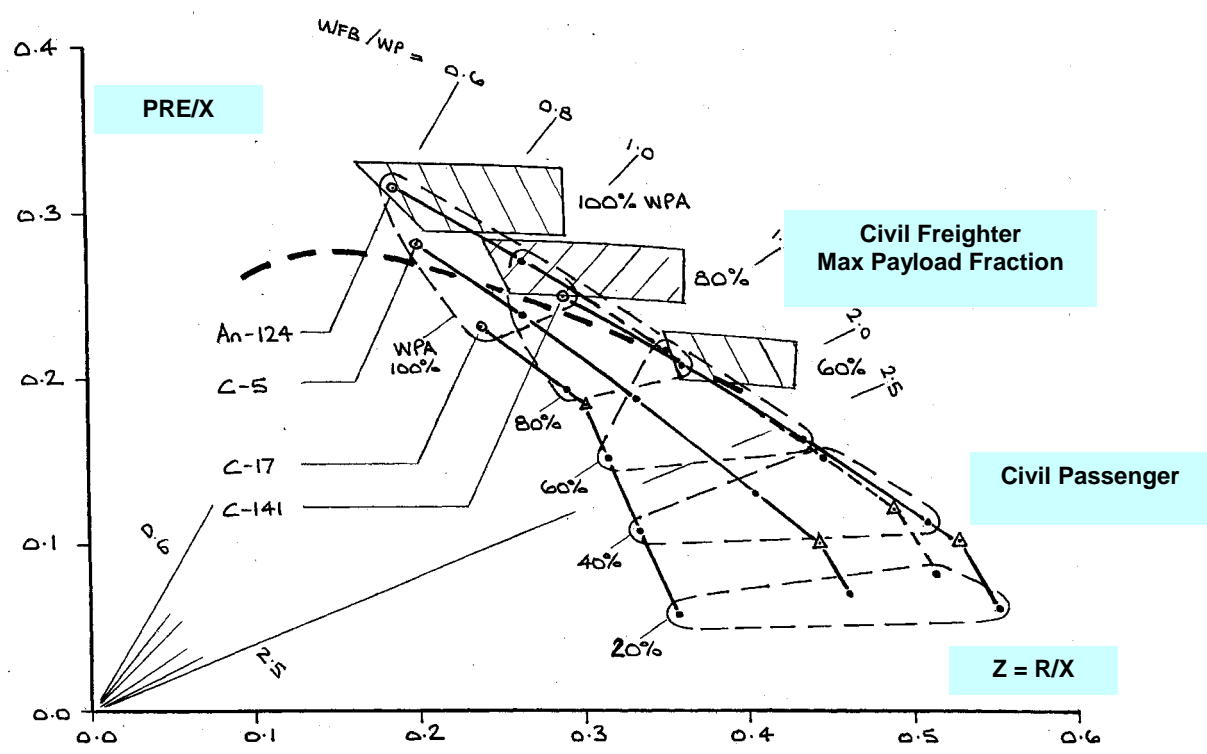


Fig. 2.1.12 PRE/X - Z, MILITARY TRANSPORTS, CIVIL PASSENGER AIRCRAFT POINT A TREND, CIVIL FREIGHTER AIRCRAFT MAX PAYLOAD FRACTION TRENDS, CONSTANT WFB/WP (RADIAL LINES)

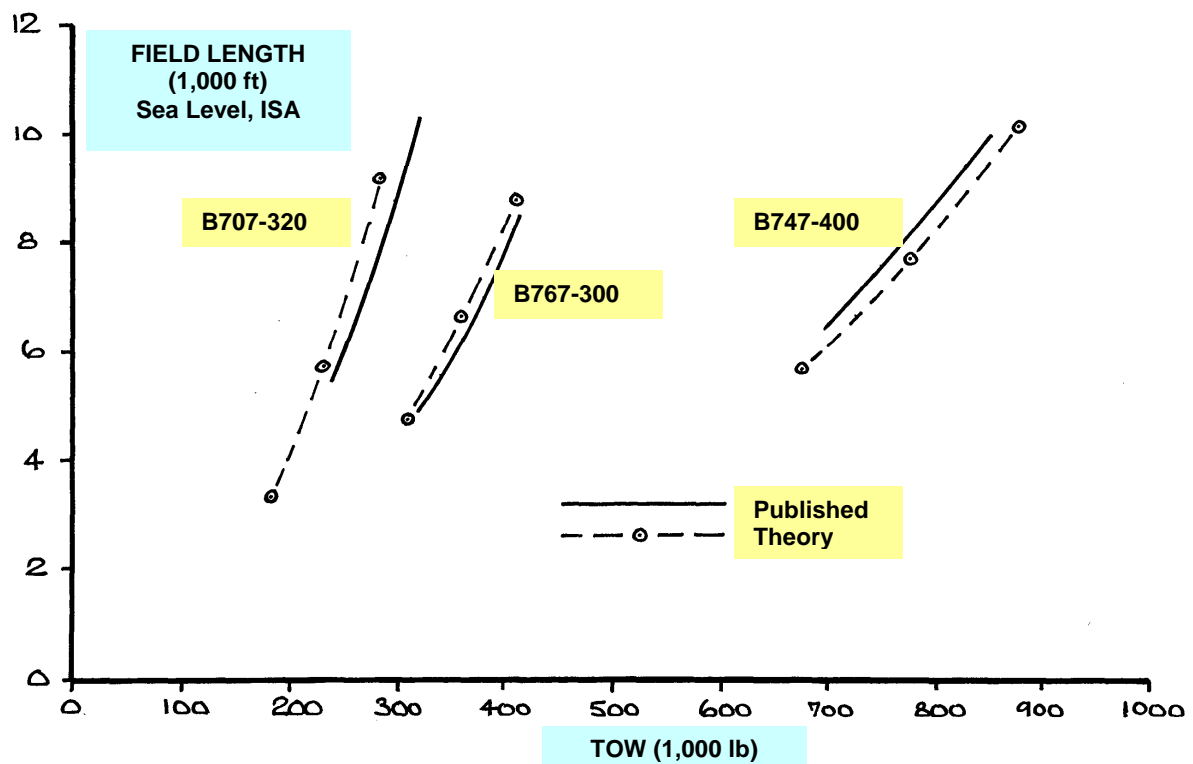


Fig. 2.3.1 TAKE-OFF FIELD LENGTH v TOW, THEORY and PUBLISHED DATA Sea Level, ISA

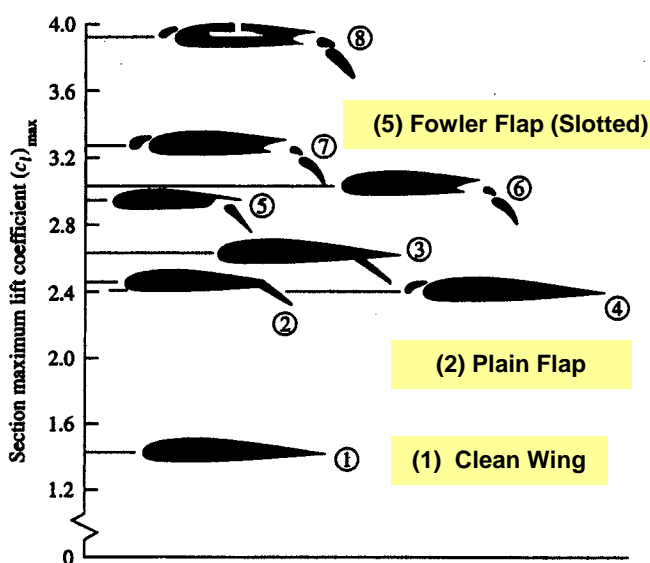


Fig. 4.1.1 HIGH-LIFT DEVICES (Anderson, Ref.17)

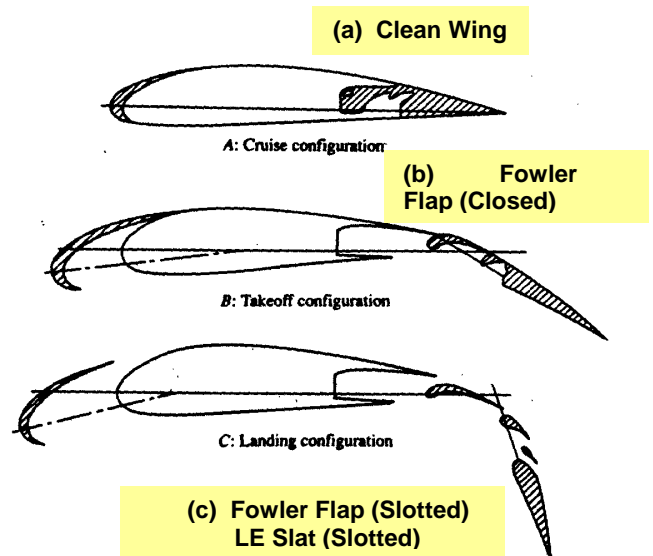
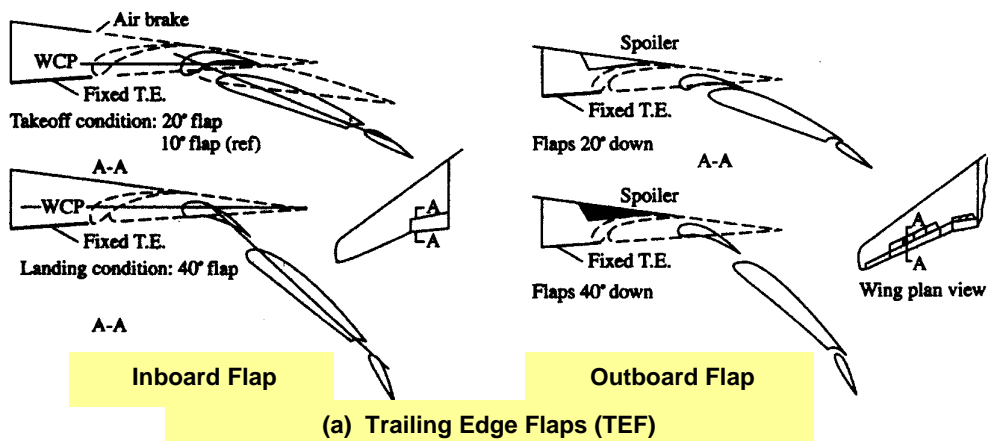


Fig. 4.1.2 HIGH-LIFT DEVICES (Ref.##)



3 • Airplane Design

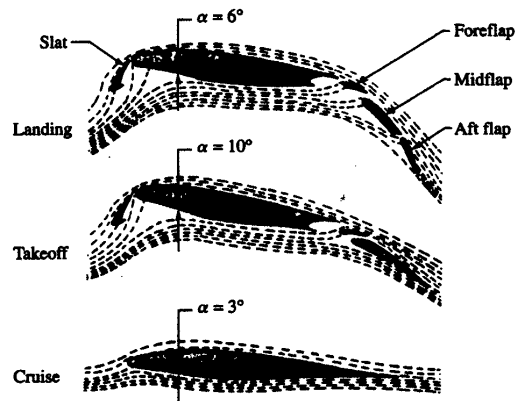
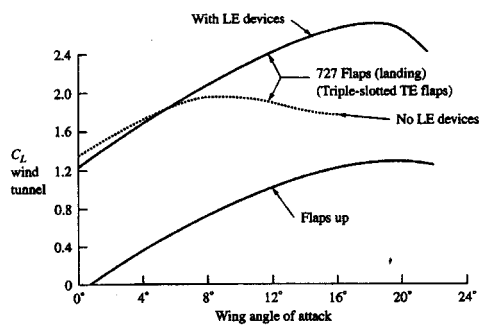
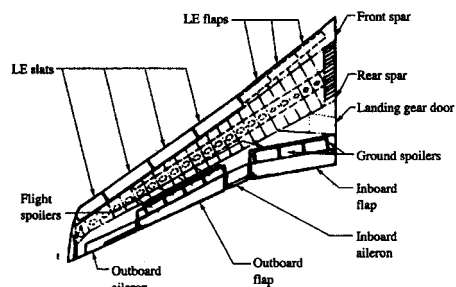
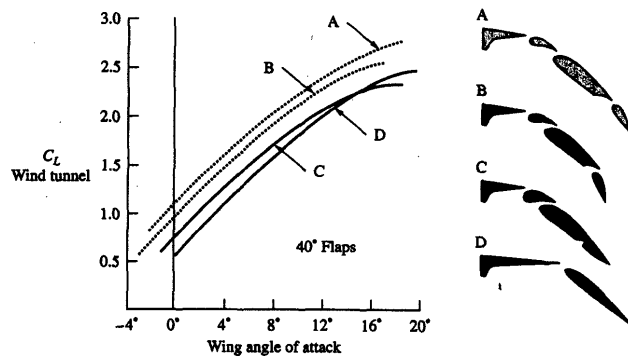
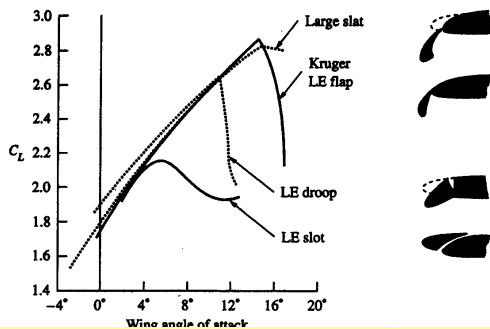
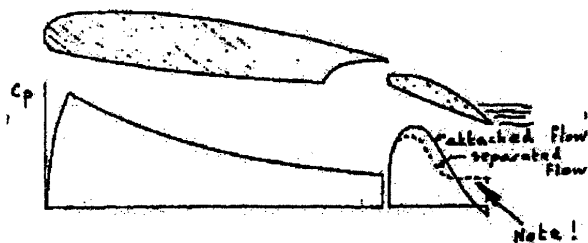
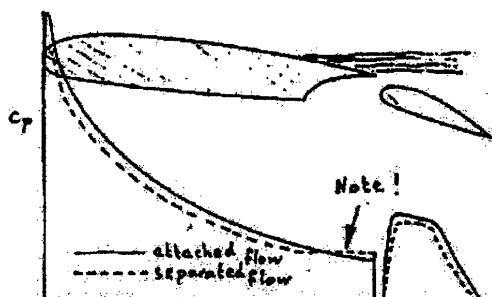


Fig. 4.1.3 HIGH-LIFT SYSTEM DEVELOPMENT FOR BOEING 727 (Ref. Anderson)

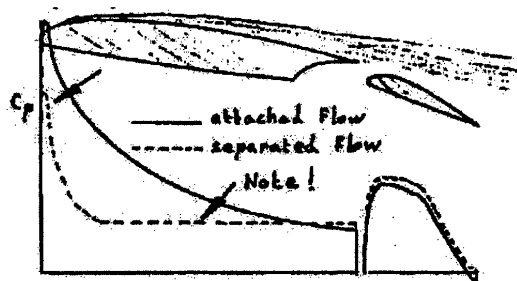
Without Leading Edge Device



(a) Trailing Edge Stall on Flap

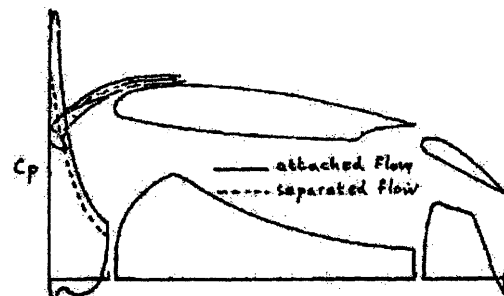


(b) Trailing Edge Stall on Main Component

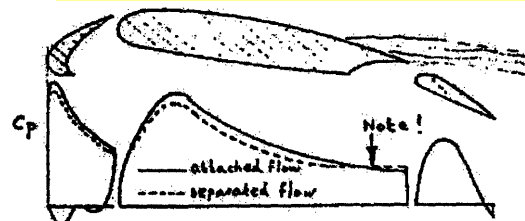


(c) Leading Edge Stall on Main Component

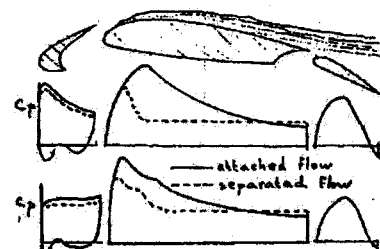
With Leading Edge Device



(d) Slat Stall



(e) Trailing Edge Stall on Main Component



(f) Leading Edge Stall on Main Component

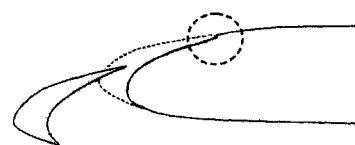
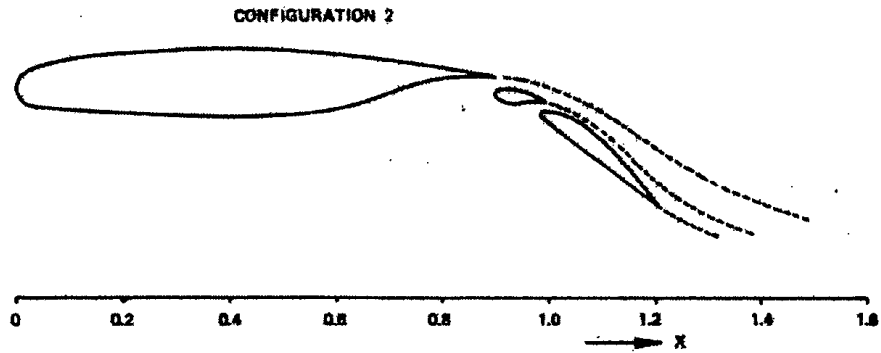
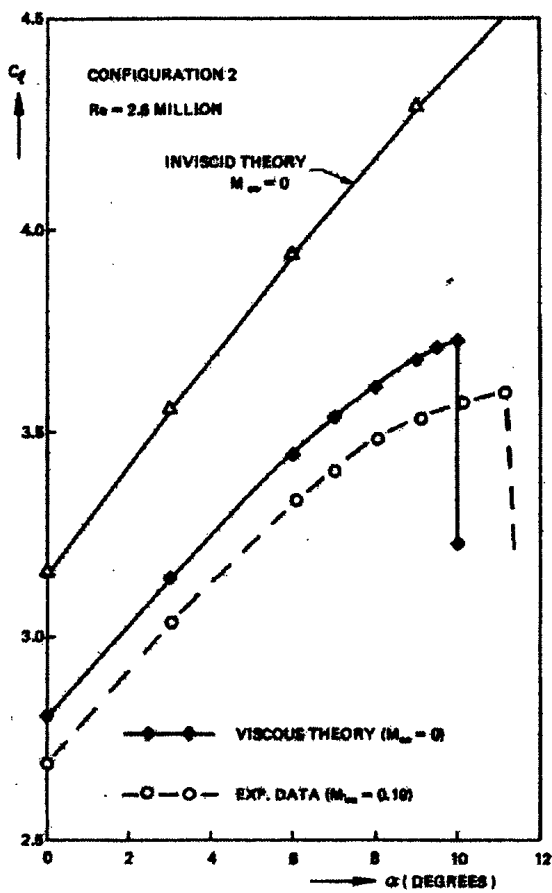


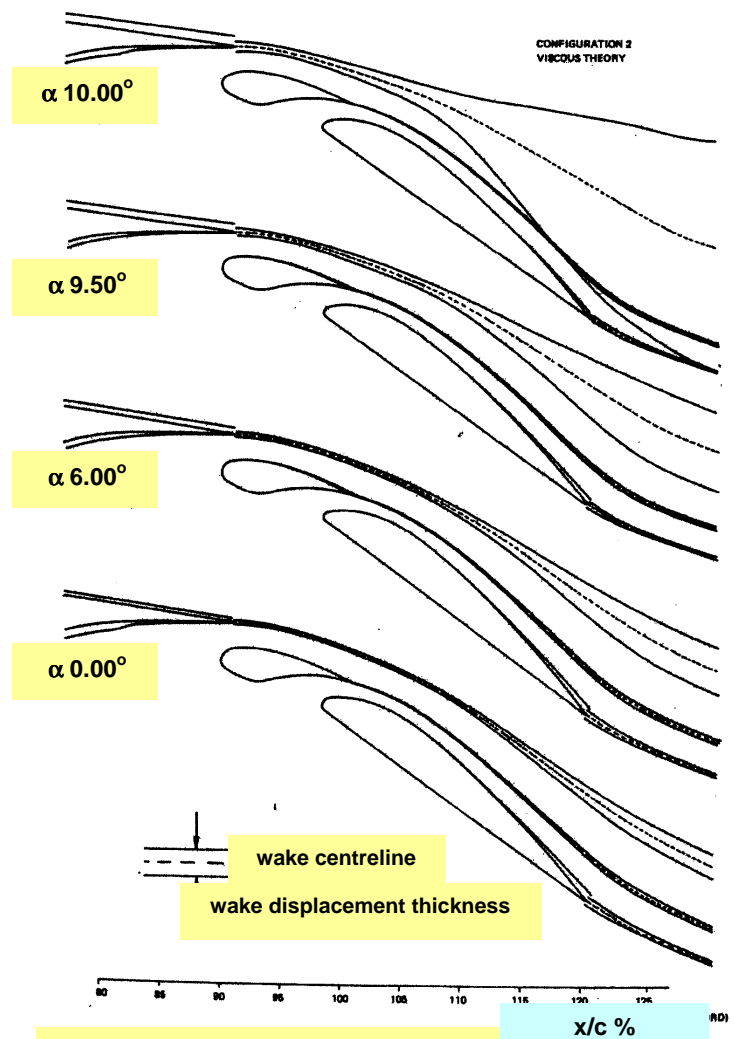
Fig. 4.1.4 TYPES OF FLOW SEPARATION ON WINGS WITH TEF (without and with LEF), (Ref. Obert)



(a) Fokker F-28 aerofoil section with $\delta_{TE} 42^\circ$



(b) $C_{LL} - \alpha$, Theory & Experiment



(c) Theoretical Wake Development

Fig. 4.1.5 FOKKER F-28 AEROFOIL SECTION WITH DOUBLE SLOTTED TEF (Ref. Obert)
EFFECT OF WAKE DEVELOPMENT, THEORY & EXPERIMENT

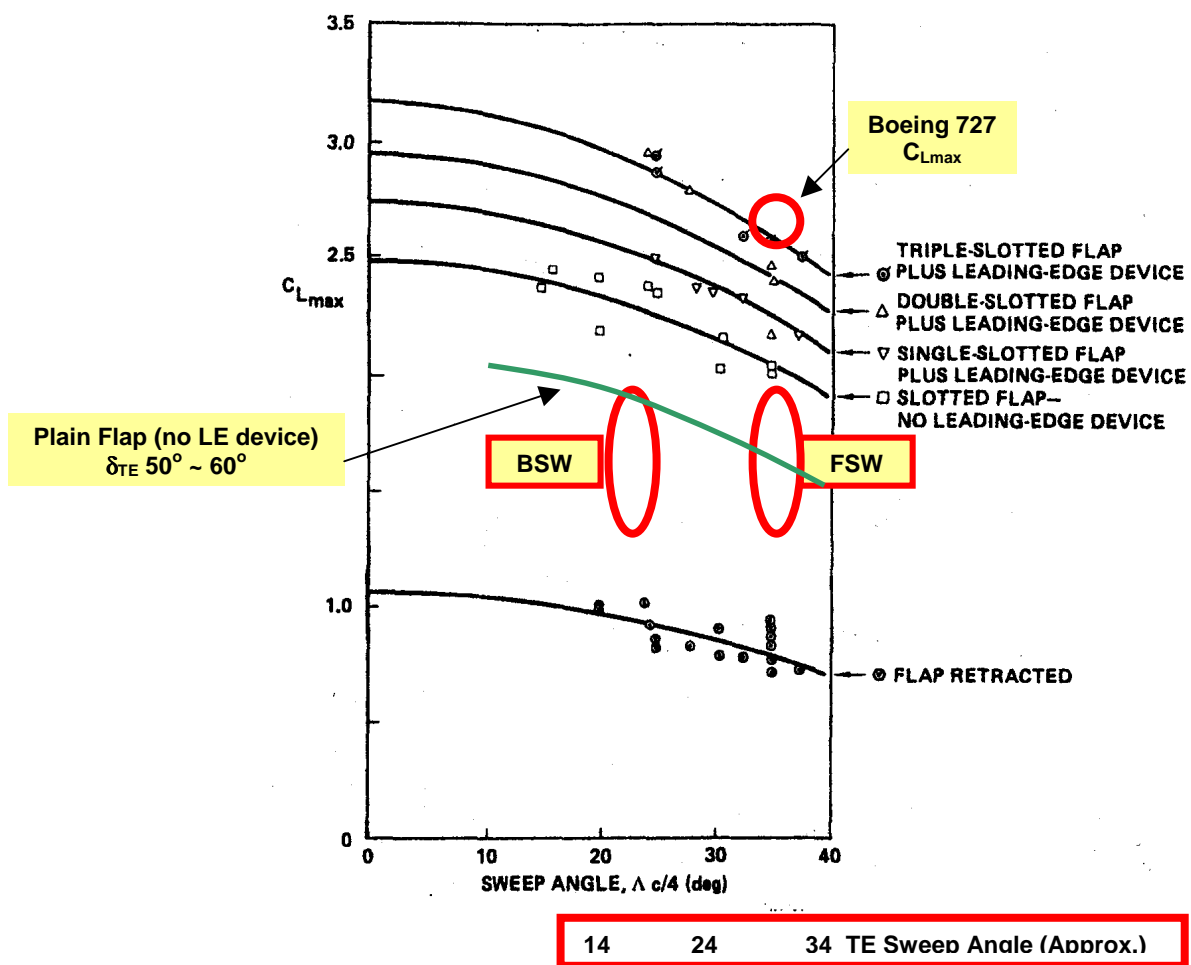


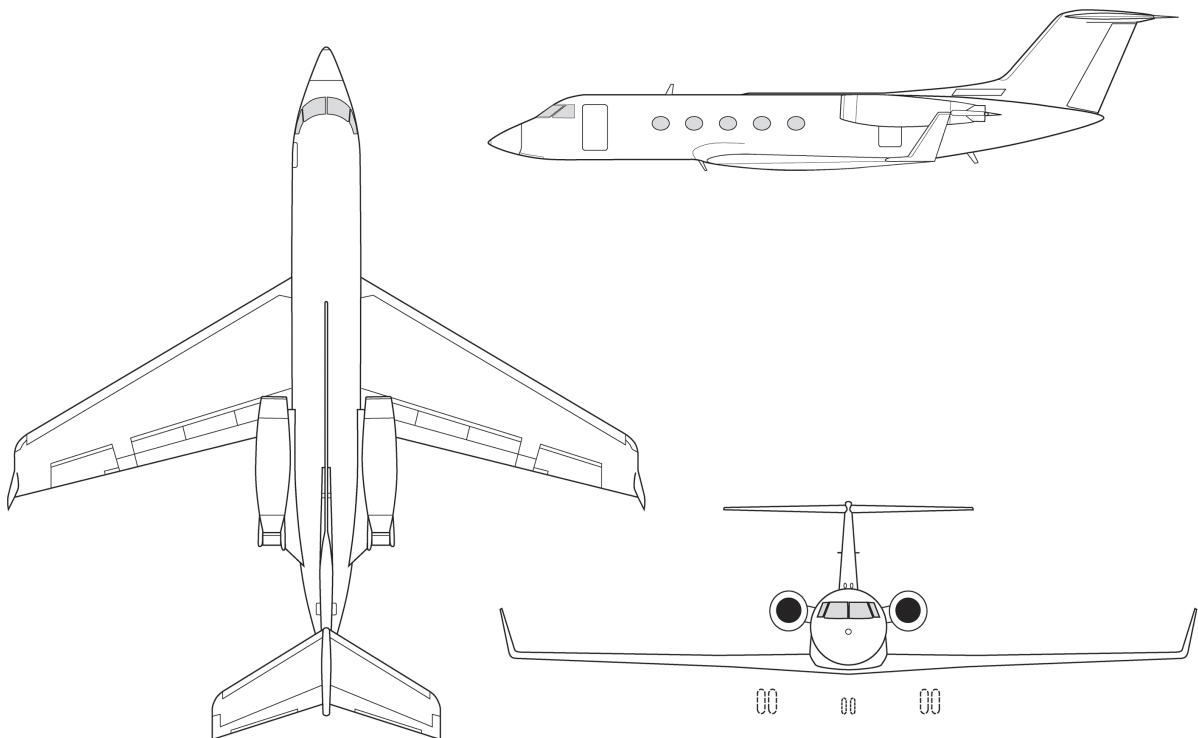
Fig. 4.1.6 STATISTICAL ANALYSIS OF MAXIMUM LIFT COEFFICIENT FOR TRANSPORT AIRCRAFT & FSW REQUIREMENTS (Based on NASA & Boeing Work)
Note the Derived Approximate Correlation with TE Sweep.

General characteristics

- **Crew:** Two or three
- **Capacity:** 19 passengers (standard seating)
- **Length:** 83 ft 1 in (25.32 m)
- **Wingspan:** 77 ft 10 in (23.72 m)
- **Height:** 24 ft 4½ in (7.43 m)
- **Wing area:** 934.6 sq ft (86.83 m²)
- **Aspect ratio:** 6.0:1
- **Empty weight:** 38,000 lb (17,236 kg)
- **Max takeoff weight:** 69,700 lb (31,615 kg)
- **Powerplant:** 2× [Rolls-Royce Spey RB.163 Mk 511-8 Turbofan](#), 11,400 lbf (50.7 kN) each

Performance

- **Maximum speed:** 576 mph (501 knots, 928 km/h) (max cruise)
- **Cruise speed:** 508 mph (442 knots, 818 km/h) (long range cruise)
- **Stall speed:** 121 mph (105 knots, 194 km/h)
- **Range:** 4,200 mi (3,650 [nmi](#), 6,760 km) (eight passengers, IFR reserves)
- **Service ceiling:** 45,000 ft (13,716 m)



Dryden Flight Research Center
Gulfstream III

March 2009

Fig. 4.1.7 GULFSTREAM III, CURRENT ADAPTIVE WING RESEARCH
General Assembly and Performance Data

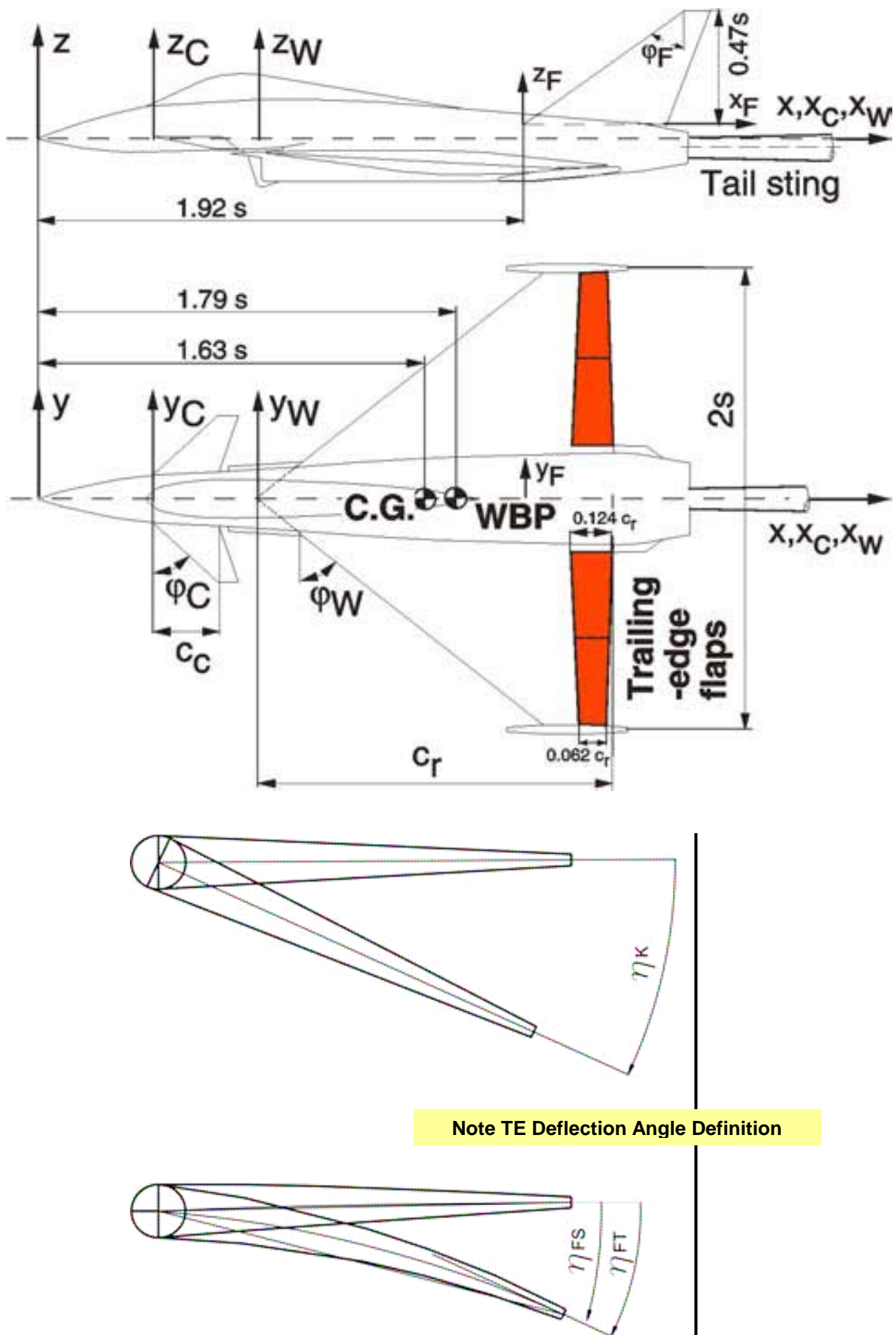
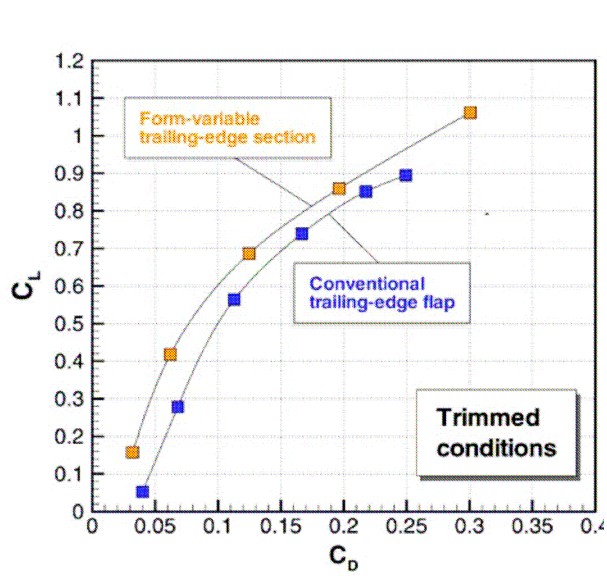
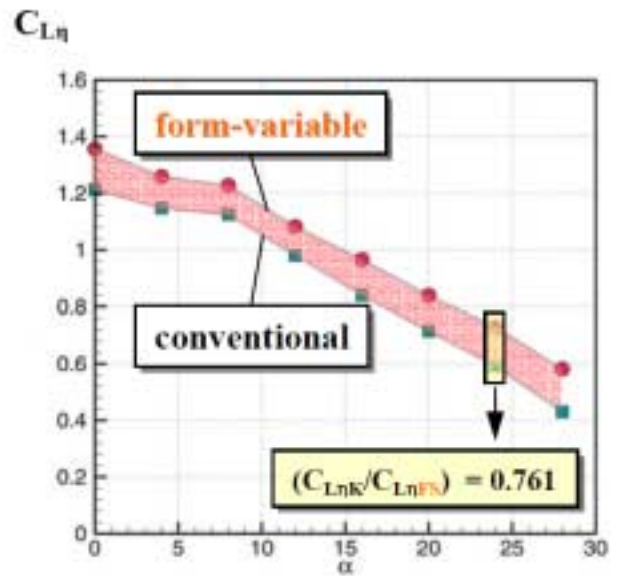


Fig. 4.1.8 TYPICAL CURRENT COMBAT AIRCRAFT GENERAL ASSEMBLY
Recent Research on Adaptive Wing Technology (Ref. Breitsamter)

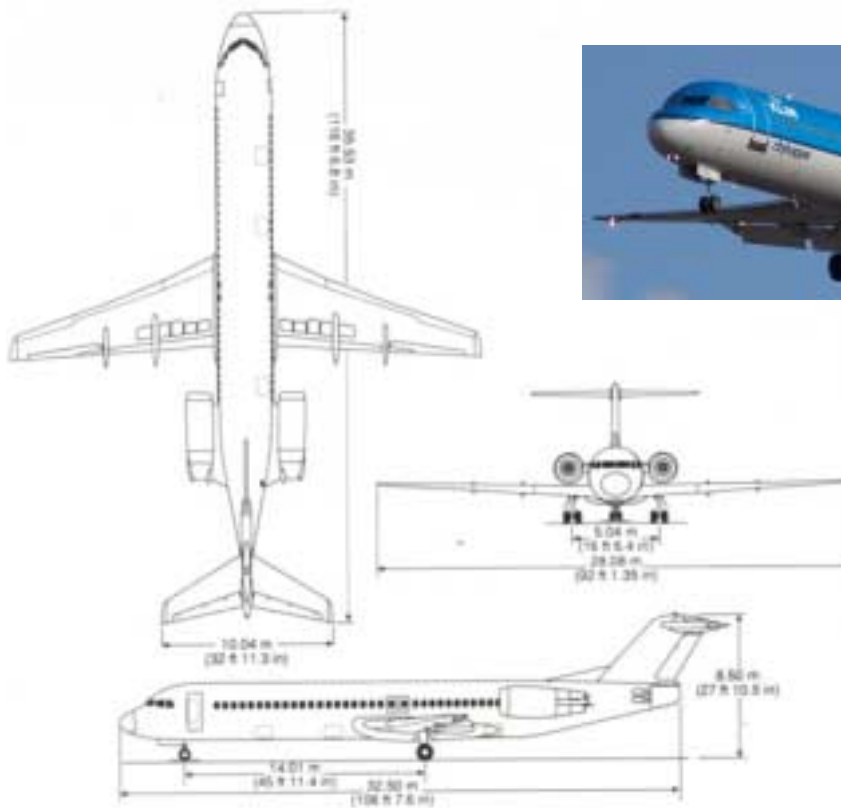


(a) $C_L - C_D$, (Trimmed)



(b) FLAP EFFICIENCY - α

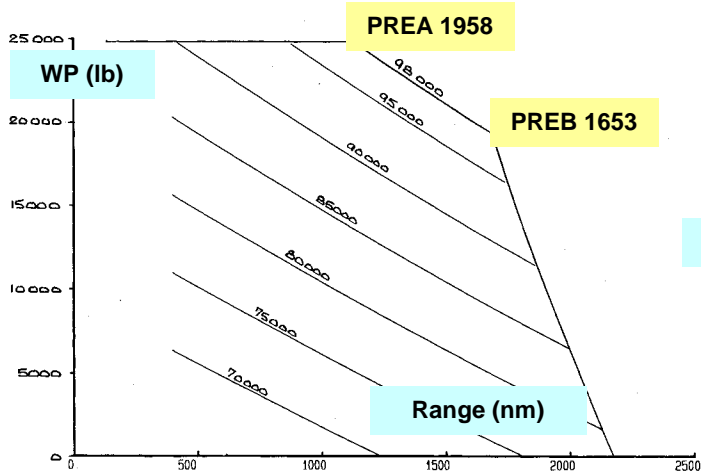
Fig. 4.1.9 "FORM VARIABLE TRAILING-EDGE SECTION" v CONVENTIONAL TRAILING EDGE FLAP



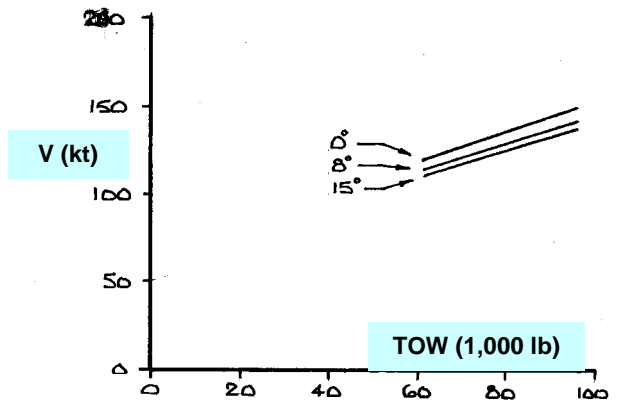
Nominal Values

Wing Reference Area 1070 ft²
 Wing Span 92.1 ft
 MTOW 101,000 lb
 Range 2100 nm

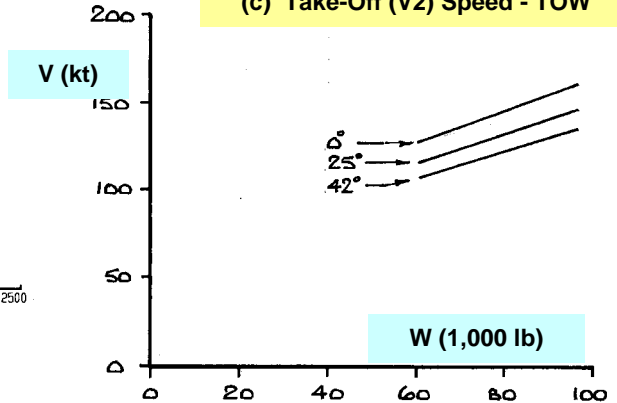
(a) General Assembly



(b) Payload - Range



(c) Take-Off (V2) Speed - TOW



(d) Landing Speed - Weight

Fig. 4.2.1 FOKKER 100, AR = 8, GENERAL ASSEMBLY, PAYLOAD – RANGE, TAKE-OFF & LANDING SPEEDS - TOW

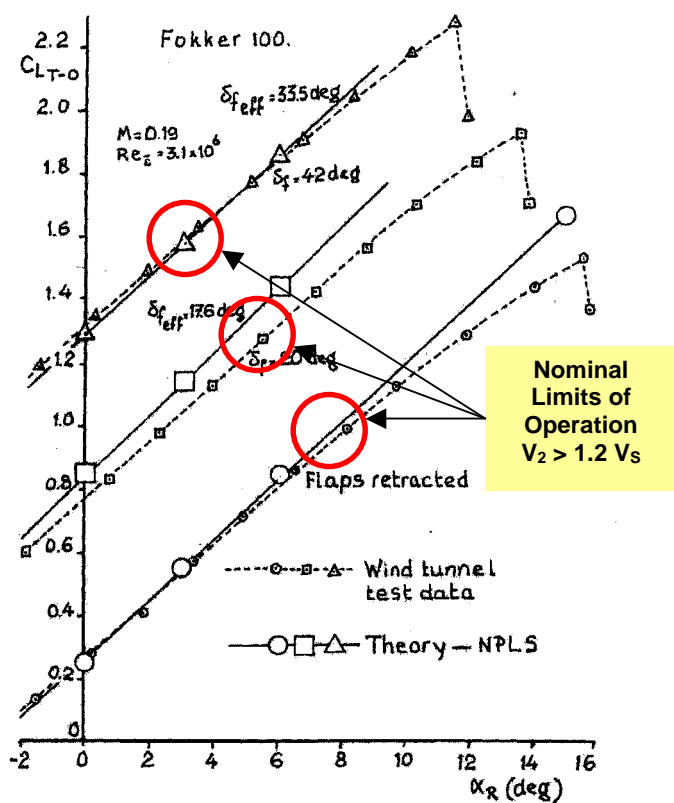


Fig. 4.2.2 $C_{L(T/O)} - \alpha$, FOKKER 100 (Tail Off), CONVENTIONAL (PART-SPAN) FLAPS

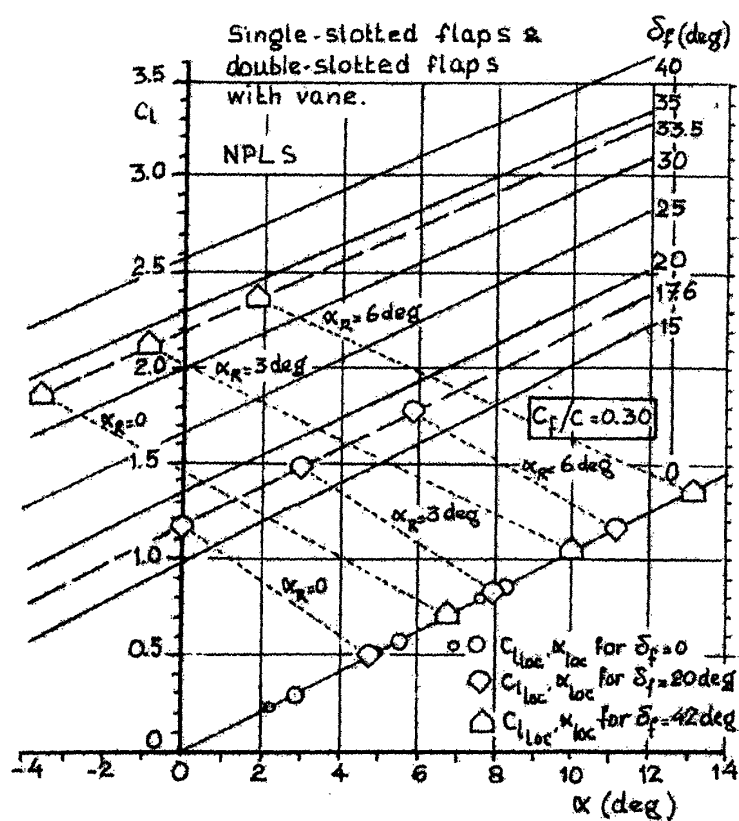


Fig. 4.2.3 $C_{LL} - \alpha$ (SECTION LIFT), FOKKER 100, SINGLE and DOUBLE SLOTTED FLAPS

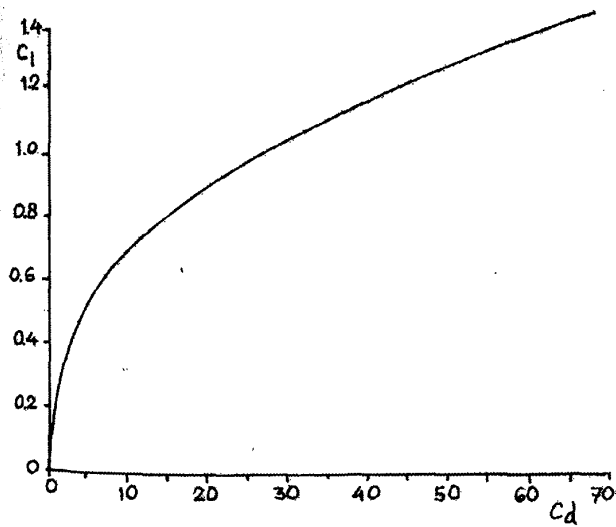


Fig. 4.2.4 $C_{LL} - C_{DL}$ (SECTIONAL PROPERTIES, FOKKER 100)

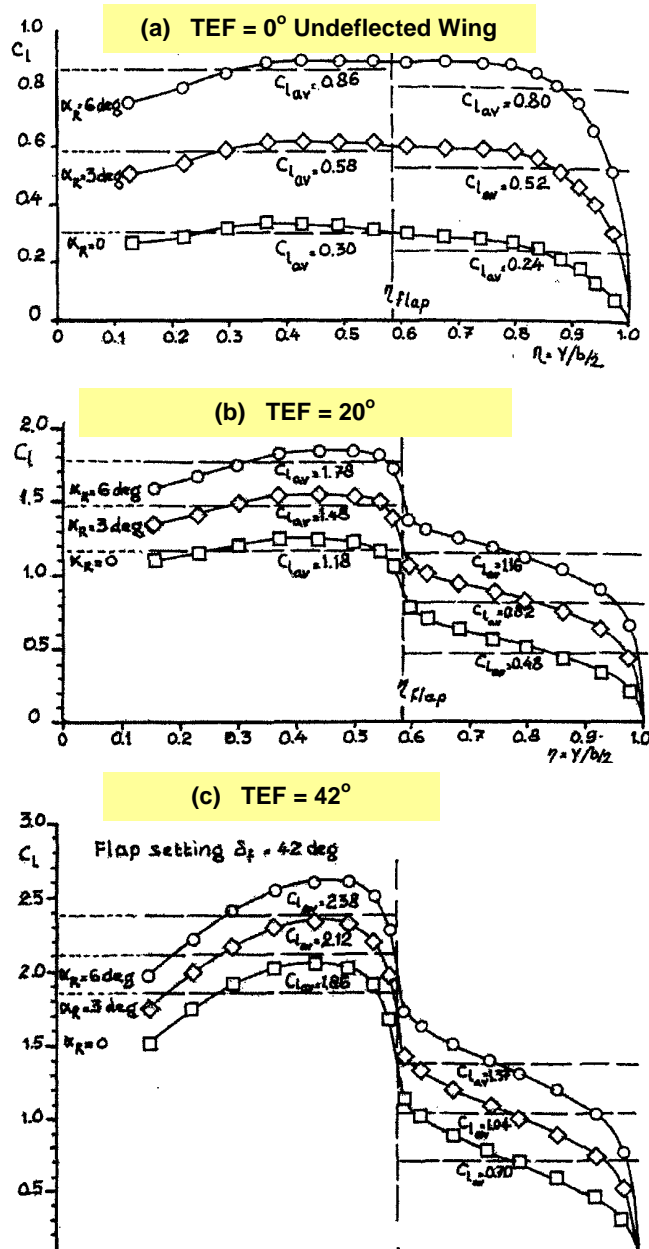


Fig. 4.2.5 FOKKER 100, CONVENTIONAL (PART-SPAN) FLAPS, Spanwise Lift Distributions

Figure 27.17 - Spanwise lift distribution with flap setting $\delta_f = 42$ deg

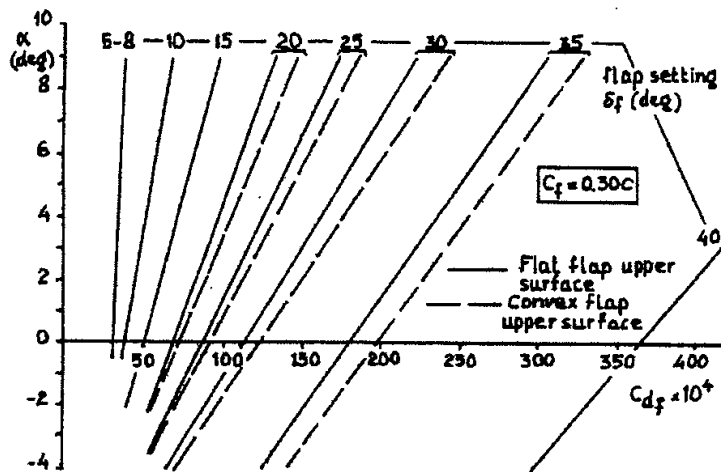


Figure 27.20 - Drag due to flap deflection, single-slotted flaps.
 (a) Single Slotted Flaps Fokker Rep. A - 166 and A - 173.

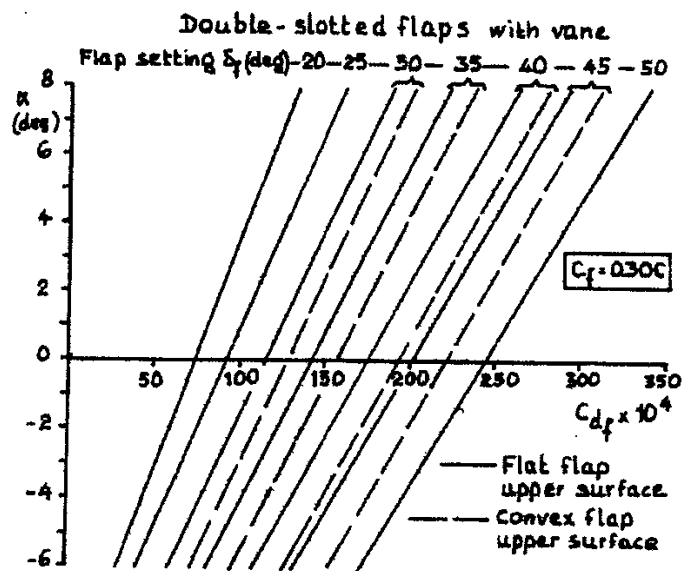
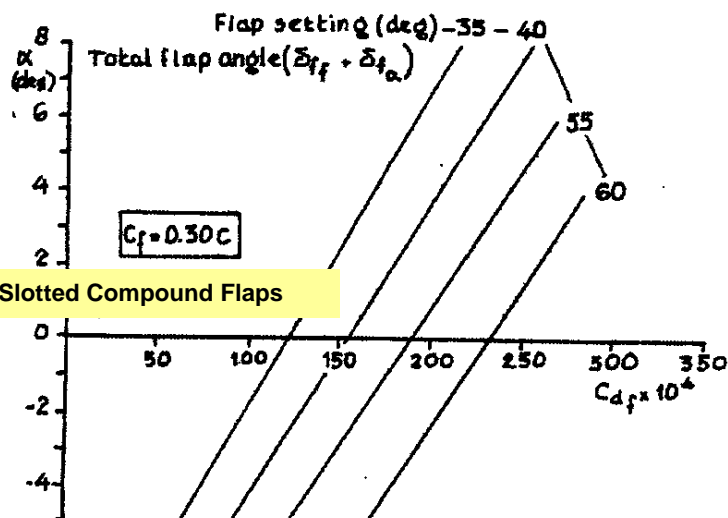


Figure 27.21 - Drag due to flap deflection, double-slotted flaps with vane.
 Source: Fokker Rep. A - 166 and A - 173.

(b) Double Slotted Flaps with Vane



(c) Double Slotted Compound Flaps

Figure 27.22 - Drag due to flap deflection, double-slotted compound flaps.

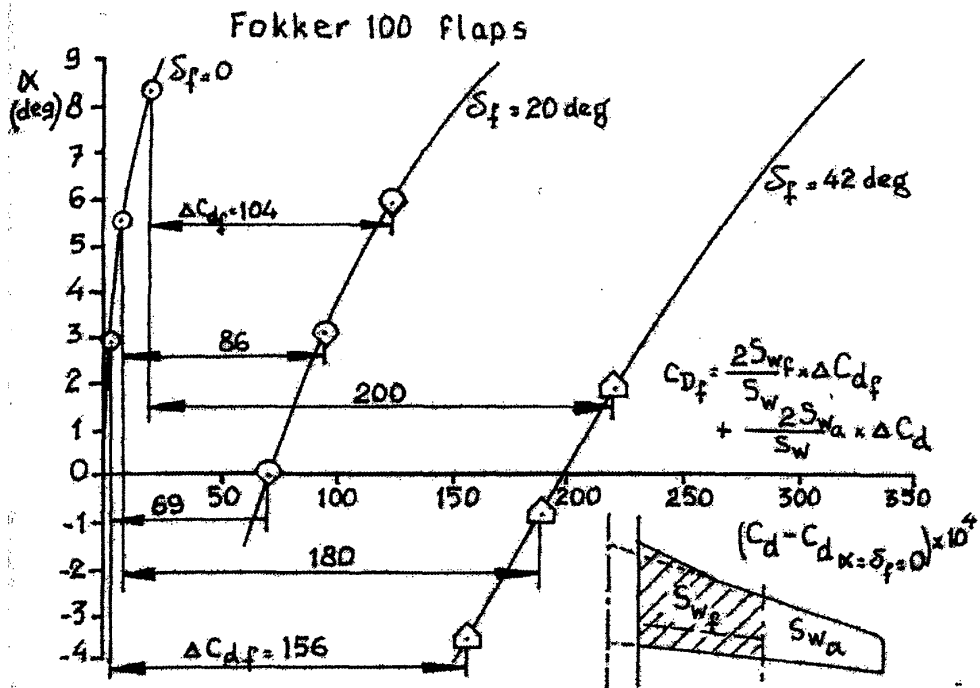


Fig. 4.2.7 DRAG DUE TO FLAP DEFLECTION, FOKKER 100

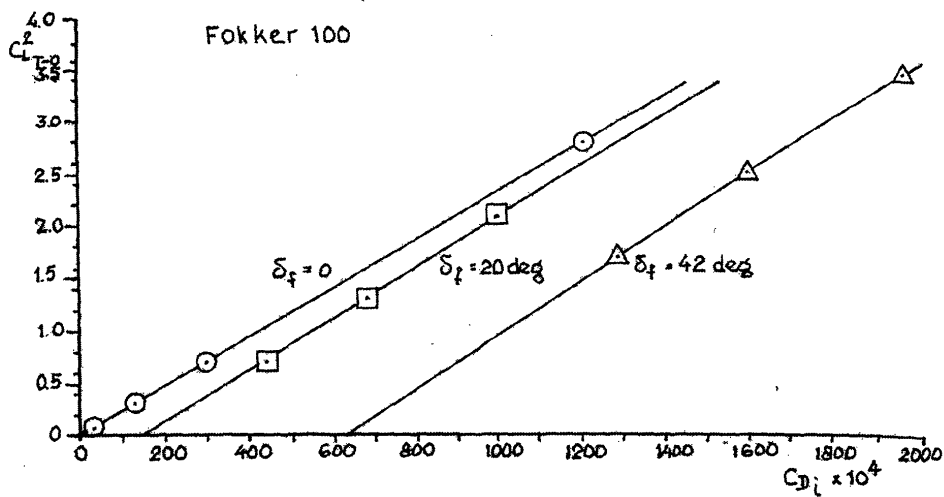


Fig. 4.2.8 $C_L^2 - C_{D_i}$, FOKKER 100, EFFECT OF FLAP ANGLE

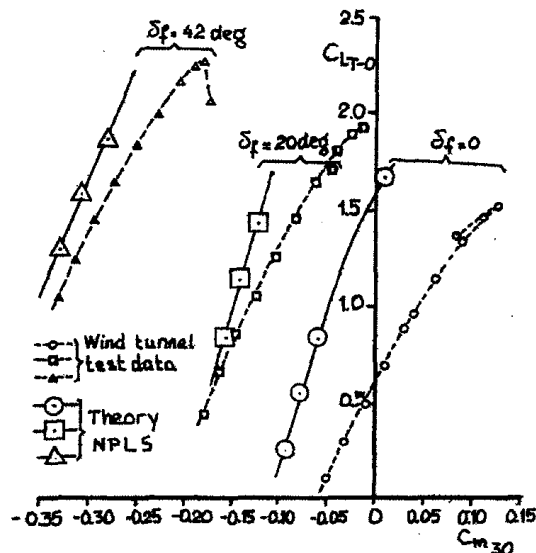


Figure 27.25 - Tail-off pitching moment curves. C.G. at 30% m.a.c.

Fig. 4.2.9 $C_m - C_L$ (TAIL OFF), c.g. at 30% mac, FOKKER 100, EFFECT OF FLAP ANGLE

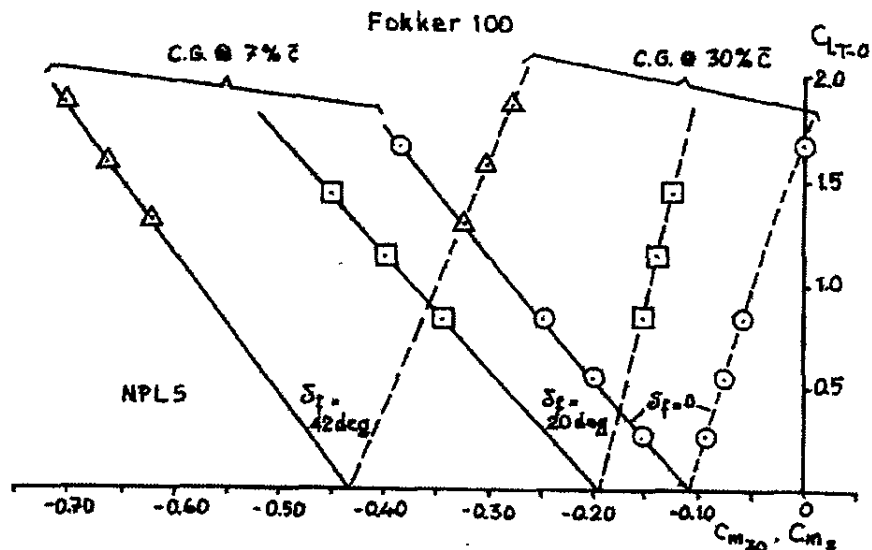


Fig. 4.2.10 $C_m - C_L$ (TAIL OFF), c.g. at 7% and 30% mac, FOKKER 100, EFFECT OF FLAP ANGLE

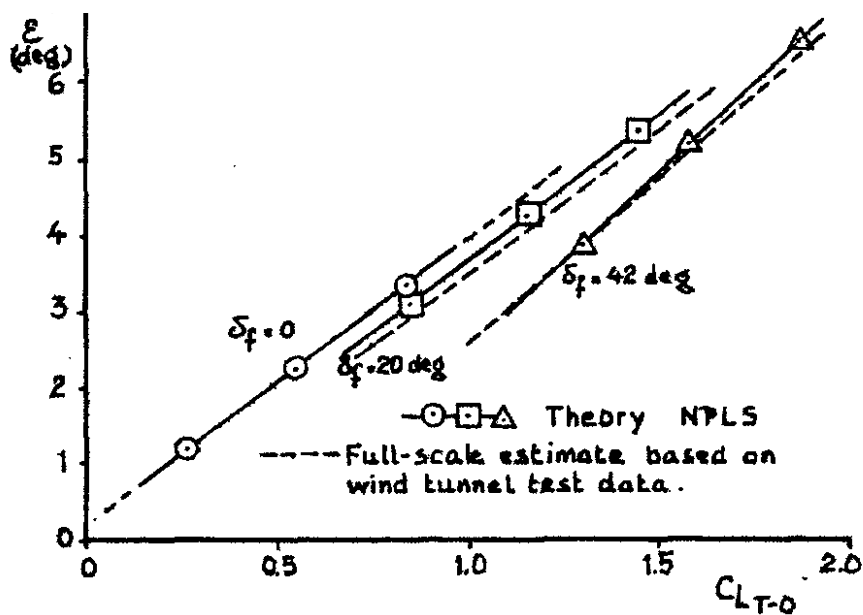


Fig. 4.2.11 AVERAGE DOWNWASH - C_L , FOKKER 100, EFFECT OF FLAP ANGLE

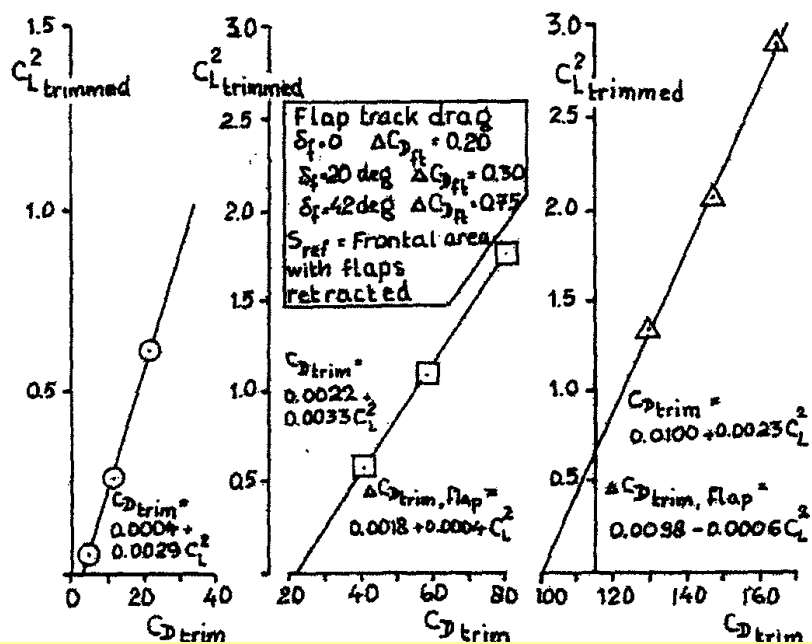


Fig. 4.2.12 TRIM DRAG - C_L^2 , FOKKER 100, EFFECT OF FLAP ANGLE

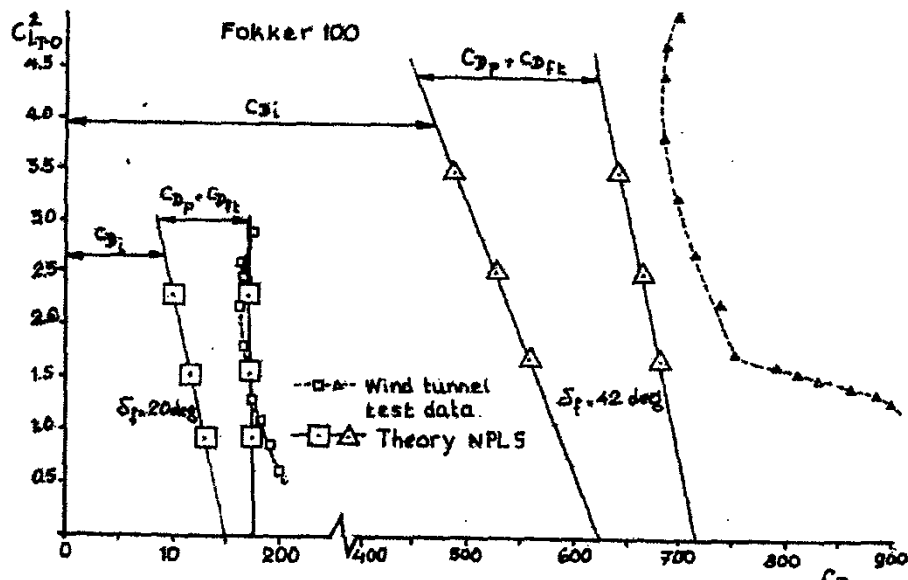
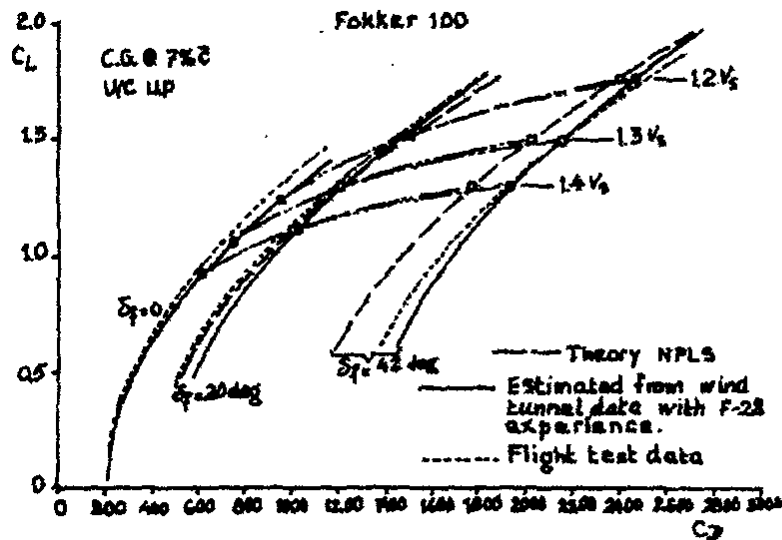


Fig. 4.2.13 DRAG DUE TO FLAP (TAIL OFF), FOKKER 100



Fokker 100 low-speed drag polars. Source: Fokker Reports A-166 and A-173

Fig. 4.2.14 $C_L - C_D$, LOW SPEED, FOKKER 100
THEORY (NPLS) and ESTIMATIONS FROM WIND TUNNEL and FLIGHT TEST, EFFECT OF FLAP

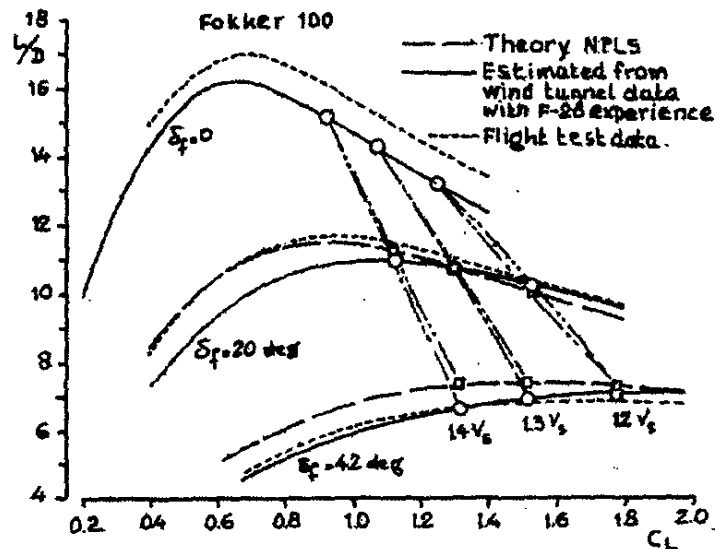


Fig. 4.2.15 $L/D - C_L$, LOW SPEED, FOKKER 100
THEORY (NPLS) and ESTIMATIONS FROM WIND TUNNEL and FLIGHT TEST, EFFECT OF FLAP

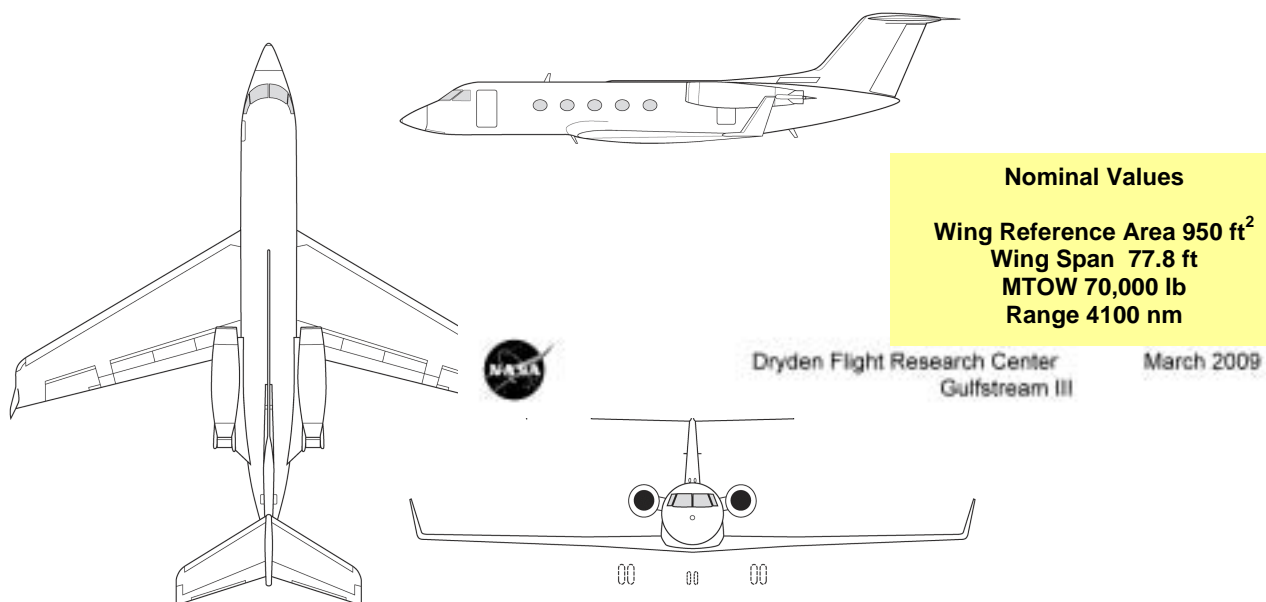
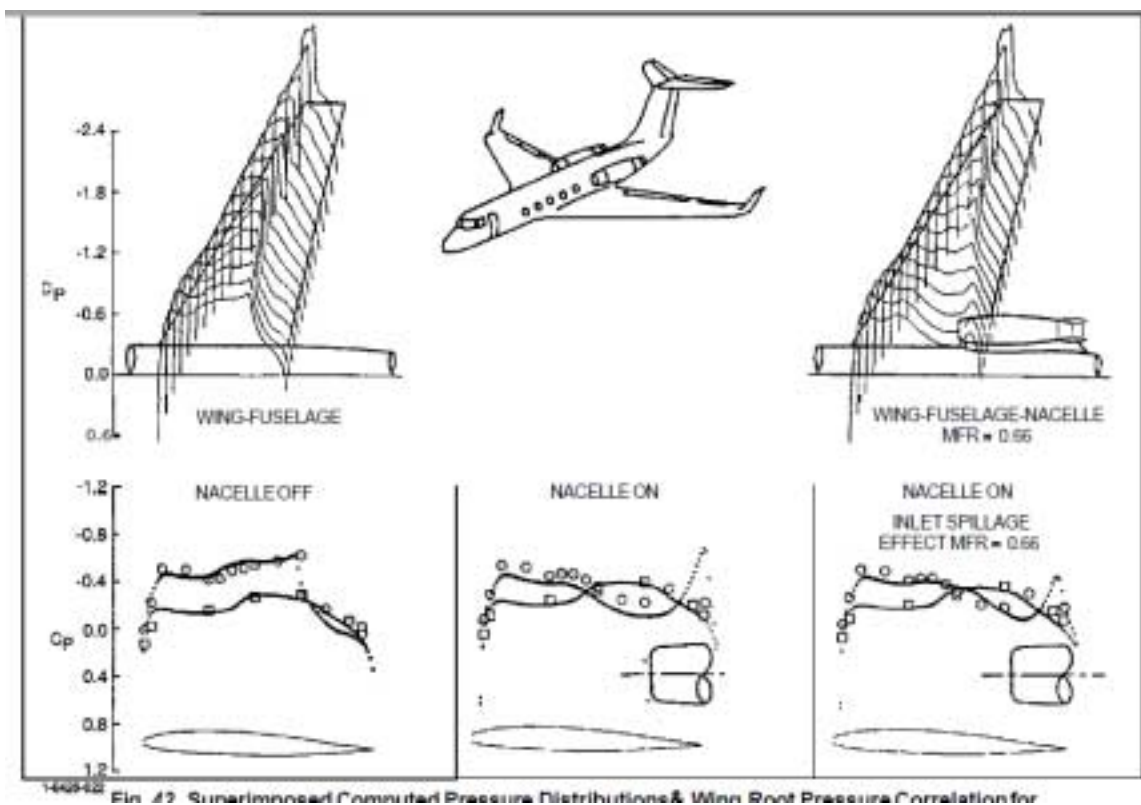
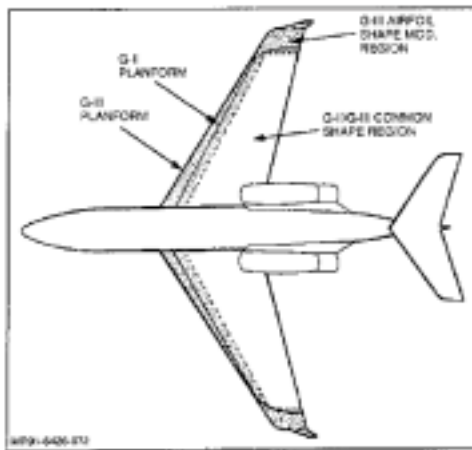


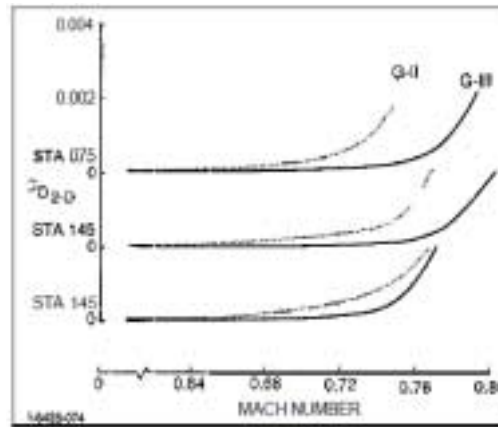
Fig. 4.3.1. GULFSTREAM III GA



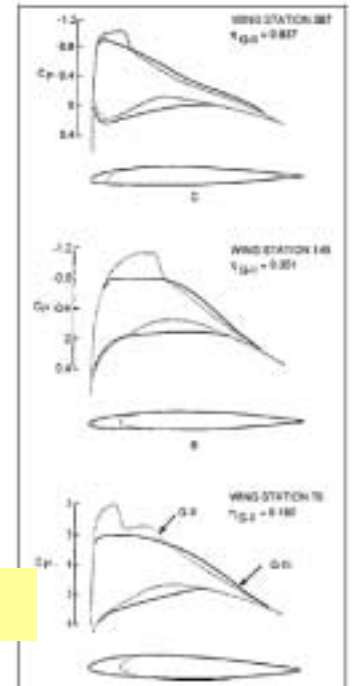
**Fig.4.3.2. CHORDWISE PRESSURE DISTRIBUTIONS, G-III, M 0.85, (BOPPE, C.W.) 1992
EFFECT OF NACELLE and INLET SPILLAGE**



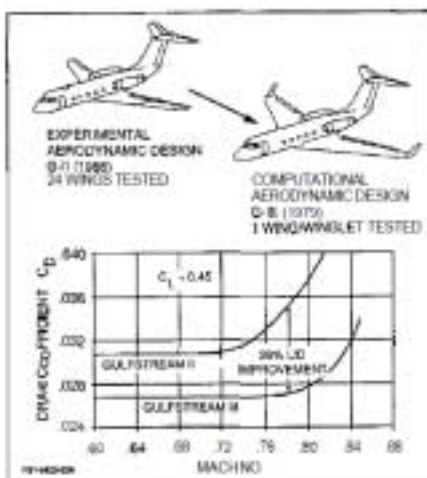
(a) Planform Development



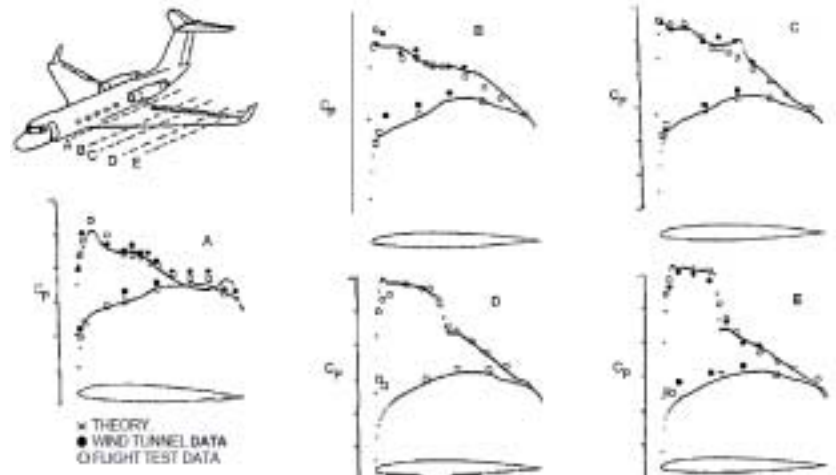
(b) Drag Divergence M Improvements



(c) Aerofoil Shape & Cp Distbn Refinements



(a) $C_D - M$ Comparison



(b) Chordwise C_p Distbns

Fig.4.3.4. G-II to G-III WING DEVELOPMENT, M 0.78, α 4° (BOPPE, C.W.) 1992

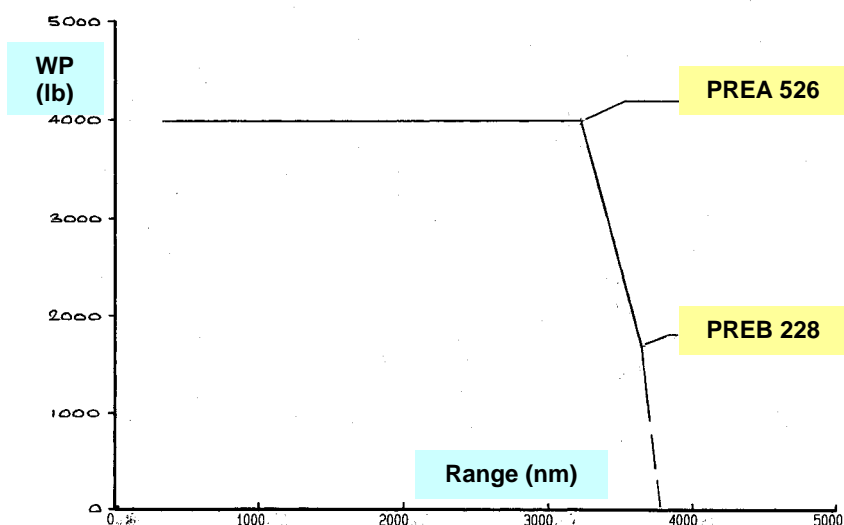


Fig.4.4.1. GULFSTREAM G-III PAYLOAD - RANGE

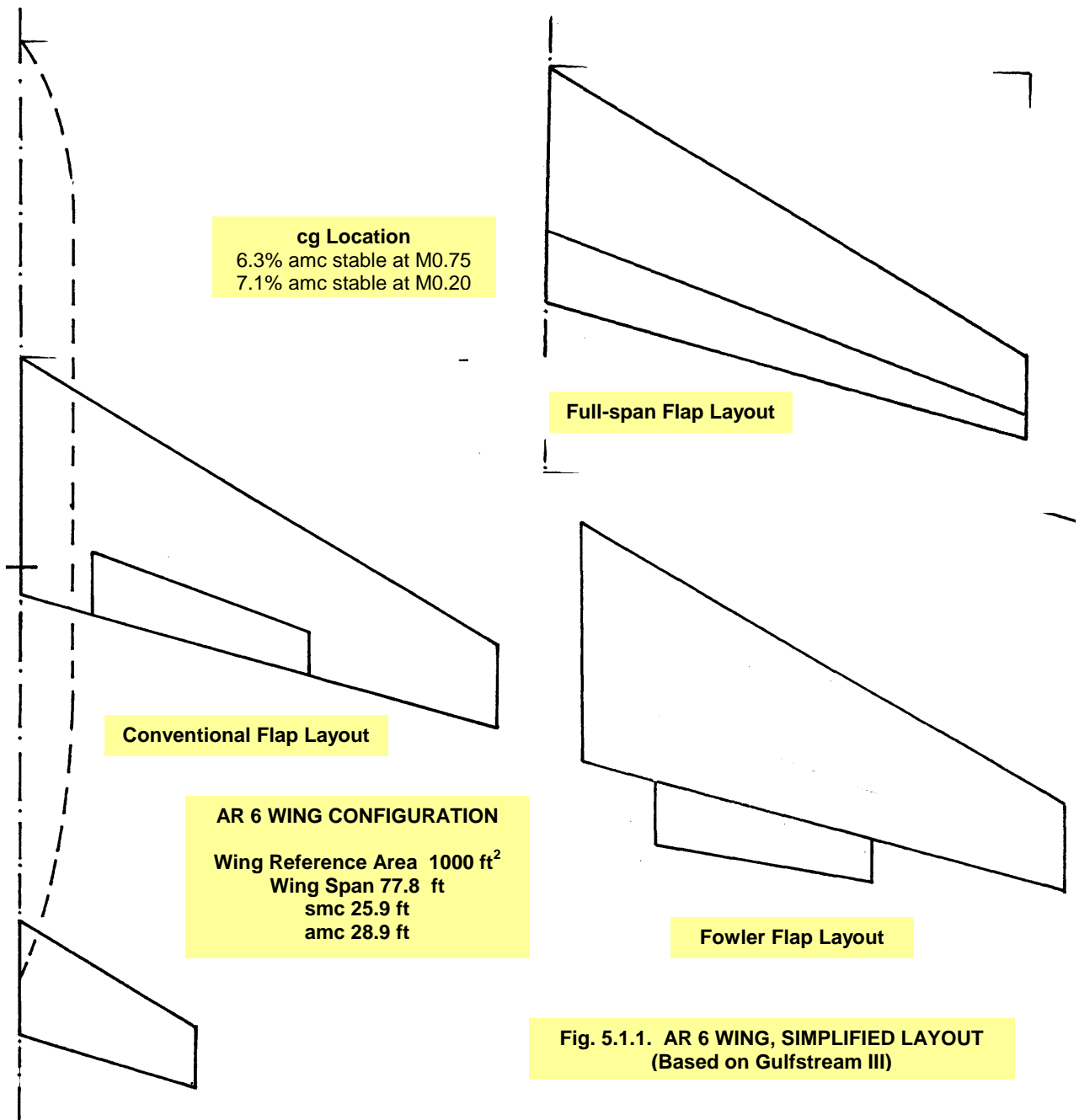


Fig. 5.1.1. AR 6 WING, SIMPLIFIED LAYOUT
 (Based on Gulfstream III)

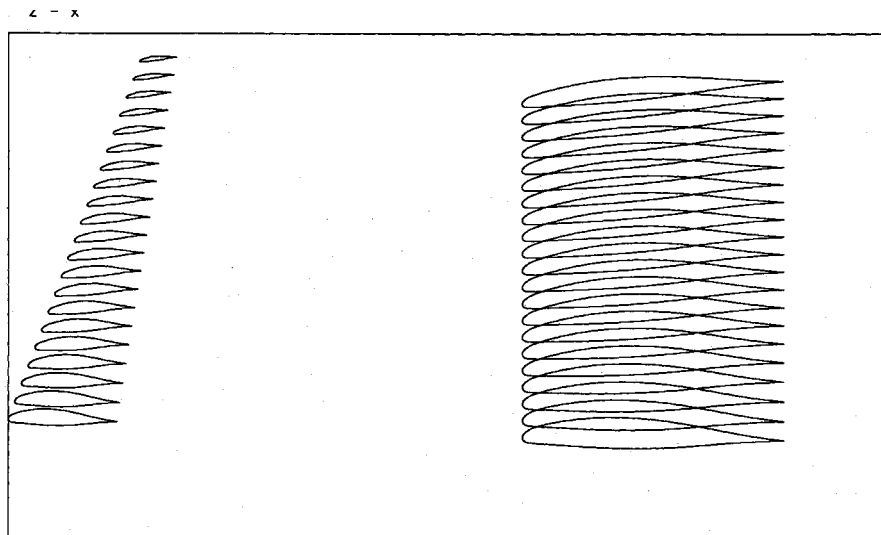


Fig. 5.1.2. AR 6 SECTION CAMBER and TWIST DISTRIBUTION
M 0.75, C_m 0.0, C_L 0.5 DESIGN

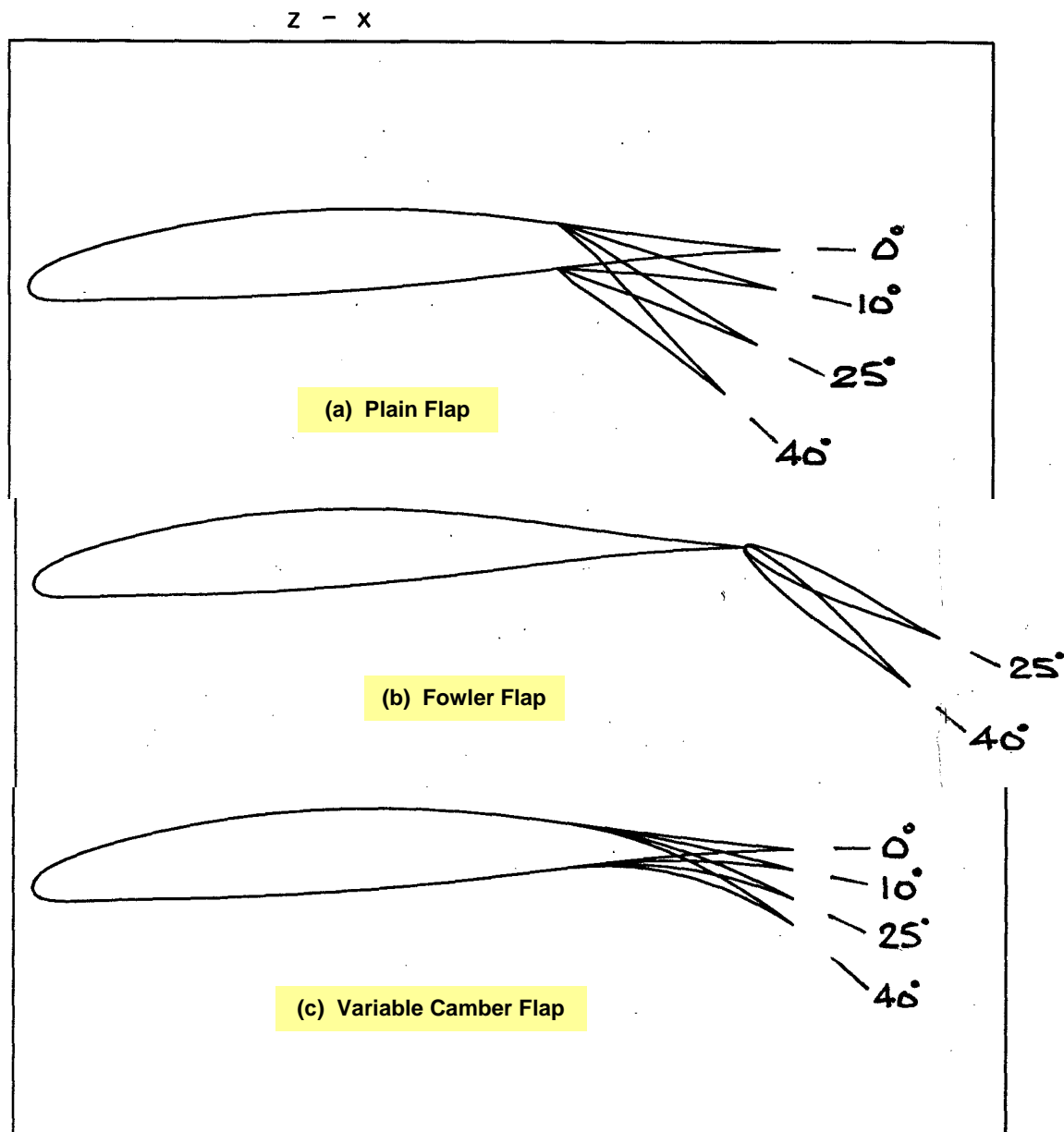


Fig. 5.1.3. TRAILING EDGE FLAP MODELLING ON TYPICAL AR 6 WING SECTION

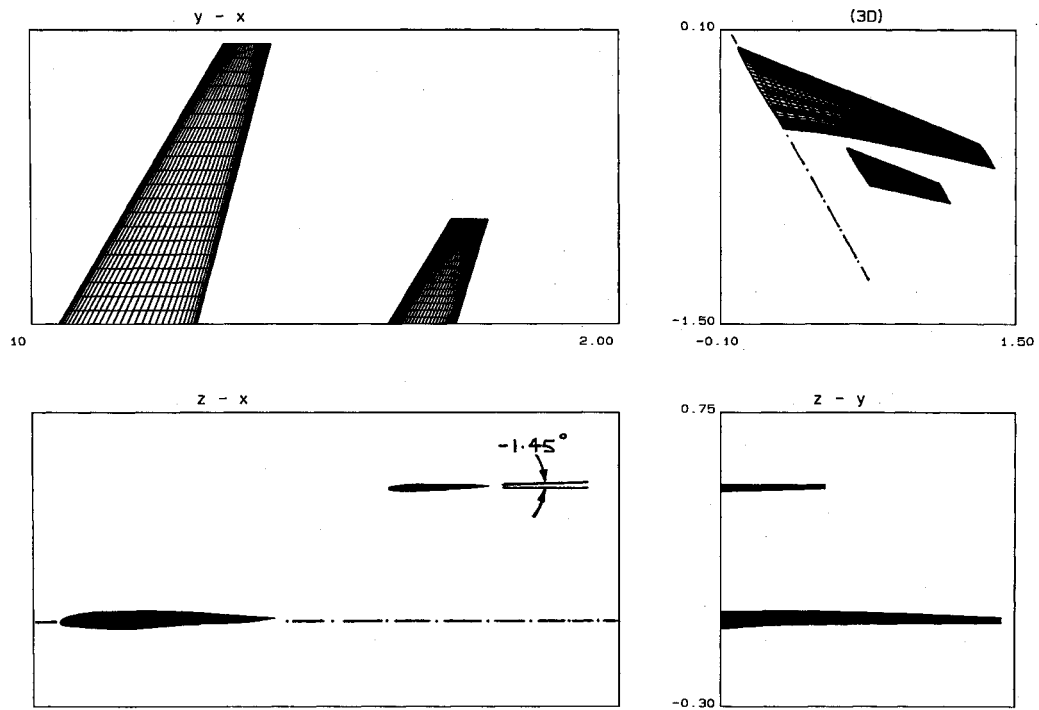


Fig. 5.1.4. AR 6 WING + TAILPLANE TYPICAL PANELLING

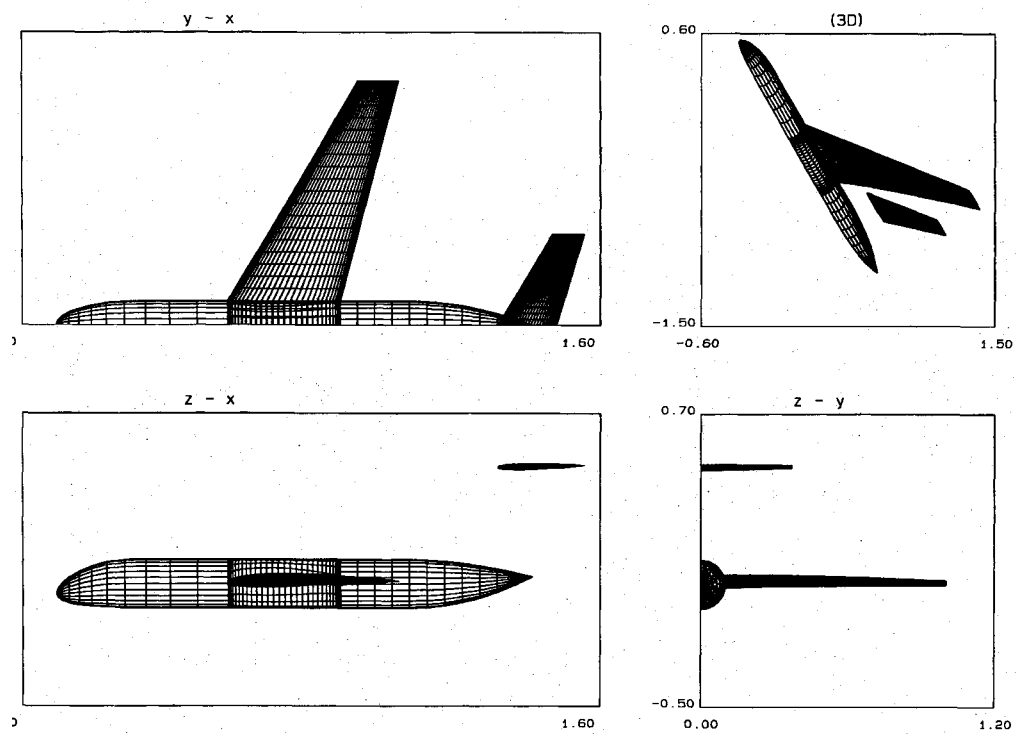
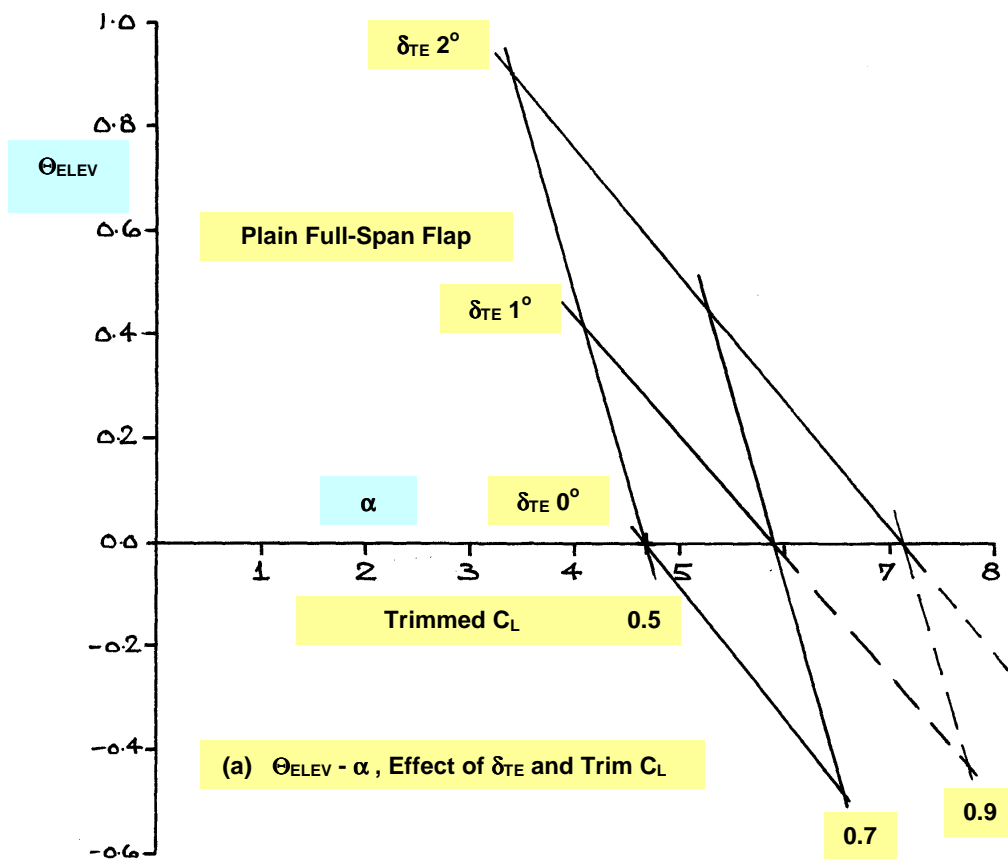
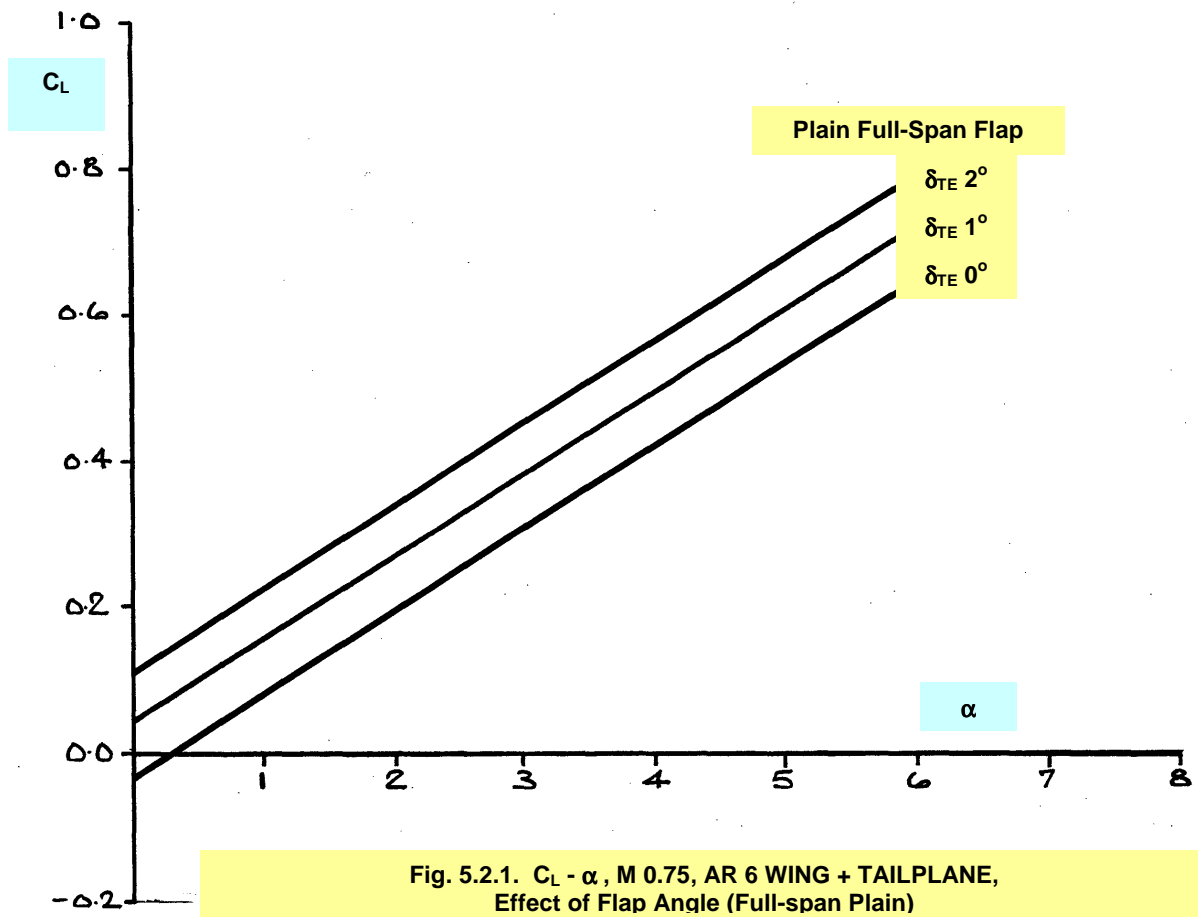


Fig. 5.1.5. AR 6 WING, FUSELAGE & TAILPLANE PANELLING



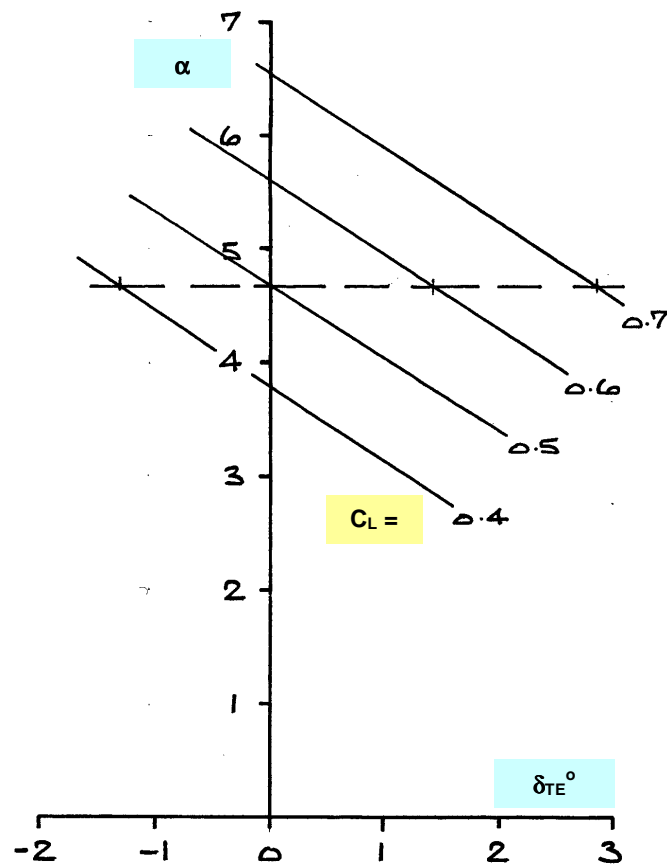
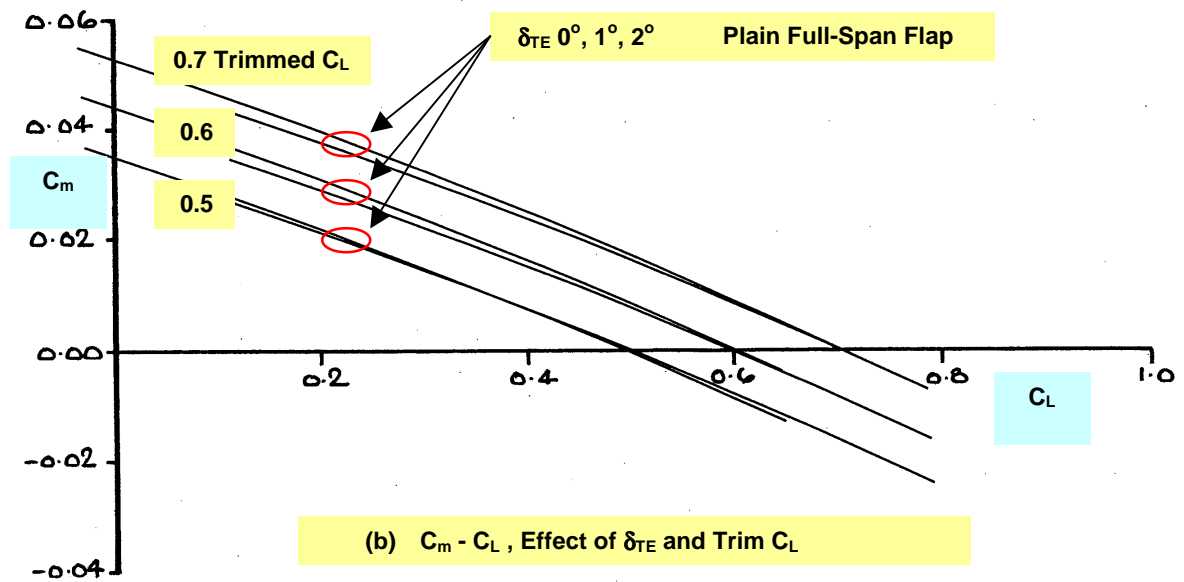
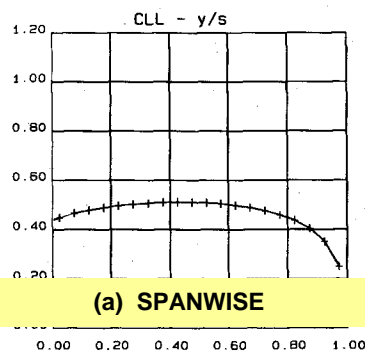
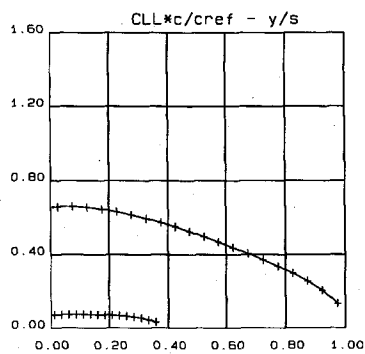
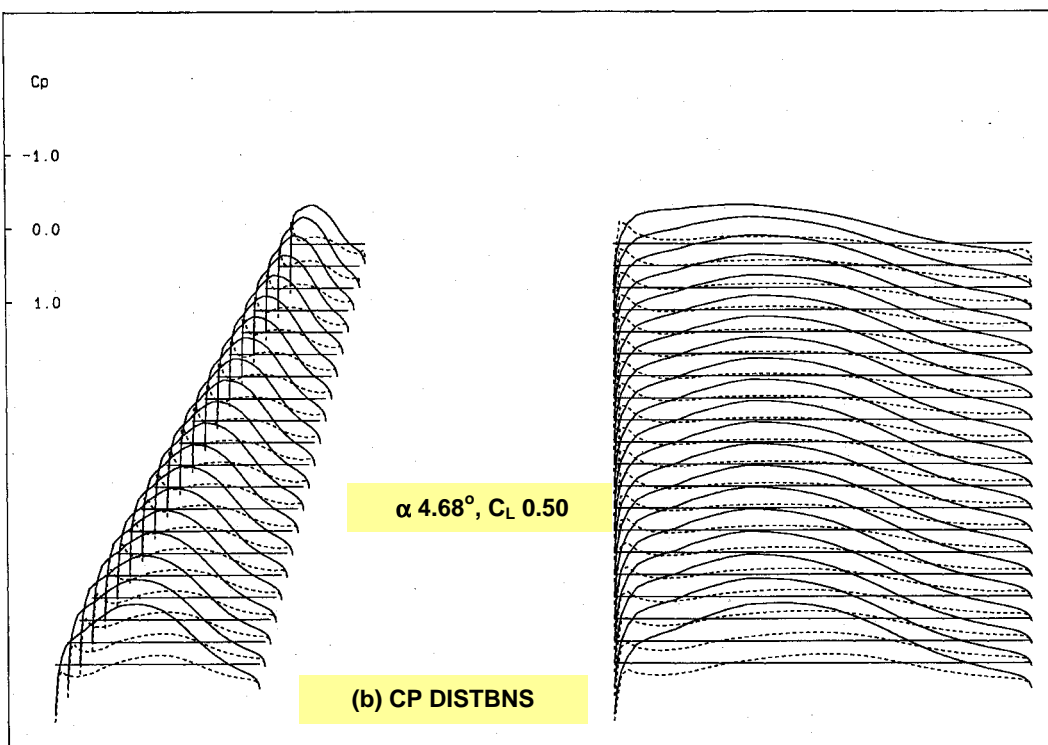


Fig. 5.2.2. $C_m - C_L$, M 0.75, AR 6 WING + TAILPLANE, Effect of δ_{TE} (Full-Span Plain)



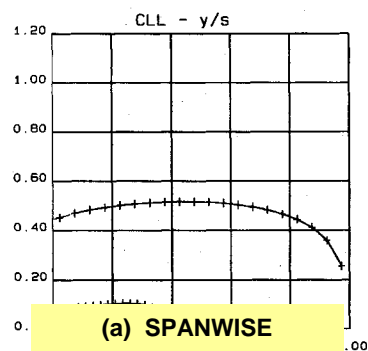
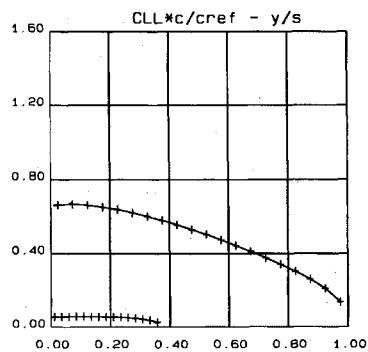
(a) SPANWISE

Cp-x (3D)



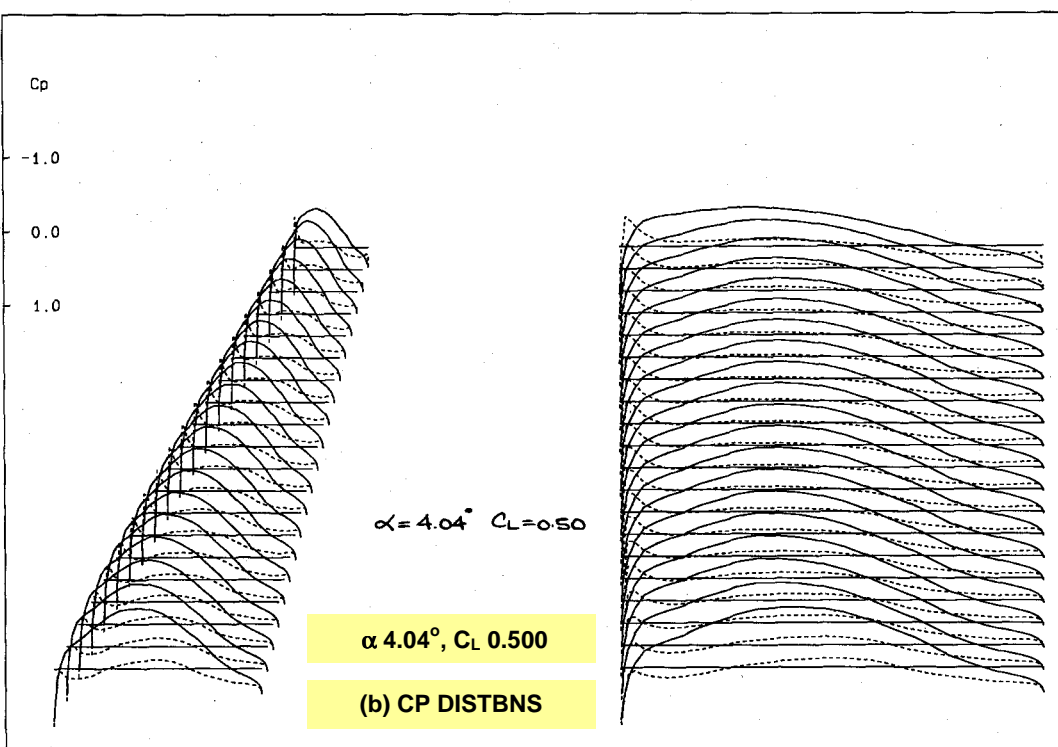
(b) CP DISTBNS

Fig. 5.2.3. CRUISE CONDITION (DATUM), LOADINGS
Trimmed C_L 0.5, M 0.75, AR 6 WING + TAILPLANE ($\Theta_{T/P} -1.45^\circ, \Theta_{ELEV} 0^\circ$)



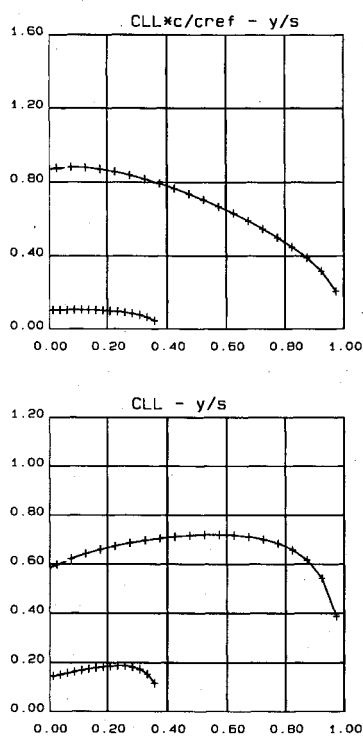
(a) SPANWISE

Cp-x (3D)

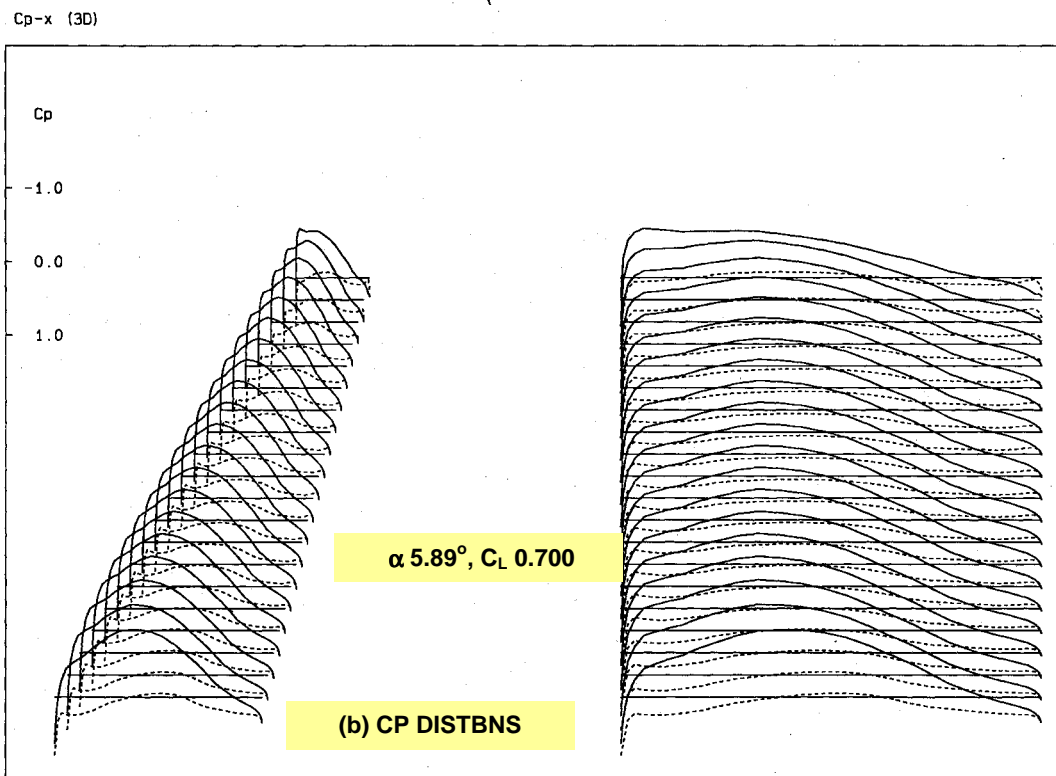


(b) CP DISTBNS

Fig. 5.2.4. $\delta_{TE} 1^\circ$ (Plain Flap), LOADINGS,
Trimmed C_L 0.5, M 0.75, AR 6 WING + TAILPLANE

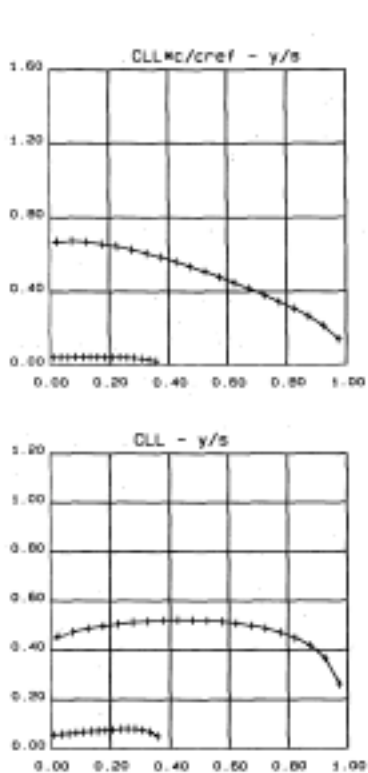


(a) SPANWISE

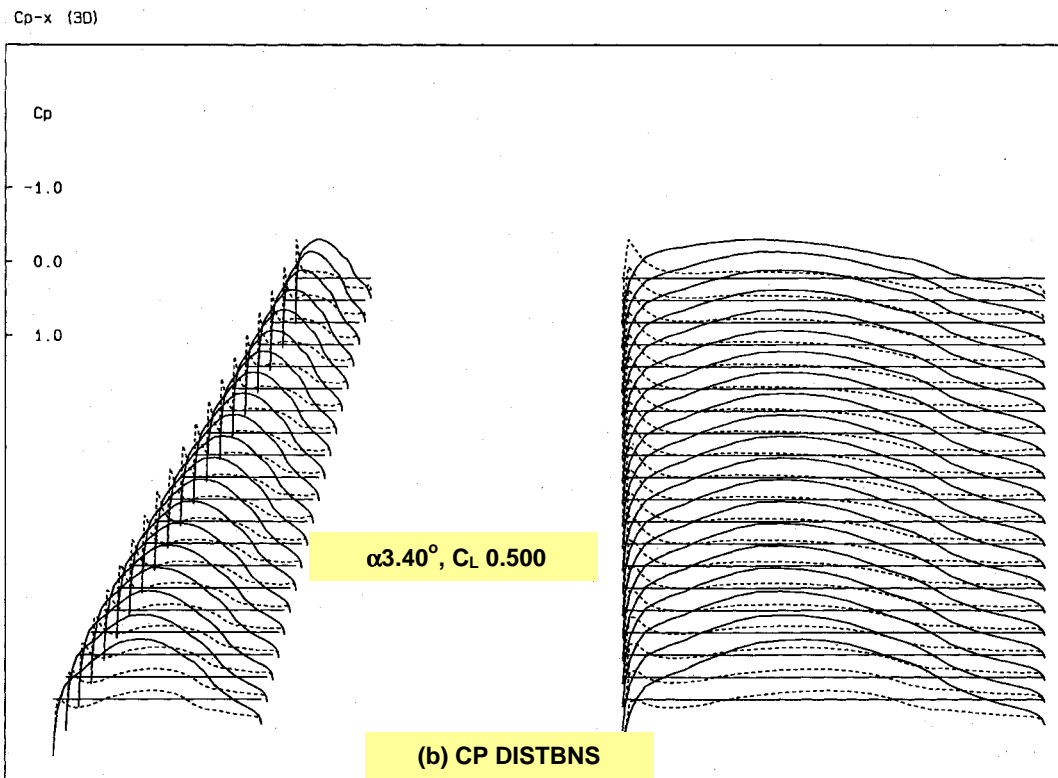


(b) CP DISTBNS

Fig. 5.2.5. $\delta_{TE} 1^\circ$ (Plain Flap), LOADINGS, Trimmed $C_L 0.7$, $M 0.75$, AR 6 WING + TAILPLANE

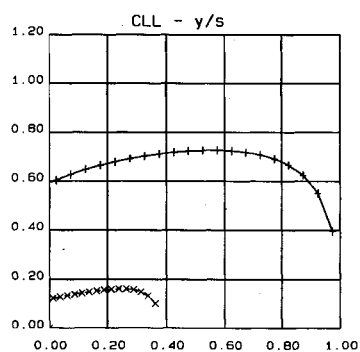
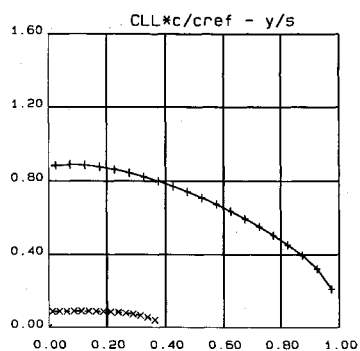


(a) SPANWISE

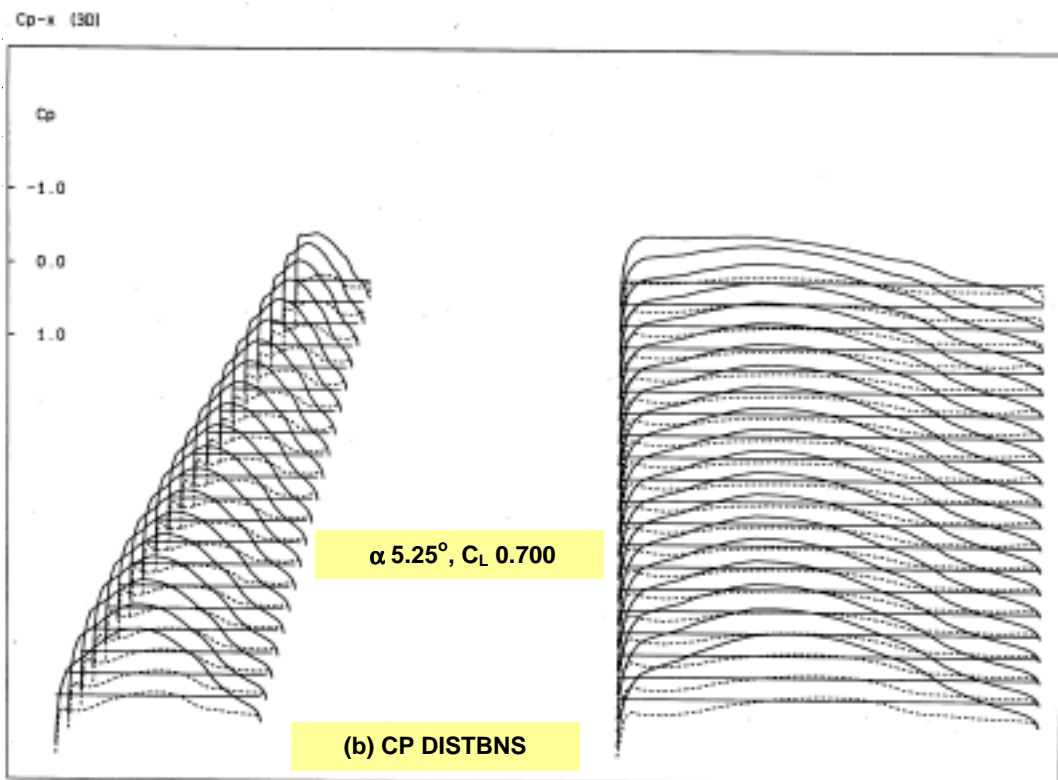


(b) CP DISTBNS

Fig. 5.2.6. $\delta_{TE} 2^\circ$ (Plain Flap), LOADINGS, Trimmed $C_L 0.5$, $M 0.75$, AR 6 WING + TAILPLANE



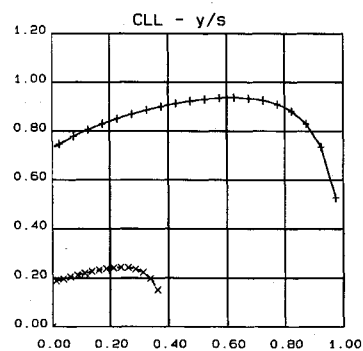
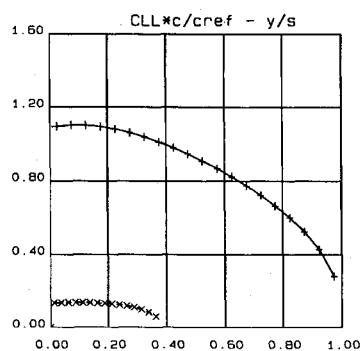
(a) SPANWISE



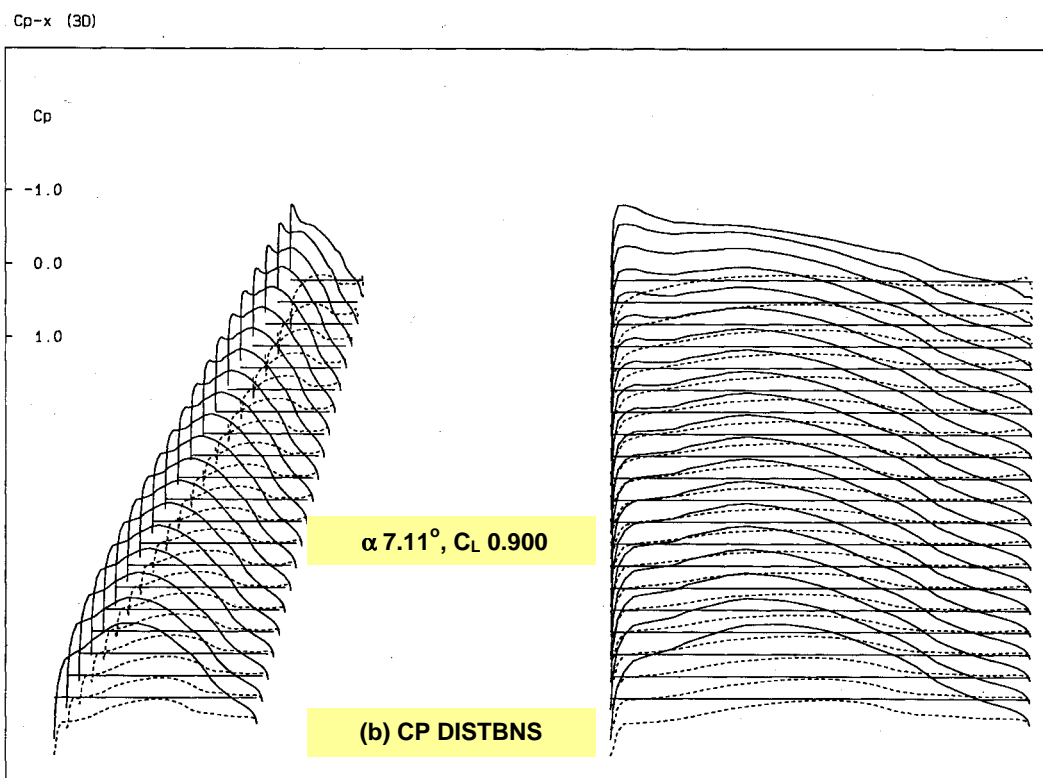
$\alpha 5.25^\circ, C_L 0.700$

(b) CP DISTBNS

Fig. 5.2.7. $\delta_{TE} 2^\circ$ (Plain Flap), LOADINGS, Trimmed $C_L 0.7$, $M 0.75$, AR 6 WING + TAILPLANE



(a) SPANWISE



$\alpha 7.11^\circ, C_L 0.900$

(b) CP DISTBNS

Fig. 5.2.8. $\delta_{TE} 2^\circ$ (Plain Flap), LOADINGS, Trimmed $C_L 0.9$, $M 0.75$, AR 6 WING + TAILPLANE

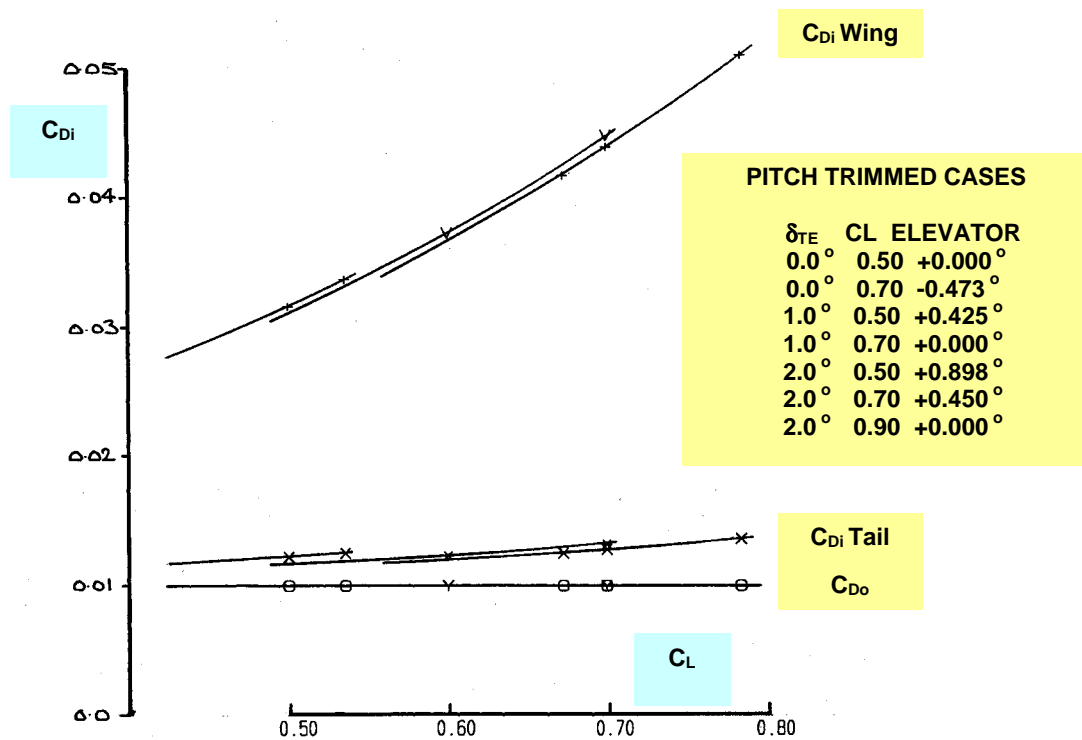


Fig. 5.2.9 $C_{Di} - C_L$, M 0.75, AR 6 WING + TAILPLANE, Effect of Flap Angle (Plain Flap)

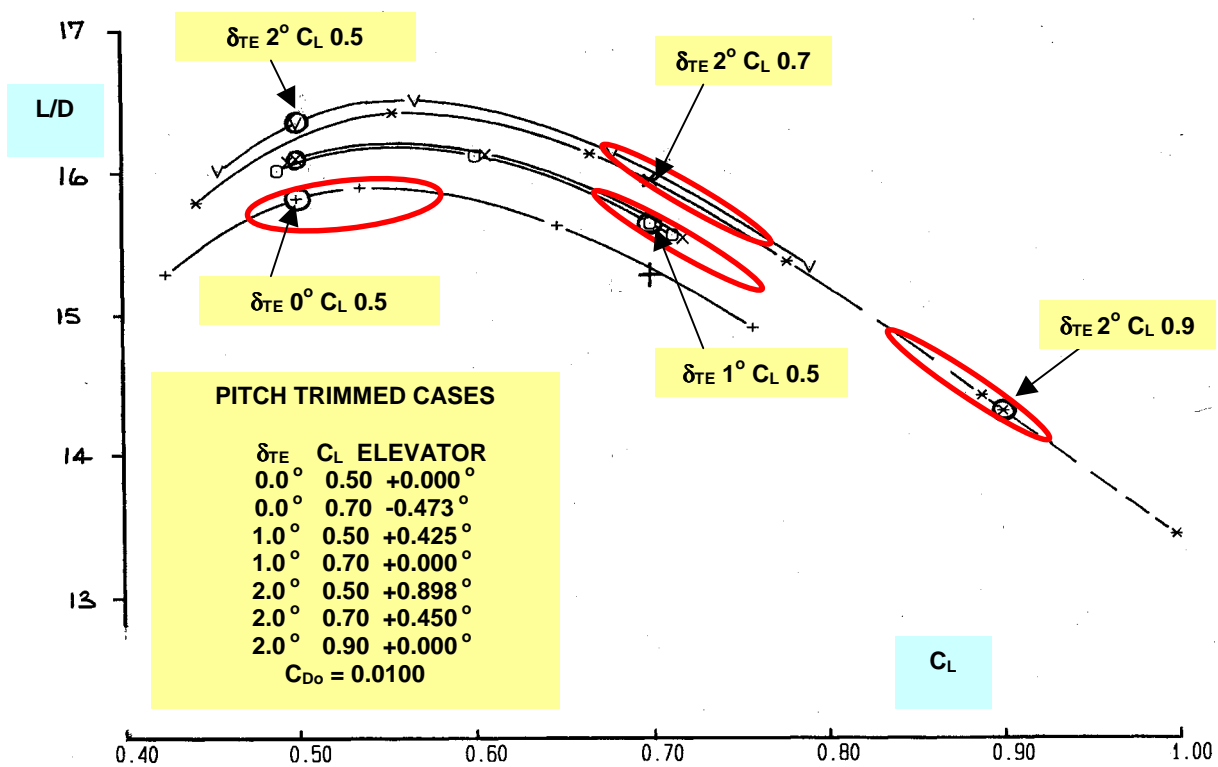


Fig. 5.2.10 $L/D - C_L$, M 0.75, AR 6 WING + TAILPLANE, Effect of Flap Angle (Plain Flap)

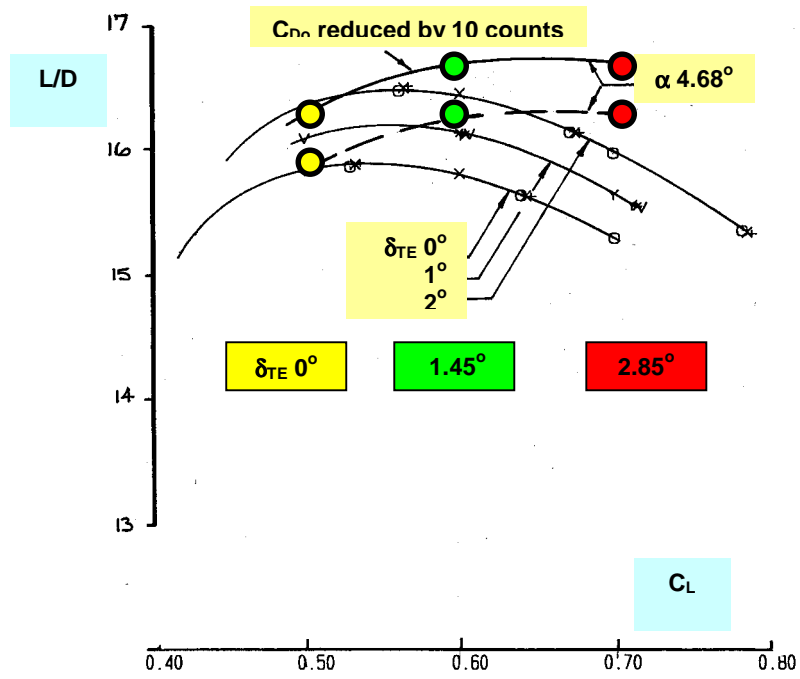


Fig. 5.2.11 L/D – C_L, M 0.75, AR 6 WING + TAILPLANE,
Effect of Flap Angle (Plain Flap)
α 4.68° Trimmed over C_L range

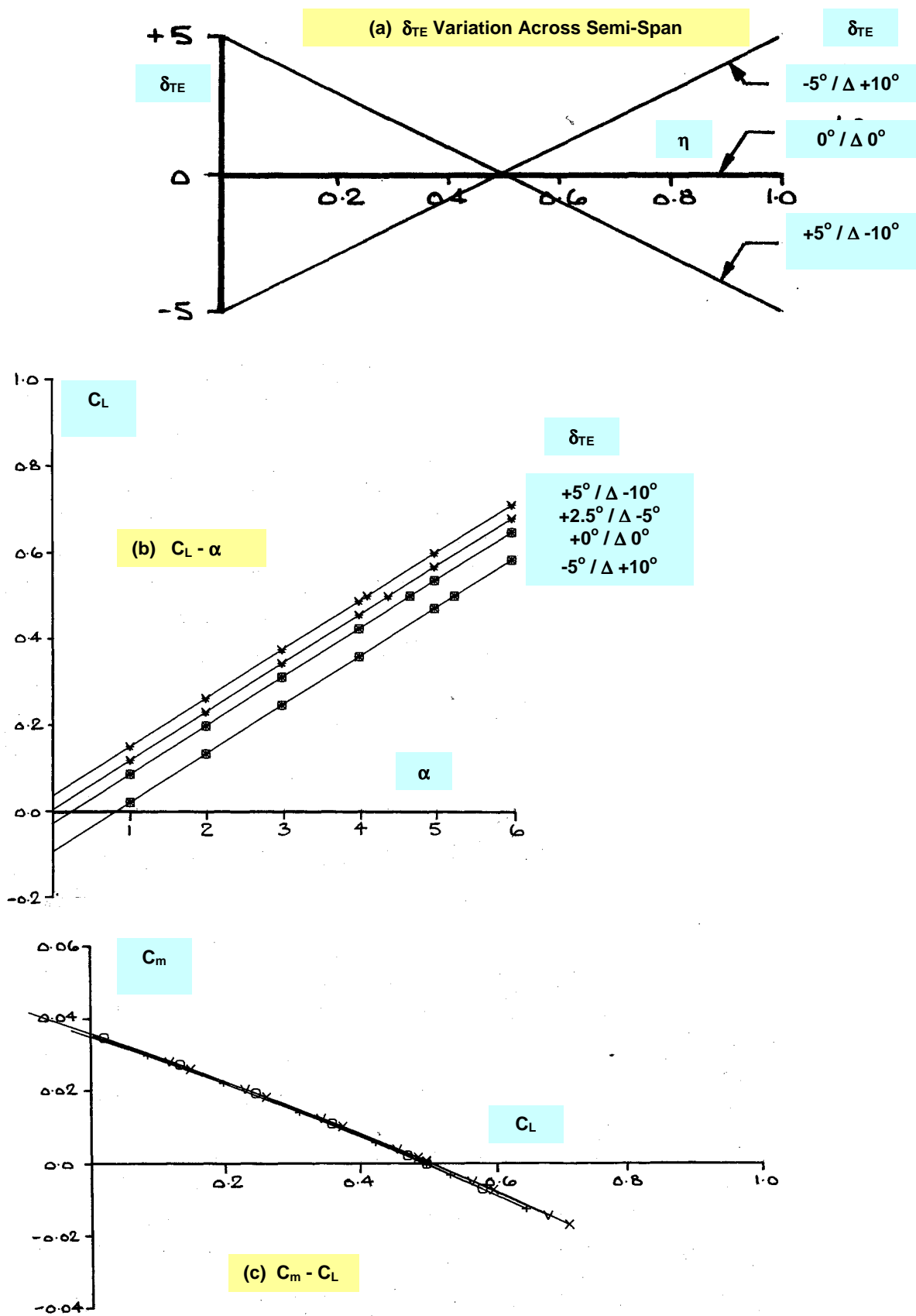
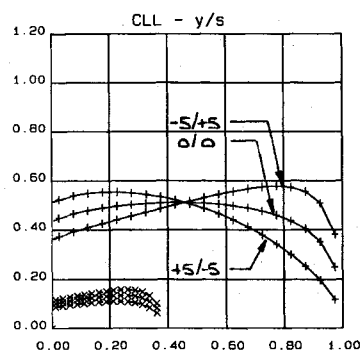
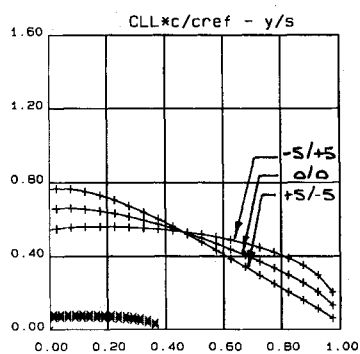


Fig. 5.2.12 $\delta_{TE} - \eta$, $C_L - \alpha$, $C_m - C_L$, $M 0.75$, $AR 6$ WING + TAILPLANE, Effect of Distributed, Full-Span Variable TE Geometry



(a) SPANWISE

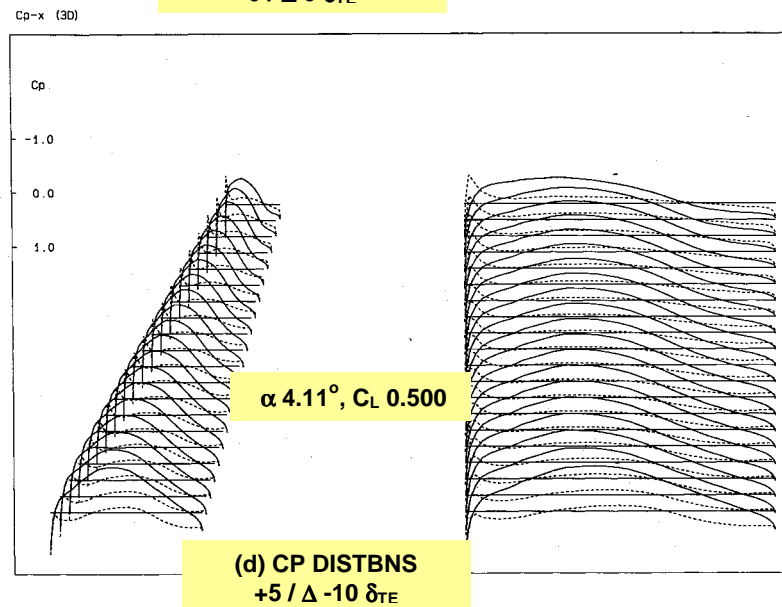
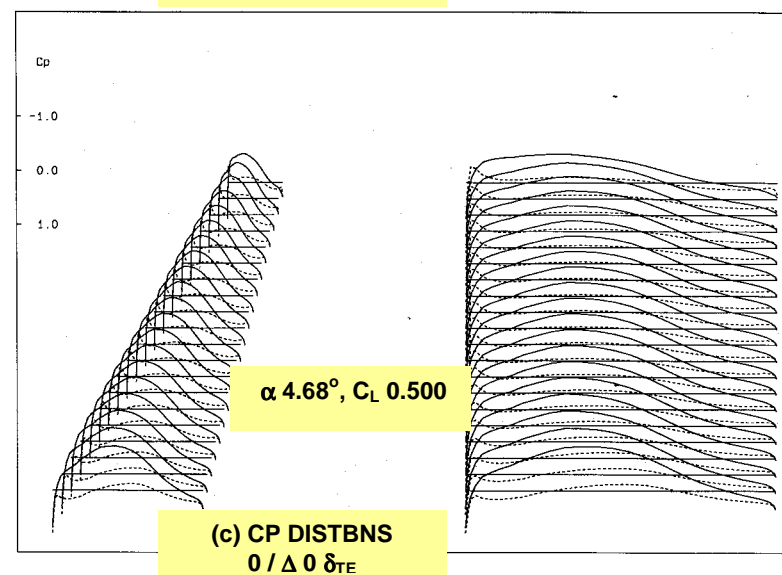
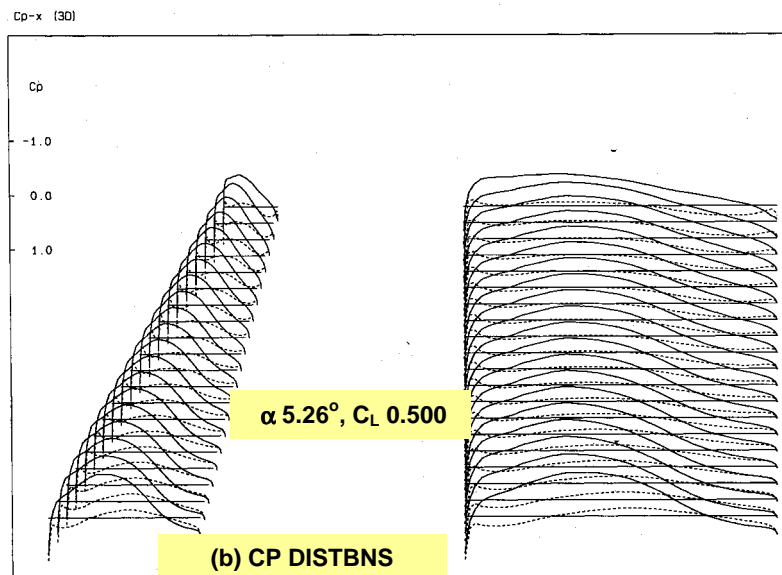


Fig. 5.2.13 LOADINGS, M 0.75, AR 6 WING + TAILPLANE,
Effect of Distributed, Full-Span Variable Camber

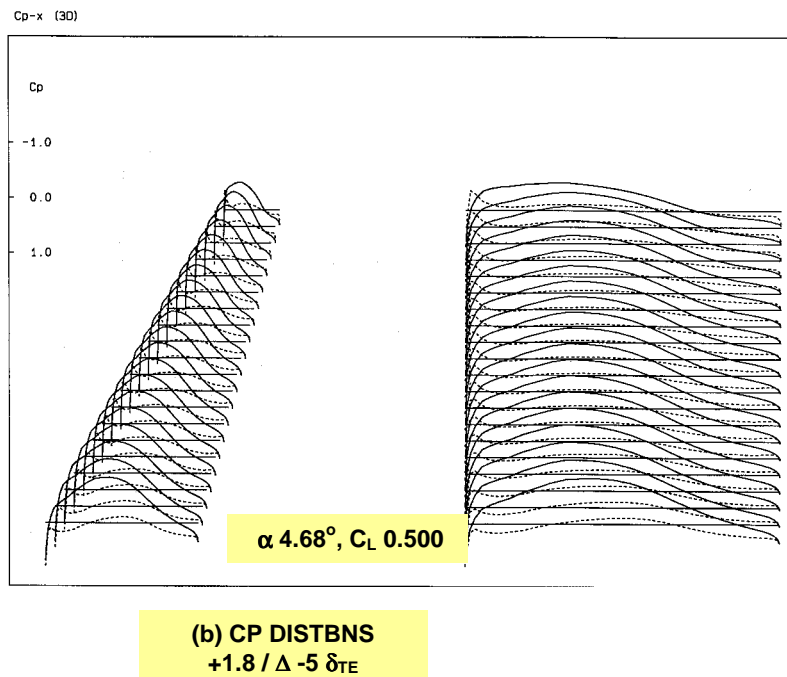
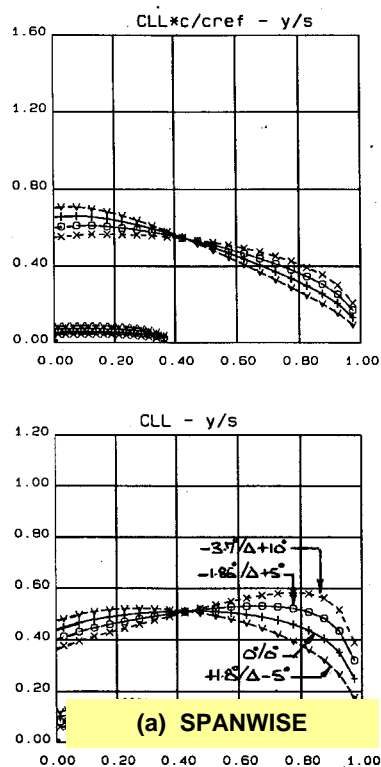


Fig. 5.2.14 LOADINGS, M 0.75, AR 6 WING + TAILPLANE,
Effect of Distributed, Full-Span Variable Camber
α 4.68° Trimmed CL

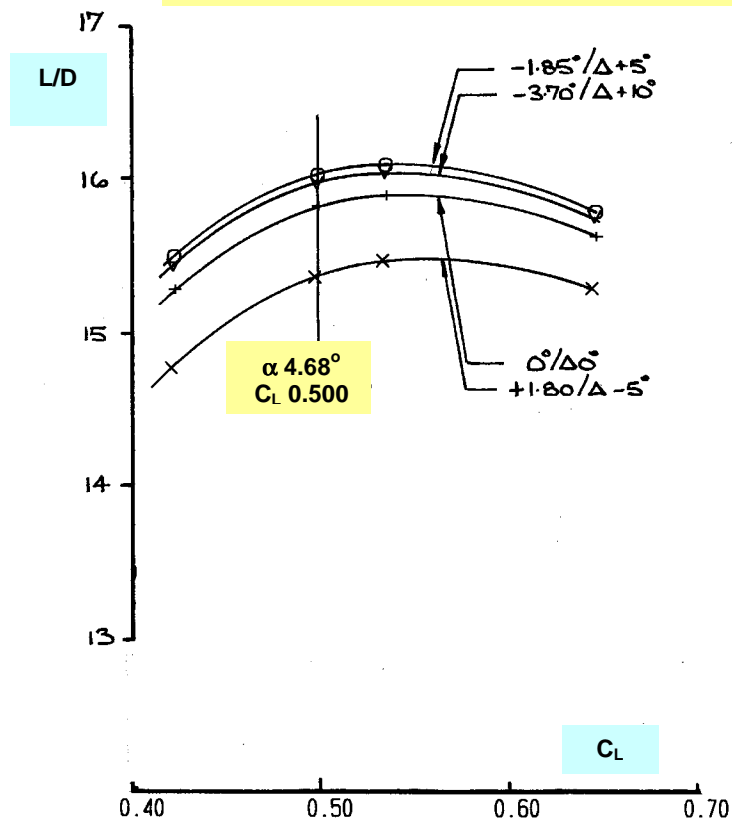


Fig. 5.2.15 L/D - CL, M 0.75, AR 6 WING + TAILPLANE,
Effect of Distributed, Full-Span Variable Camber
α 4.68° Trimmed CL 0.5

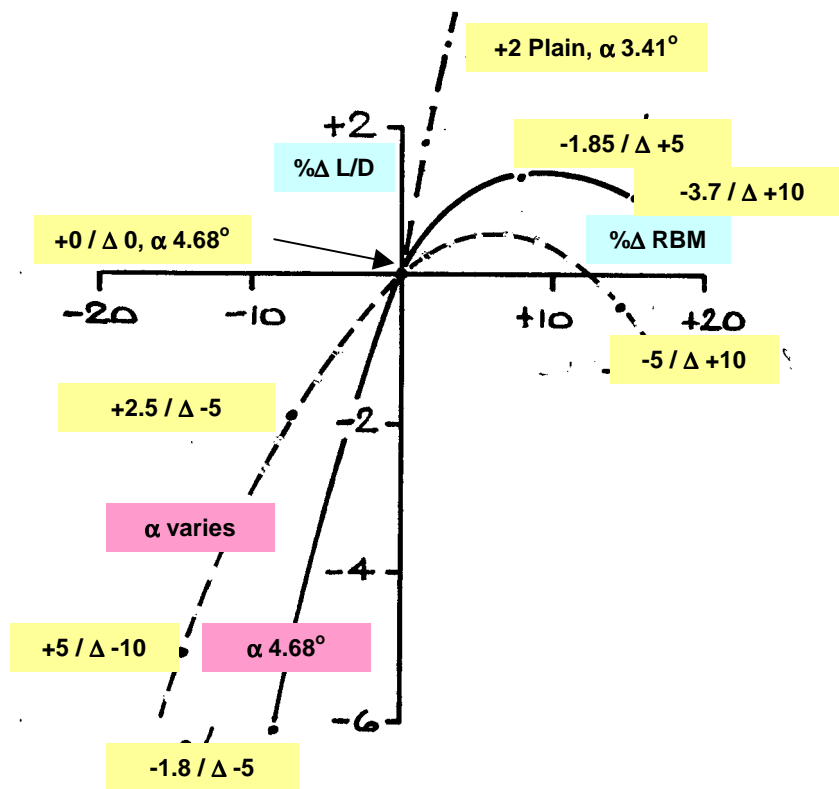


Fig. 5.2.16. L/D and RBM % CHANGES BASED ON DESIGN WING ($\delta_{TE} 0^\circ$)
Effect of Flap Angle and Trimming
(Plain, Distributed Plain and Distributed Variable TE Geometry)
M0.75, AR 6 WING + TAILPLANE

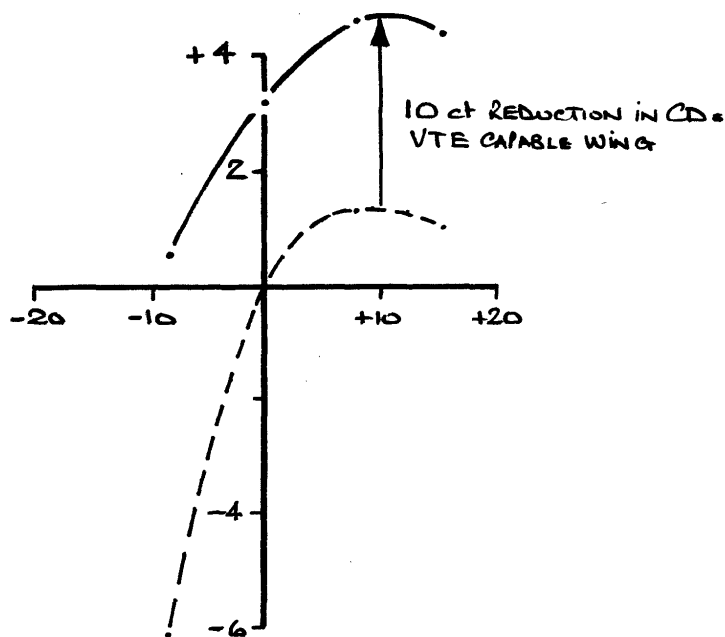


Fig. 5.2.17. L/D and RBM % CHANGES BASED ON DESIGN WING ($\delta_{TE} 0^\circ$)
Effect of Distributed VTE Deflections on VTE Capable Designed Wing
M0.75, AR 6 WING + TAILPLANE

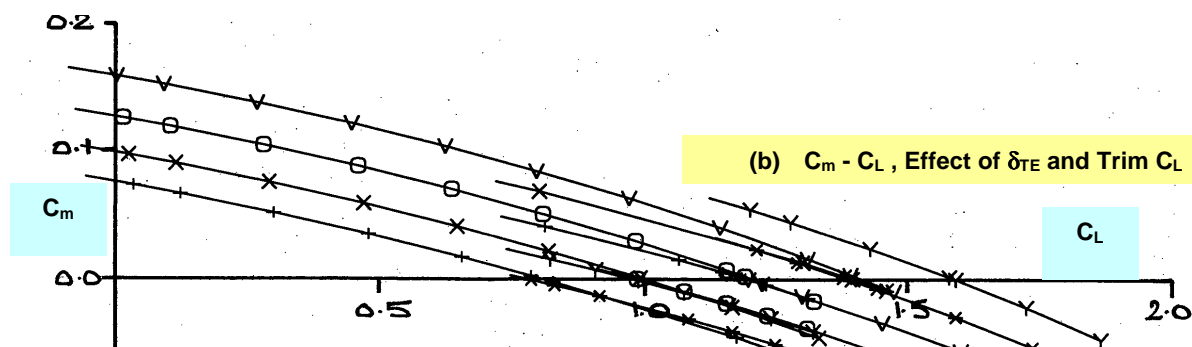
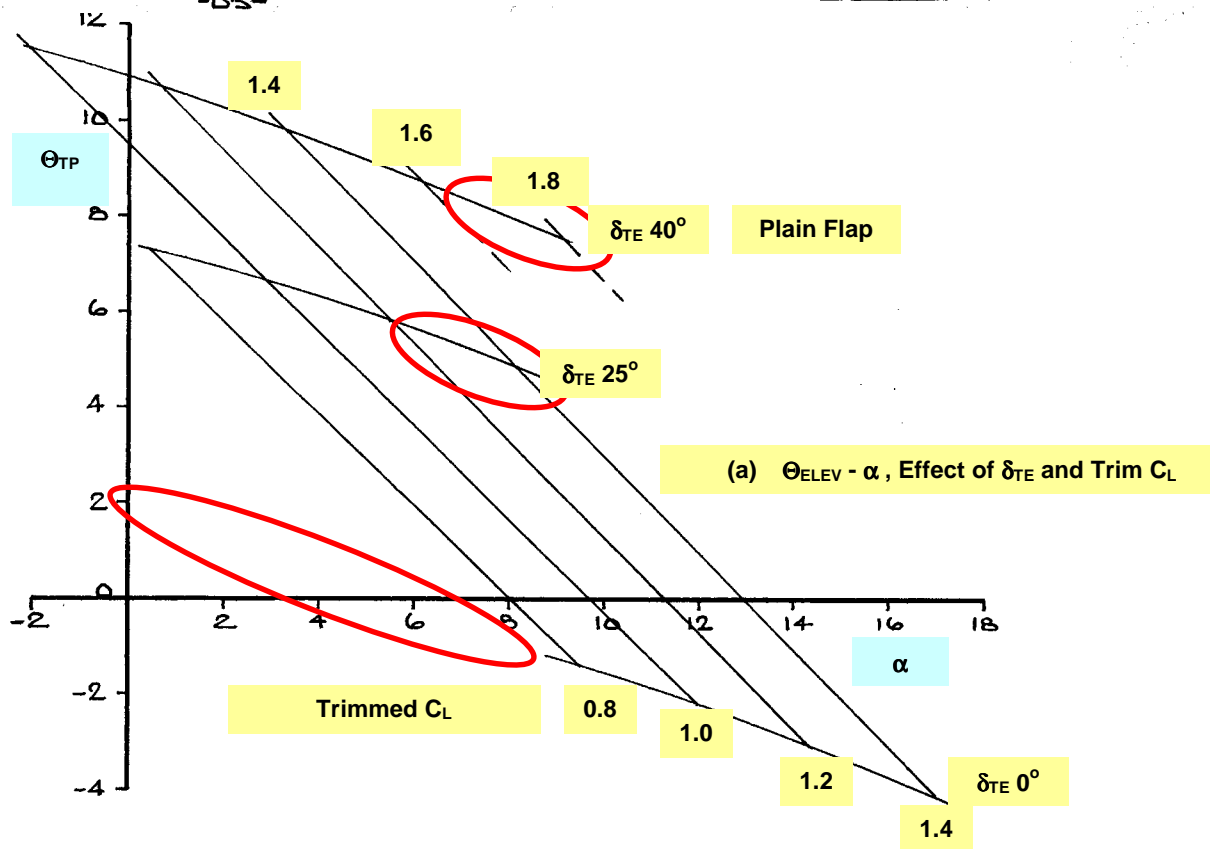
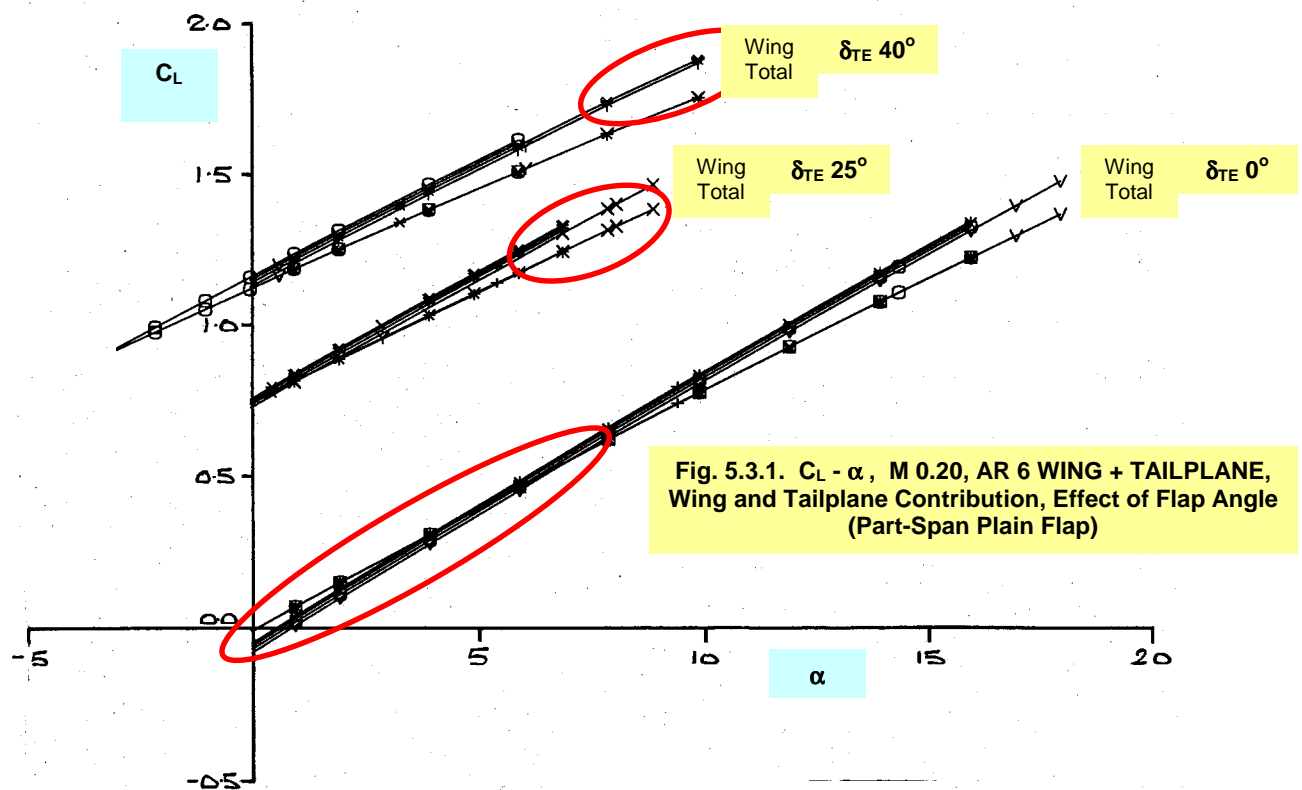
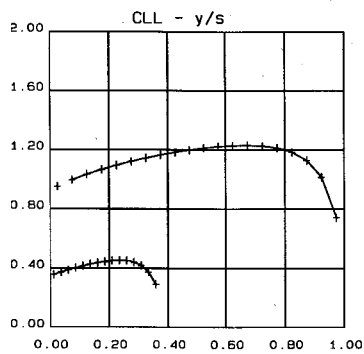
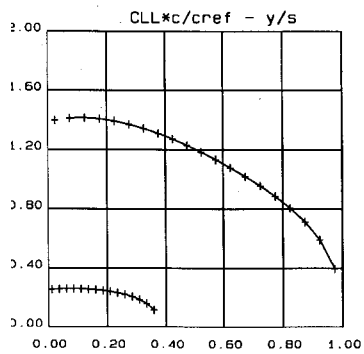


Fig. 5.3.2. $C_m - C_L$, $M 0.20$, $AR 6$ WING + TAILPLANE, TRIM REQUIREMENTS Effect of δ_{TE} (Part-Span Plain Flap)



(a) SPANWISE

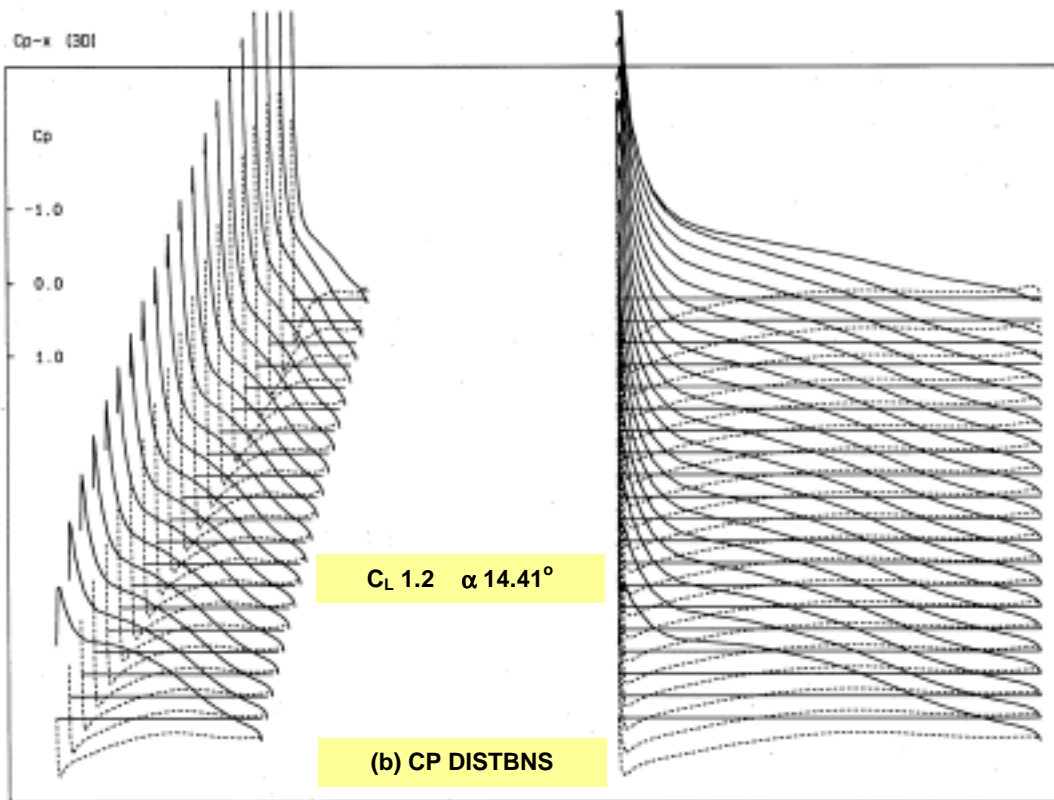
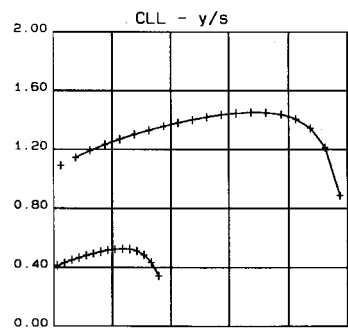
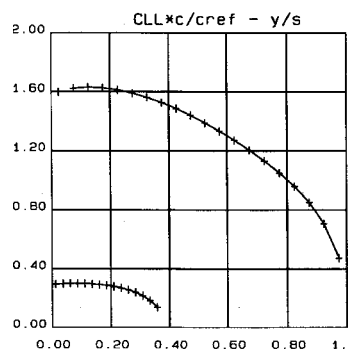


Fig. 5.3.3. CLEAN WING ($\delta_{TE} 0^\circ$), LOADINGS,
Trimmed $C_L 1.2$, M 0.20, AR 6 WING + TAILPLANE



(a) SPANWISE

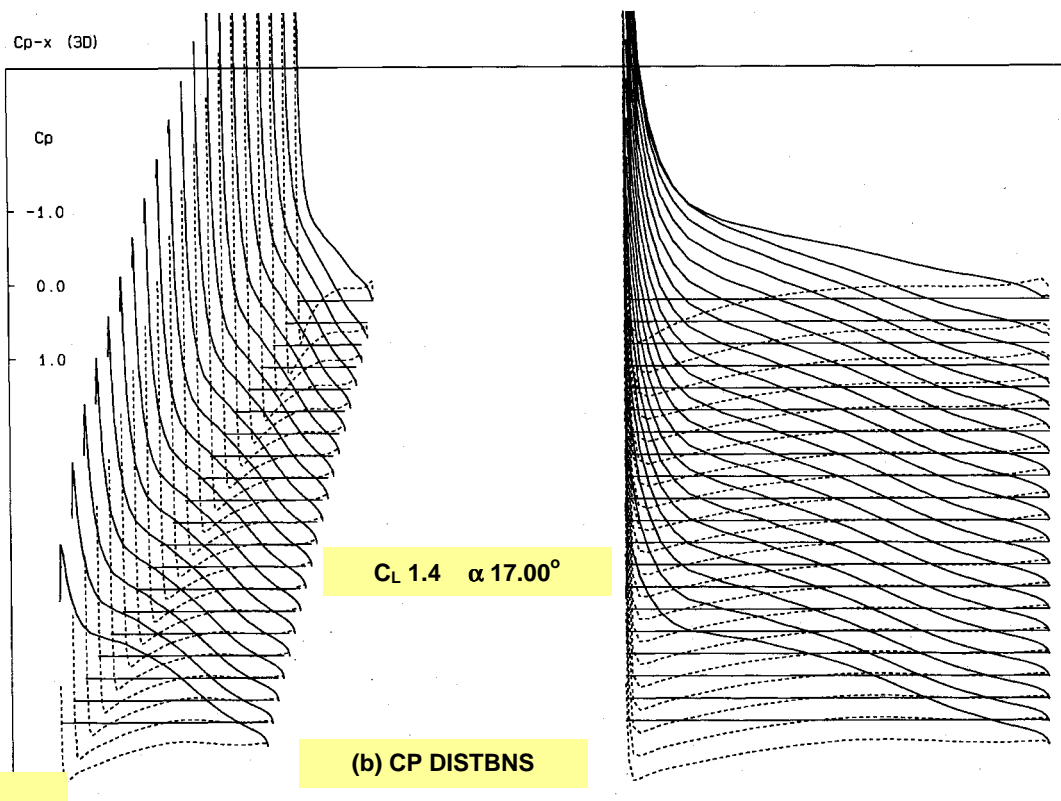
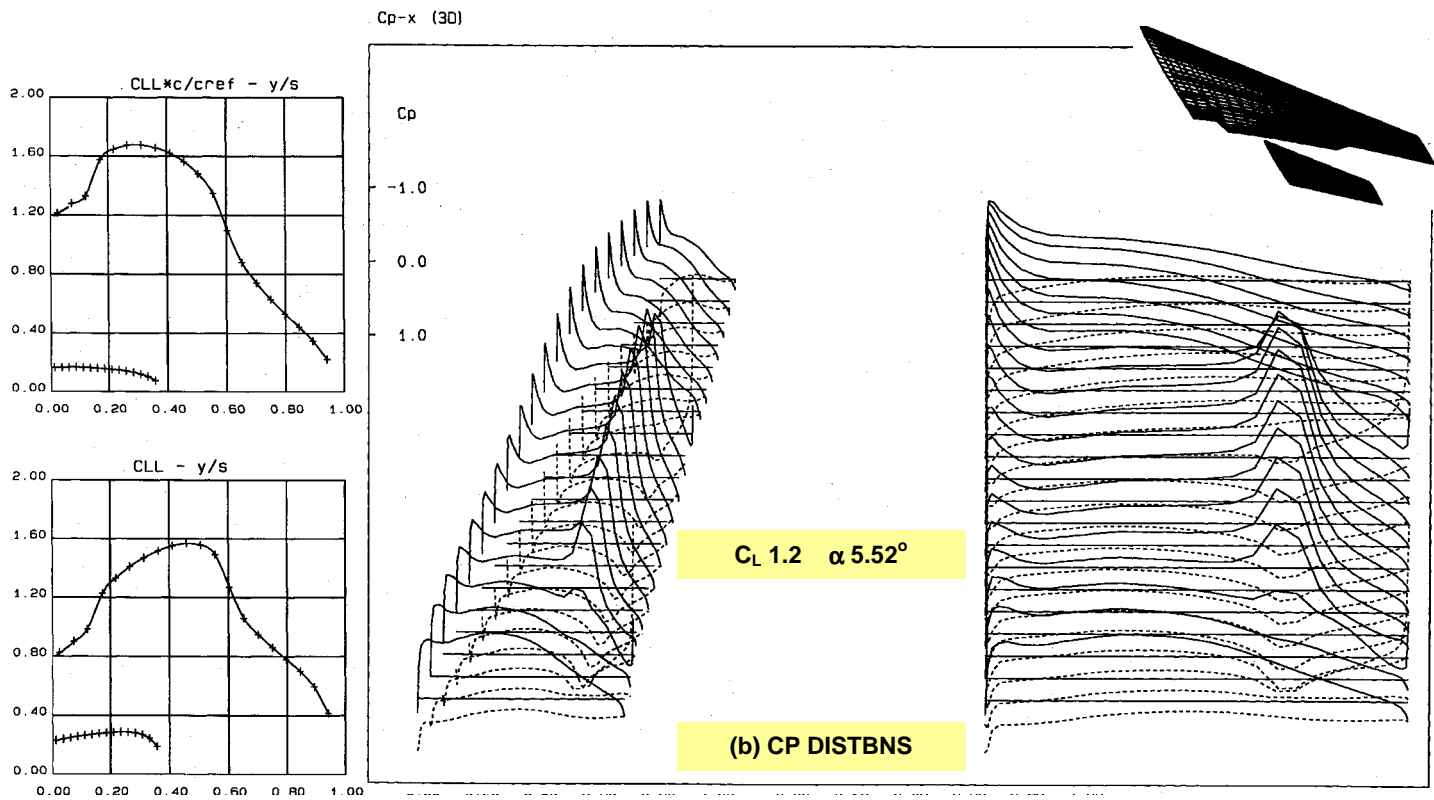
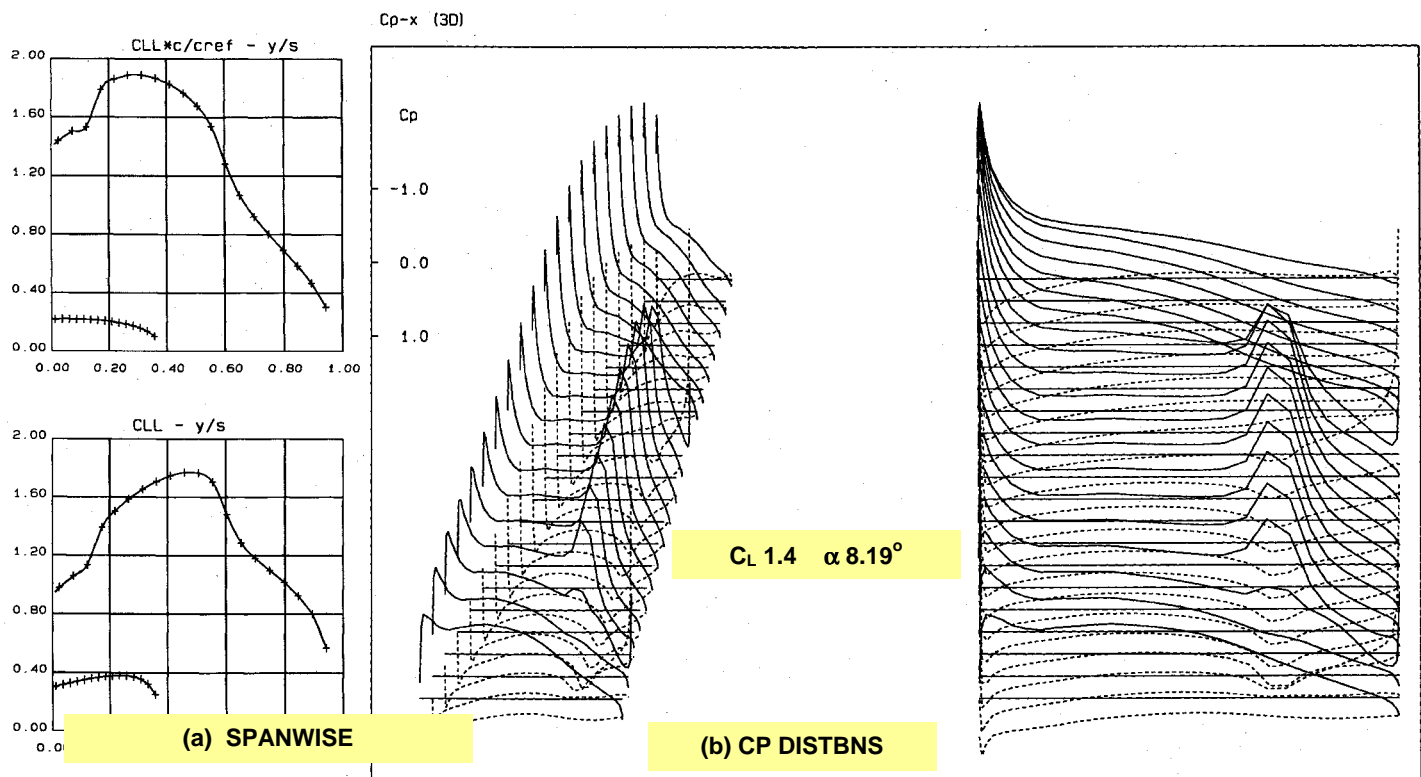


Fig. 5.3.4. CLEAN WING ($\delta_{TE} 0^\circ$), LOADINGS,
Trimmed $C_L 1.4$, M 0.20, AR 6 WING + TAILPLANE



(a) SPANWISE

Fig. 5.3.5. $\delta_{TE} 25^\circ$ (Plain Flap), LOADINGS, Trimmed $C_L 1.2$, $M 0.20$, AR 6 WING + TAILPLANE



(a) SPANWISE

Fig. 5.3.6. $\delta_{TE} 25^\circ$ (Plain Flap), LOADINGS, Trimmed $C_L 1.4$, $M 0.20$, AR 6 WING + TAILPLANE

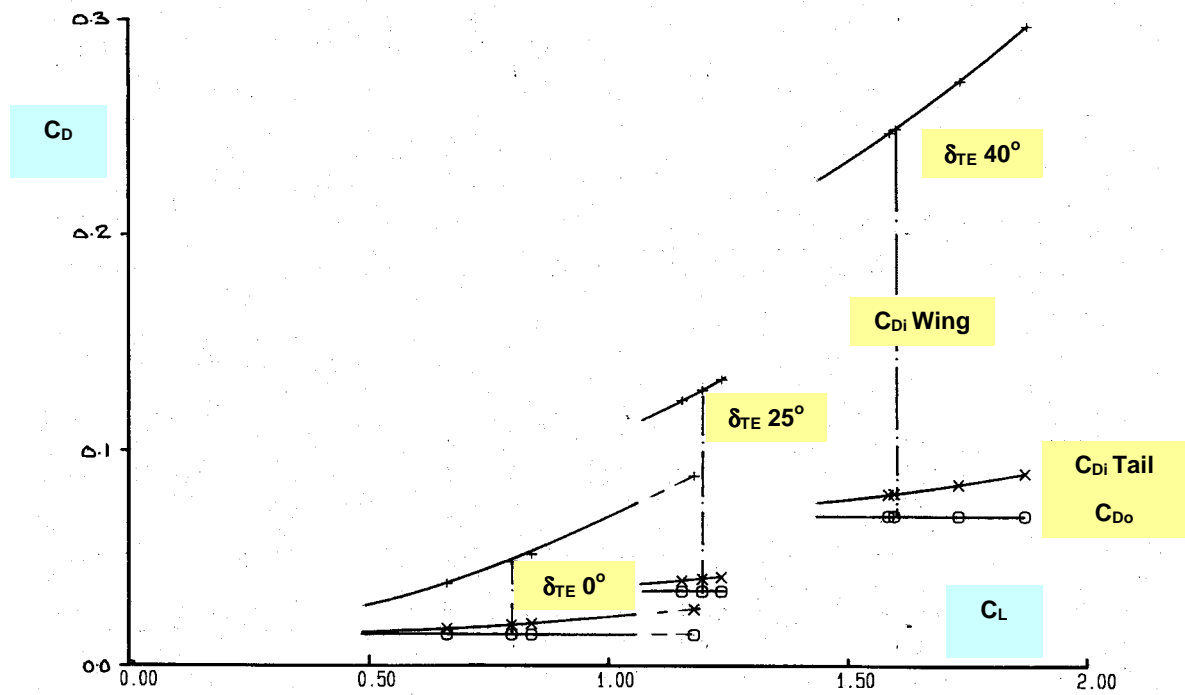


Fig. 5.3.7 $C_D - C_L$, M 0.20, AR 6 WING + TAILPLANE, Drag Breakdown, Effect of Flap Angle (Part-Span Plain Flap)

5.3.7

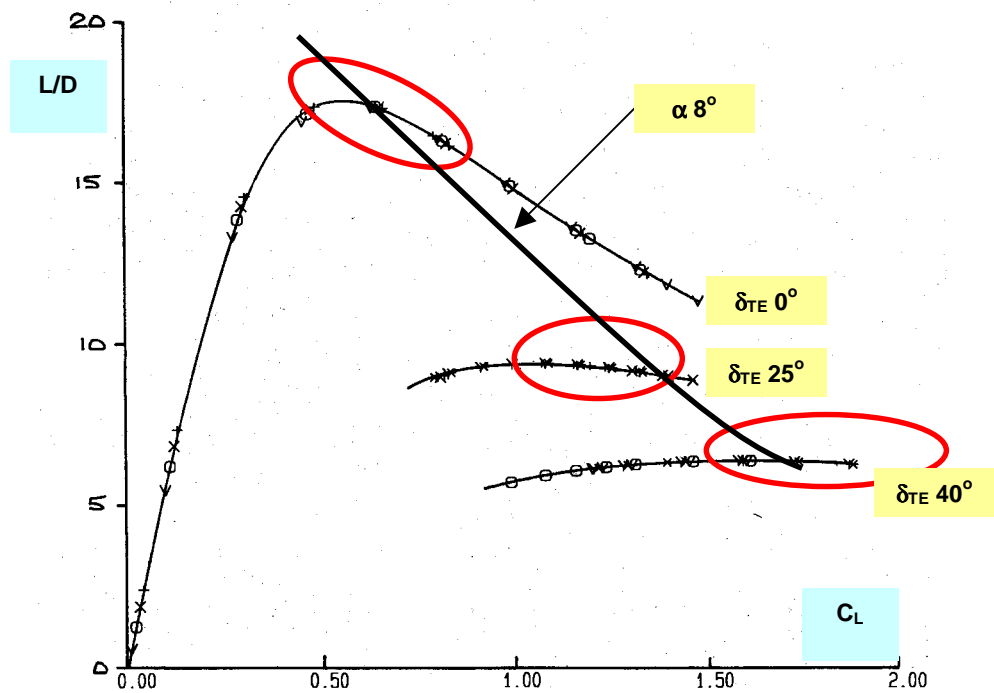
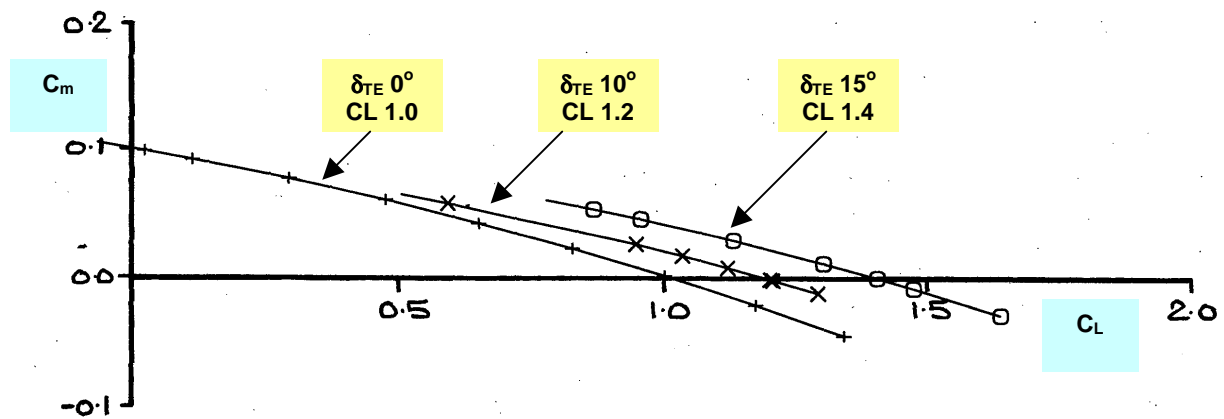
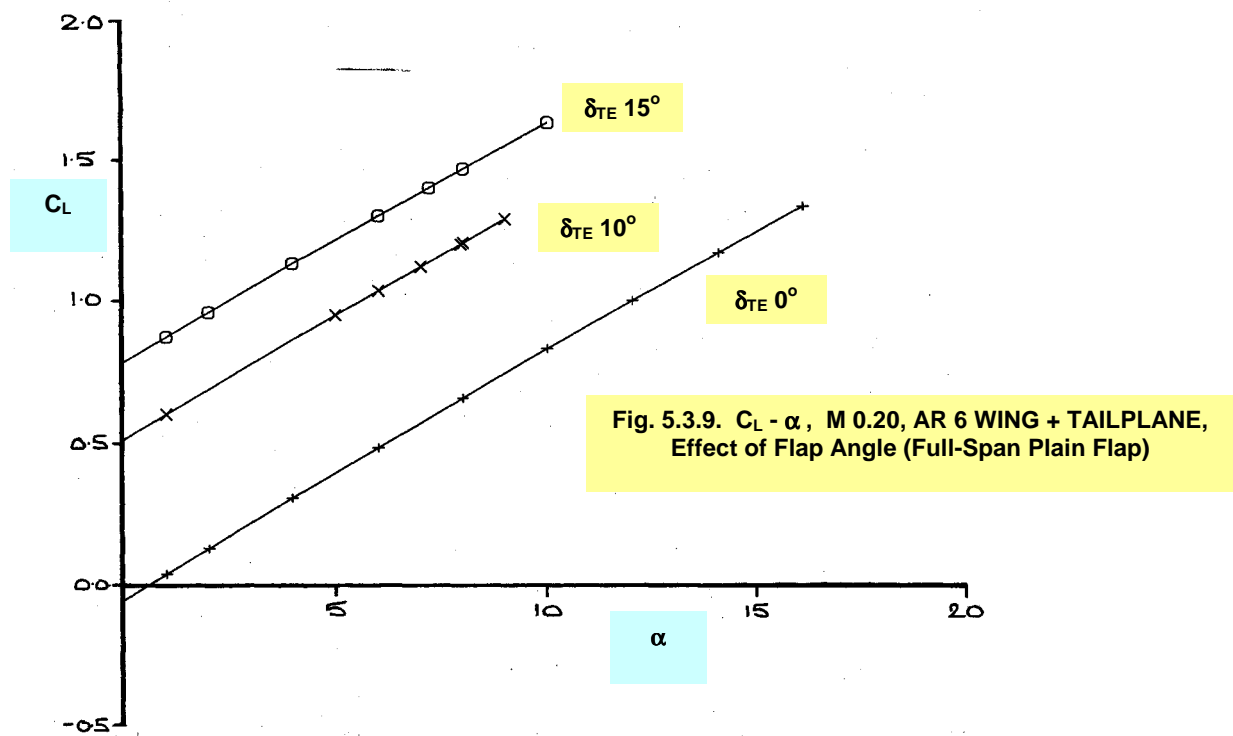


Fig. 5.3.8 $L/D - C_L$, M 0.20, AR 6 WING + TAILPLANE, Effect of Flap Angle (Part-Span Plain Flap)



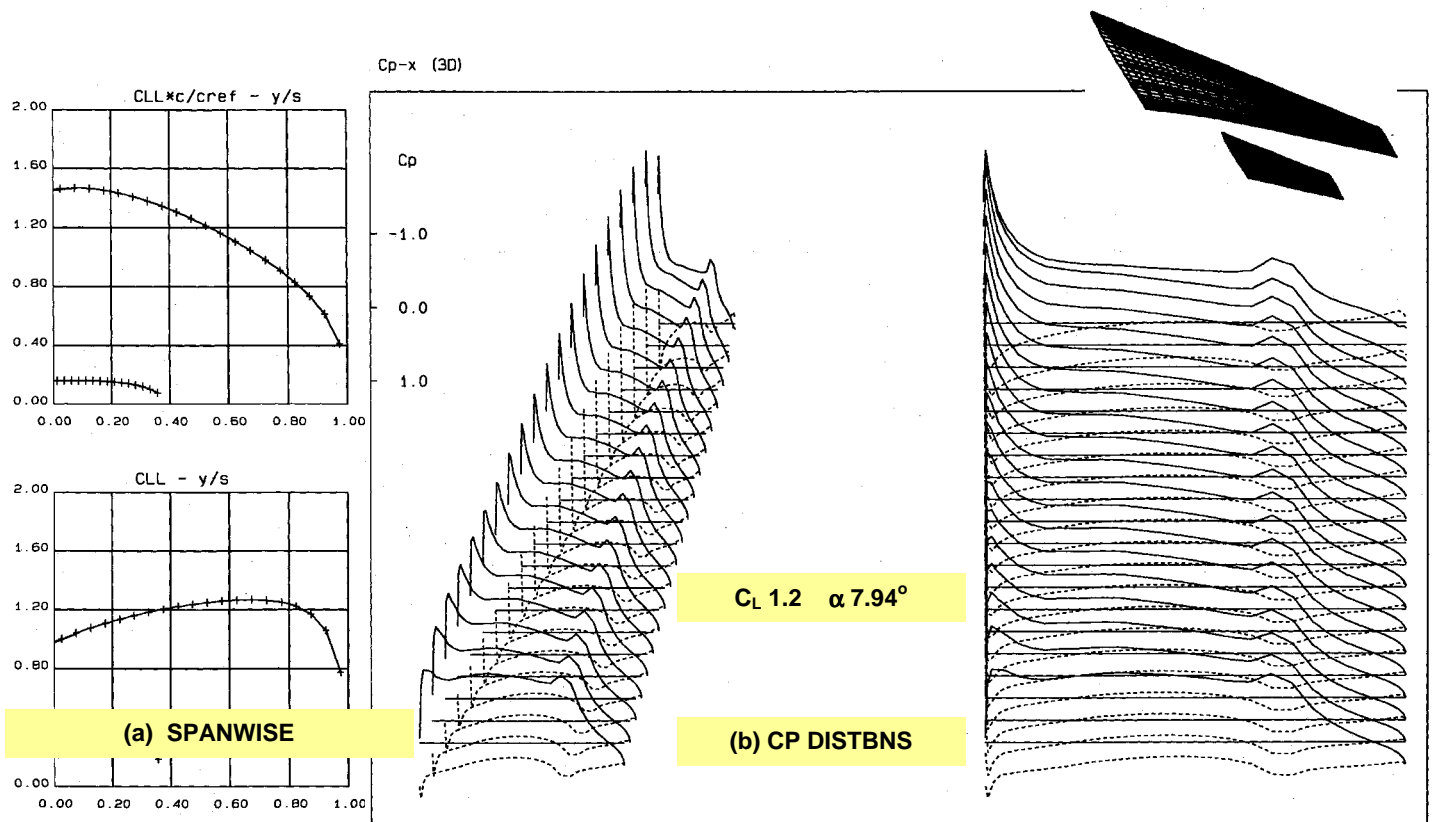


Fig. 5.3.11. $\delta_{TE} 10^\circ$ (Full-span Plain Flap), LOADINGS, Trimmed $C_L 1.2$, $M 0.20$, AR 6 WING + TAILPLANE

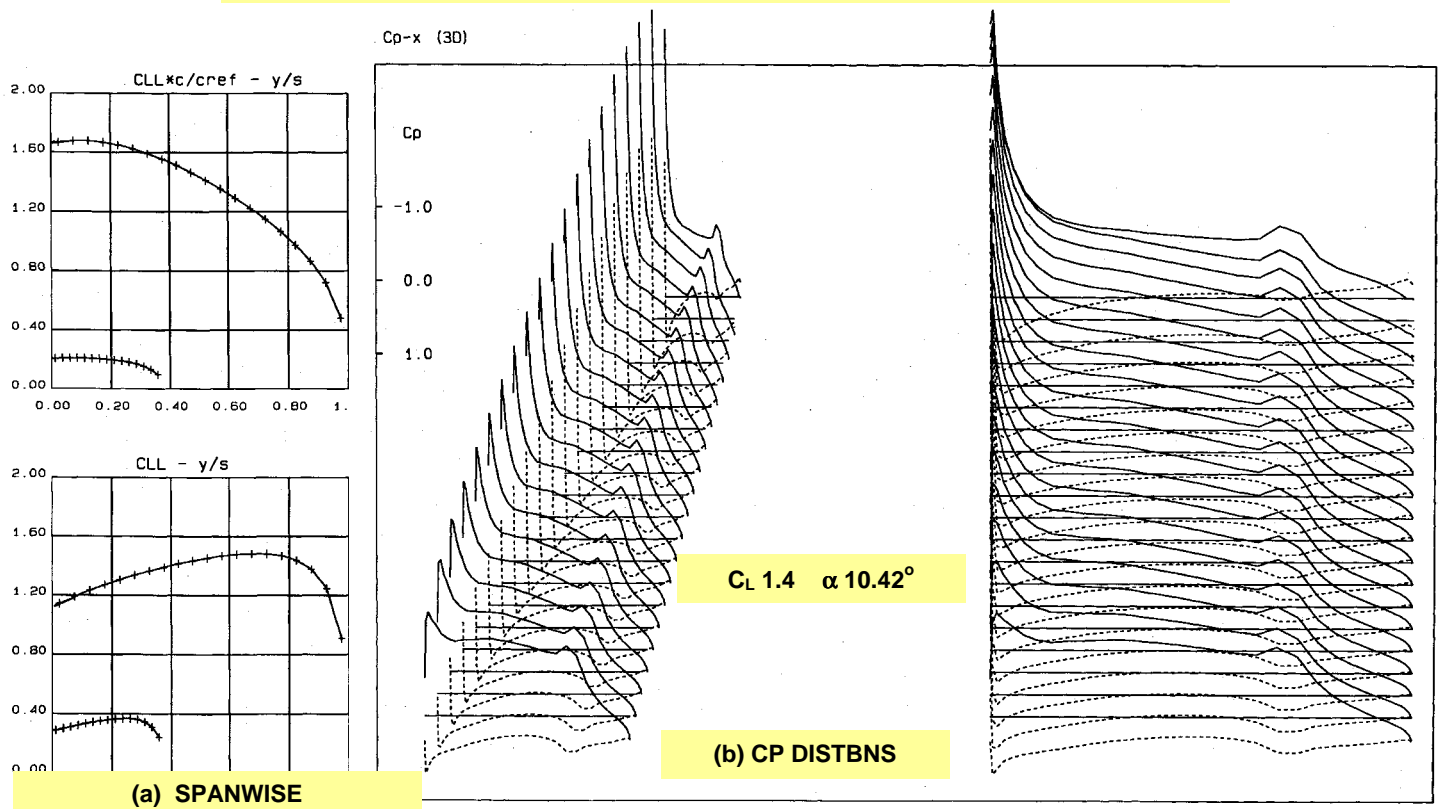
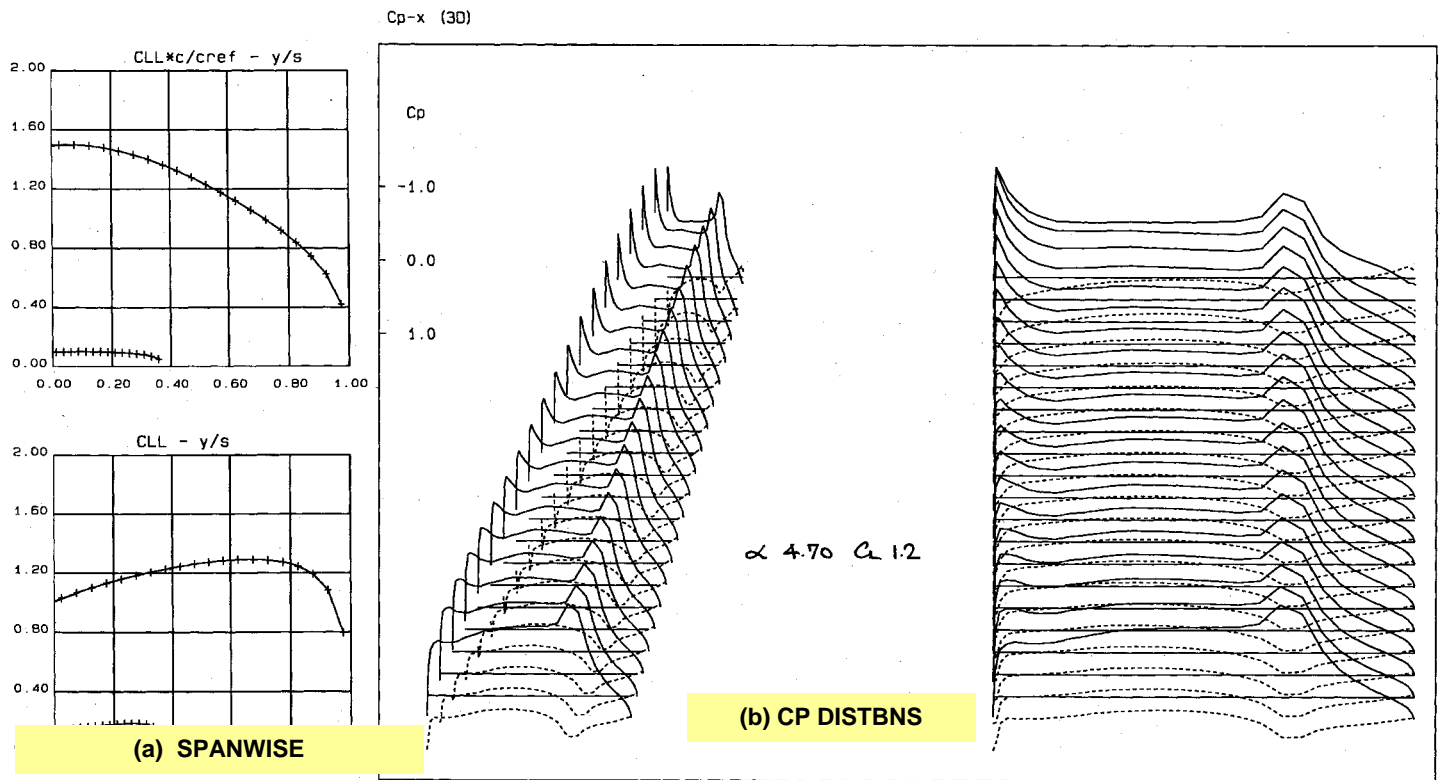


Fig. 5.3.12. $\delta_{TE} 10^\circ$ (Full-span Plain Flap), LOADINGS, Trimmed $C_L 1.4$, $M 0.20$, AR 6 WING + TAILPLANE



M=0.2 15°

Fig. 5.3.13. $\delta_{TE} 15^\circ$ (Full-span Flap), LOADINGS, Trimmed $C_L 1.2$, M 0.20, AR 6 WING + TAILPLANE

NN.3.11

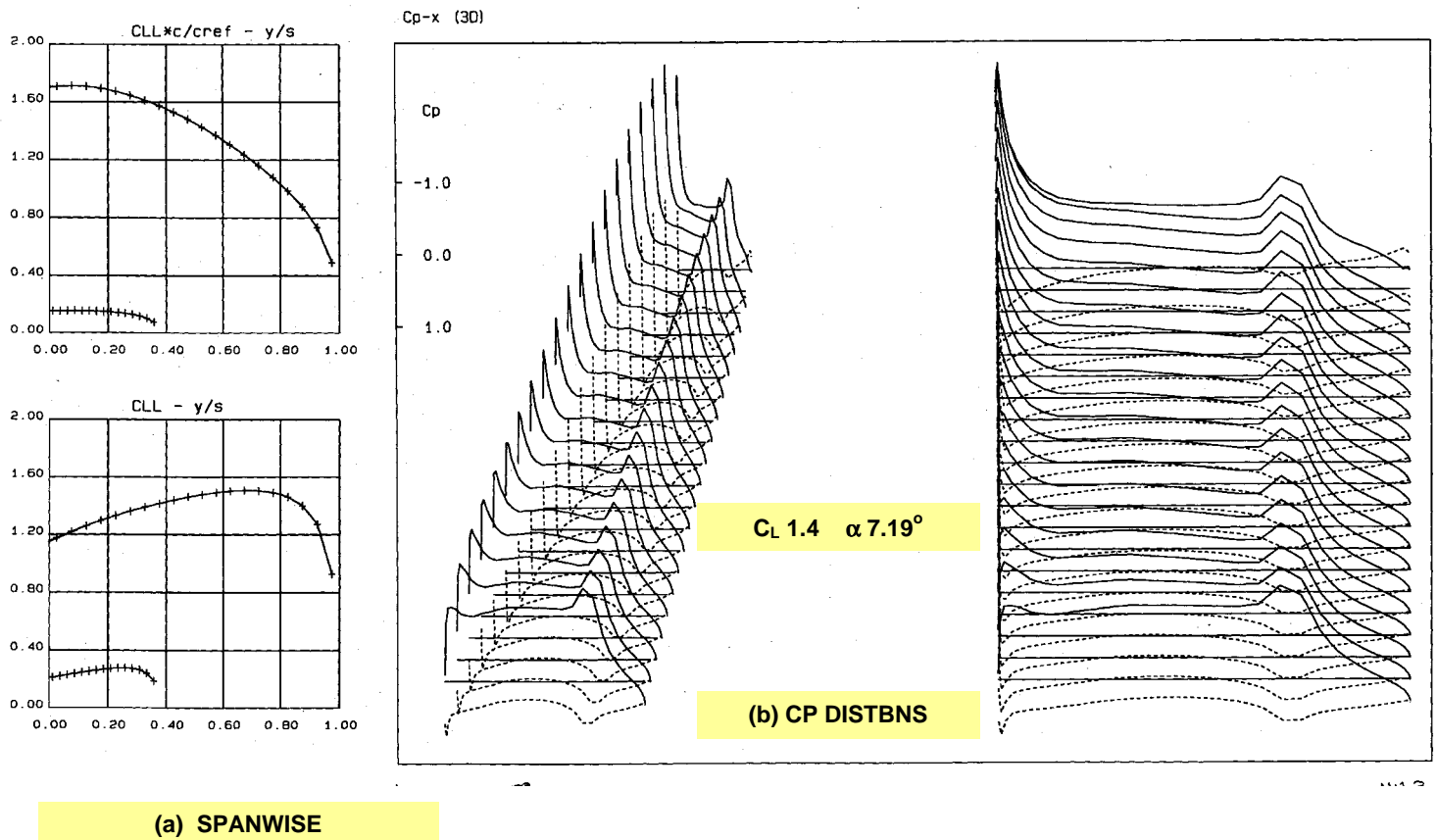


Fig. 5.3.14. $\delta_{TE} 15^\circ$ (Full-span Flap), LOADINGS, Trimmed $C_L 1.4$, M 0.20, AR 6 WING + TAILPLANE

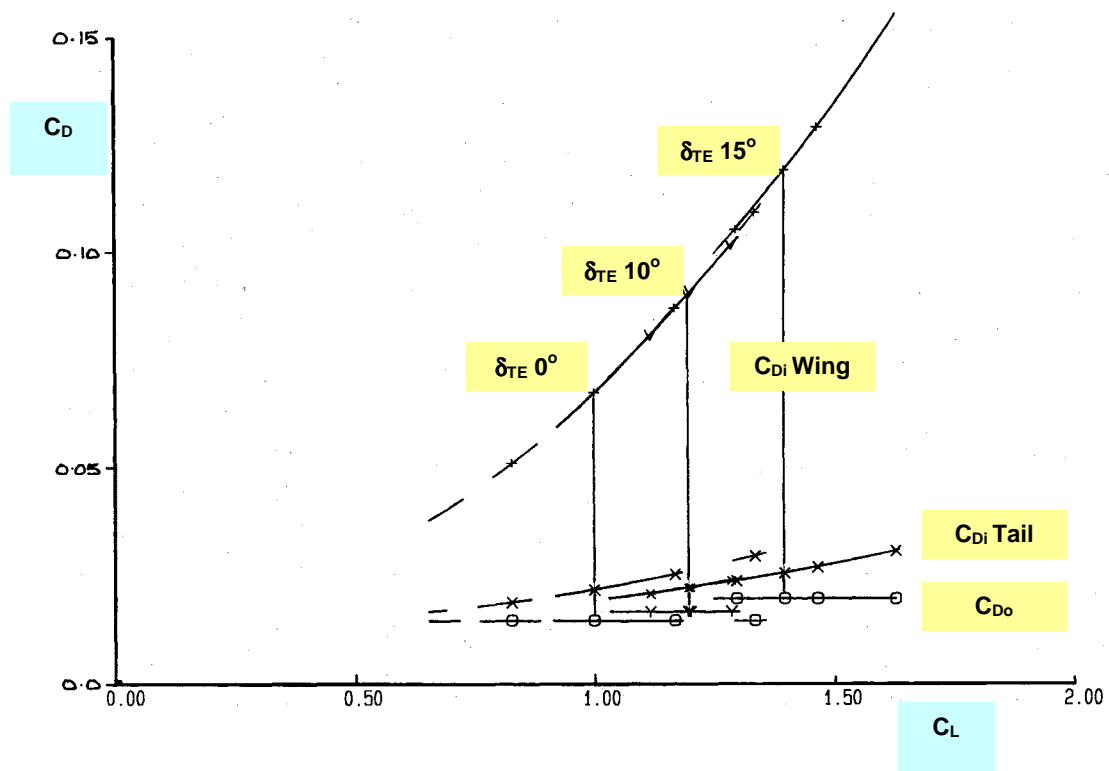


Fig. 5.3.15 $C_D - C_L$, M 0.20, AR 6 WING + TAILPLANE, Drag Breakdown, Effect of Flap Angle (Full-Span Plain Flap)

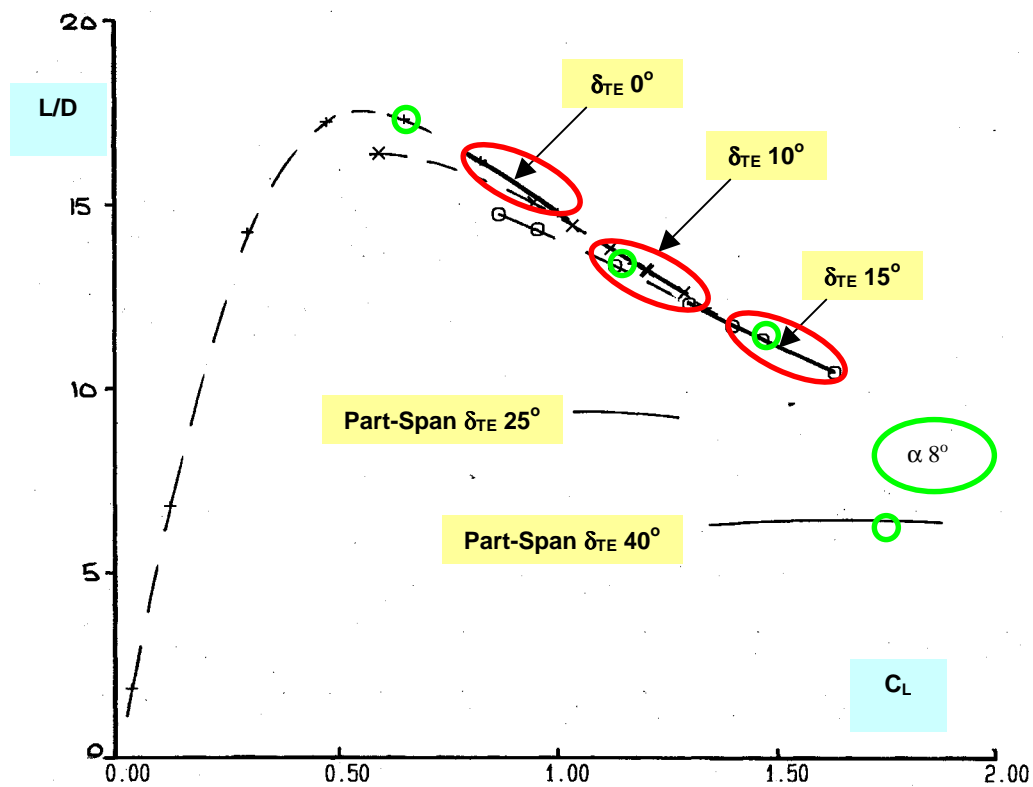
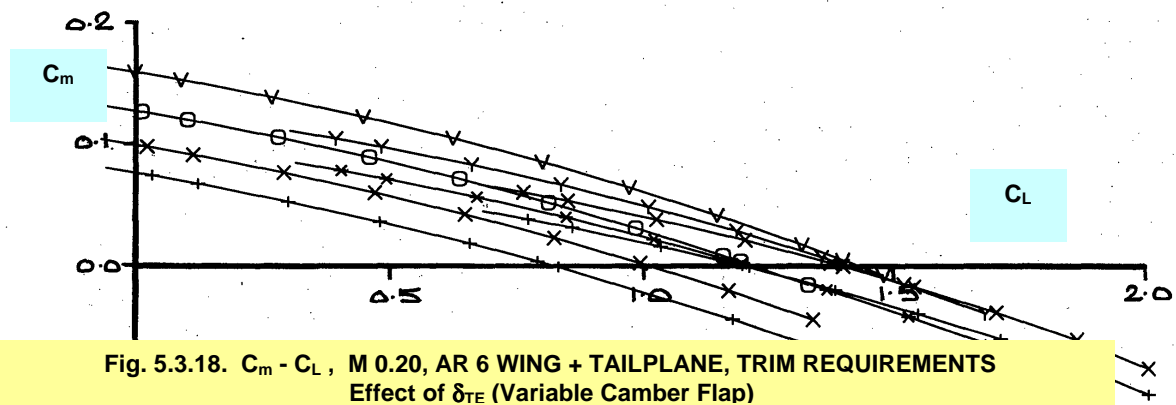
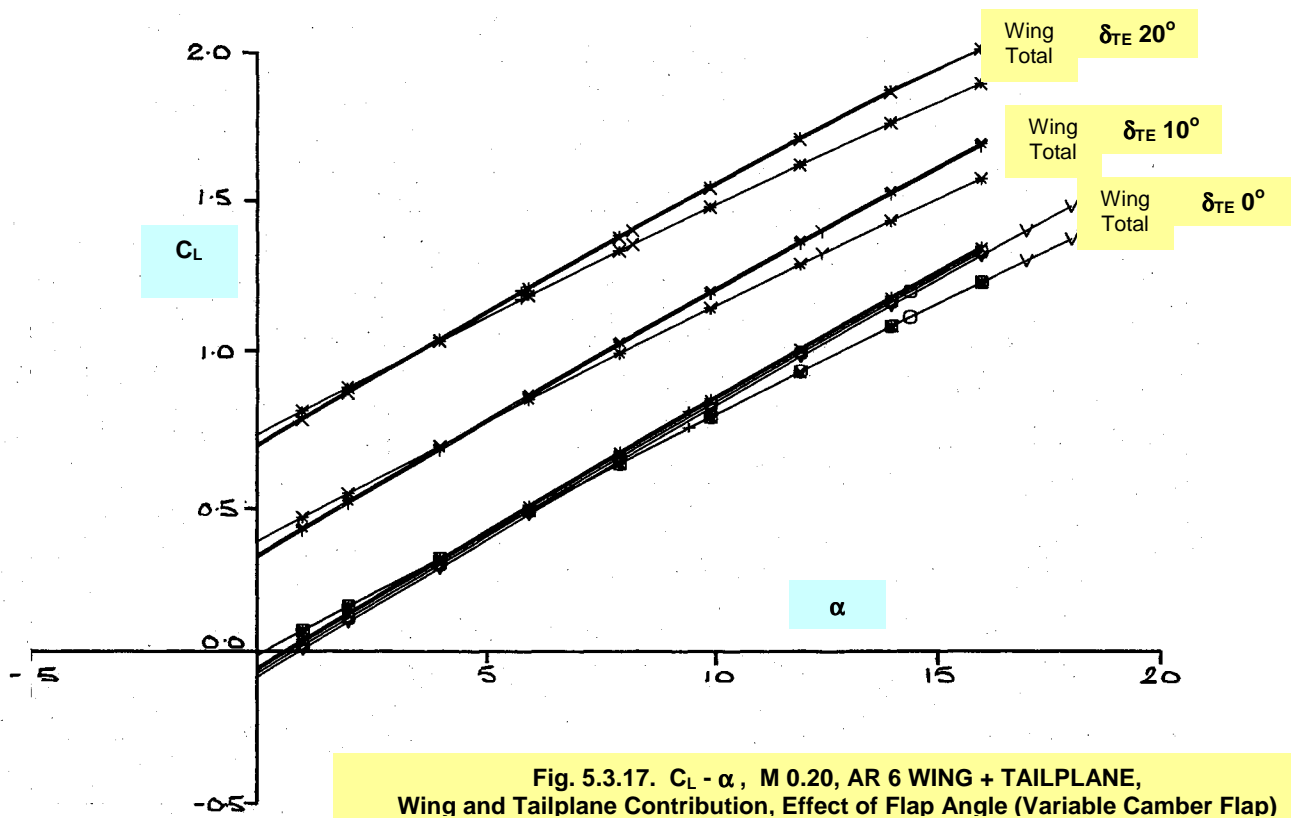
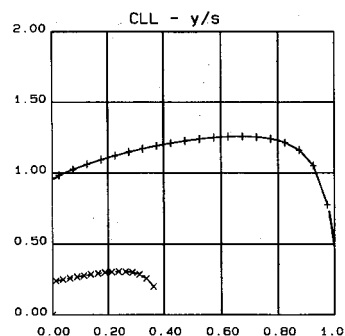
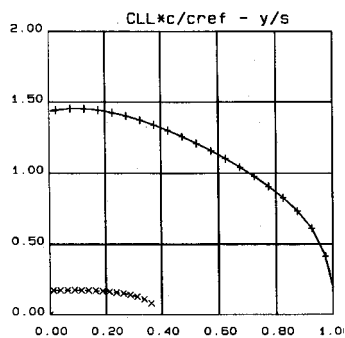


Fig. 5.3.16 $L/D - C_L$, M 0.20, AR 6 WING + TAILPLANE, Effect of Flap Angle (Full-Span Plain Flap)





(a) SPANWISE

Cp-x (3D)

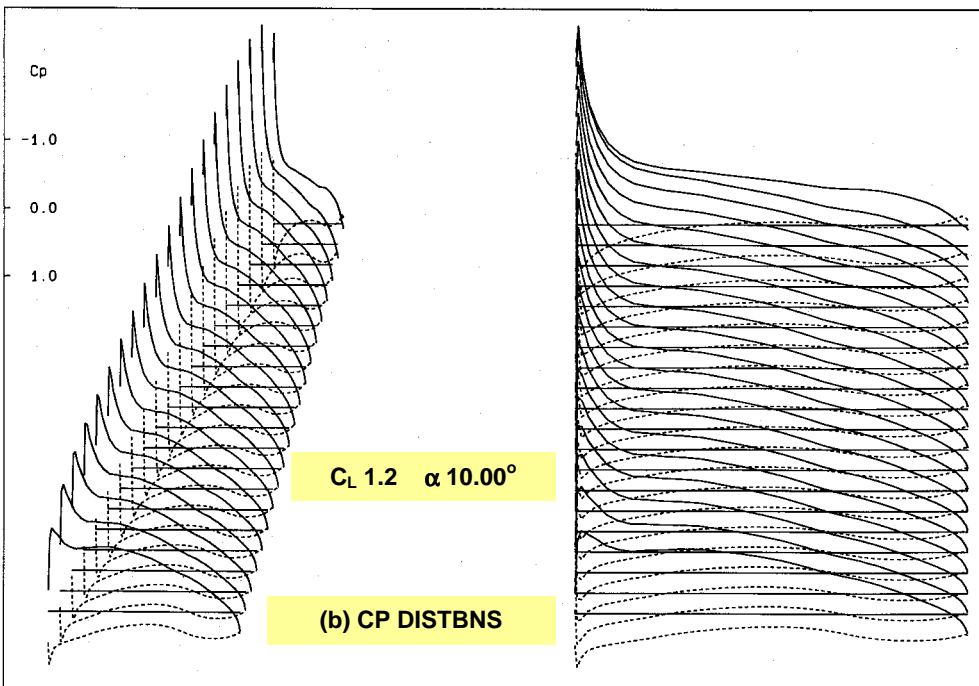
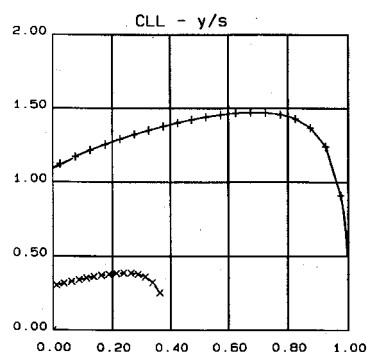
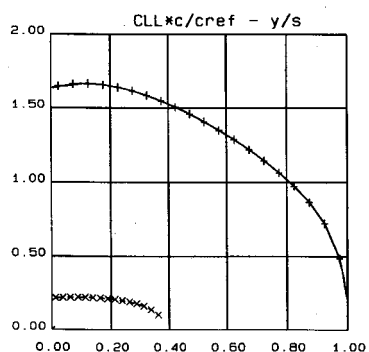


Fig. 5.3.19. $\delta_{TE} 10^\circ$ (Full-Span, Vari-Camber), LOADINGS, Trimmed $C_L 1.2$, $M 0.20$, AR 6 WING + TAILPLANE



(a) SPANWISE

Cp-x (3D)

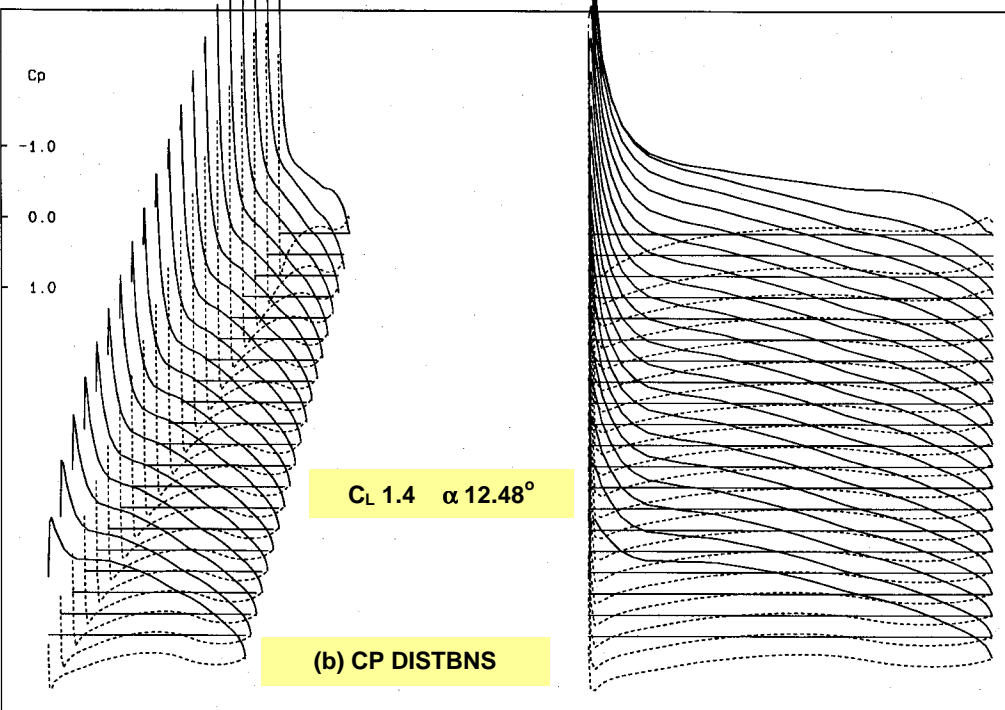


Fig. 5.3.20. $\delta_{TE} 10^\circ$ (Full-Span, Vari-Camber), LOADINGS, Trimmed $C_L 1.4$, $M 0.20$, AR 6 WING + TAILPLANE

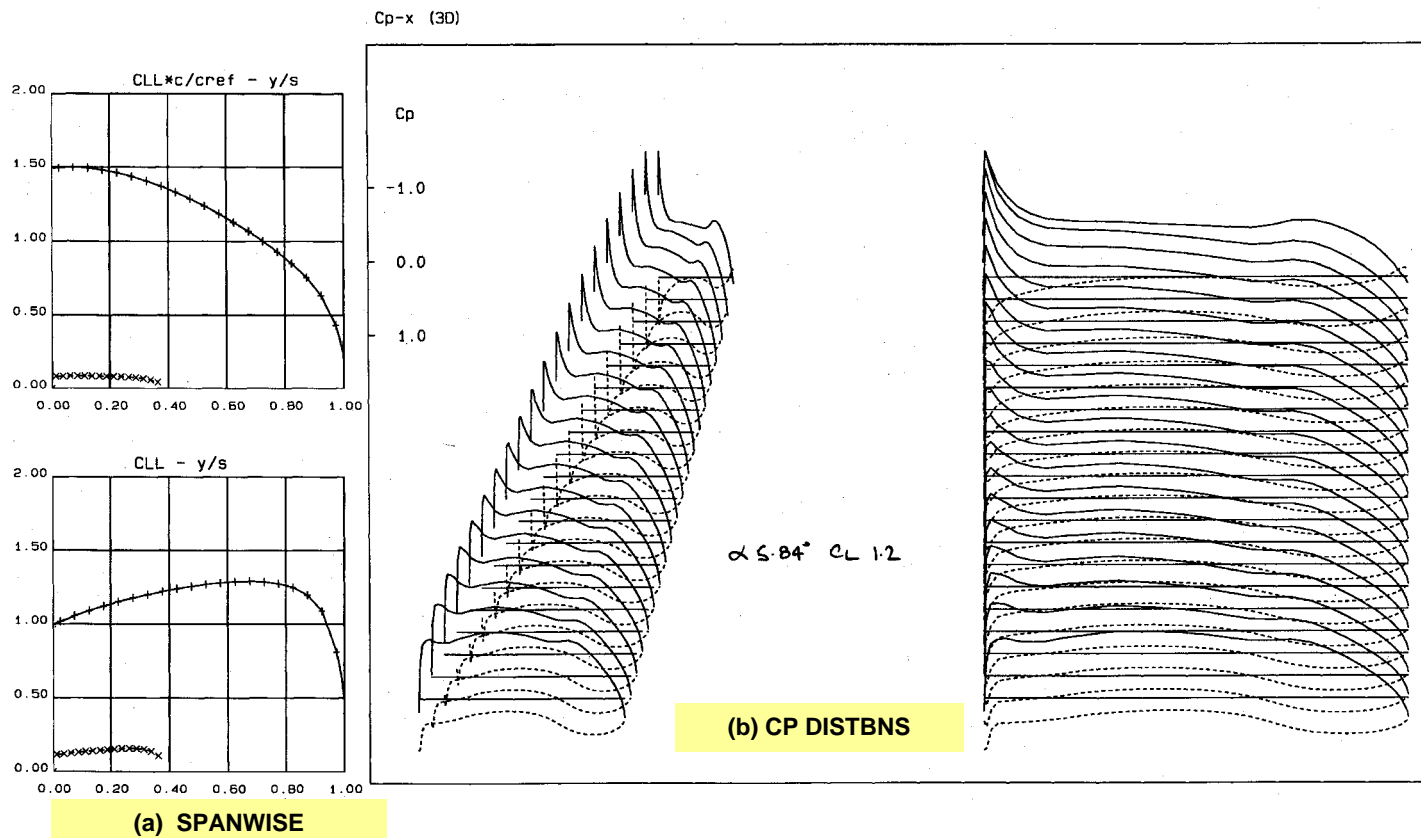


Fig. 5.3.21. $\delta_{TE} 20^\circ$ (Full-Span, Vari-Camber), LOADINGS, Trimmed $C_L 1.2$, M 0.20, AR 6 WING + TAILPLANE

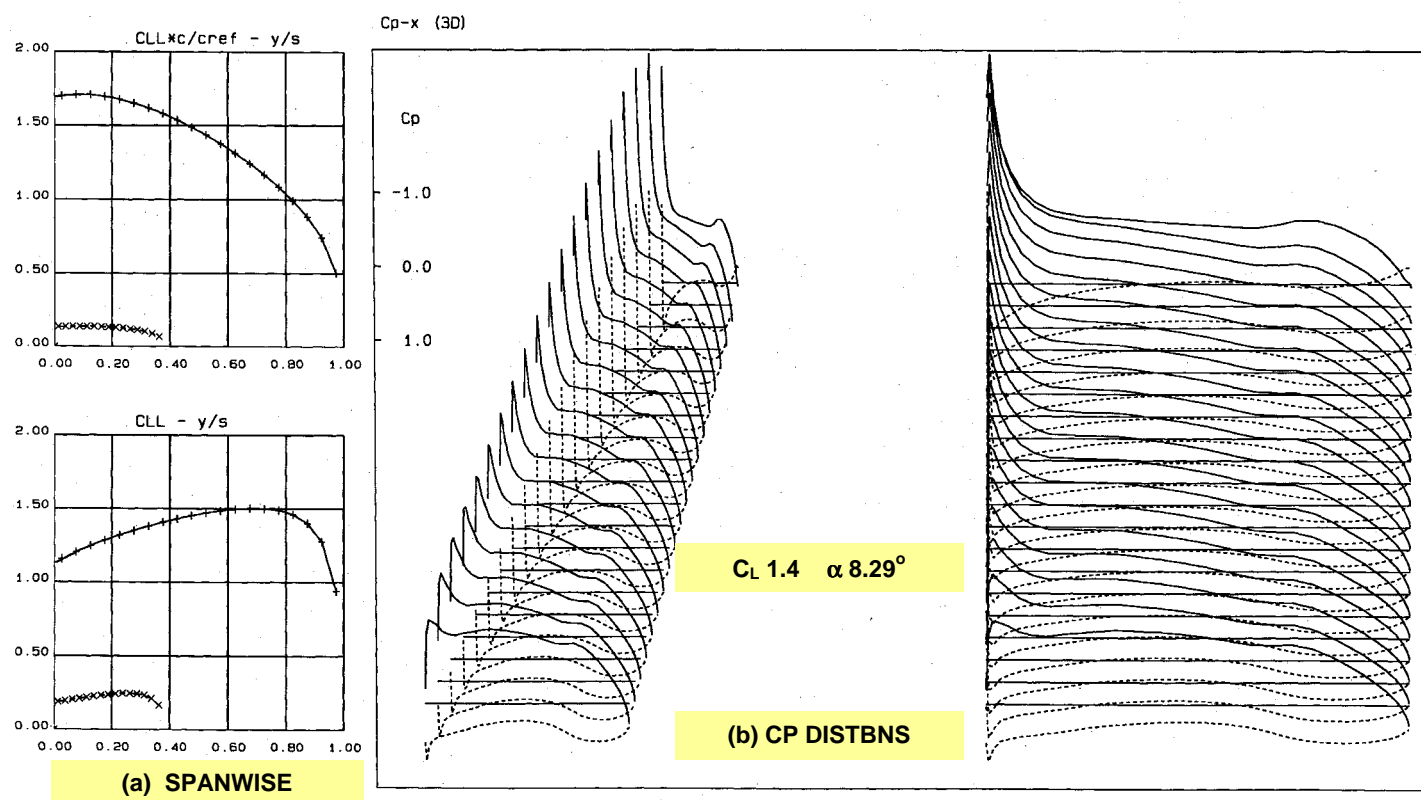


Fig. 5.3.22. $\delta_{TE} 20^\circ$ (Full-Span, Vari-Camber), LOADINGS, Trimmed $C_L 1.4$, M 0.20, AR 6 WING + TAILPLANE

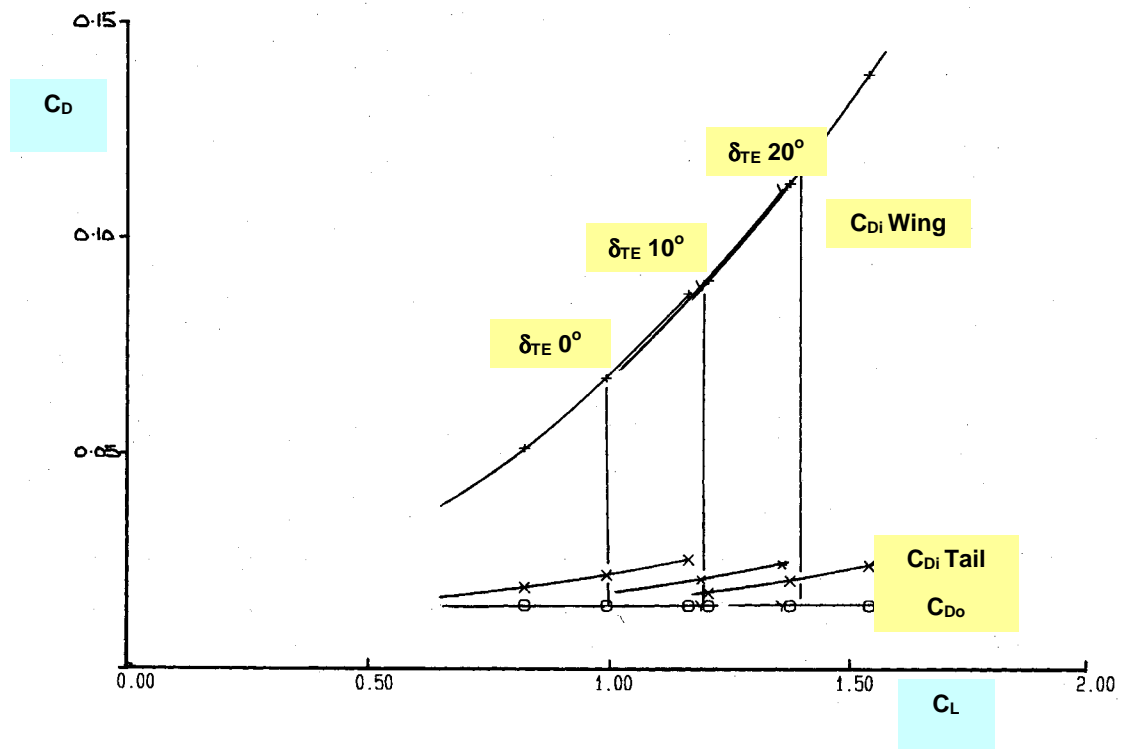


Fig. 5.3.23 $C_D - C_L$, M 0.20, AR 6 WING + TAILPLANE, Drag Breakdown, Effect of Flap Angle (Vari-Camber)

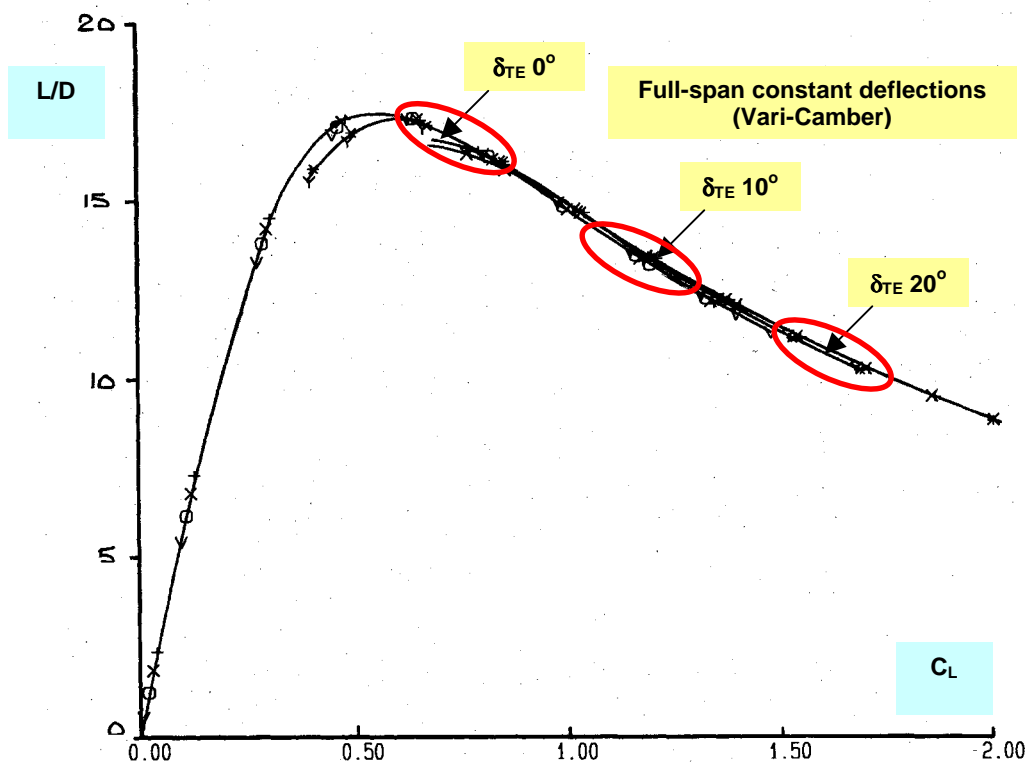
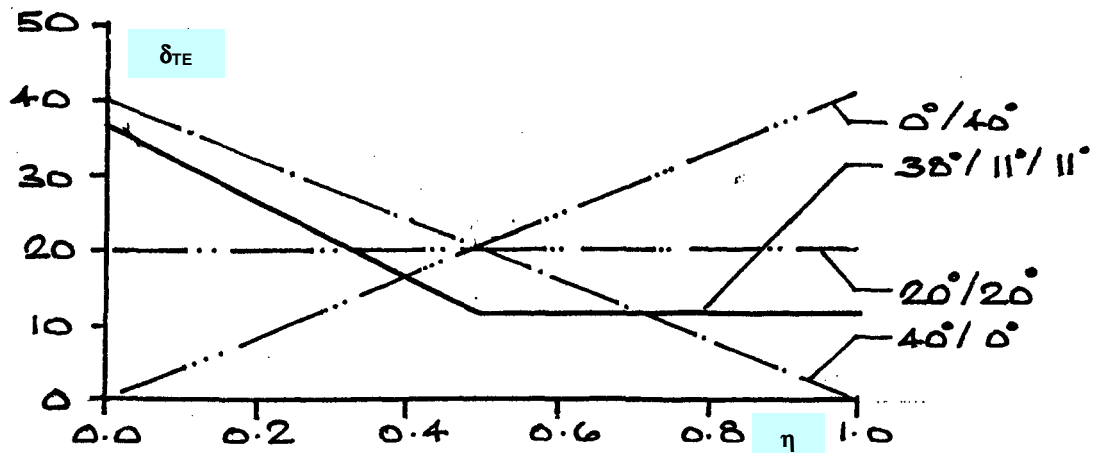
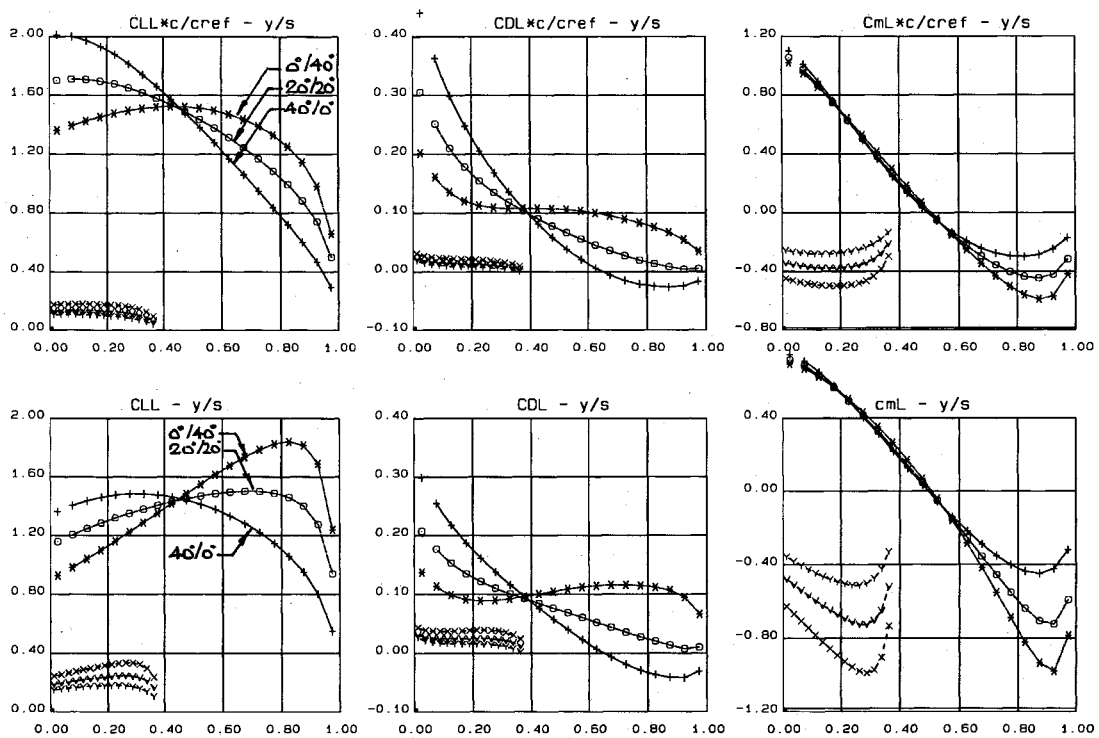


Fig. 5.3.24 $L/D - C_L$, M 0.20, AR 6 WING + TAILPLANE, Effect of Flap Angle (Vari-Camber)



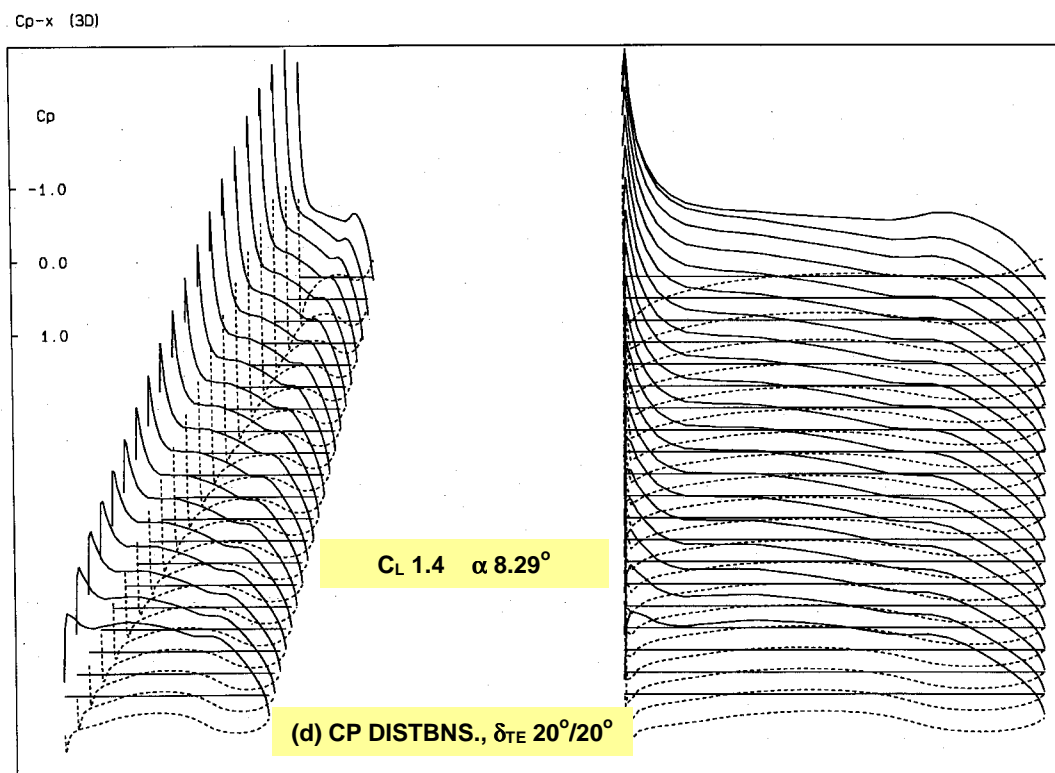
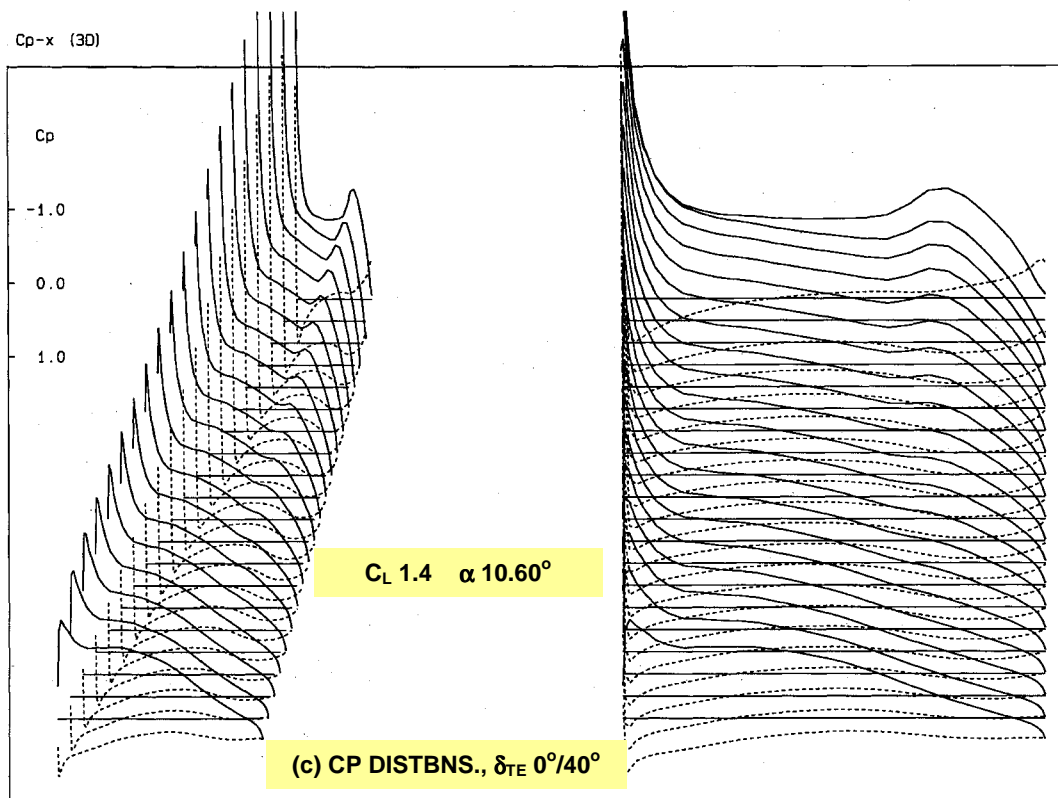
(a) δ_{TE} VARIATION ACROSS SEMI-SPAN



(b) SPANWISE LOADINGS FOR 0°/40°, 20°/20° and 40°/0° δ_{TE} DISTRIBUTIONS, TRIMMED C_L 2.0

AR 6 M-2 VARI-CAMBER

5.3. (b)



Cp-x (3D)

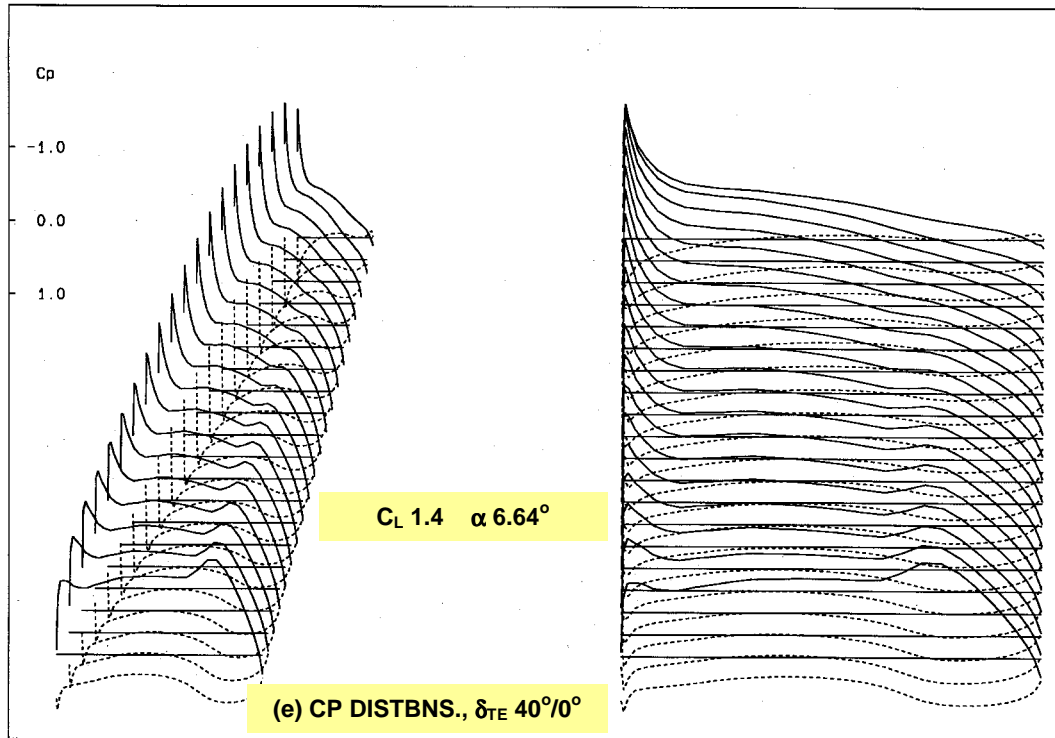


Fig. 5.3.25. DISTRIBUTED δ_{TE} (Full-Span, Vari-Camber), DEFLECTION DISTRIBUTIONS and LOADINGS, Trimmed $C_L 1.4$, $M 0.20$, AR 6 WING + TAILPLANE

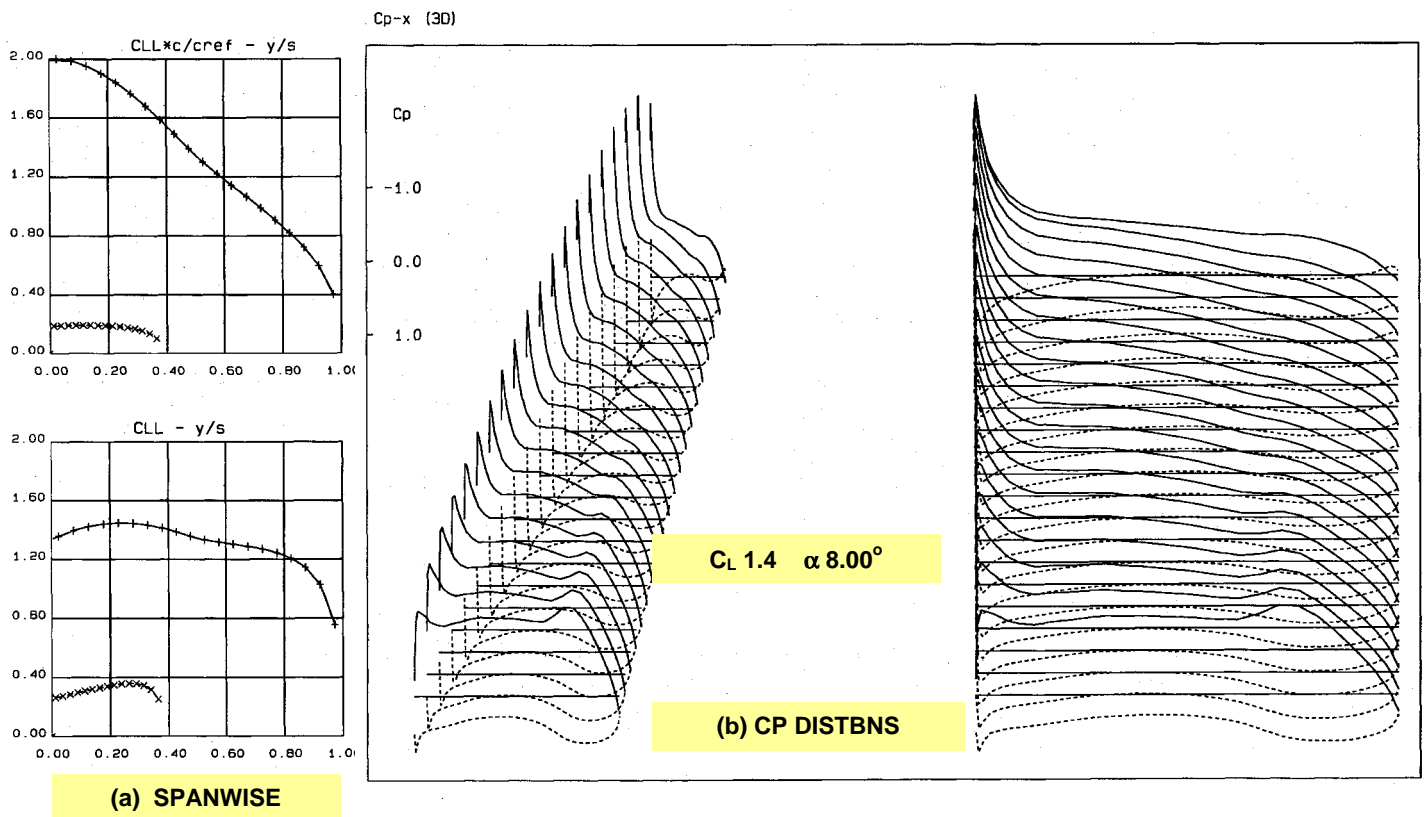


Fig. 5.3.26. DISTRIBUTED $\delta_{TE} 38^\circ/11^\circ/11^\circ$ (Full-Span, Variable TE), LOADINGS, Trimmed $C_L 1.4$, $M 0.20$, $\alpha 8^\circ$, AR 6 WING + TAILPLANE

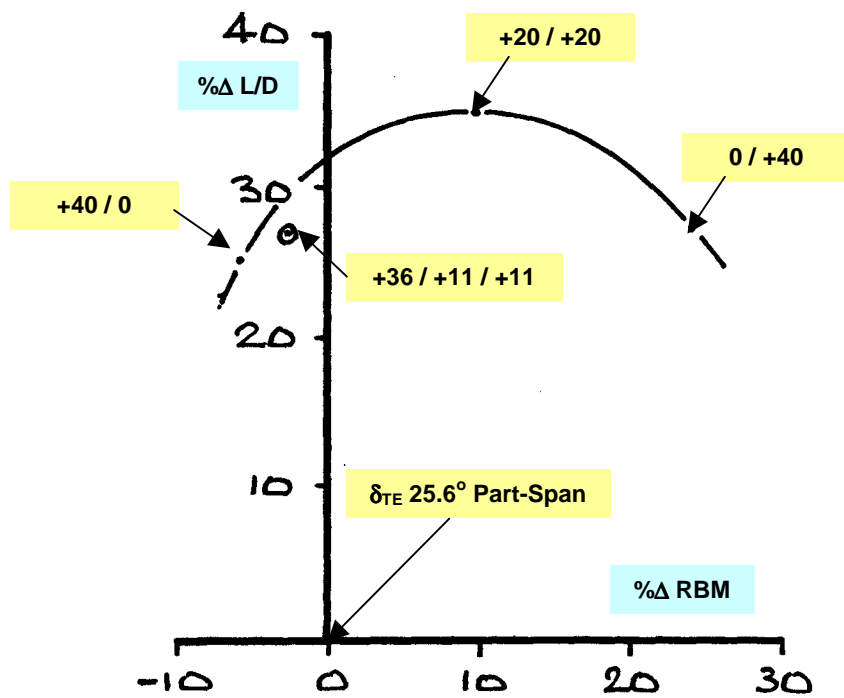


Fig. 5.3.27. L/D and RBM % CHANGES BASED ON δ_{TE} 25.6° Part-Span TEF
Effect of Flap Angle and Trimming, C_L 1.4, M 0.20, α 8°, AR 6 WING + TAILPLANE
(Distributed Variable TE Geometry)

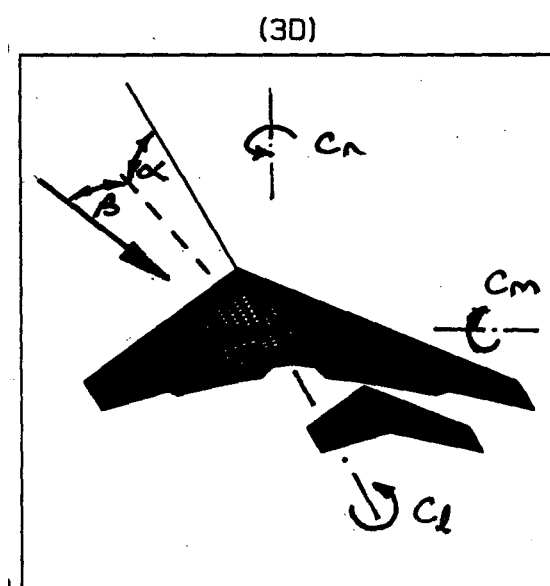
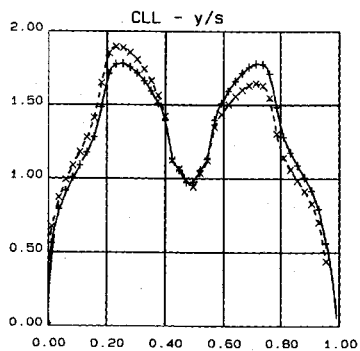
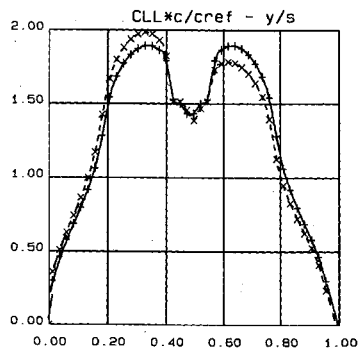
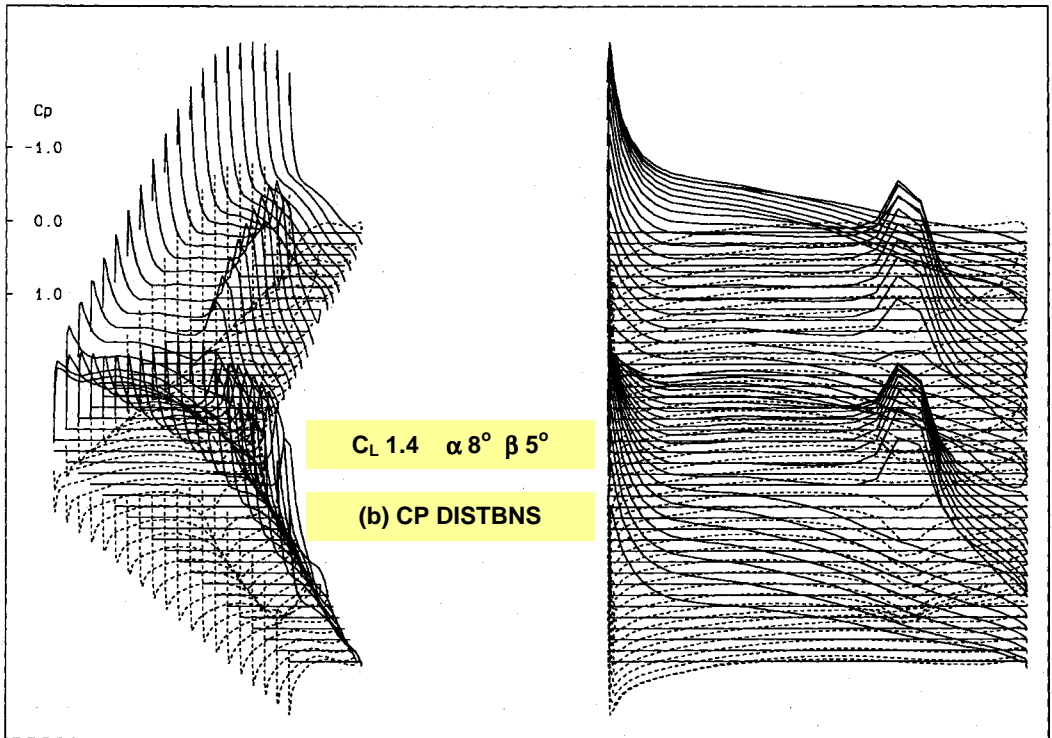


Fig. 5.4.1. AR 6 WING + TAILPLANE TYPICAL PANELLING, SIDESLIP CASES, SIGN CONVENTIONS



$C_L 1.4 \quad \alpha 8^\circ \quad \beta 0^\circ/5^\circ$
(a) SPANWISE

Cp-x (3D)

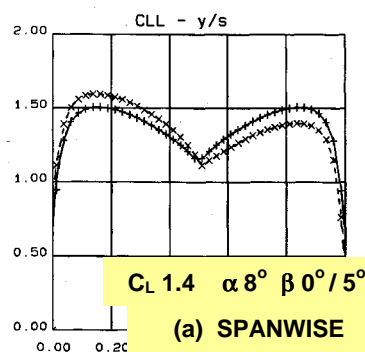
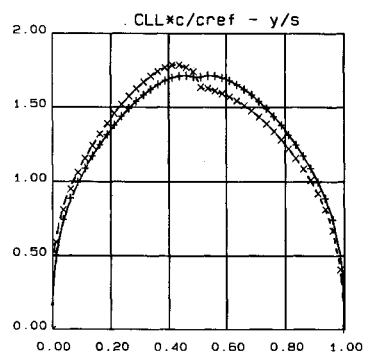


$C_L 1.4 \quad \alpha 8^\circ \quad \beta 5^\circ$

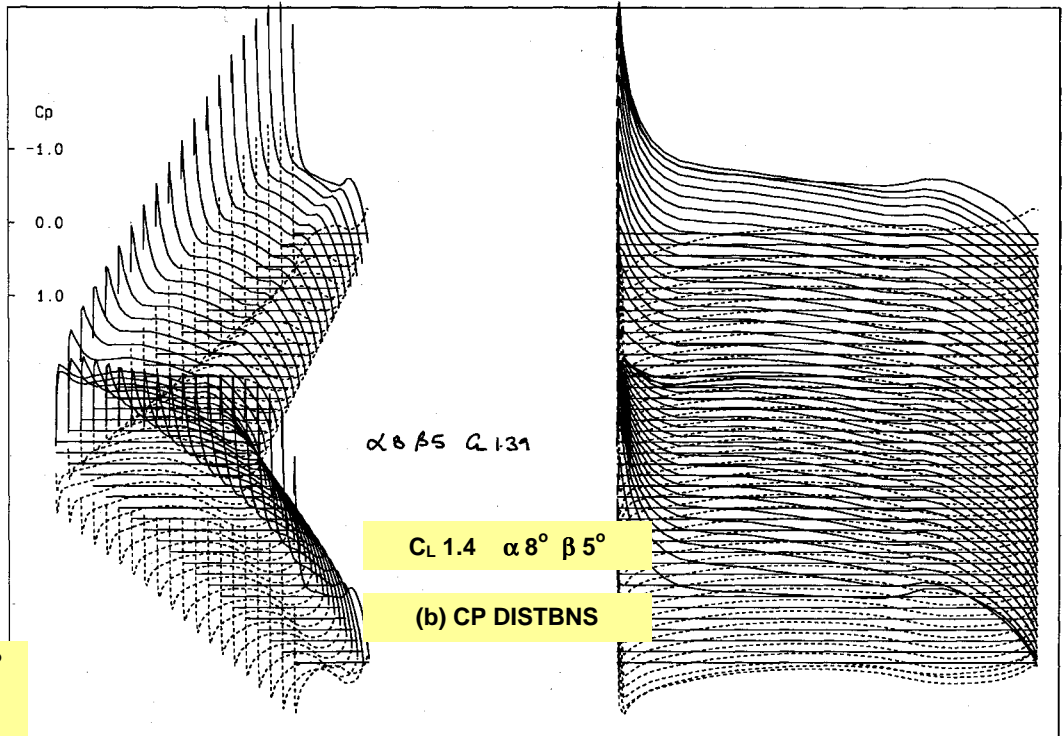
(b) CP DISTBNS

Fig. 5.4.2. $\delta_{TE} 25^\circ$ (Plain Flap), LOADINGS,
Trimmed $C_L 1.4$, $M 0.20$, $\alpha 8^\circ$, $\beta 5^\circ$, AR 6 WING + TAILPLANE

Cp-x (3D)



$C_L 1.4 \quad \alpha 8^\circ \quad \beta 0^\circ/5^\circ$
(a) SPANWISE



$\alpha 8^\circ \quad \beta 5^\circ \quad Q 1.31$

$C_L 1.4 \quad \alpha 8^\circ \quad \beta 5^\circ$

(b) CP DISTBNS

Fig. 5.4.3. $\delta_{TE} 20.7^\circ$ (Full-Span Vari-Camber), LOADINGS,
Trimmed $C_L 1.4$, $M 0.20$, $\alpha 8^\circ$, $\beta 5^\circ$, AR 6 WING + TAILPLANE

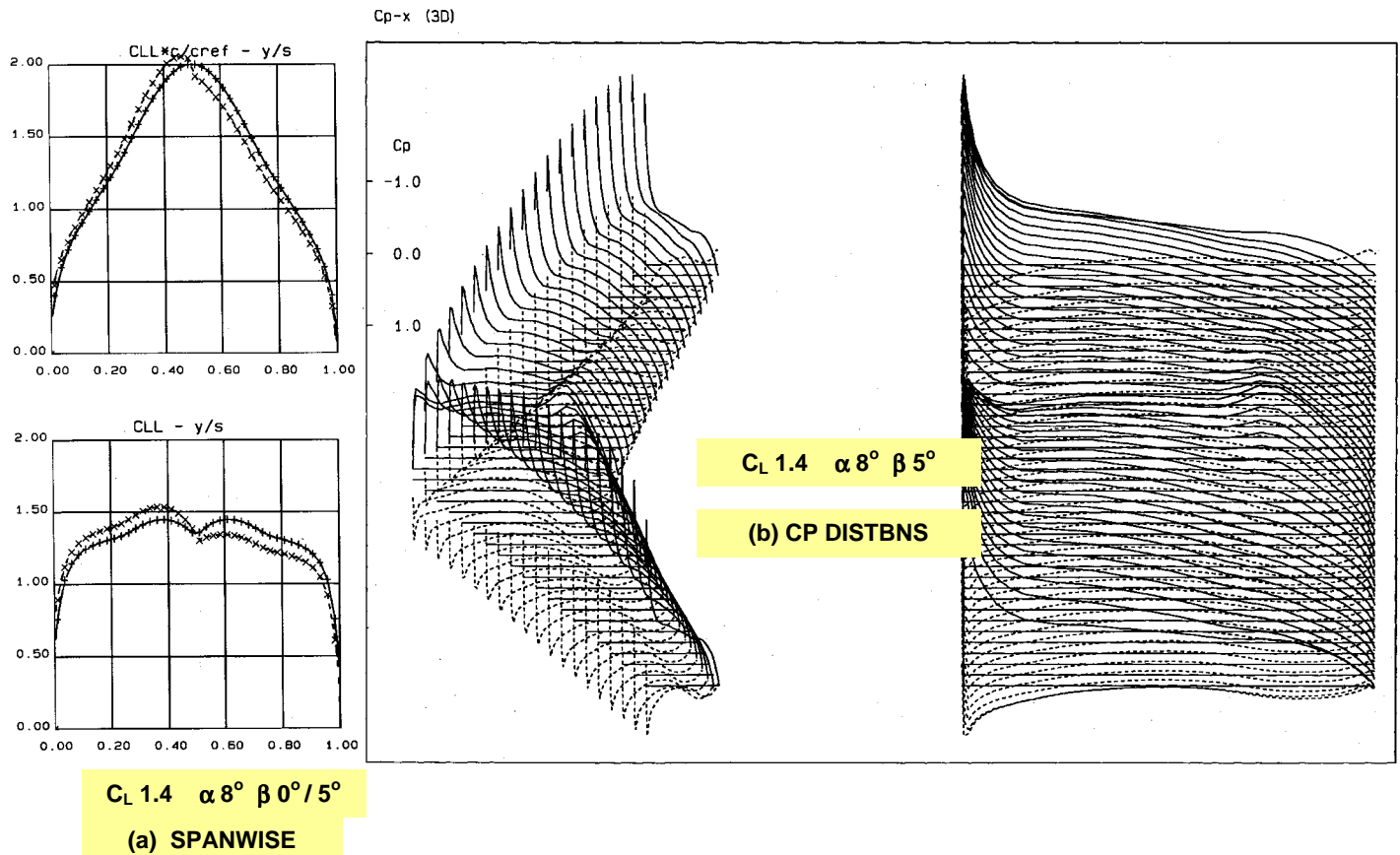


Fig. 5.4.4. DISTRIBUTED $\delta_{TE} 36.3^\circ / 11.3^\circ / 11.3^\circ$ (Full-Span Vari-Camber), LOADINGS, Trimmed $C_L 1.4$, $M 0.20$, $\alpha 8^\circ$, $\beta 5^\circ$, AR 6 WING + TAILPLANE

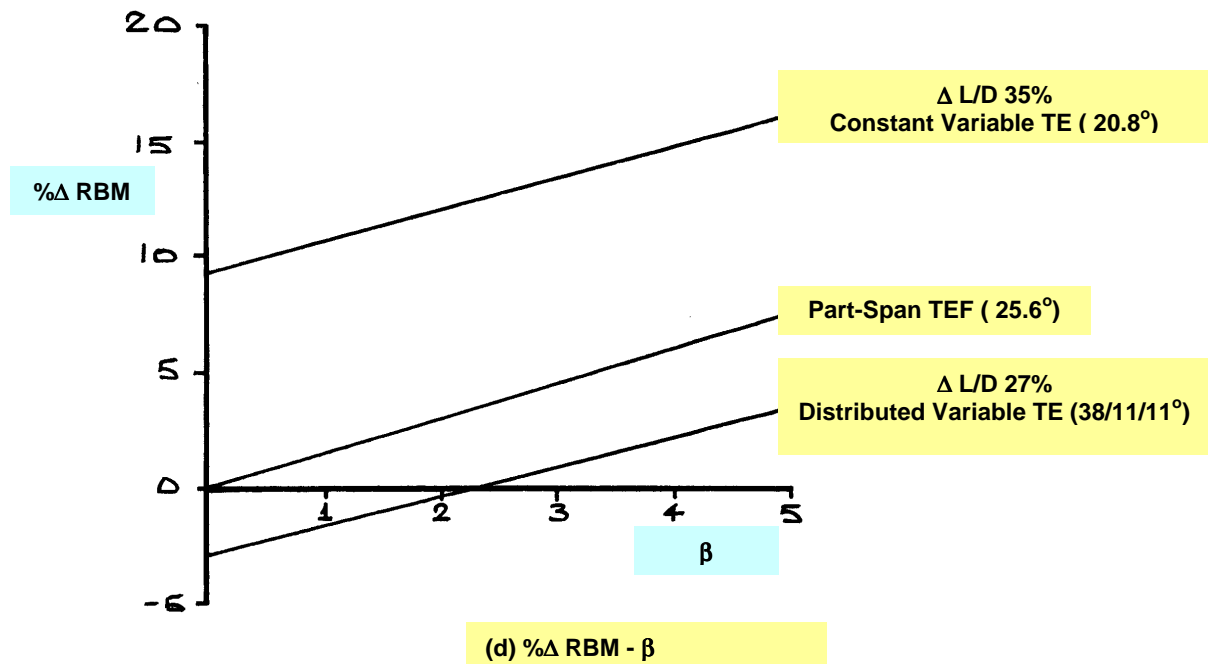


Fig. 5.4.5. RBM INCREMENTS - β
FULL-SPAN VARIABLE TE ($\delta_{TE} 20.7^\circ$), DISTRIBUTED ($\delta_{TE} 36.3^\circ / 11.3^\circ / 11.3^\circ$) & PART-SPAN ($\delta_{TE} 25.6^\circ$)
REFERENCED TO PART-SPAN ($\delta_{TE} 25.6^\circ$) AT $\beta 0^\circ$
Trimmed $C_L 1.4$, $M 0.20$, $\alpha 8^\circ$, AR 6 WING + TAILPLANE

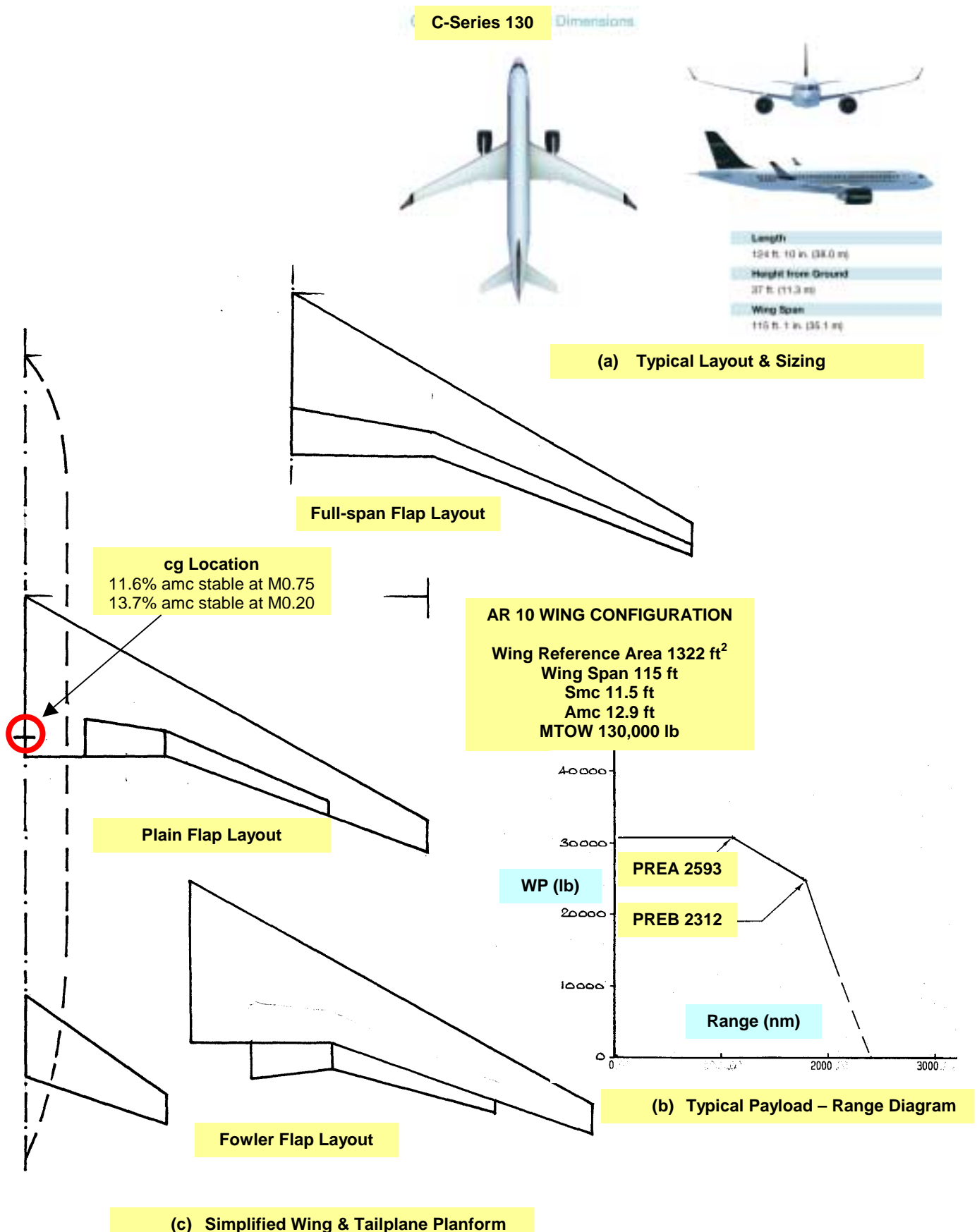
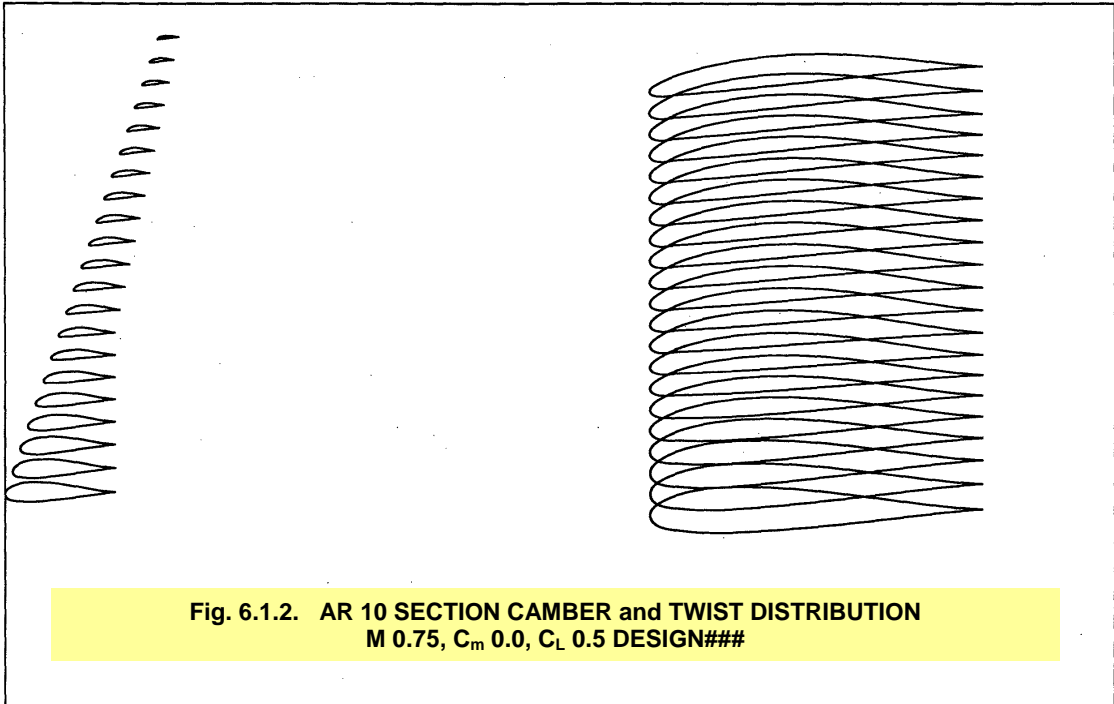


Fig. 6.1.1. MODERN MEDIUM CAPACITY - MEDIUM RANGE AR 10 WING CONFIGURATION
(Based on Bombardier C-Series 110 & 130)



Z - X

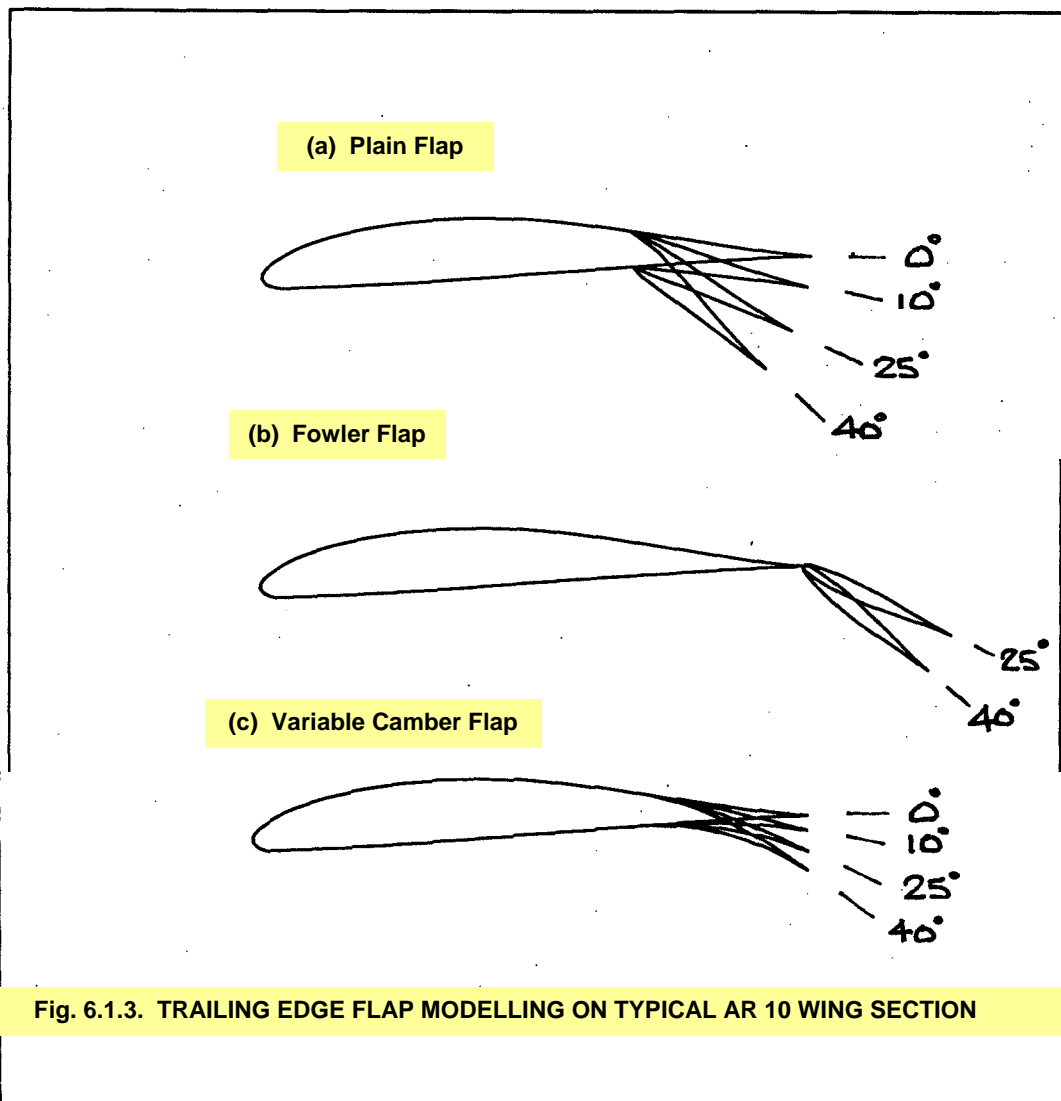


Fig. 6.1.3. TRAILING EDGE FLAP MODELLING ON TYPICAL AR 10 WING SECTION

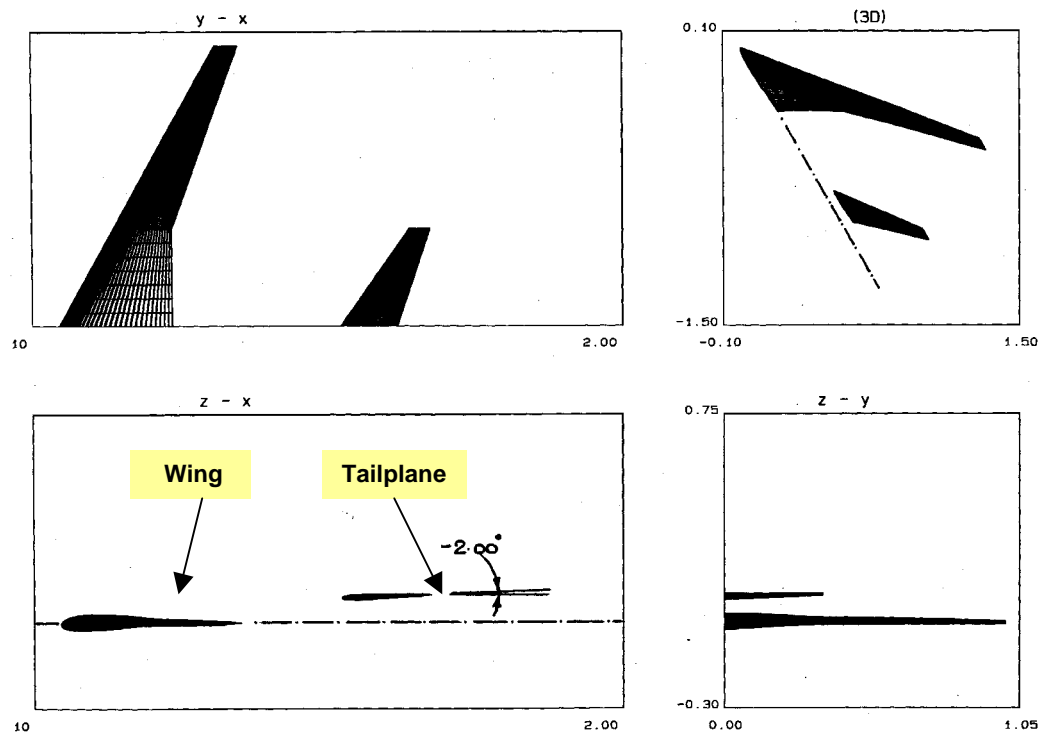


Fig. 6.1.4. AR 10 WING + TAILPLANE TYPICAL PANELLING

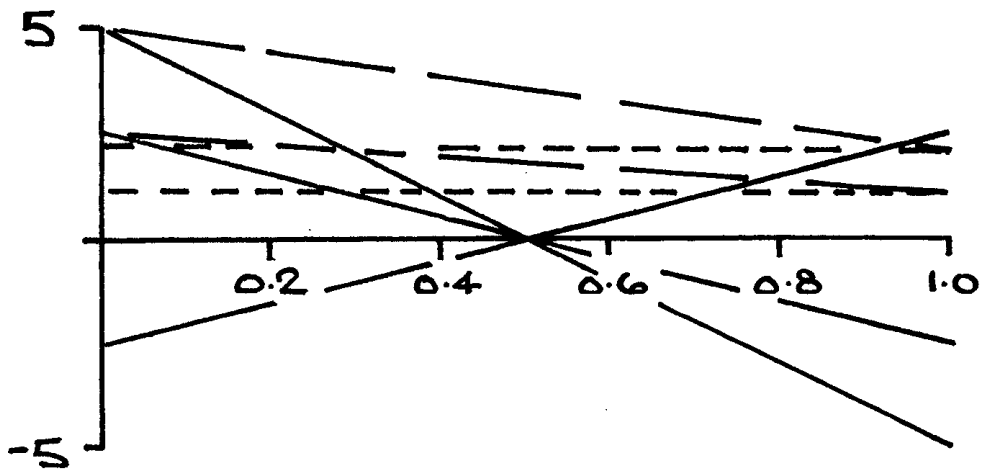


Fig. 6.2.1. TEF DEFLECTION SPANWISE DISTRIBUTION, $\delta - \eta$, VARIOUS FLAP TYPES
M 0.75, AR 10 WING + TAILPLANE

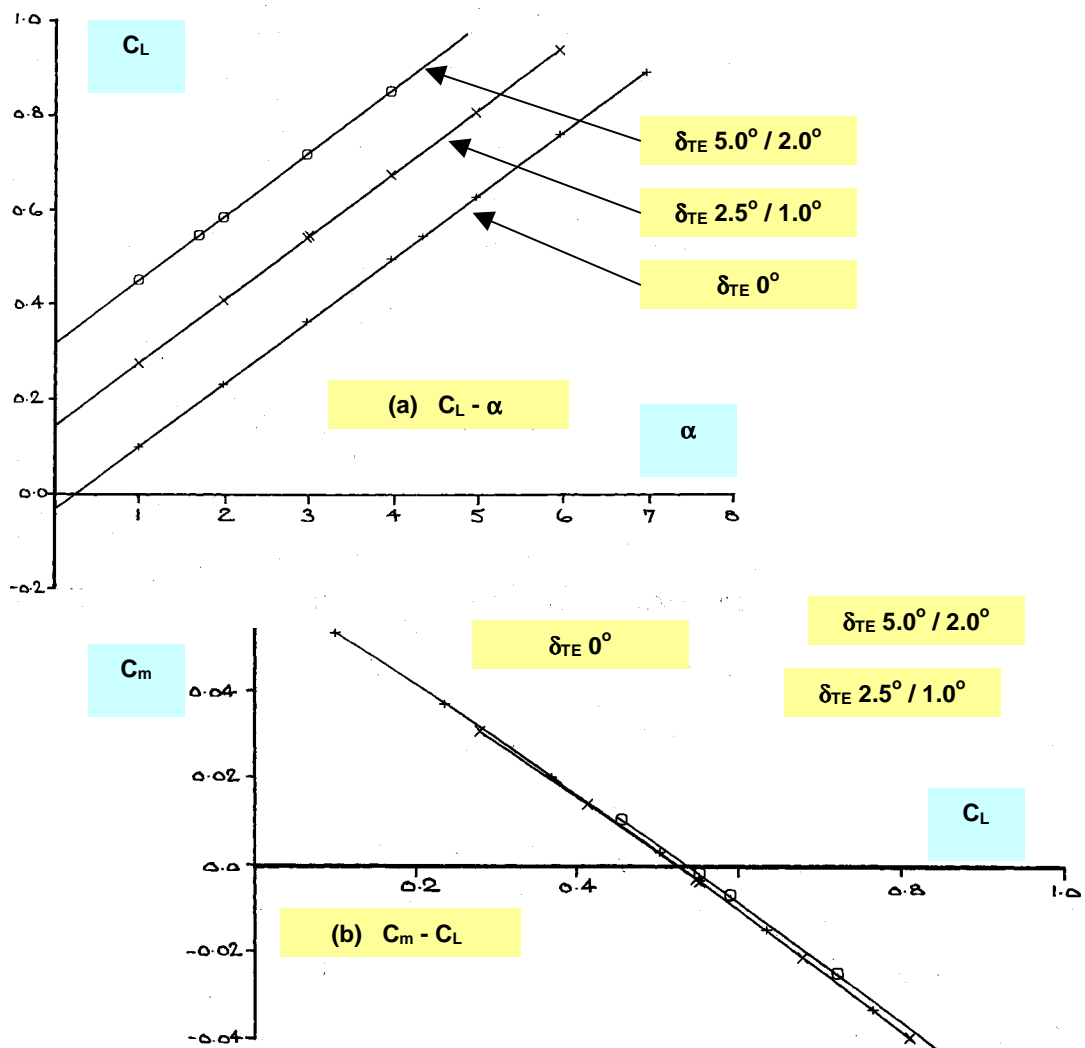
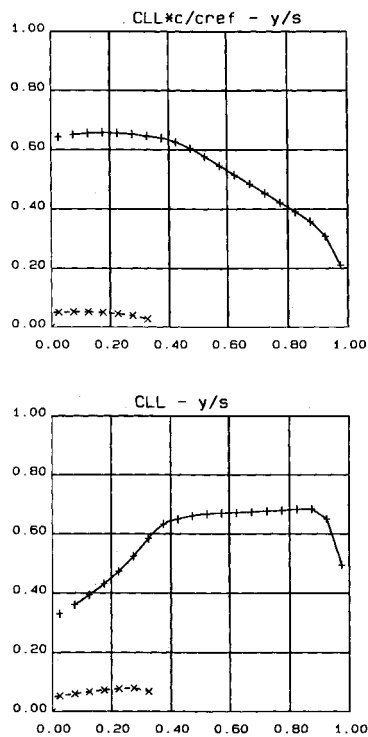


Fig. 6.2.2. $C_L - \alpha$, $C_m - C_L$, M 0.75, AR 10 WING + TAILPLANE,
Effect of Flap Type and Angle



(a) SPANWISE

Cp-x (3D)

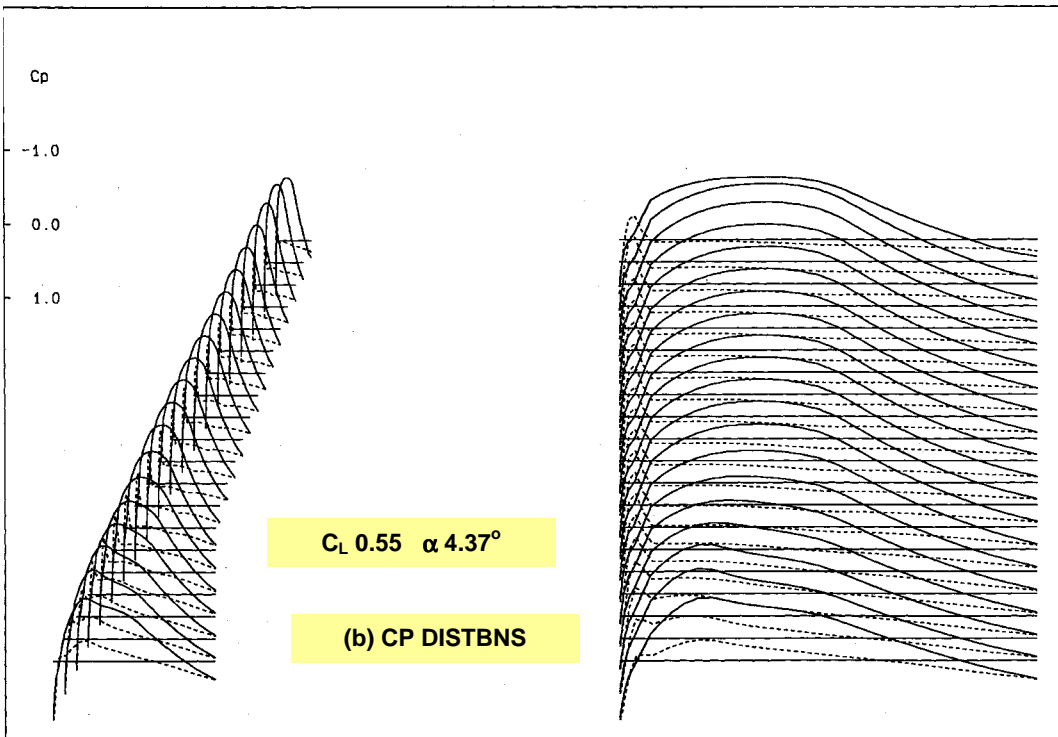
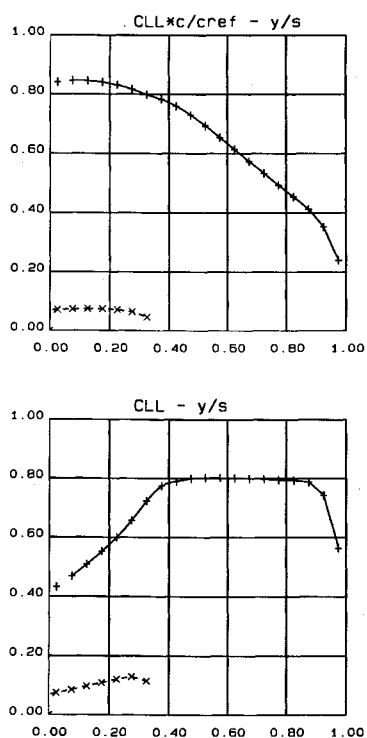


Fig. 6.2.3. CRUISE CONDITION (DATUM), LOADINGS, Trimmed $C_L 0.55$, M 0.75, AR 10 WING + TAILPLANE

6.2.2 (b)



(a) SPANWISE

Cp-x (3D)

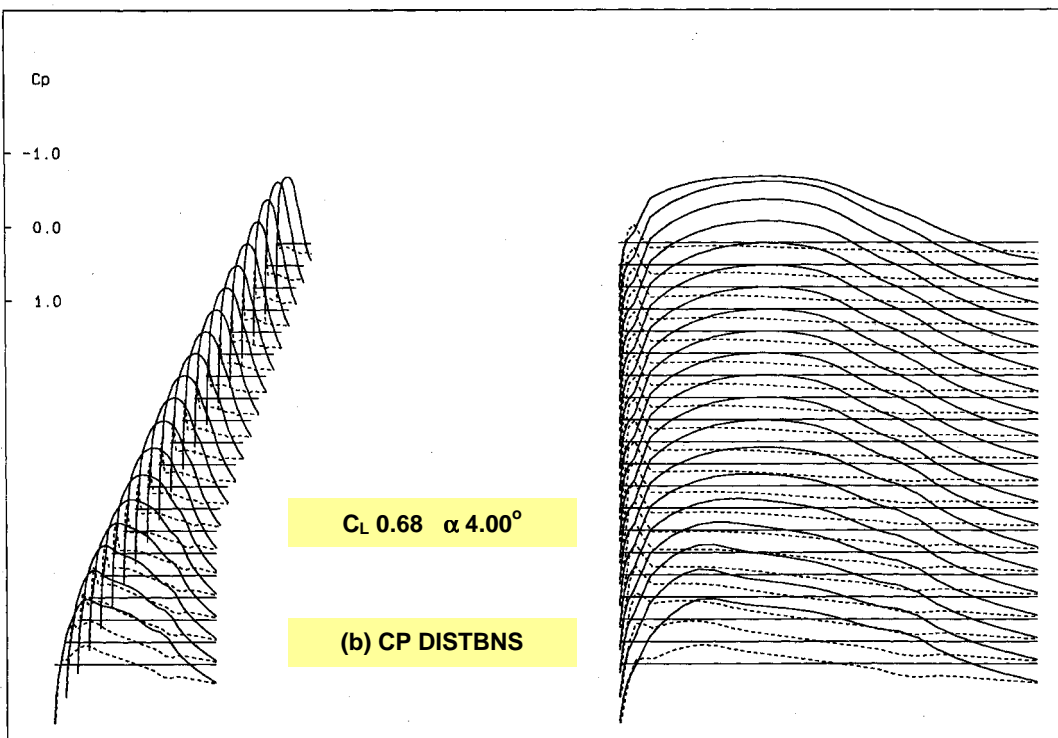
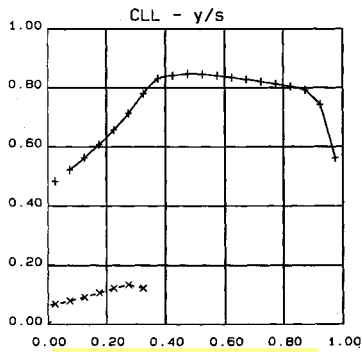
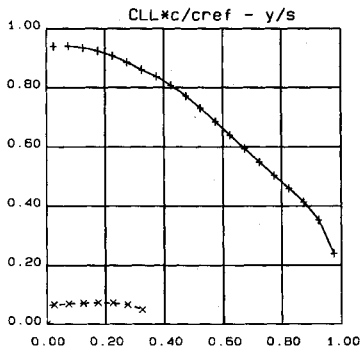


Fig. 6.2.4. PLAIN FLAP, ROOT to TIP VARIATION ($\delta_{TE} 2.5^\circ / 1.0^\circ$), LOADINGS, M 0.75, AR 10 WING + TAILPLANE



(a) SPANWISE

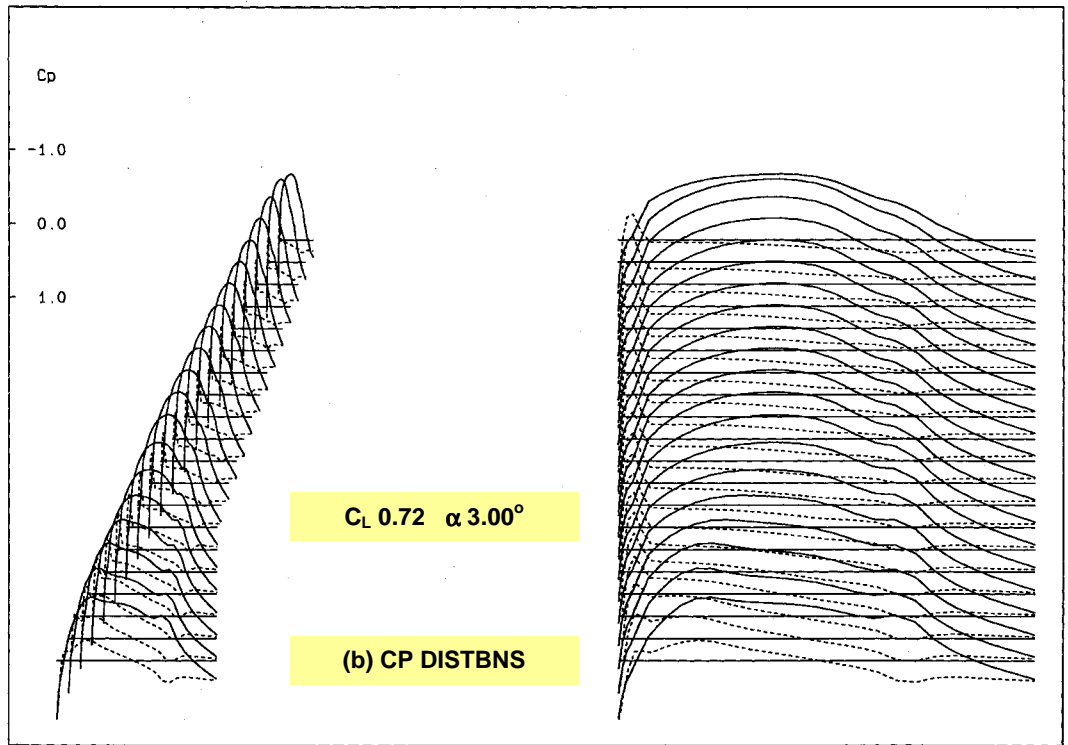


Fig. 6.2.5. PLAIN FLAP, ROOT to TIP VARIATION ($\delta_{TE} 5.0^\circ / 2.0^\circ$), LOADINGS, M 0.75, AR 10 WING + TAILPLANE

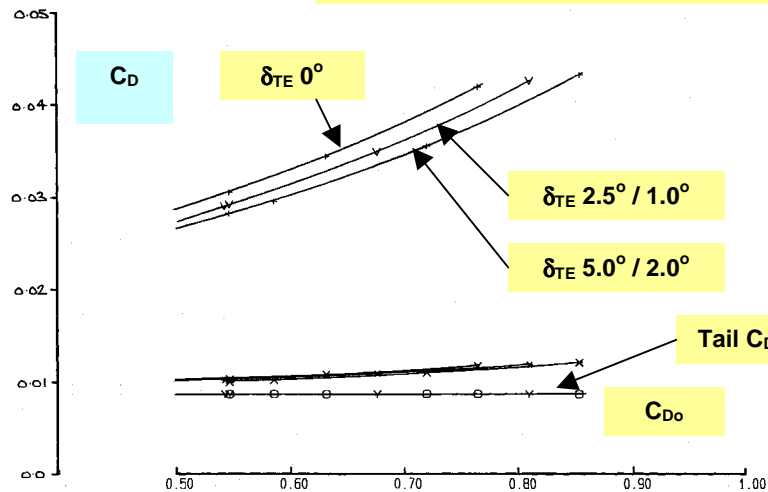


Fig. 6.2.6 $C_D - C_L$, M 0.75, AR 10 WING + TAILP
Drag Breakdown, Effect of Flap Angle (Full-Span P

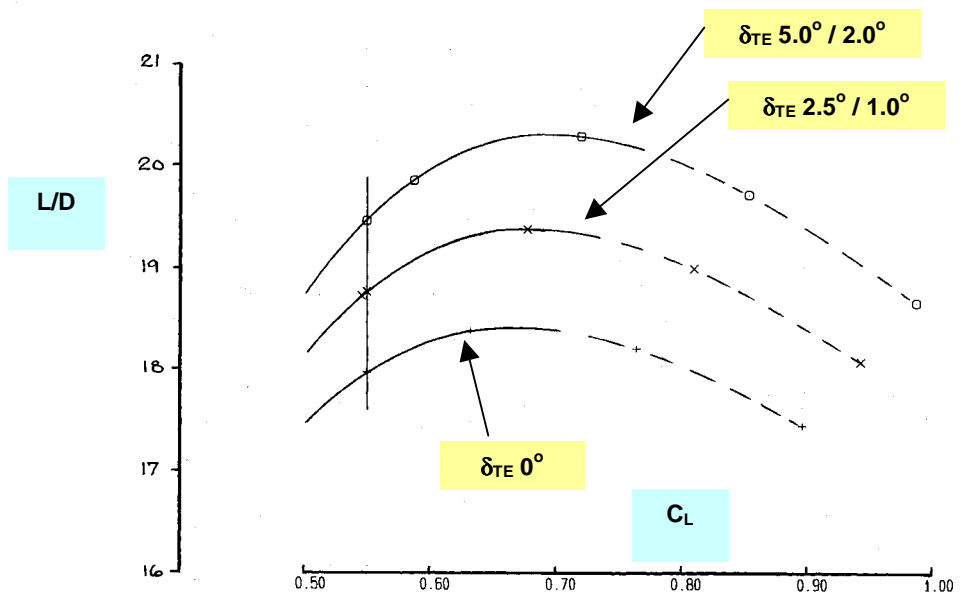
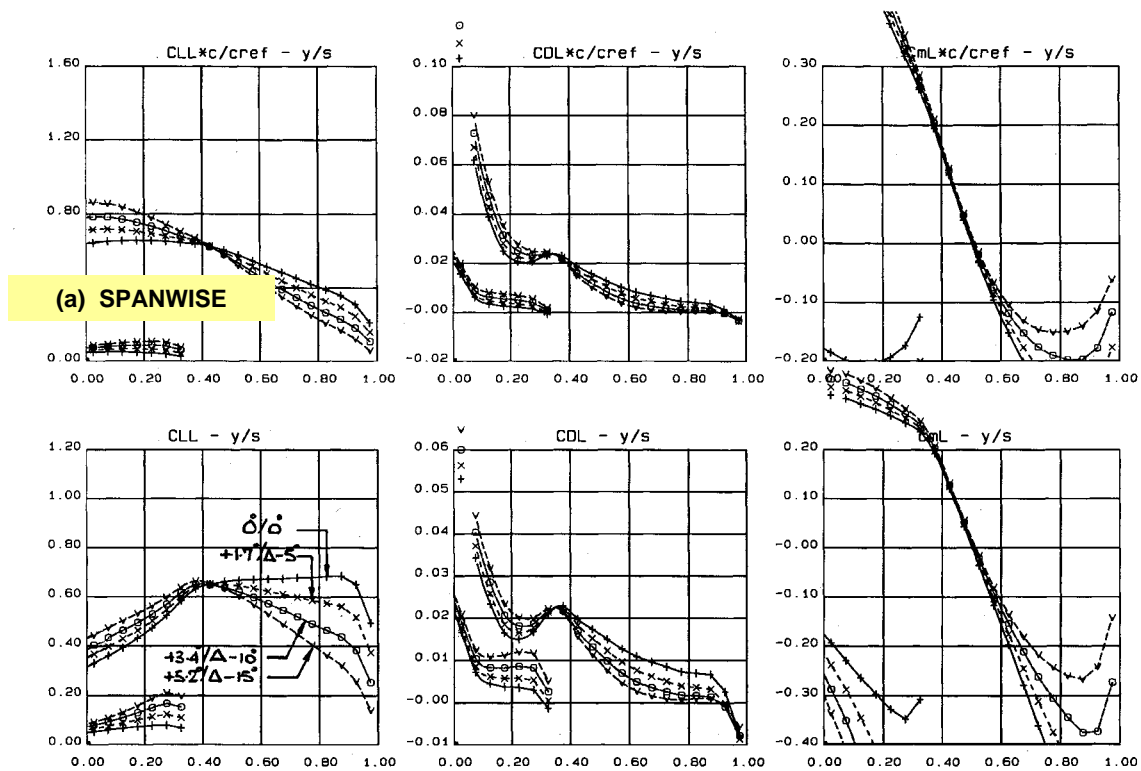


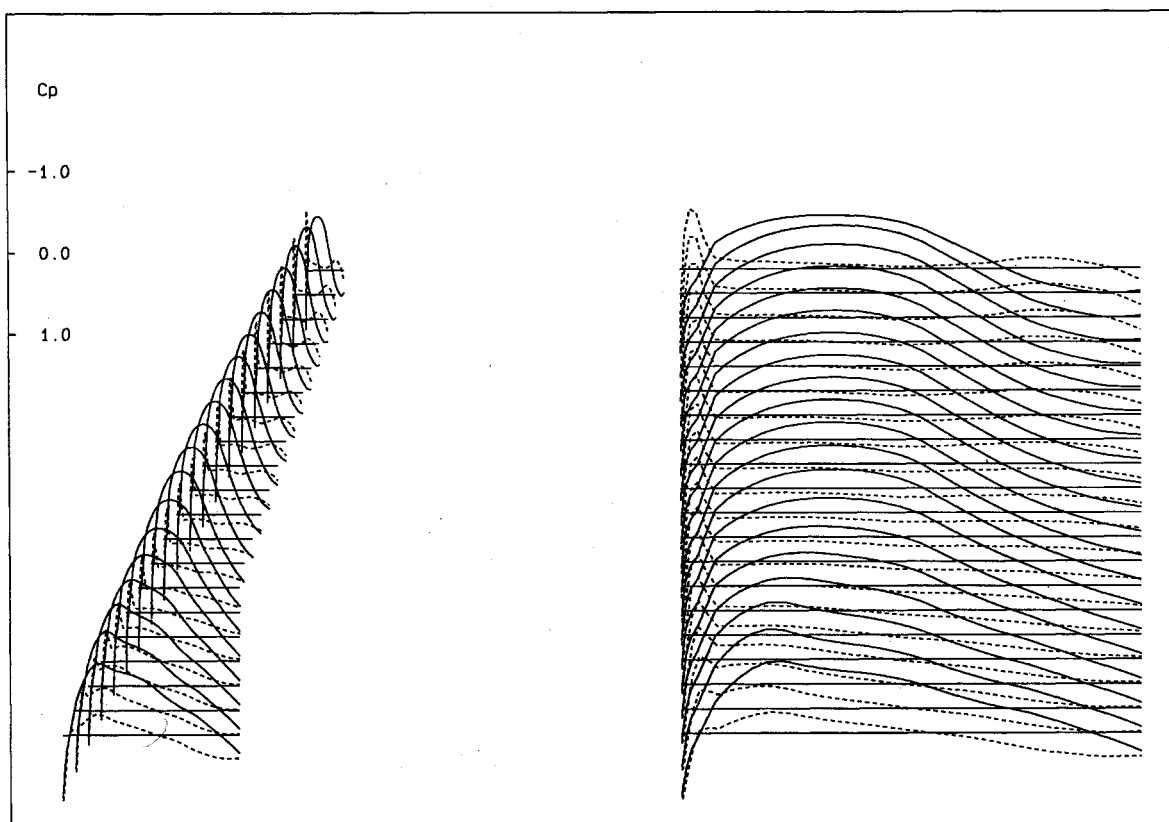
Fig. 6.2.7 $L/D - C_L$, M 0.75, AR 10 WING + TAILPLANE,
Effect of Flap Angle (Full-Span Plain Flap)



$C_L 0.55 \quad \alpha 4.37^\circ$

AR 10
CU-X (30)

6.2.8(a)



(b) CP DISTBNS, $\delta_{TE} +5.2^\circ / \Delta -15^\circ$

Fig. 6.2.8. VARYING DISTRIBUTED, FULL-SPAN, VTE, LOADINGS
M 0.75, AR 10 WING + TAILPLANE, $\alpha 4.37^\circ$ Trimmed $C_L 0.55$

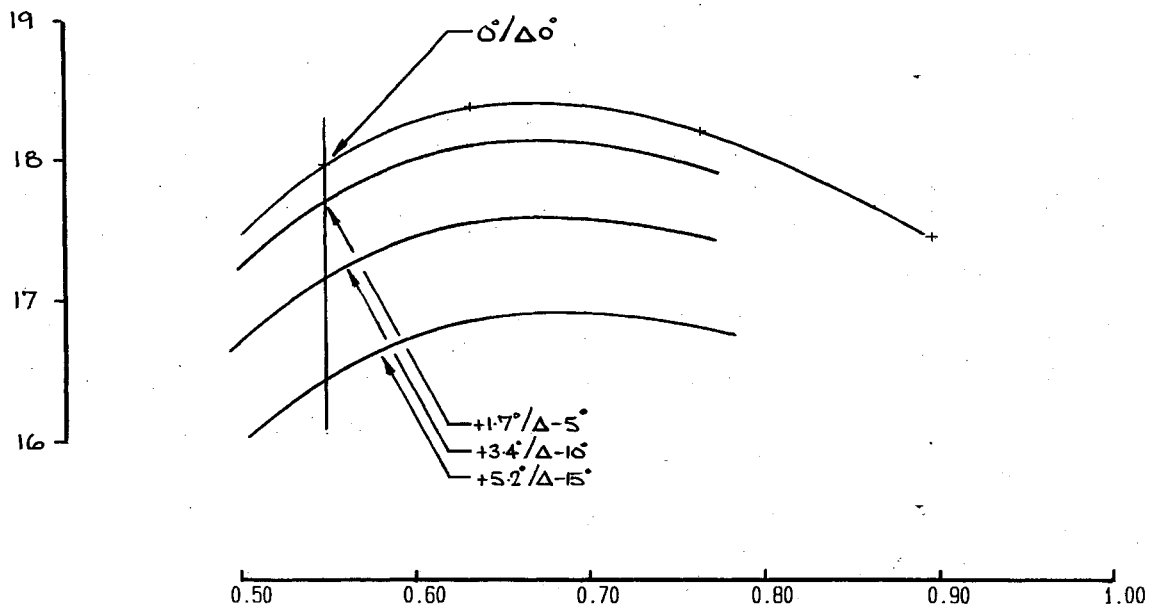


Fig. 6.2.9 L/D - C_L , M 0.75, AR 10 WING + TAILPLANE,
Effect of Distributed, Full-Span Variable Camber
 α 4.37° Trimmed C_L 0.55

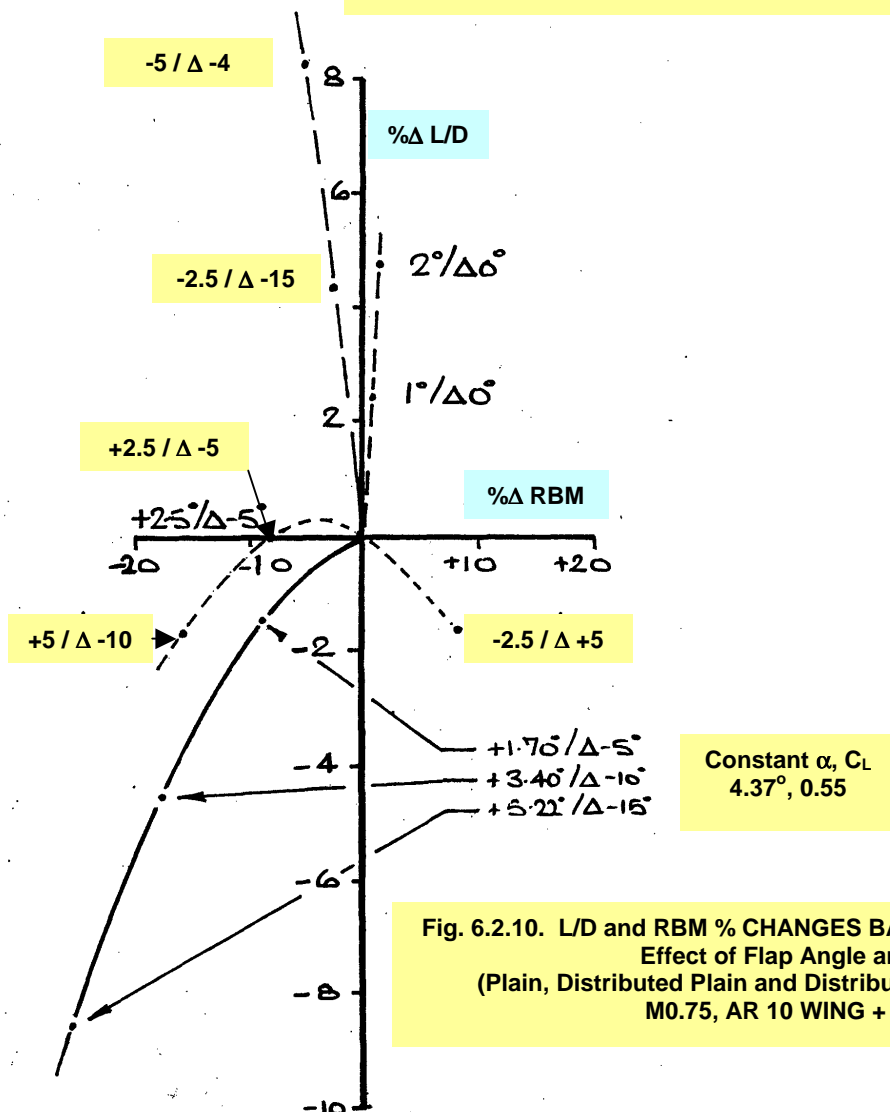


Fig. 6.2.10. L/D and RBM % CHANGES BASED ON DESIGN WING ($\delta_{TE} 0^\circ$)
Effect of Flap Angle and Trimming
(Plain, Distributed Plain and Distributed Variable TE Geometry)
M0.75, AR 10 WING + TAILPLANE

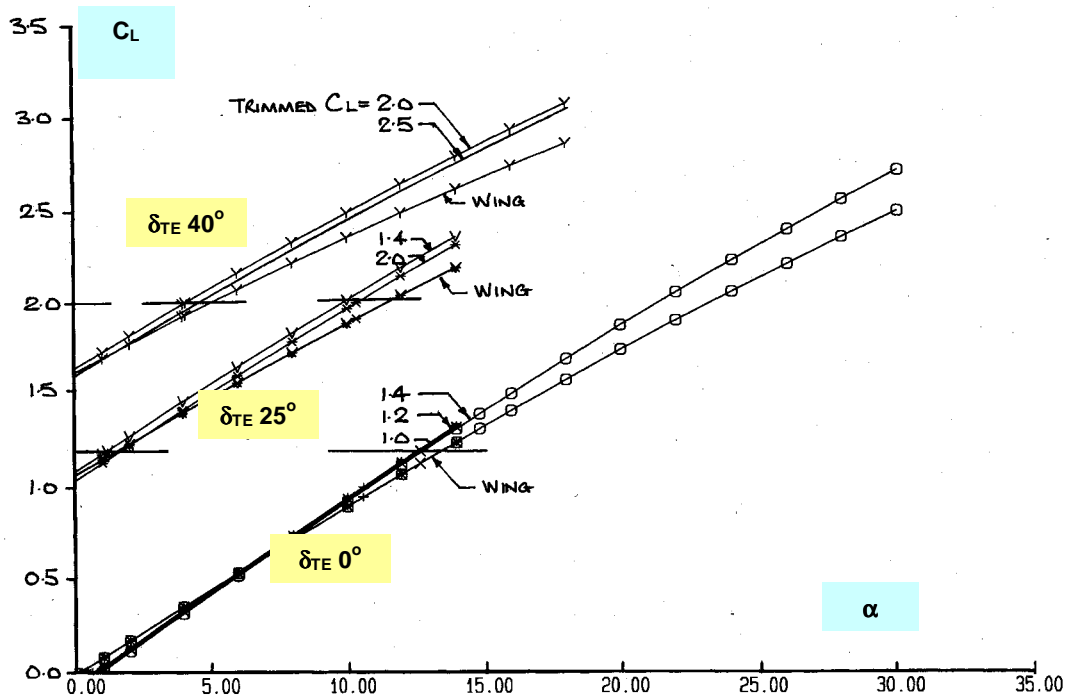
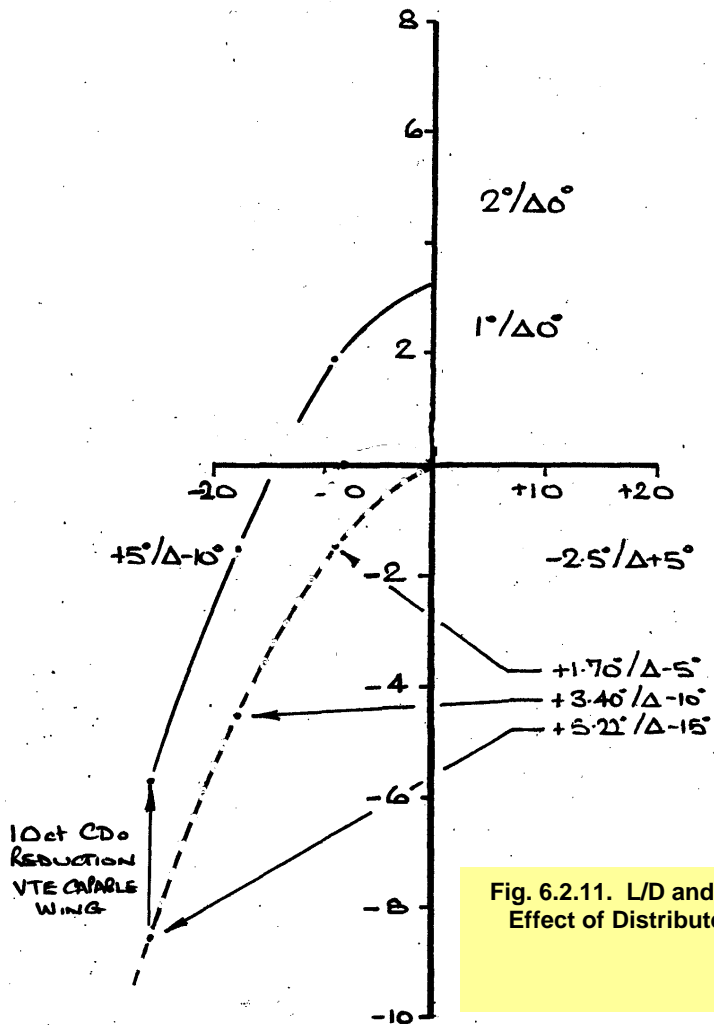
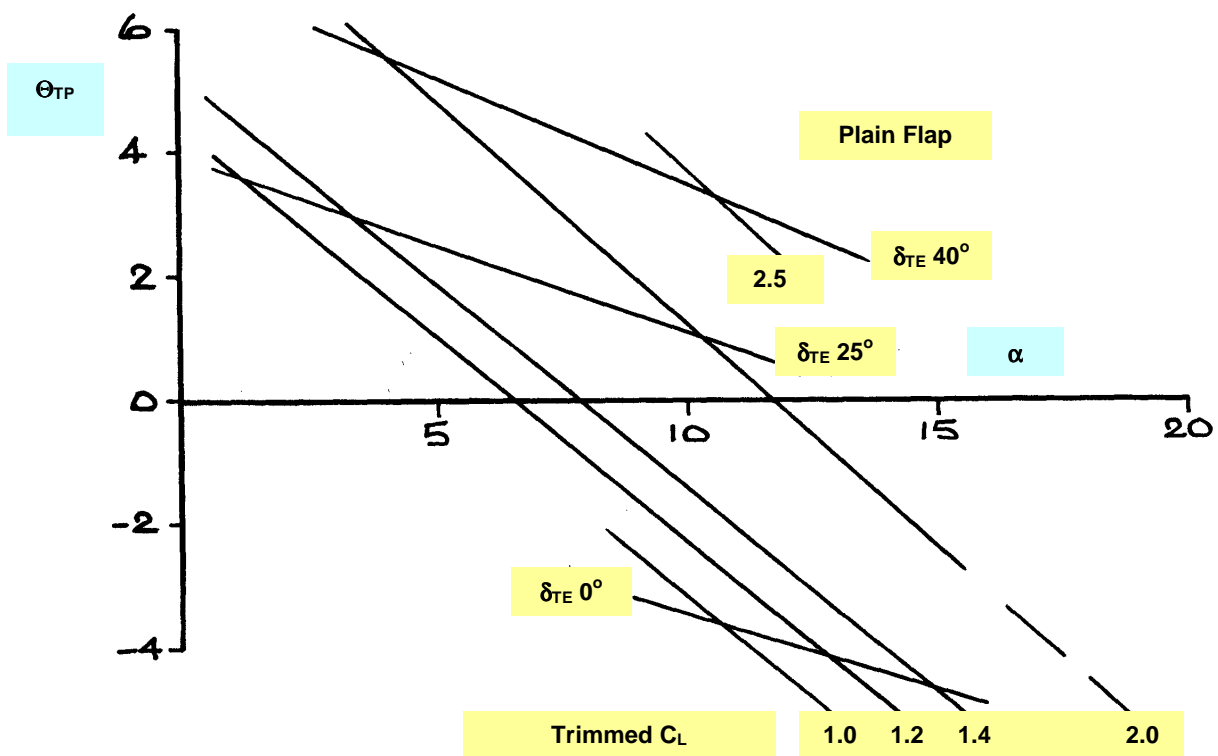
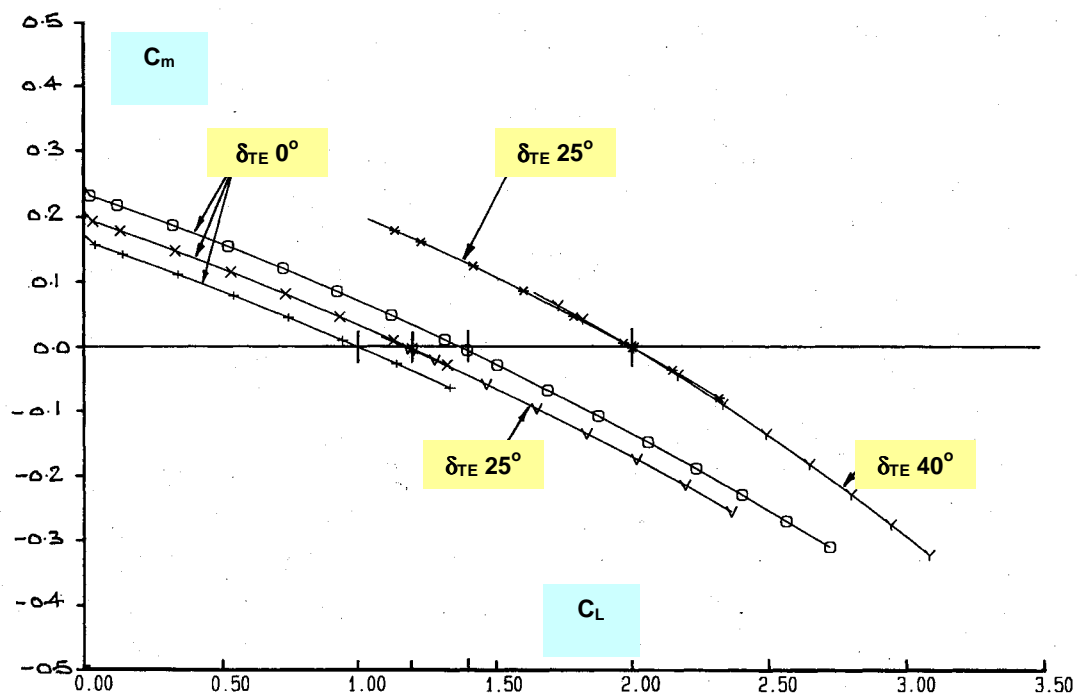


Fig. 6.3.1. $C_L - \alpha$, $M=0.20$, AR 10 WING + TAILPLANE,
Wing and Tailplane Contribution, Effect of Flap Angle (Plain Flap)

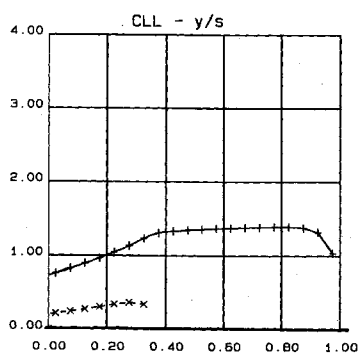
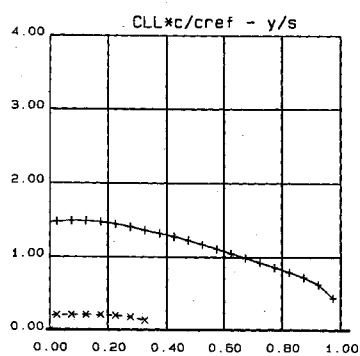


(a) $\theta_{TP} - \alpha$, Effect of δ_{TE} and Trim C_L



(b) $C_m - C_L$, Effect of δ_{TE} and Trim C_L

Fig. 6.3.2. $C_m - C_L$, M 0.20, AR 10 WING + TAILPLANE, TRIM REQUIREMENTS
Effect of δ_{TE} (Plain Flap)



(a) SPANWISE

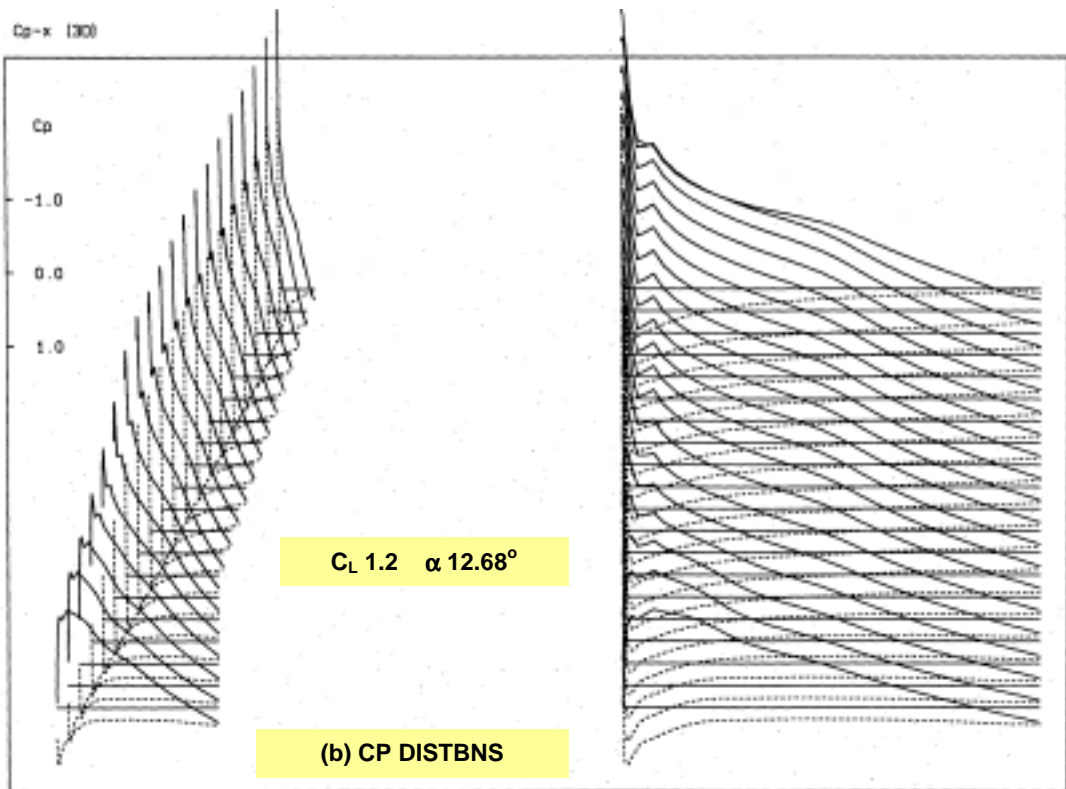
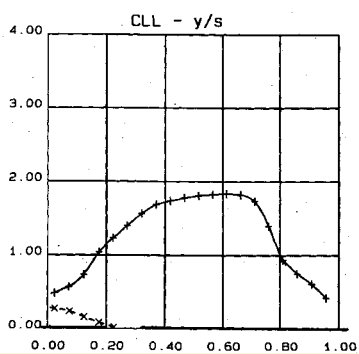
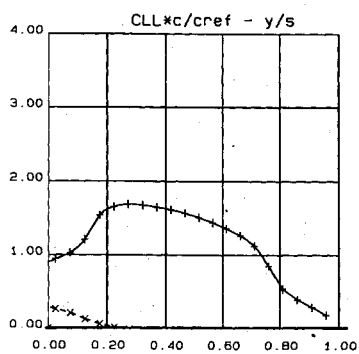


Fig. 6.3.3. CLEAN WING ($\delta_{TE} 0^\circ$), LOADINGS,
Trimmed $C_L 1.2$, $M 0.20$, AR 10 WING + TAILPLANE



(a) SPANWISE

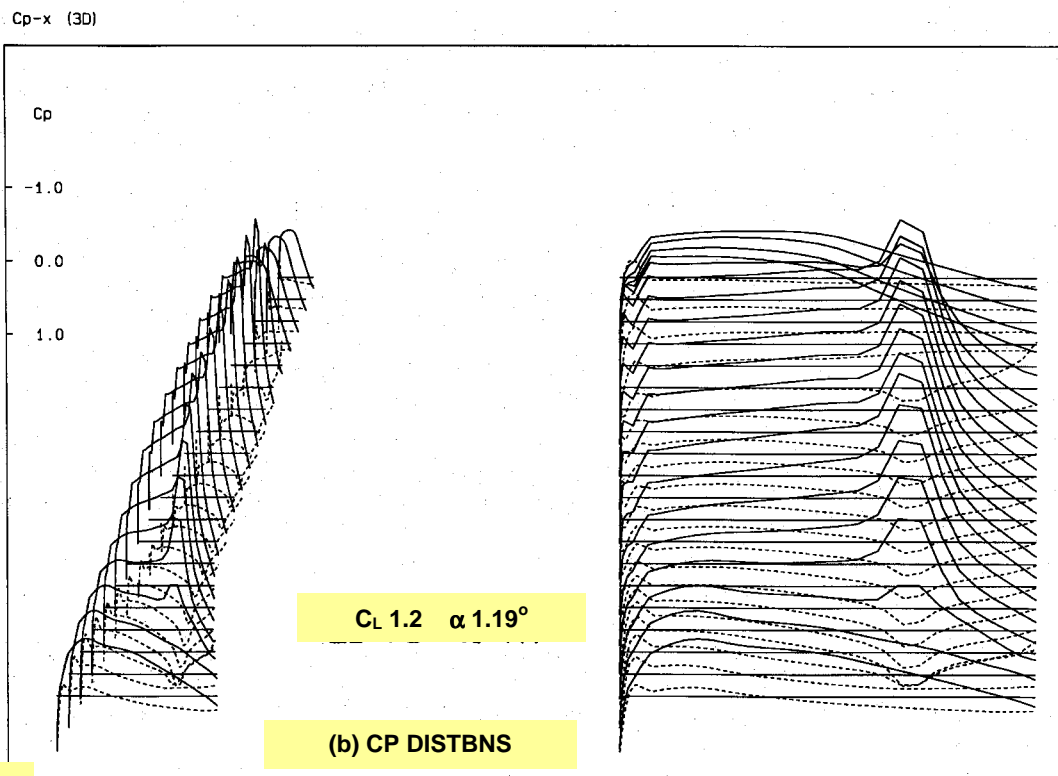


Fig. 6.3.4. $\delta_{TE} 25^\circ$ (Plain Flap), LOADINGS,
Trimmed $C_L = 1.2$, $M=0.20$, AR 10 WING + TAILPLANE

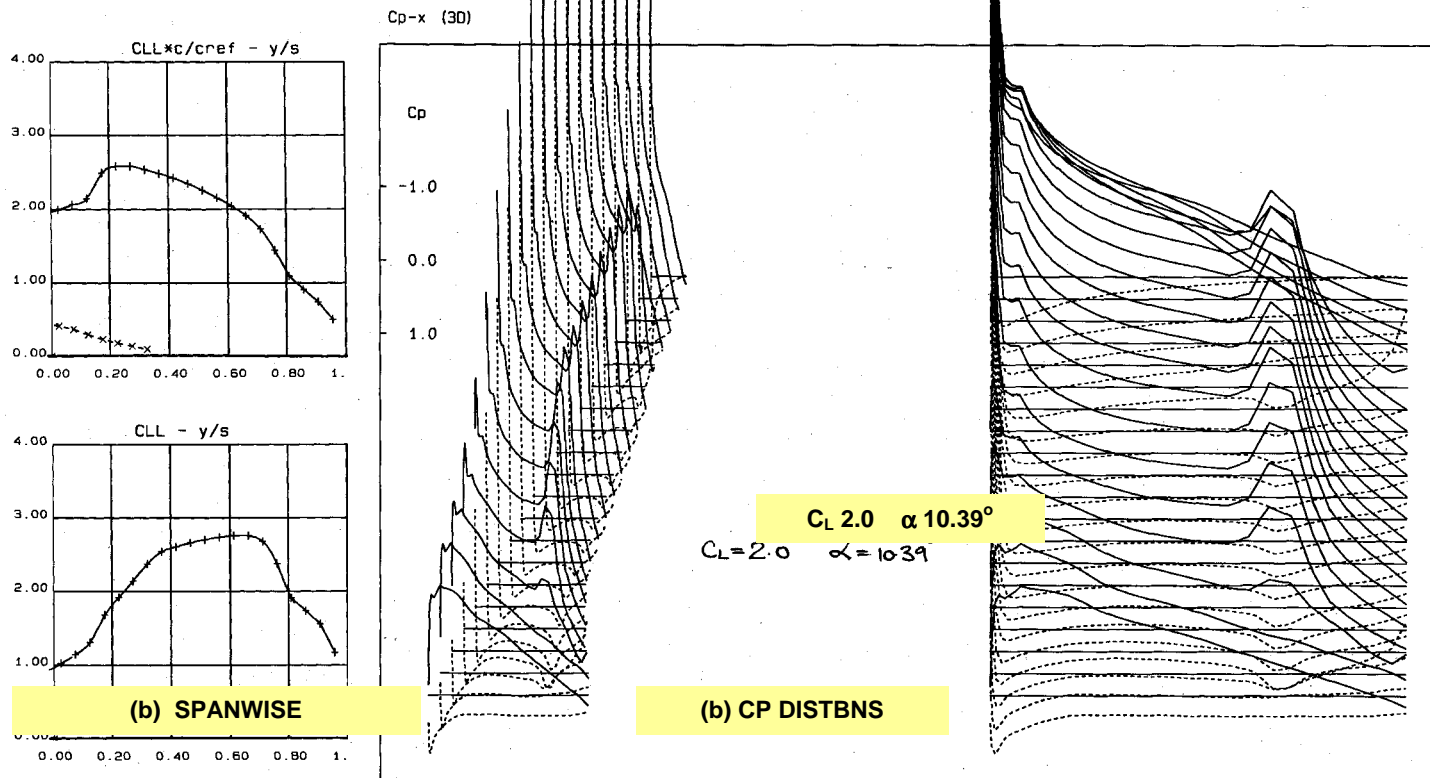


Fig. 6.3.5. $\delta_{TE} 25^\circ$ (Plain Flap), LOADINGS, Trimmed $C_L = 2.0$, $M = 0.20$, AR 10 WING + TAILPLANE

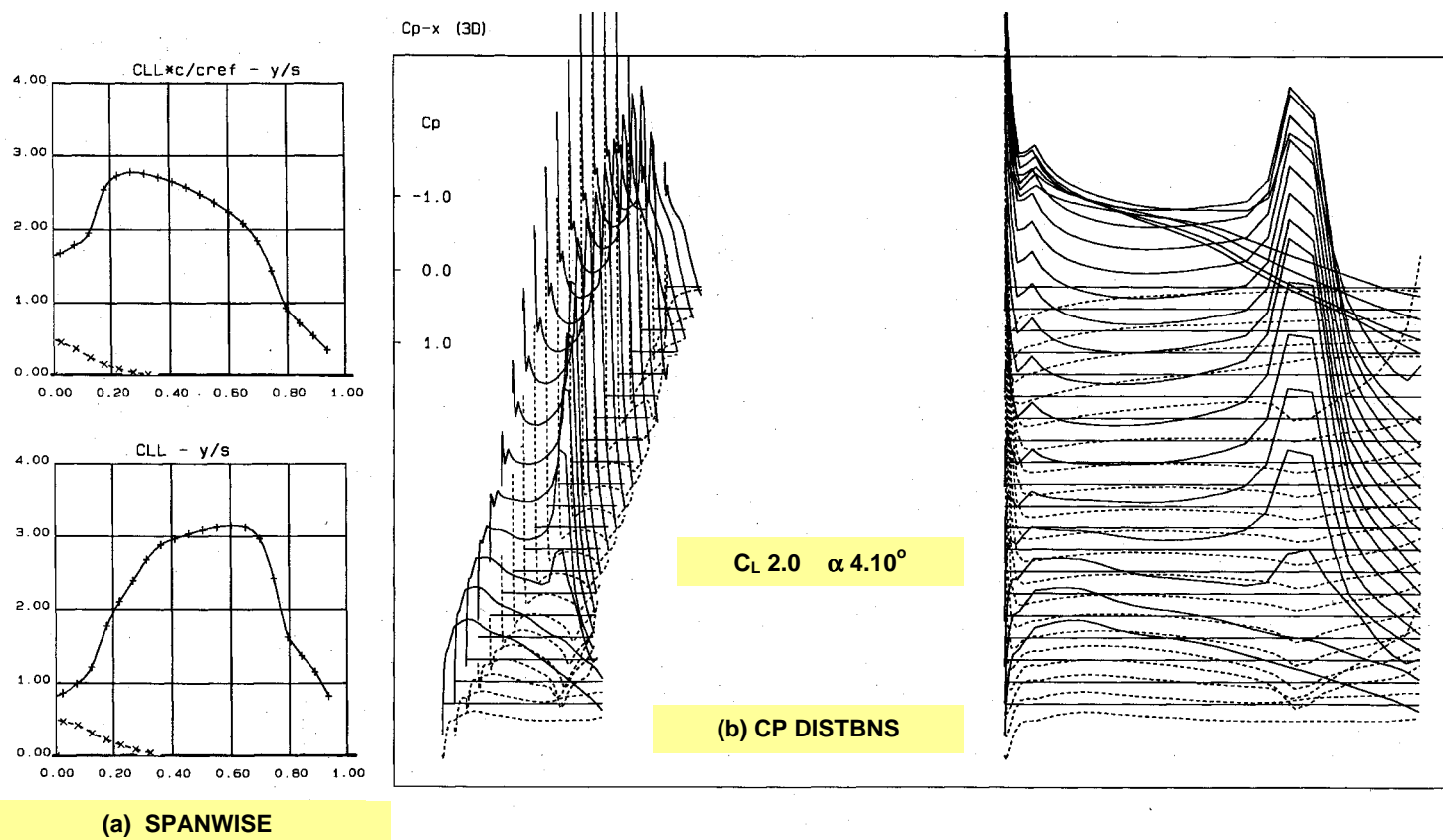


Fig. 6.3.6. $\delta_{TE} 40^\circ$ (Plain Flap), LOADINGS, Trimmed $C_L = 2.0$, $M = 0.20$, AR 10 WING + TAILPLANE

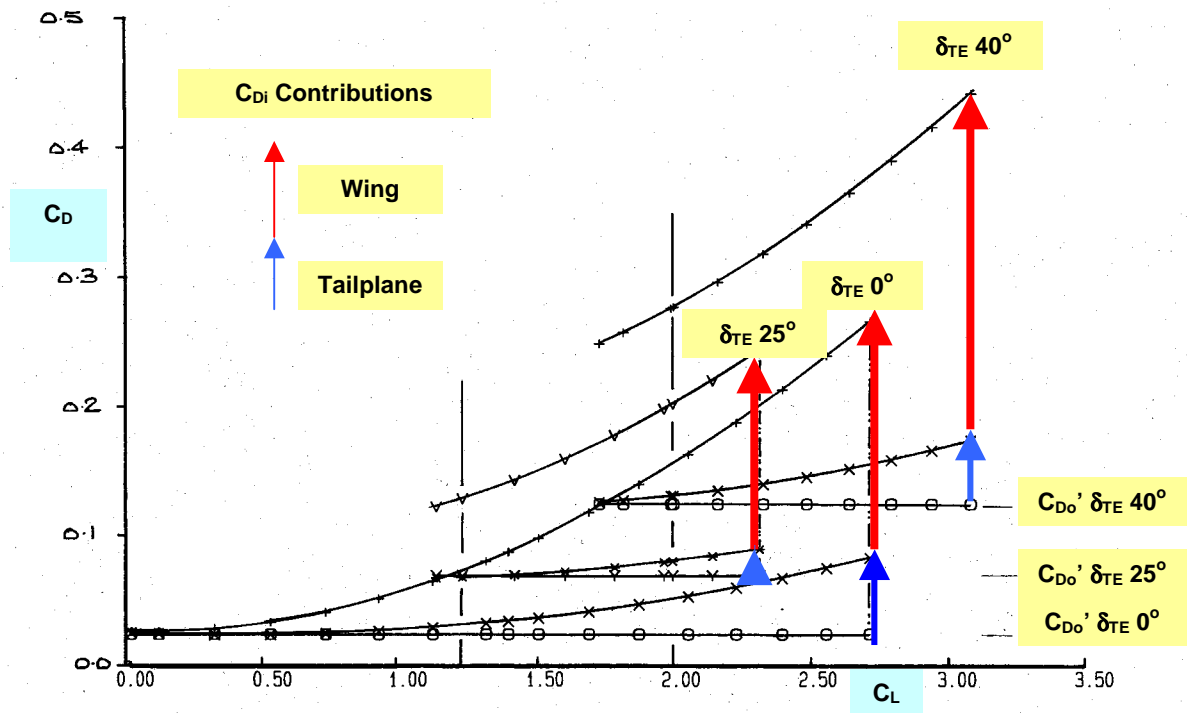


Fig. 6.3.7 $C_D - C_L$, M 0.20, AR 10 WING + TAILPLANE, Drag Breakdown, Effect of Flap Angle (Plain Flap)

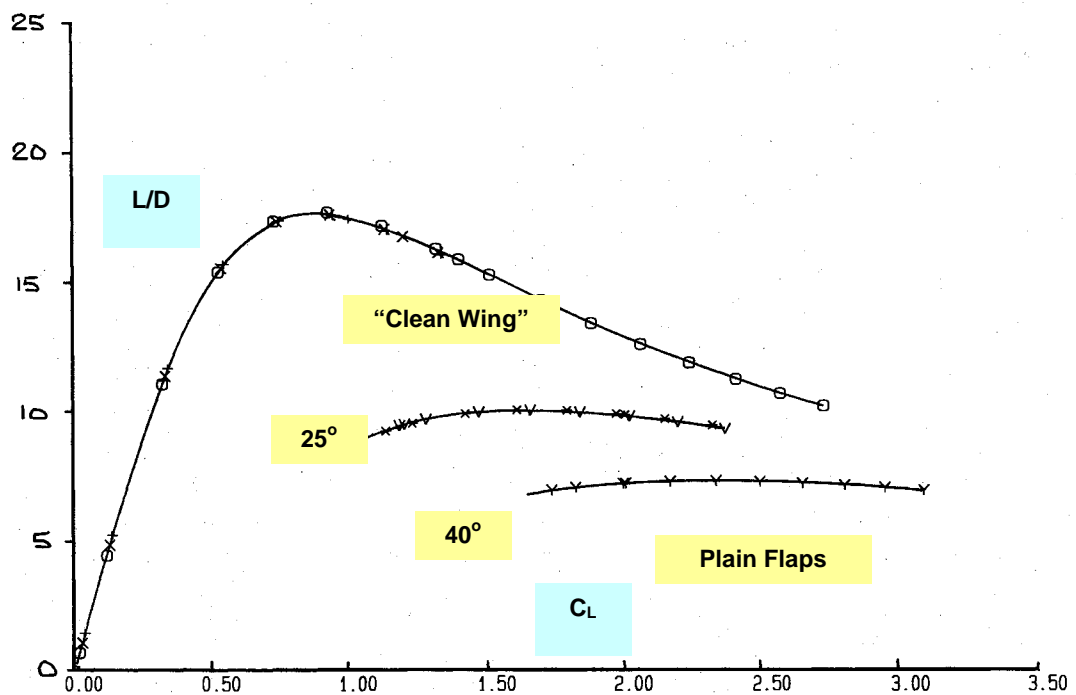


Fig. 6.3.8 $L/D - C_L$, M 0.20, AR 10 WING + TAILPLANE, Effect of Flap Angle (Plain Flap)

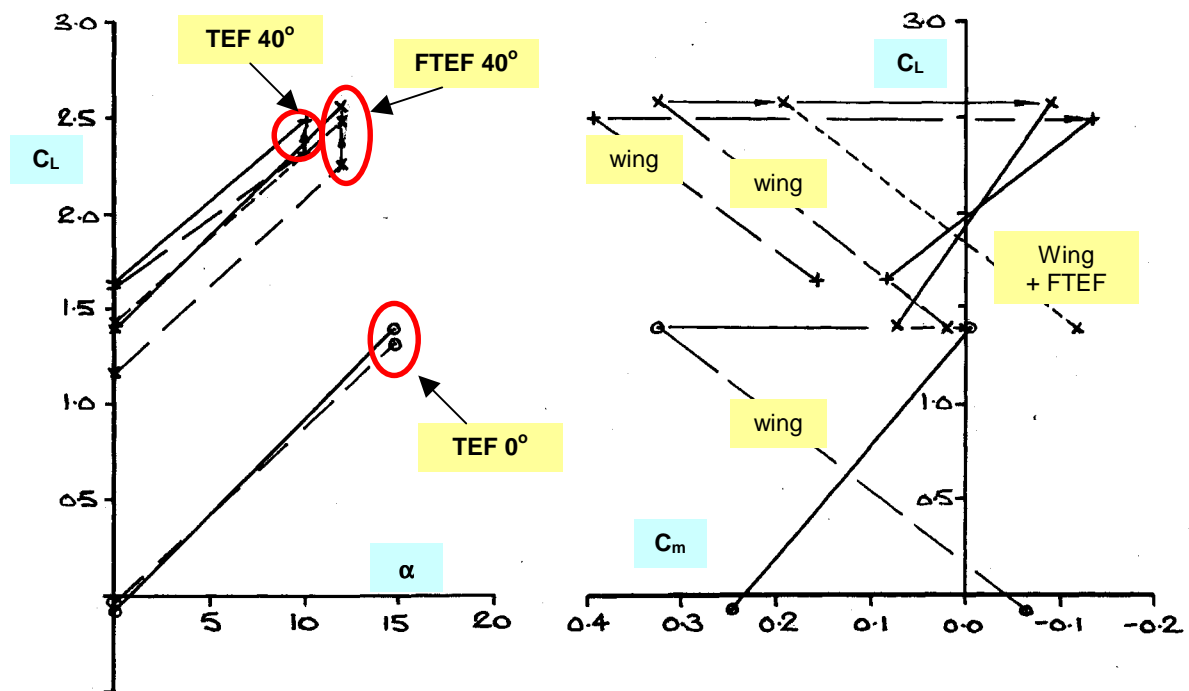
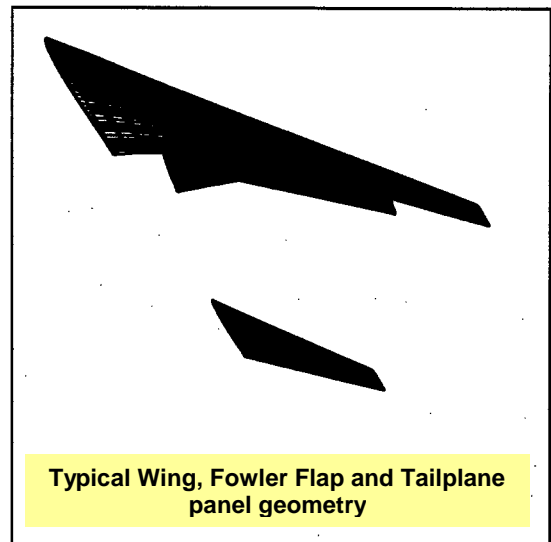
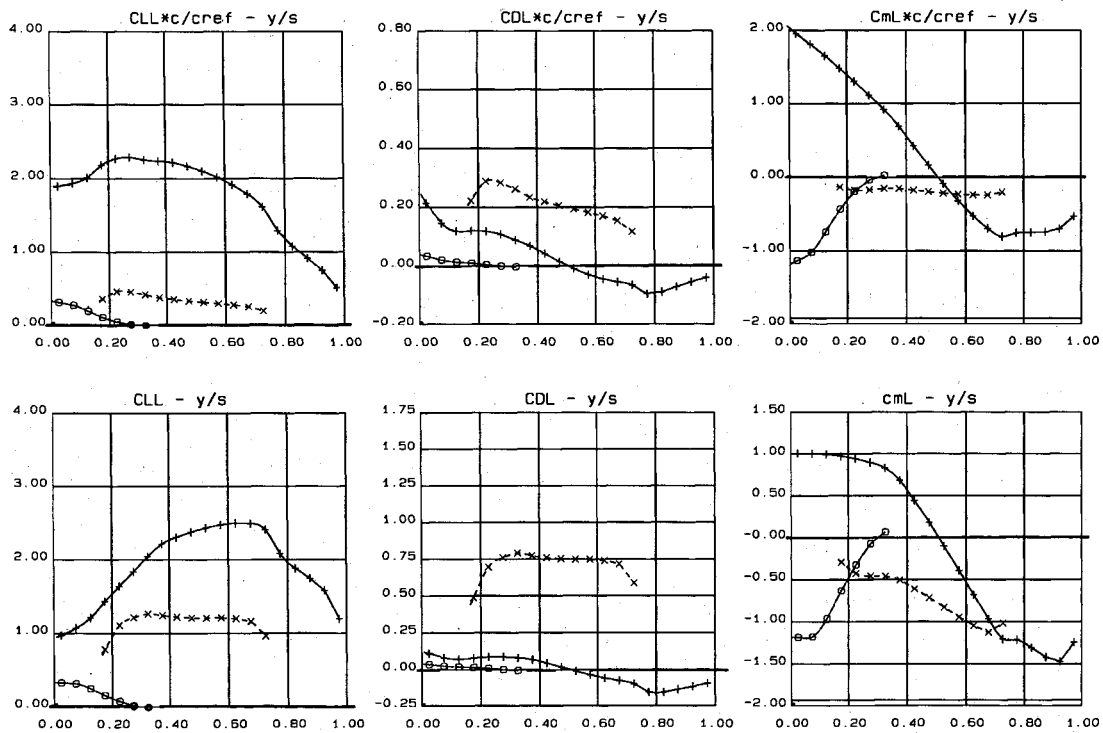
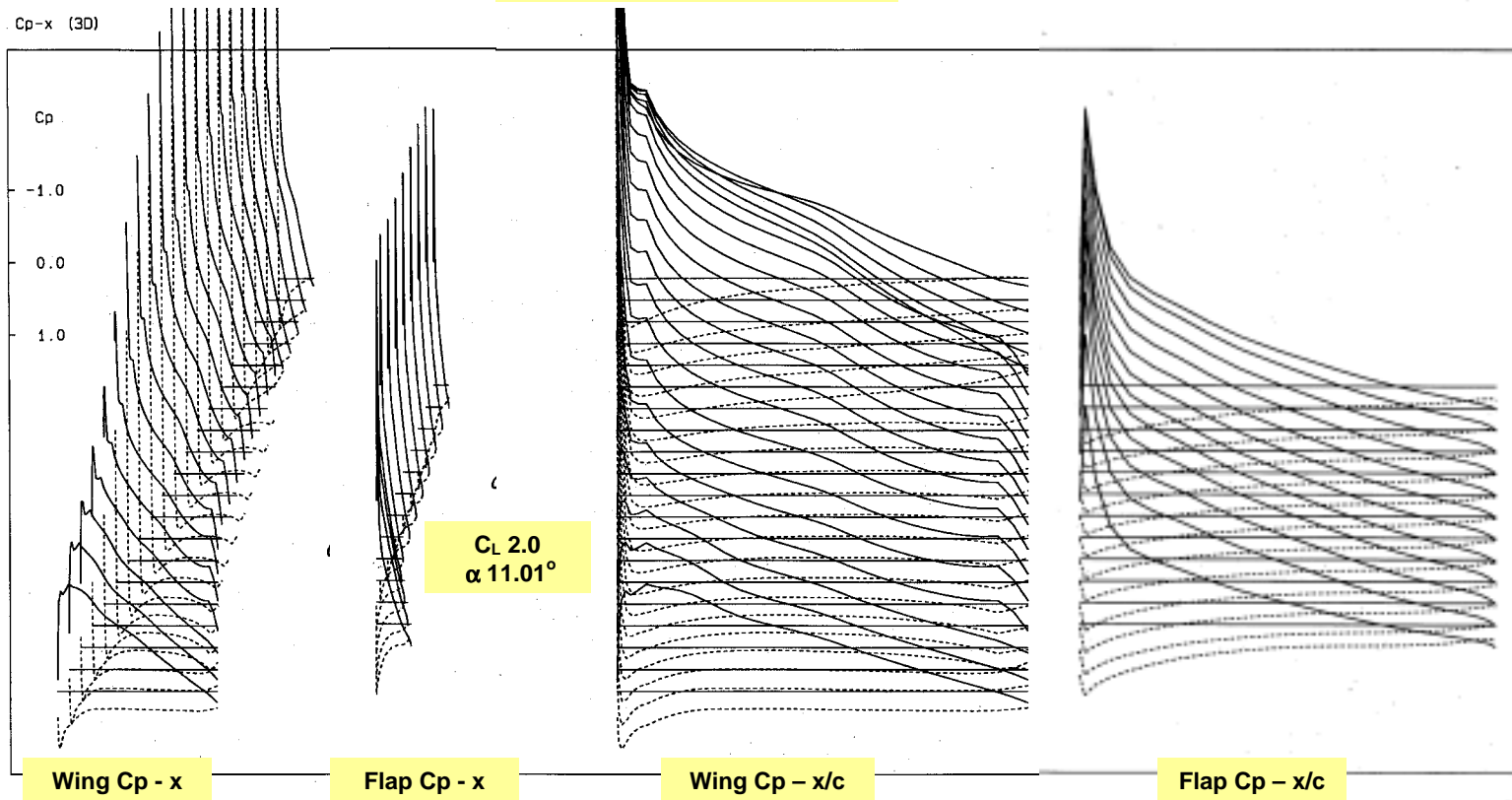


Fig. 6.3.9. $C_L - \alpha$, $C_m - C_L$, $M 0.20$, $AR 10$ WING + TAILPLANE, Wing. Flap and Tail Contributions. Effect of Flap Angle (Plain and Fowler Flap. $\delta_{TF} 40^\circ$)

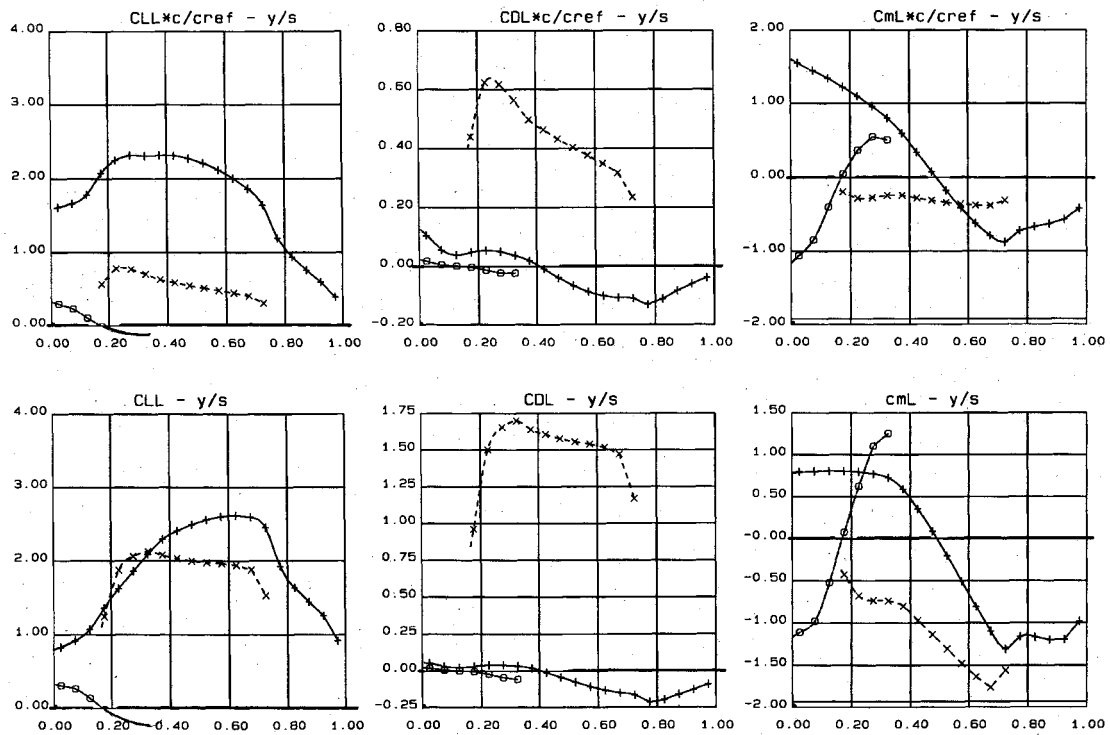


(a) SPANWISE

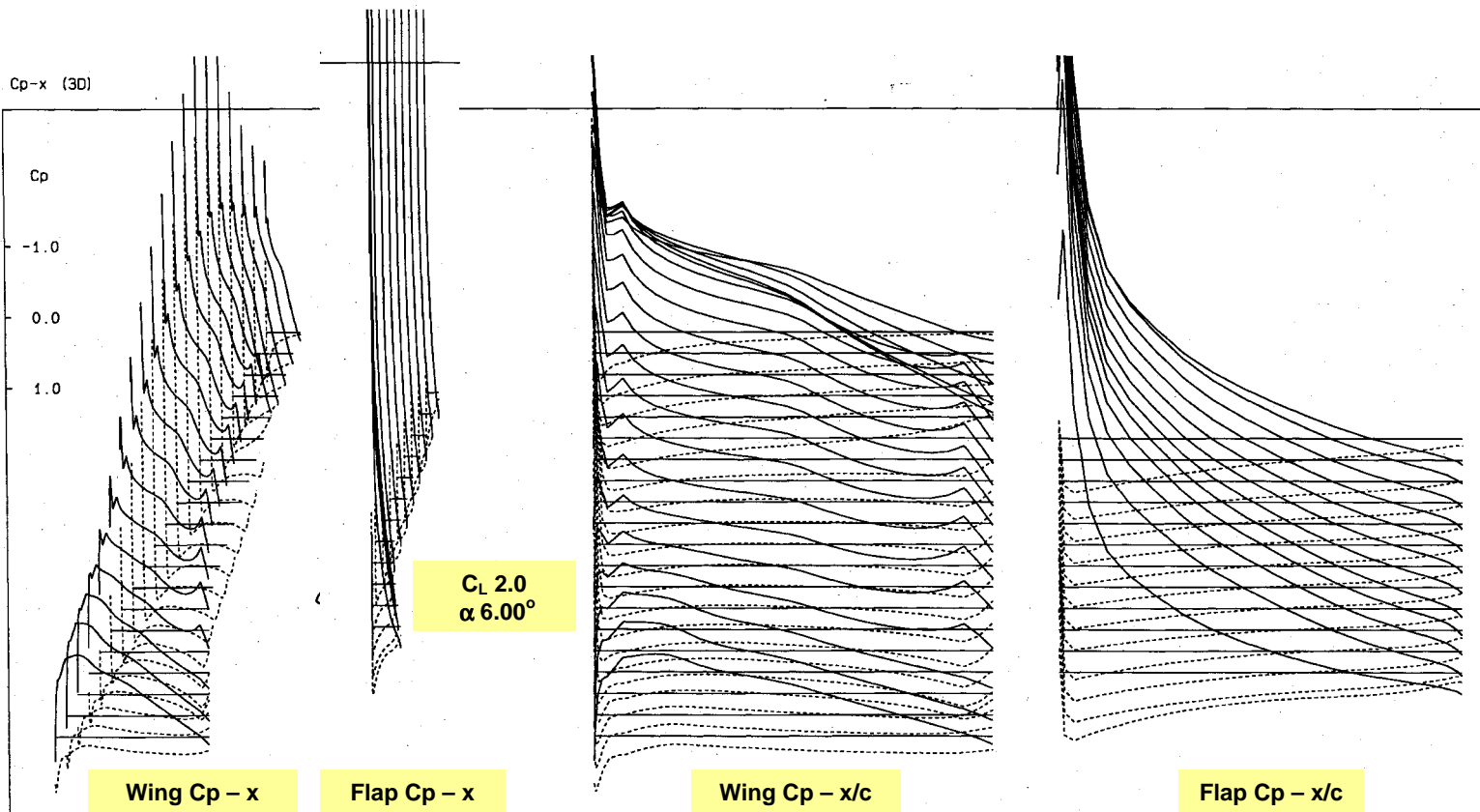


(b) CP DISTBNS

Fig. 6.3.10. FTEF $\delta_{TE} 25^\circ$ (Fowler Flap), LOADINGS, Trimmed $C_L 2.0$, $M 0.20$, AR 10 WING + TAILPLANE



(a) SPANWISE



(b) CP DISTBNS

Fig. 6.3.11. FTEF $\delta_{TE} 40^\circ$ (Fowler Flap), SPANWISE and CHORDWISE CP DISTBNS, Trimmed $C_L 2.0$, $M 0.20$, $AR 10$ WING + TAILPLANE

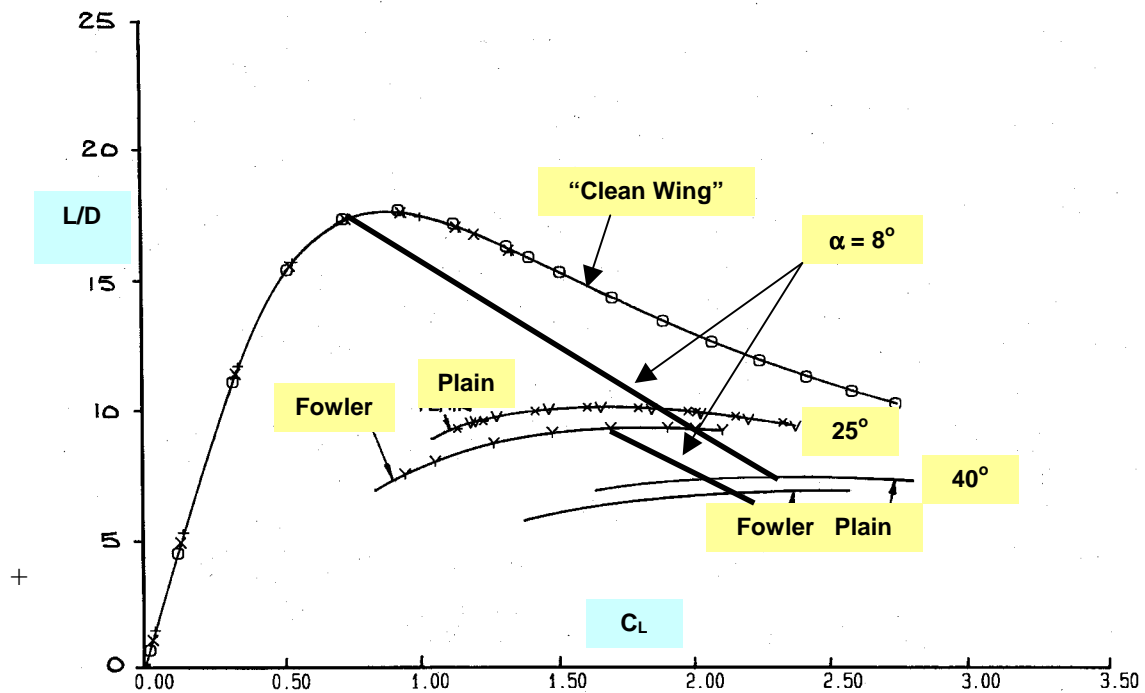


Fig. 6.3.12. L/D – C_L, M 0.20, AR 10 WING + TAILPLANE, Effect of Flap Type at 25° & 40° Deflection (Plain & Fowler Flap)

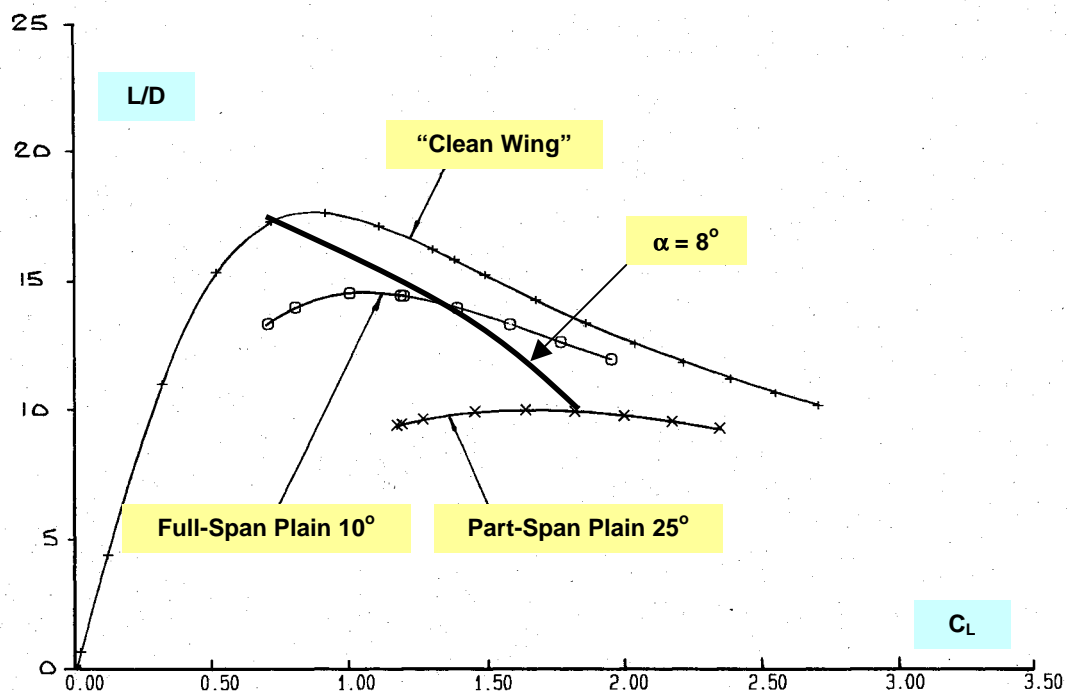


Fig. 6.3.13. L/D – C_L, M 0.20, AR 10 WING + TAILPLANE, Plain Flaps, Full-span 10°, Part-span 25° Deflection & Clean Wing

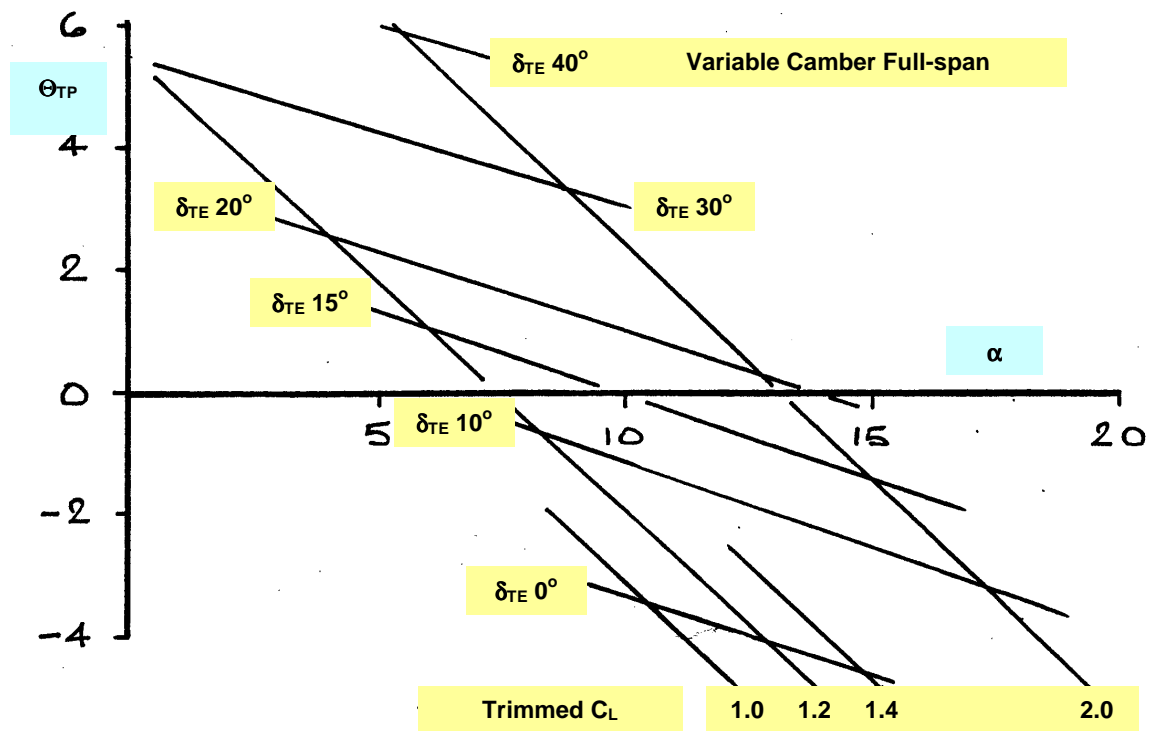


Fig. 6.3.14. AR 10 WING + TAILPLANE, TRIM REQUIREMENTS, M 0.20
Effect of δ_{TE} (Variable Camber Flap)

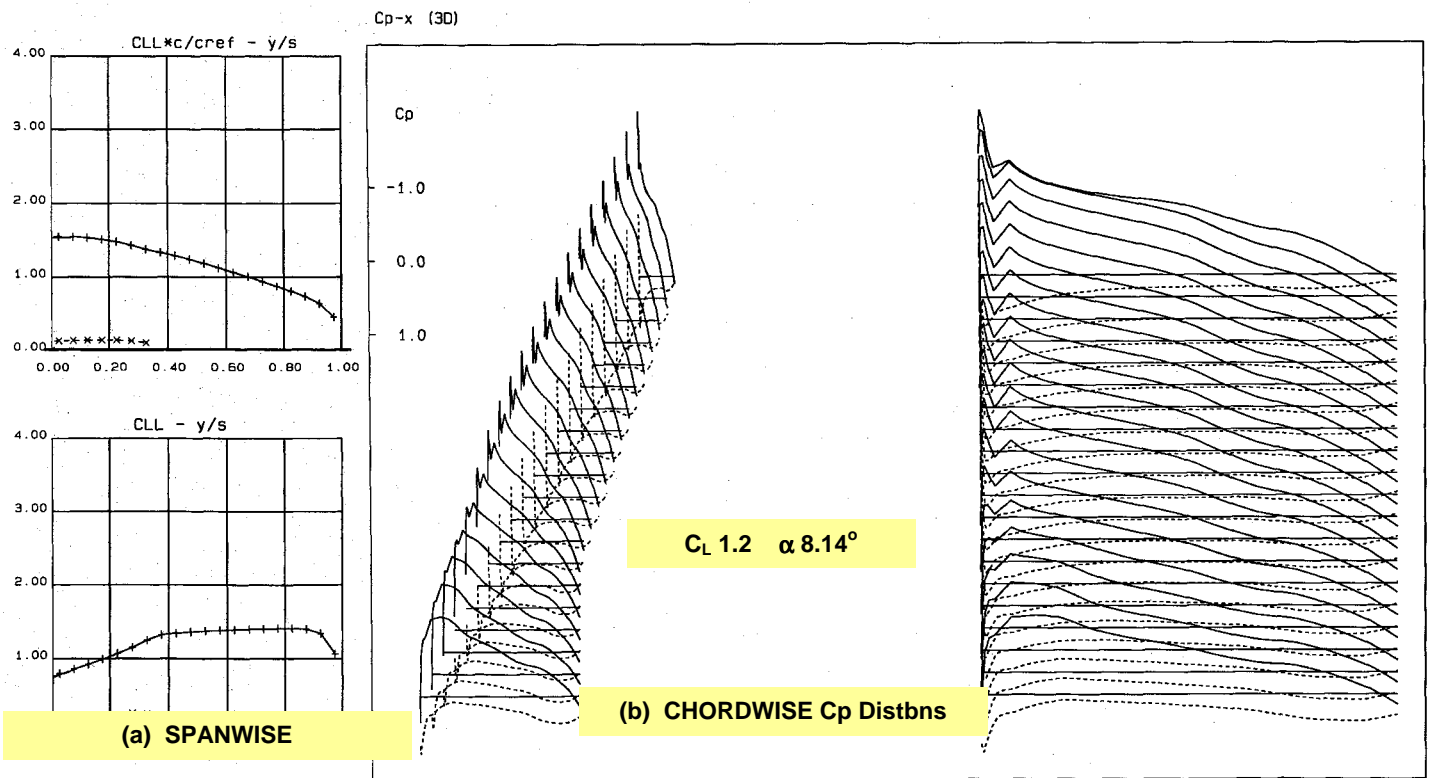


Fig. 6.3.15. $\delta_{TE} 10^\circ$ (Full-Span, Vari-Camber), LOADINGS, Trimmed $C_L 1.2$, M 0.20, AR 10 WING + TAILPLANE

6.3.16 b

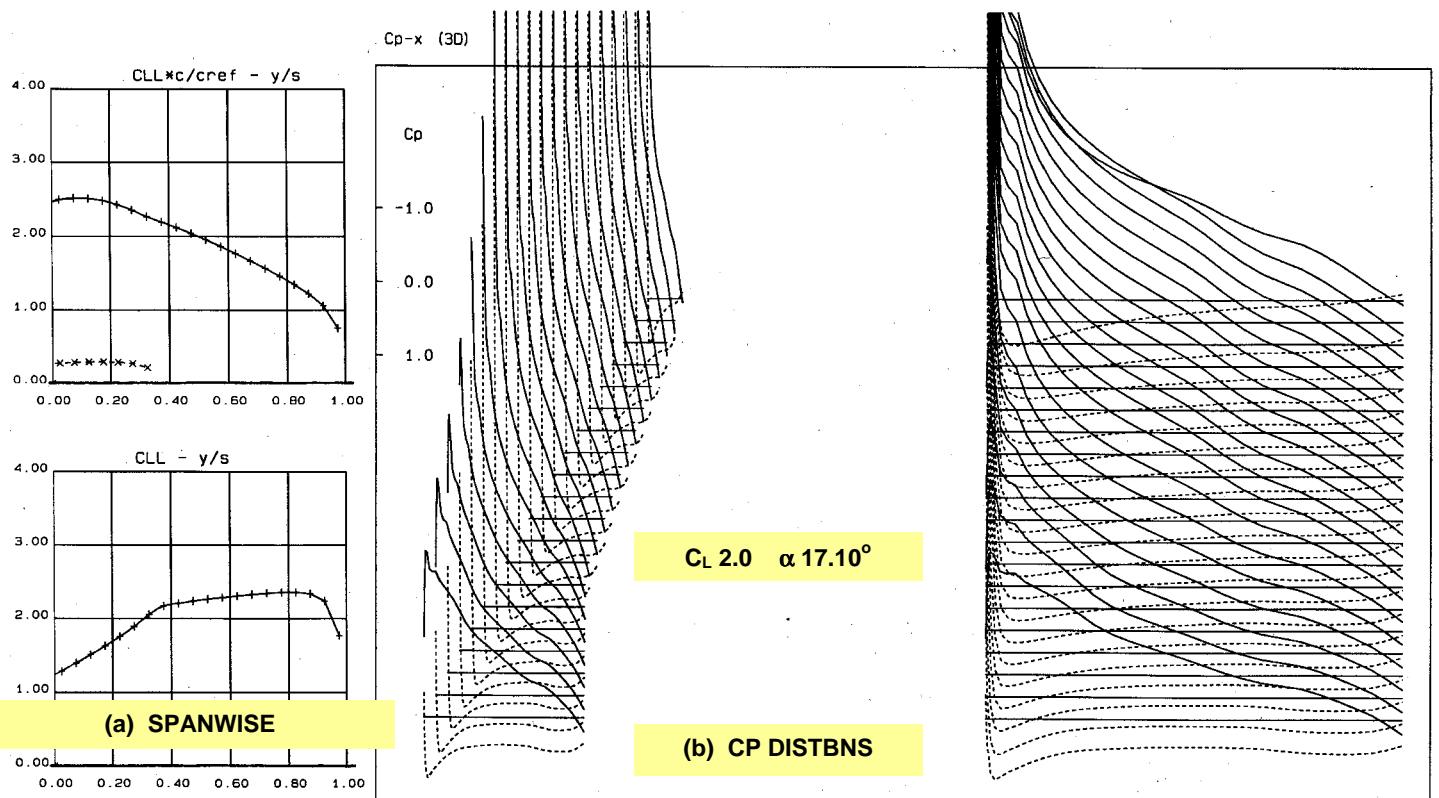


Fig. 6.3.16. $\delta_{TE} 10^\circ$ (Full-Span, Vari-Camber), LOADINGS, Trimmed $C_L 2.0$, M 0.20, AR 10 WING + TAILPLANE

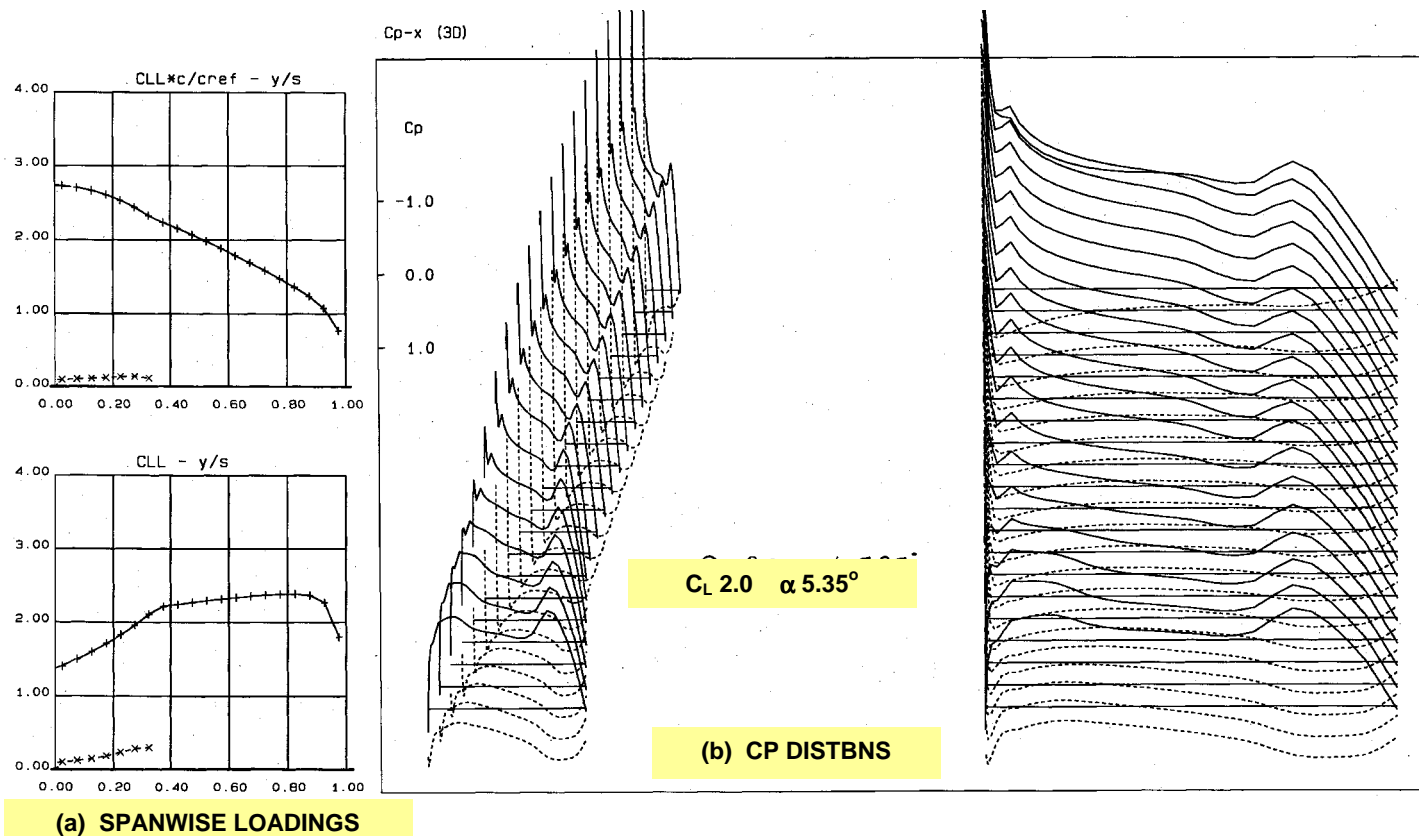


Fig. 6.3.17. $\delta_{TE} 40^\circ$ (Full-Span, Vari-Camber), LOADINGS, Trimmed $C_L 2.0$, $M 0.20$, $AR 10$ WING + TAILPLANE

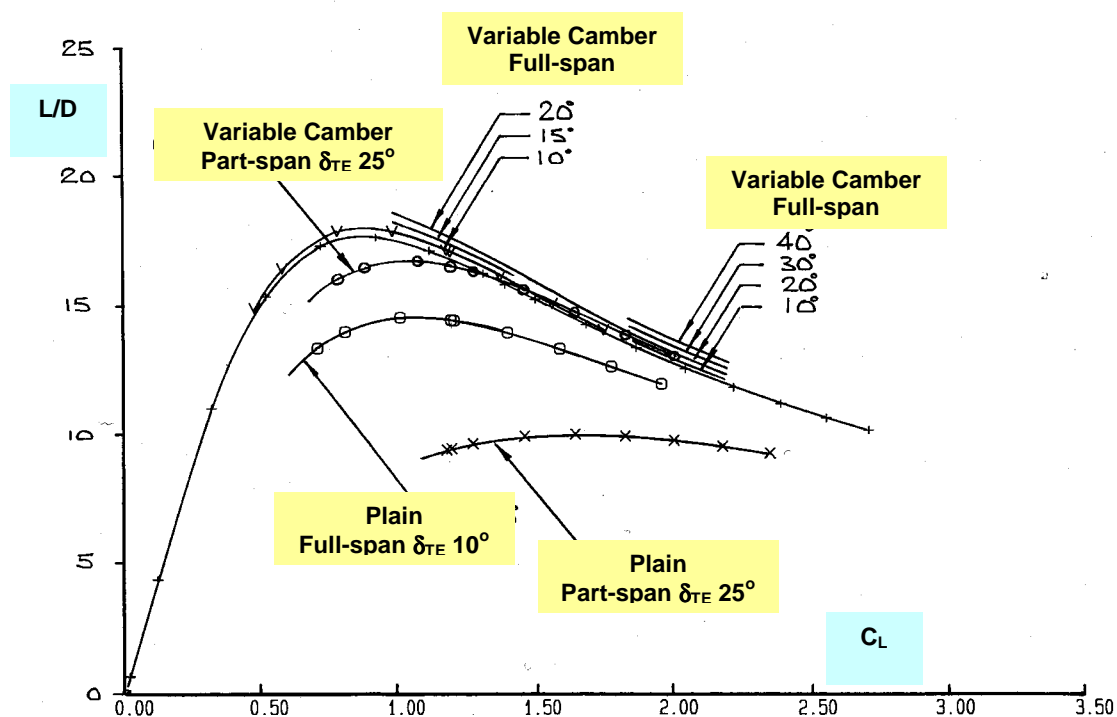
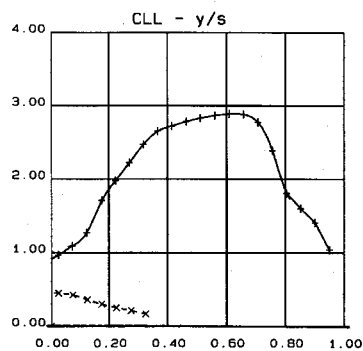
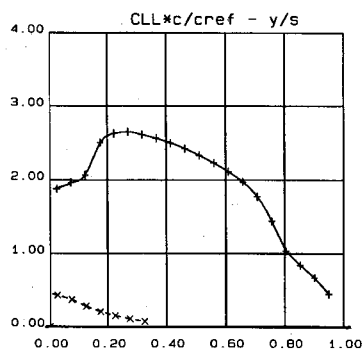


Fig. 6.3.18. $L/D - C_L$, $M 0.20$, $AR 10$ WING + TAILPLANE, Full-Span Vari-Camber 10° to 40° , Full-Span Plain Flap 10° , Part-Span Plain Flap 25° . Part-Span Vari-Camber 25°



(a) SPANWISE

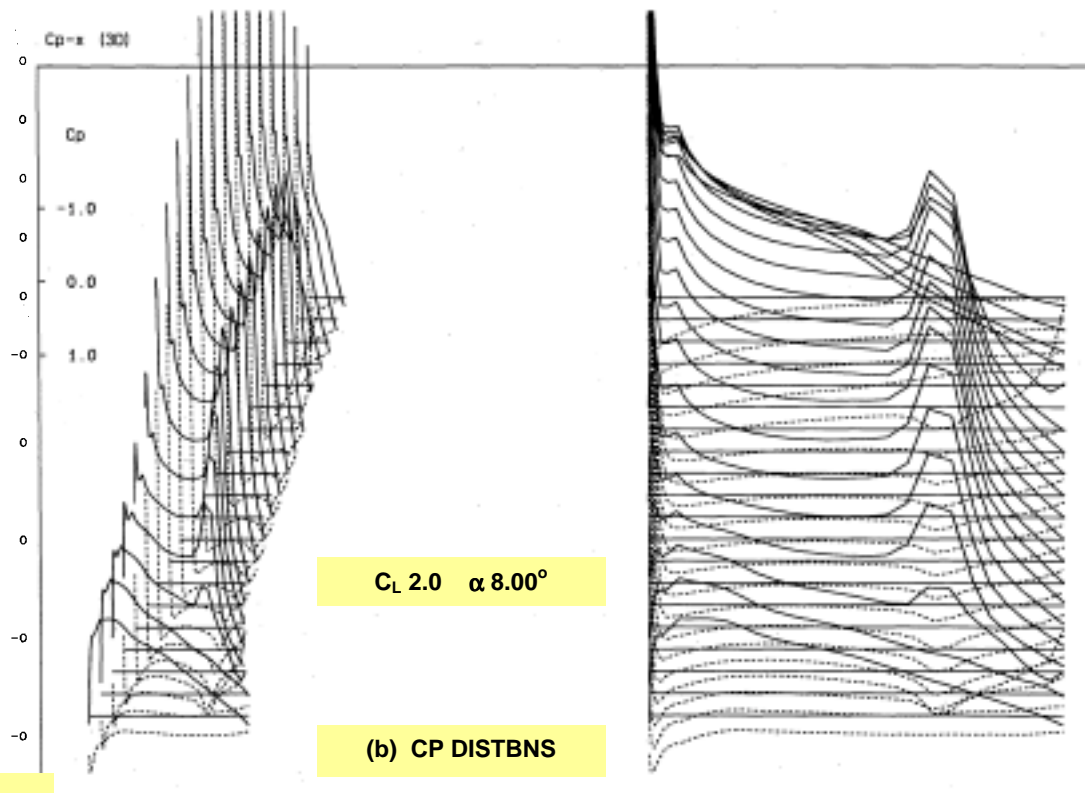
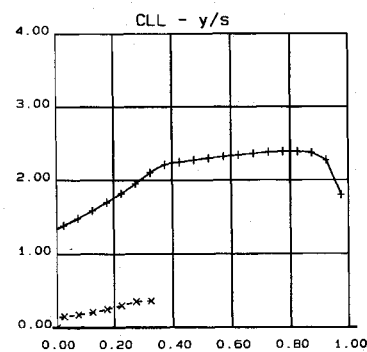
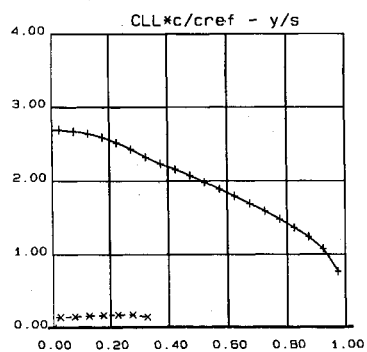


Fig. 6.3.19. $\delta_{TE} 30.5^\circ$ (Part-Span), LOADINGS,
Trimmed $C_L 2.0$, $M 0.20$, $AR 10$ WING + TAILPLANE



(a) SPANWISE

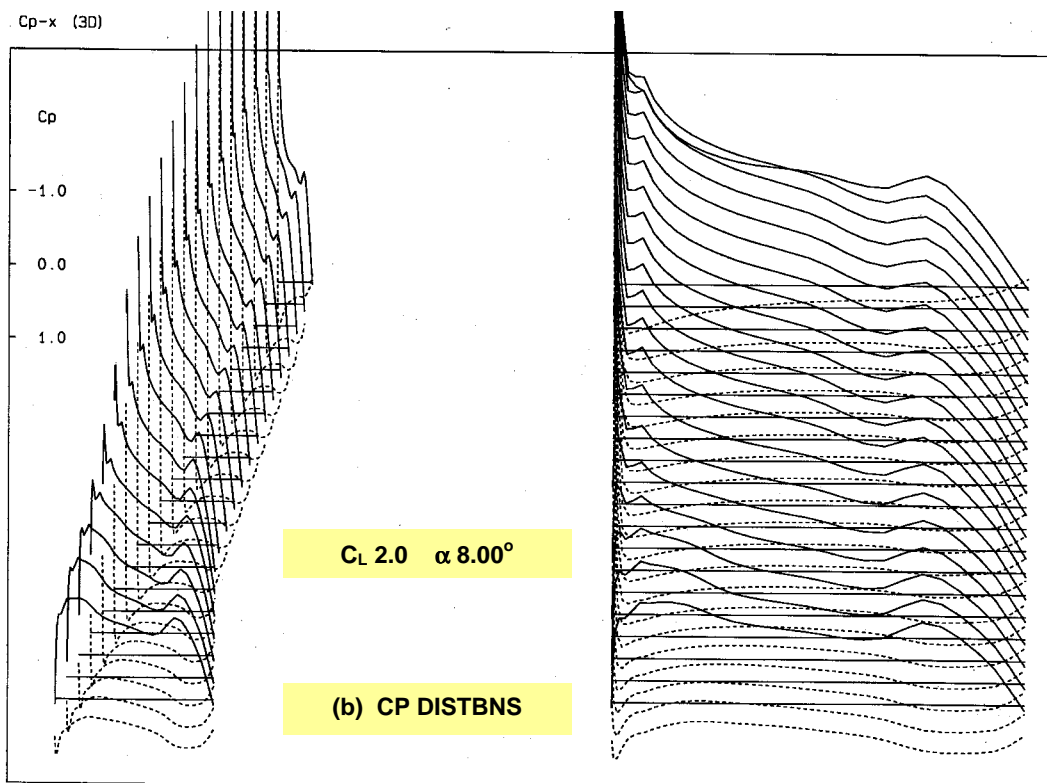


Fig. 6.3.20. $\delta_{TE} 32.4^\circ$ (Full-Span, Vari-Camber), LOADINGS,
Trimmed $C_L 2.0$, $M 0.20$, $AR 10$ WING + TAILPLANE

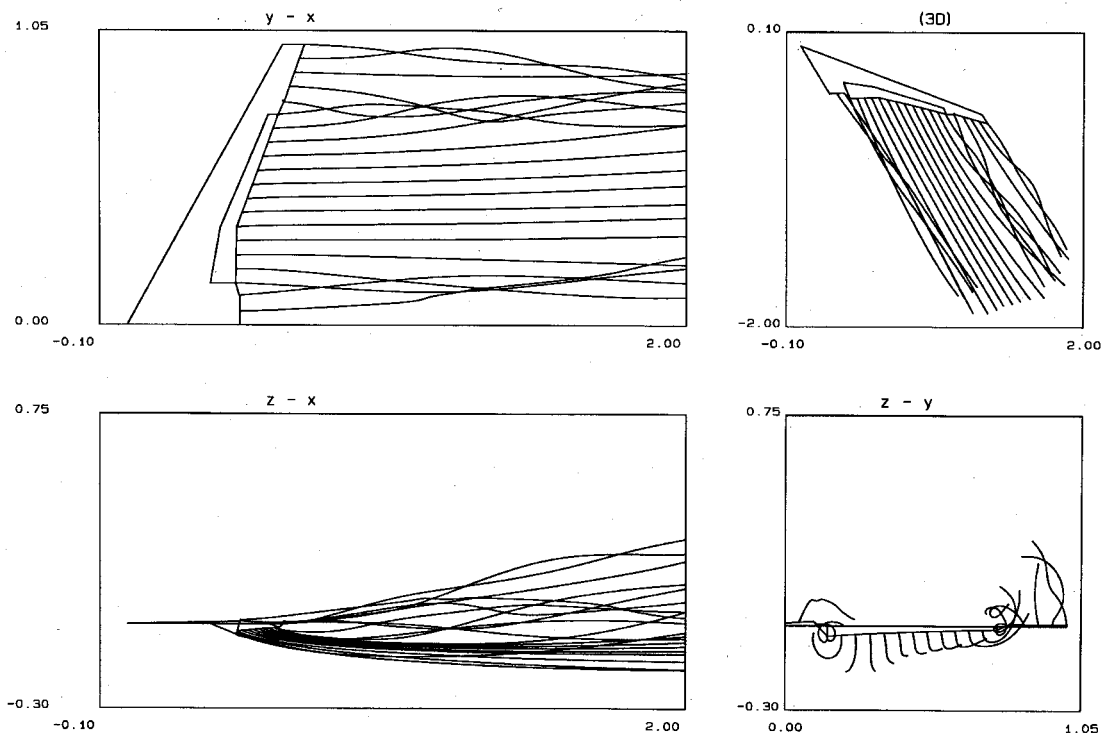


Fig. 6.3.21. $\delta_{TE} 30.5^\circ$ (Part-Span), RELAXED WAKE GEOMETRY, Trimmed $C_L 2.0$, $M 0.20$, AR 10 WING + TAILPLANE

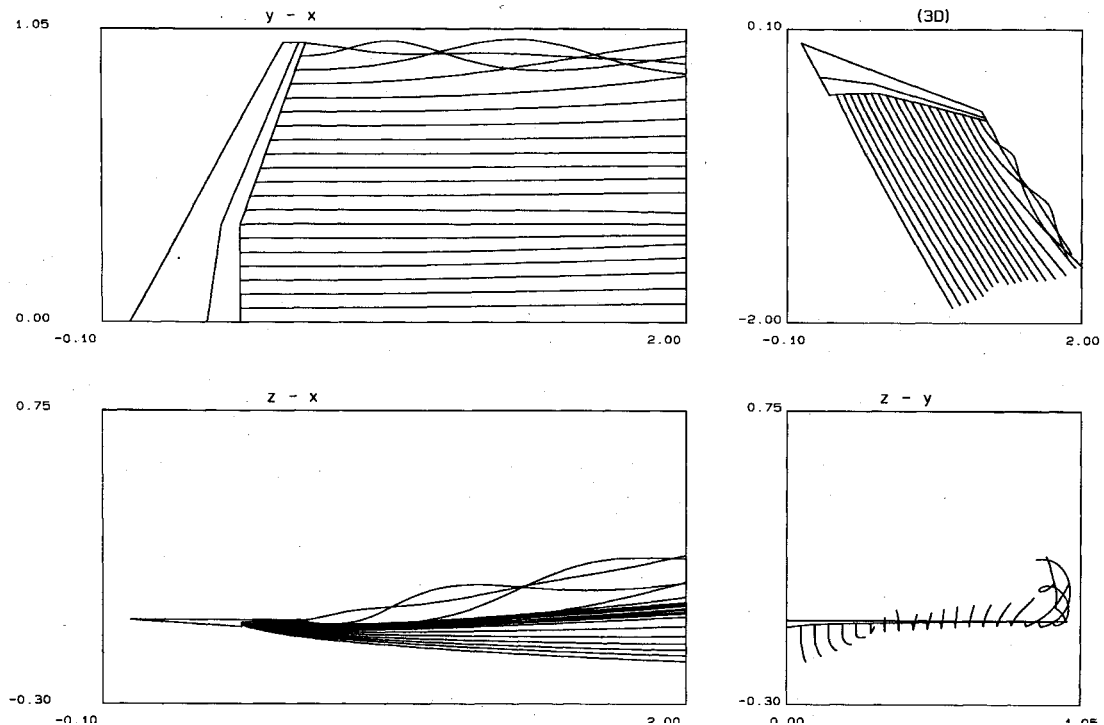
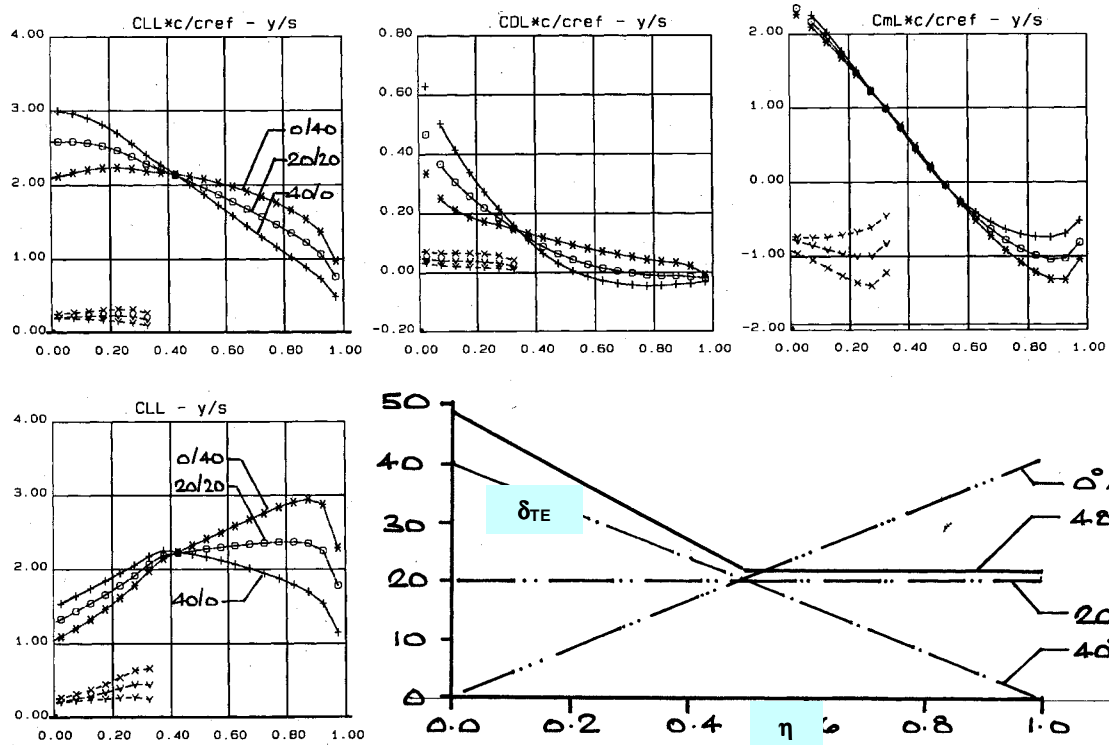
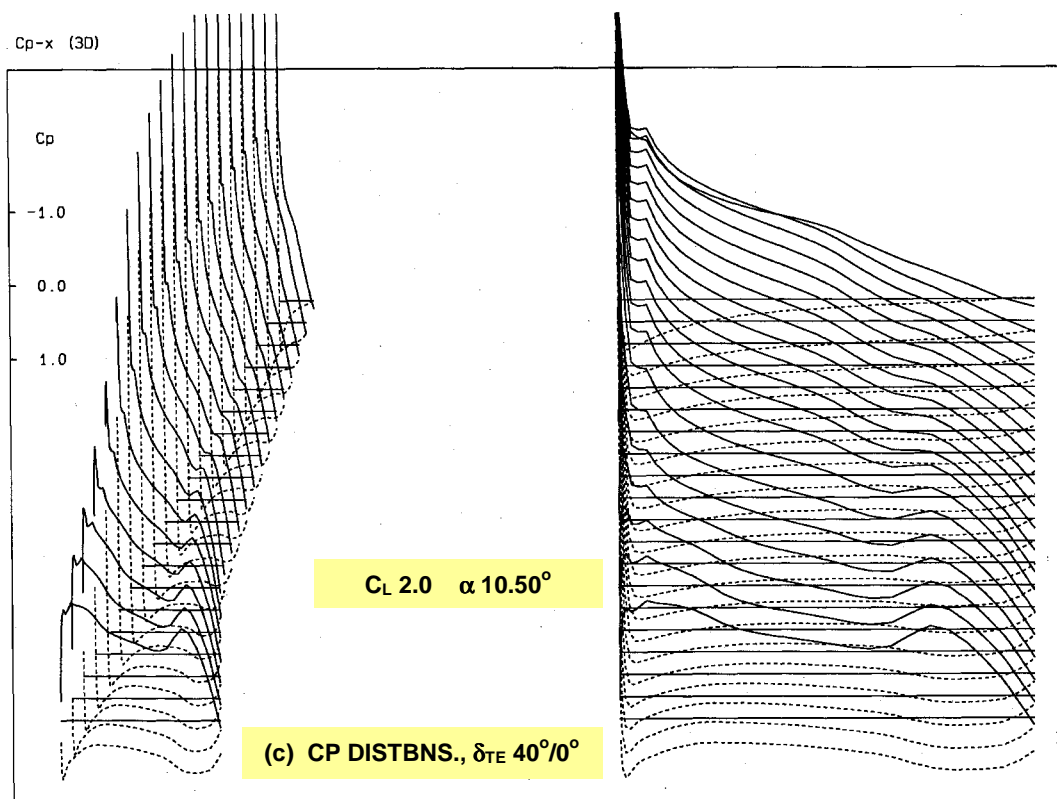


Fig. 6.3.22. $\delta_{TE} 32.4^\circ$ (Full-Span, Vari-Camber), RELAXED WAKE GEOMETRY, Trimmed $C_L 2.0$, $M 0.20$, AR 10 WING + TAILPLANE



(b) SPANWISE LOADINGS
 $0^\circ/40^\circ$, $20^\circ/20^\circ$ & $40^\circ/0^\circ$ δ_{TE}

(a) δ_{TE} VARIATION ACROSS SEMI-SPAN



(c) CP DISTBNS., $\delta_{TE} 40^\circ/0^\circ$

Fig. 6.3.23. DISTRIBUTED δ_{TE} (Full-Span, Vari-Camber), DEFLECTION DISTRIBUTIONS and LOADINGS, Trimmed $C_L 2.0$, $M 0.20$, AR 10 WING + TAILPLANE

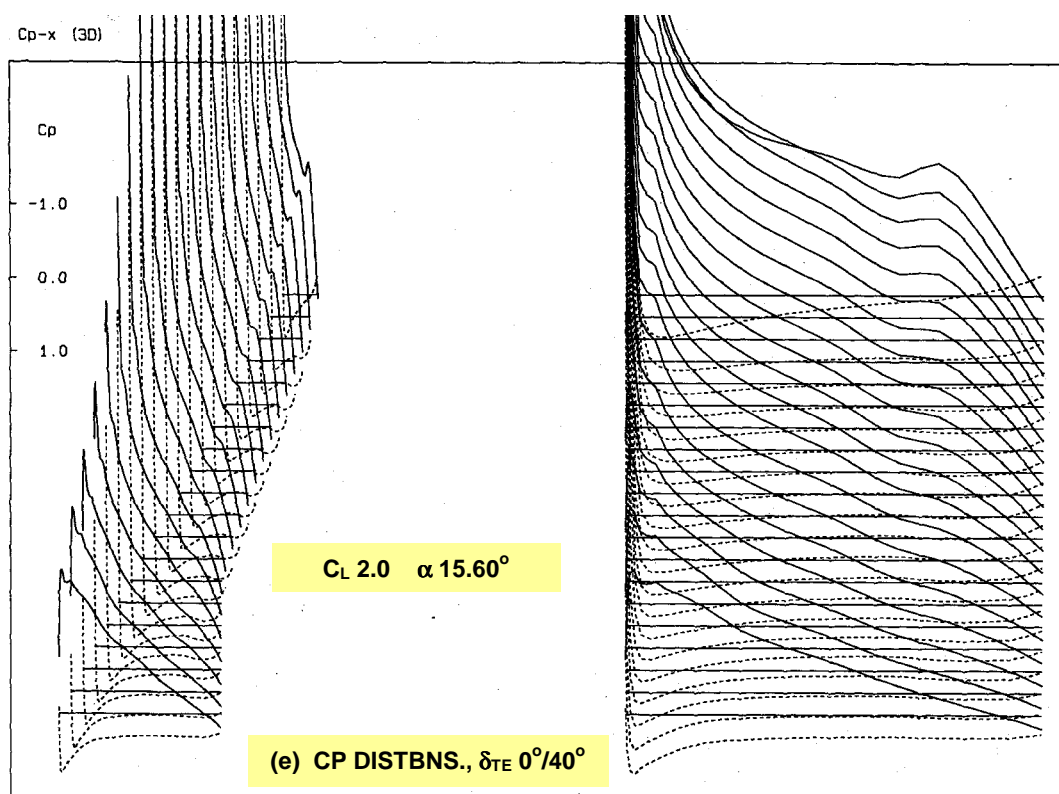
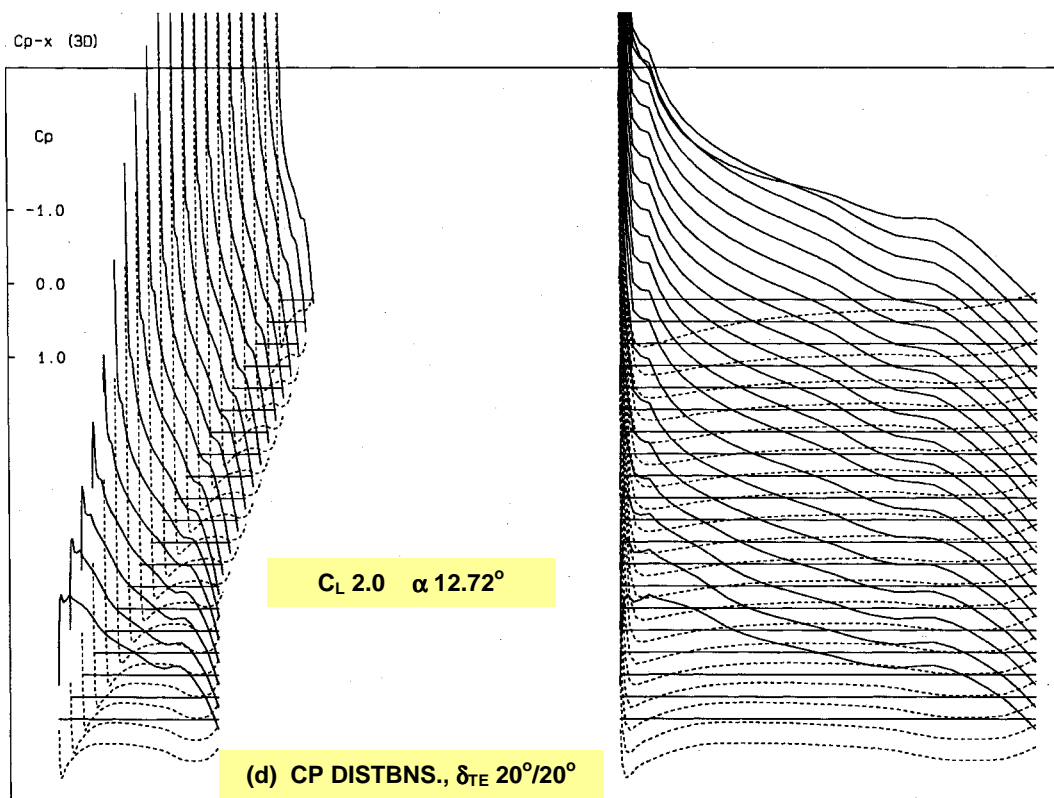
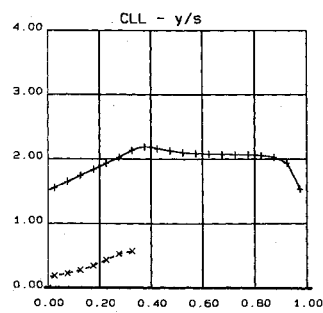
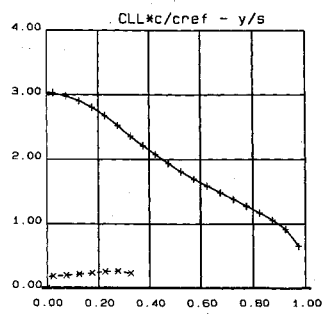
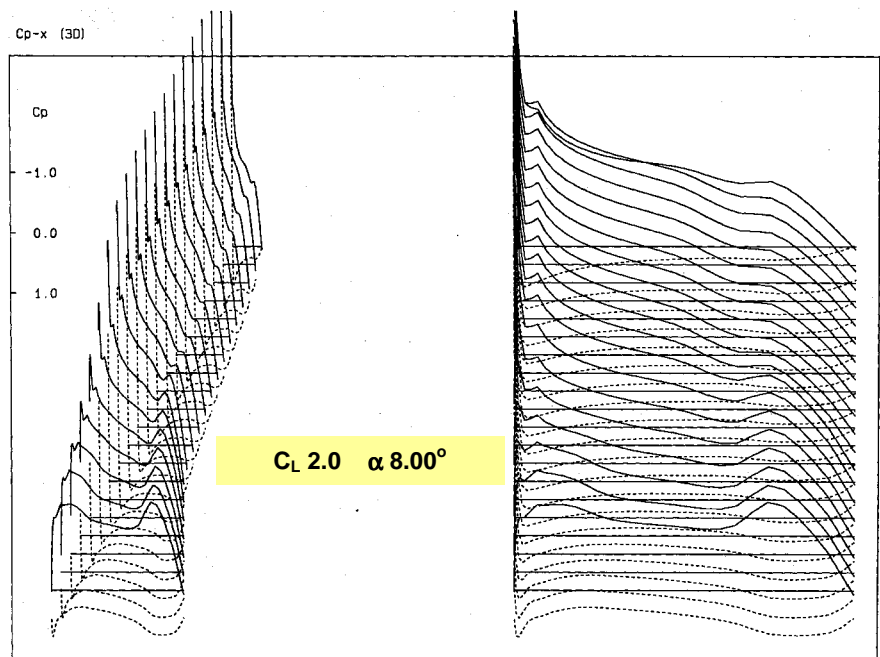


Fig. 6.3.23. Contd



(b) SPANWISE



(b) CP DISTBNS

Fig. 6.3.24. DISTRIBUTED $\delta_{TE} 48^\circ/21^\circ/21^\circ$ (Full-Span, Vari-Camber), LOADINGS, Trimmed $C_L 2.0$, $M 0.20$, $\alpha 8^\circ$, AR 10 WING + TAILPLANE

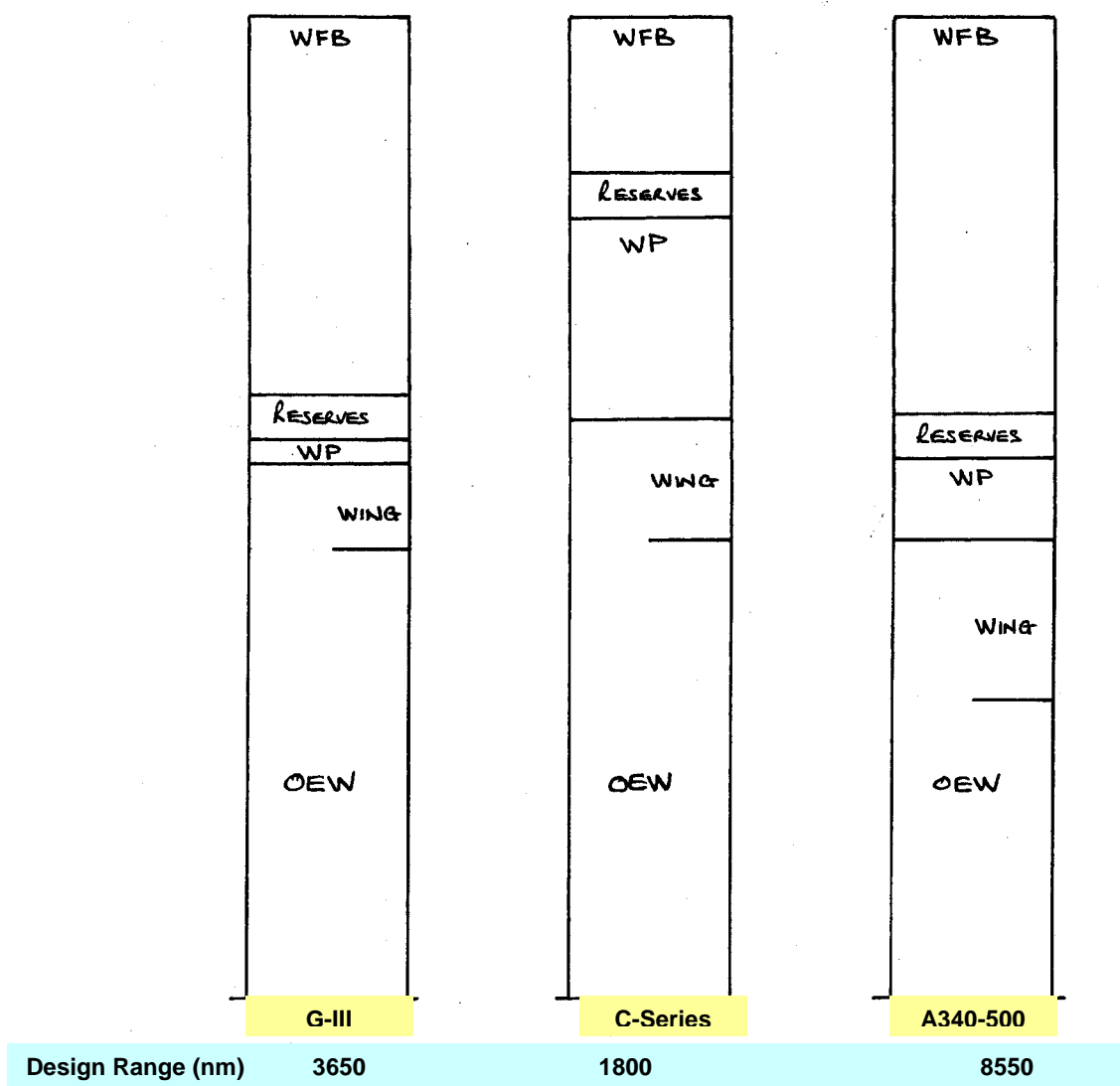


FIG. 7.2.1. COMPONENT WEIGHT BREAKDOWN – DESIGN POINT. G-III. C-SERIES & A340-500

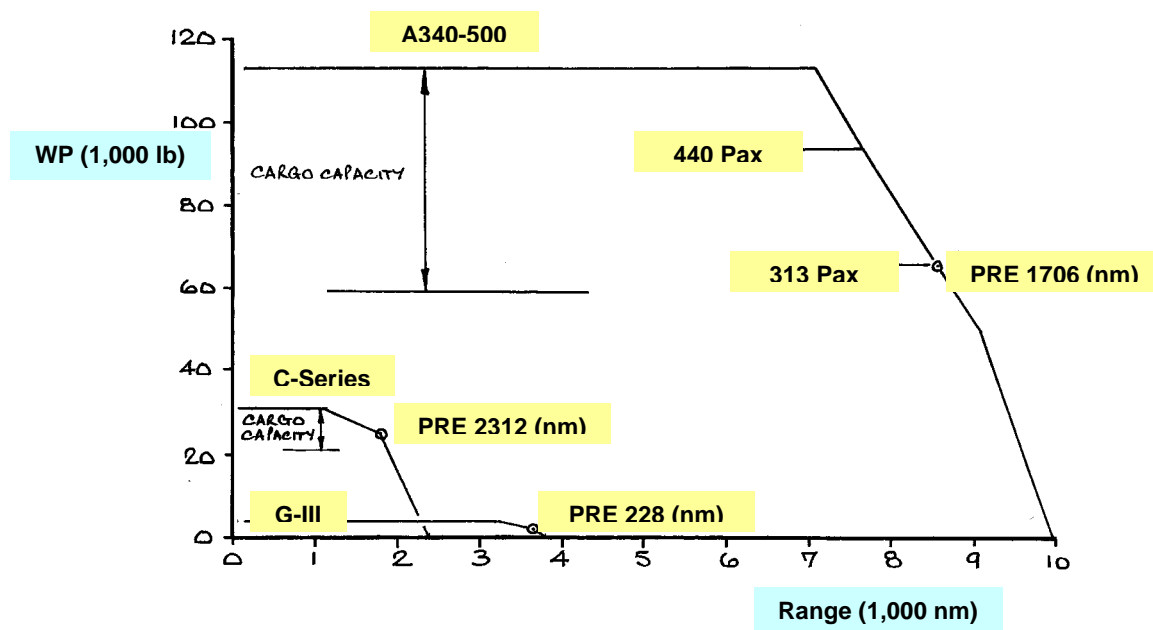


FIG. 7.2.2. PAYLOAD – RANGE DIAGRAM. G-III. C-SERIES & A340-500

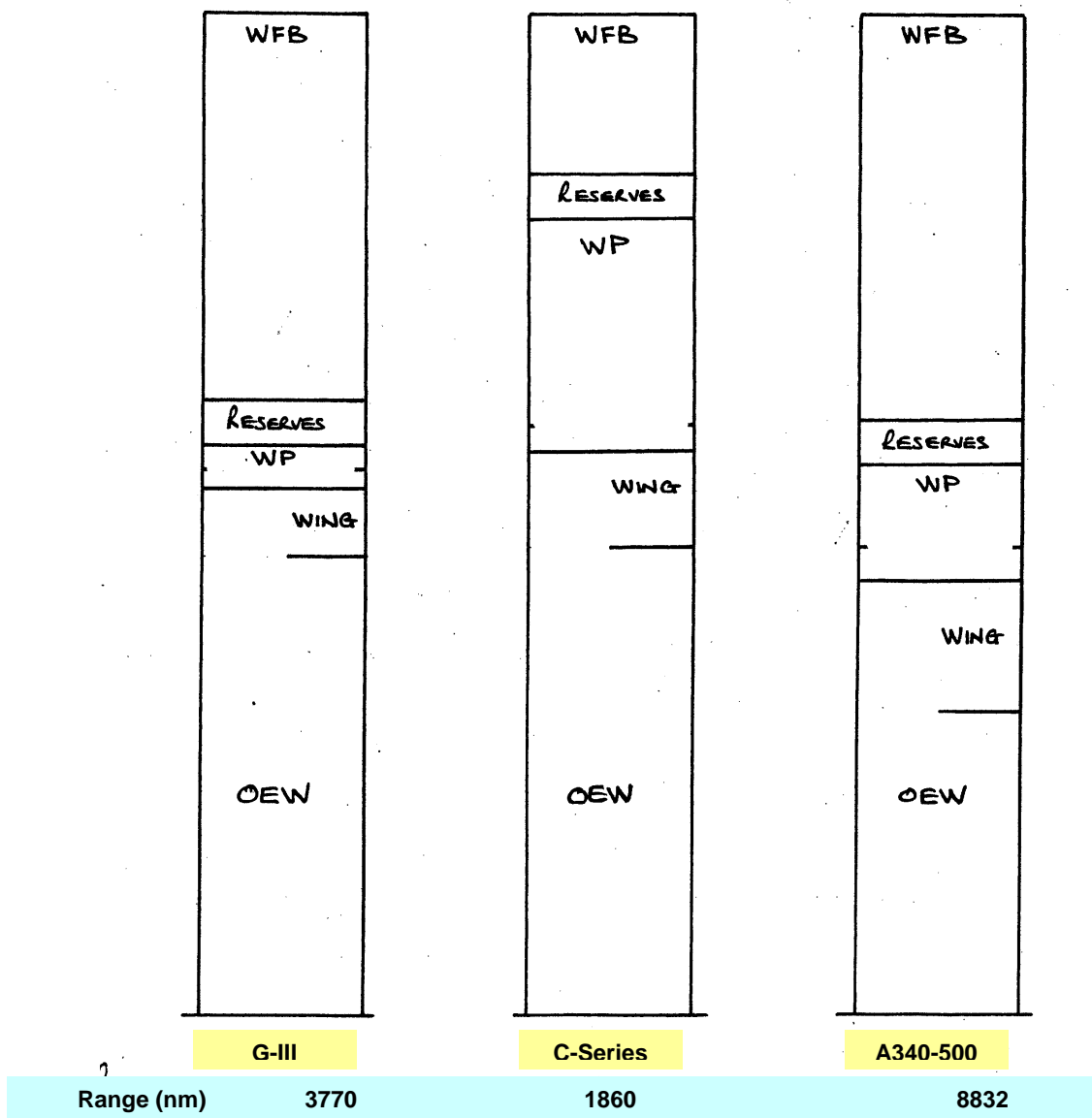


Fig. 7.2.3. COMPONENT WEIGHT BREAKDOWN – DESIGN POINT. G-III. C-SERIES & A340-500

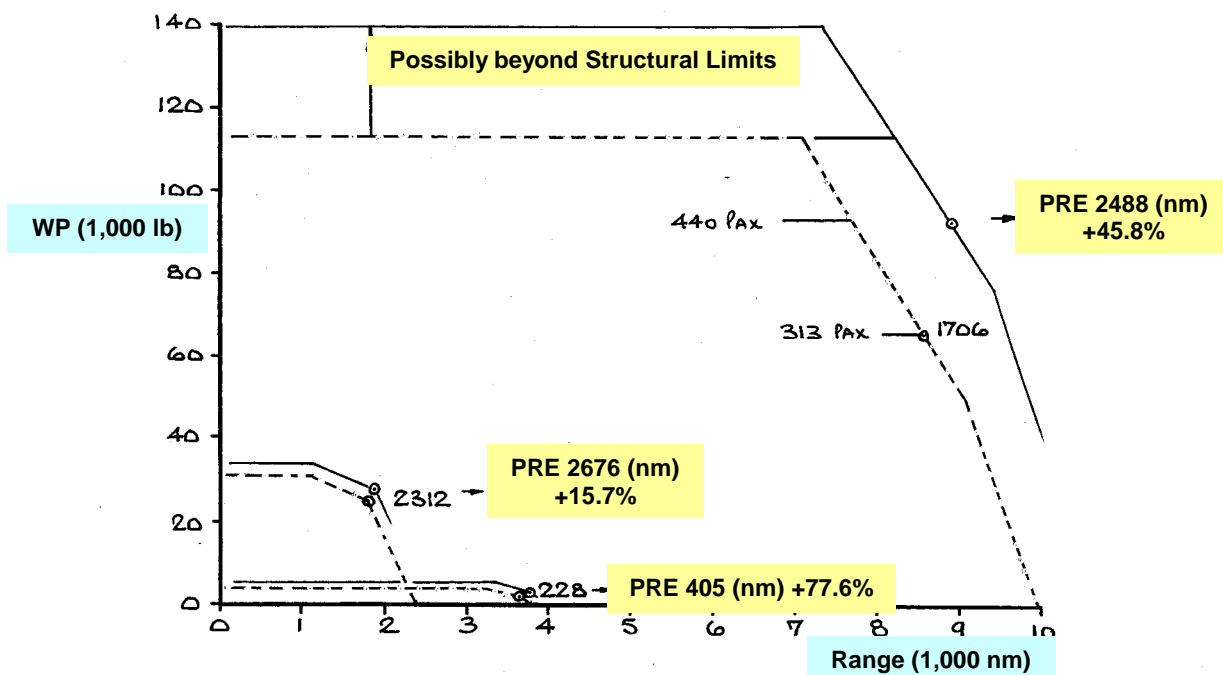


Fig. 7.2.4. PAYLOAD – RANGE DIAGRAM, G-III, C-SERIES & A340-500 RE-CONFIGURED VTE CAPABLE WINGS

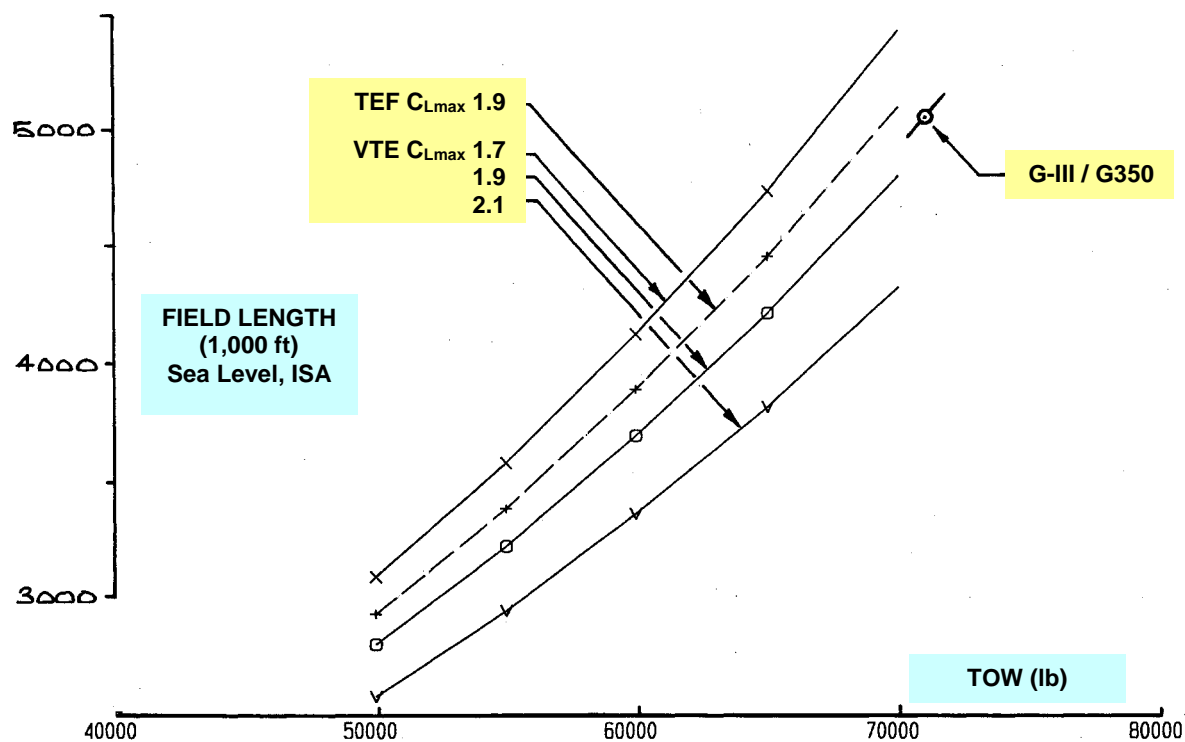


Fig. 7.3.1. TAKE-OFF FIELD LENGTH – TAKE-OFF WEIGHT, AR 6 THEORY, CONVENTIONAL TEF & VTE CAPABLE

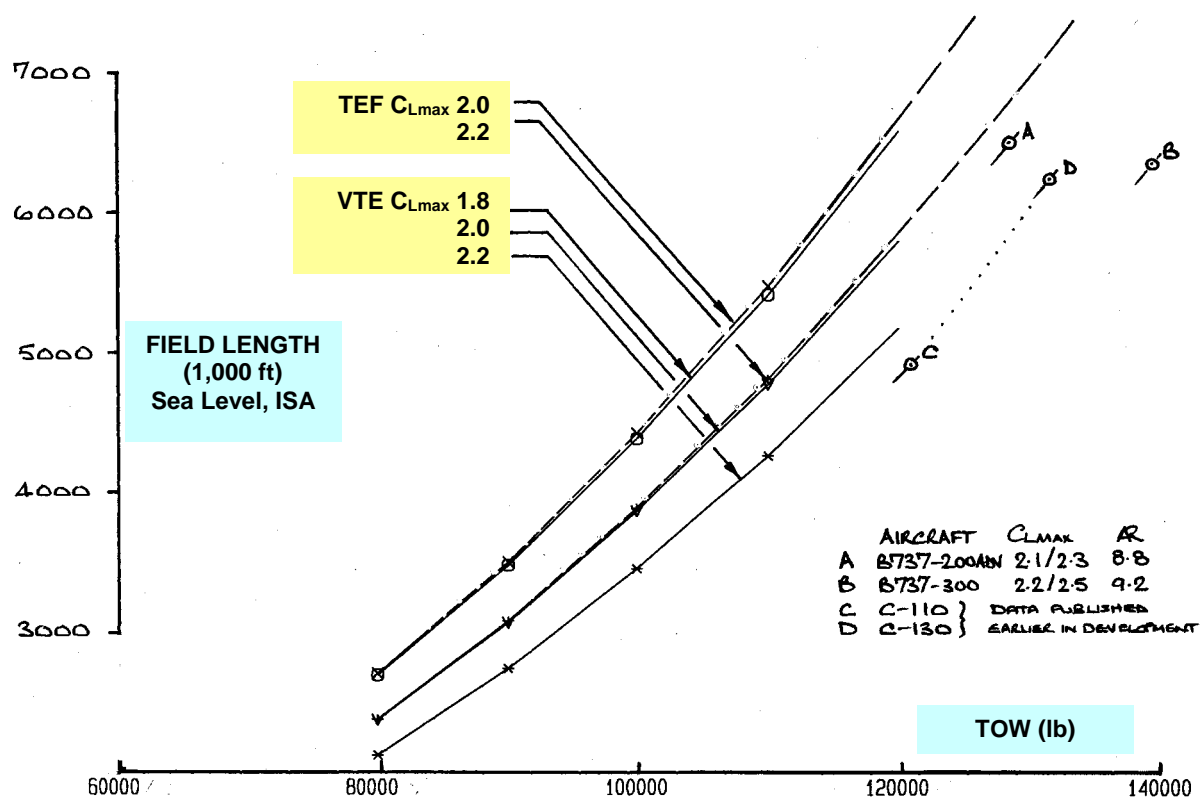


Fig. 7.3.2. TAKE-OFF FIELD LENGTH – TAKE-OFF WEIGHT, AR 10 THEORY, CONVENTIONAL TEF & VTE CAPABLE

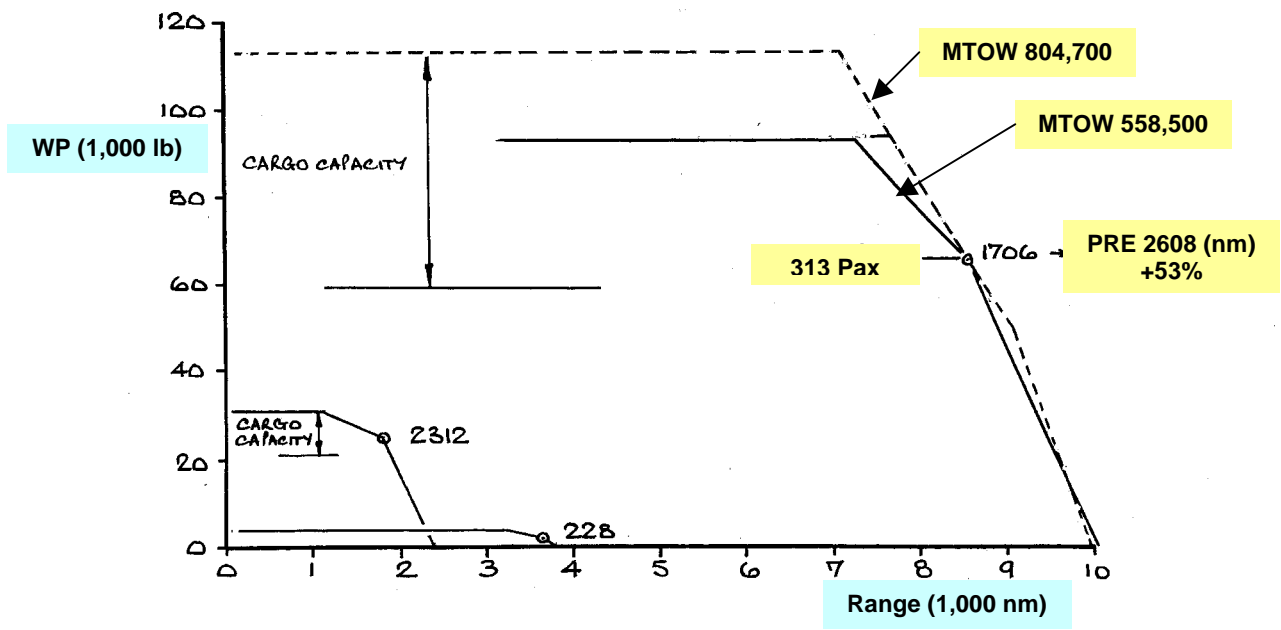


Fig. 7.4.1. PAYLOAD – RANGE DIAGRAM, G-III, C-SERIES, A340-500 & RE-SIZED A340-500

